VOL. 689 NO. 1 6 JANUARY 1995

JOURNAL OF CHROMATOGRAPHY A

INCLUDING ELECTROPHORESIS AND OTHER SEPARATION METHODS

ELSEVIER

JOURNAL OF CHROMATOGRAPHY A

INCLUDING ELECTROPHORESIS AND OTHER SEPARATION METHODS

Scope. The *Journal of Chromatography A* publishes papers on all aspects of **chromatography, electrophoresis** and related methods. Contributions consist mainly of research papers dealing with chromatographic theory, instrumental developments and their applications. In the *Symposium volumes*, which are under separate editorship, proceedings of symposia on chromatography, electrophoresis and related methods are published. *Journal of Chromatography B: Biomedical Applications* —This journal, which is under separate editorship, deals with the following aspects: developments in and applications of chromatographic and electrophoretic techniques related to clinical diagnosis or alterations during medical treatment; screening and profiling of body fluids or tissues related to the analysis of active substances and to metabolic disorders; drug level monitoring and pharmacokinetic studies; clinical toxicology; forensic medicine; veterinary medicine; occupational medicine; results from basic medical research with direct consequences in clinical practice.

Submission of Papers. The preferred medium of submission is on disk with accompanying manuscript (see *Electronic manuscripts* in the Instructions to Authors, which can be obtained from the publisher, Elsevier Science B.V., P.O. Box 330, 1000 AH Amsterdam, Netherlands). Manuscripts (in English; *four* copies are required) should be submitted to: Editorial Office of *Journal of Chromatography A*, P.O. Box 681, 1000 AR Amsterdam, Netherlands, Telefax (+31-20) 485 2304, or to: The Editor of *Journal of Chromatography B: Biomedical Applications*, P.O. Box 681, 1000 AR Amsterdam, Netherlands. Review articles are invited or proposed in writing to the Editors who welcome suggestions for subjects. An outline of the proposed review should first be forwarded to the Editors for preliminary discussion prior to preparation. Submission of an article is understood to imply that the article is original and unpublished and is not being considered for publication elsewhere. For copyright regulations, see below.

Publication information. *Journal of Chromatography A* (ISSN 0021-9673): for 1995 Vols. 683–714 are scheduled for publication. *Journal of Chromatography B: Biomedical Applications* (ISSN 0378-4347): for 1995 Vols. 663–674 are scheduled for publication. Subscription prices for *Journal of Chromatography A*, *Journal of Chromatography B: Biomedical Applications* or a combined subscription are available upon request from the publisher. Subscriptions are accepted on a prepaid basis only and are entered on a calendar year basis. Issues are sent by surface mail except to the following countries where air delivery via SAL is ensured: Argentina, Australia, Brazil, Canada, China, Hong Kong, India, Israel, Japan, Malaysia, Mexico, New Zealand, Pakistan, Singapore, South Africa, South Korea, Taiwan, Thailand, USA. For all other countries airmail rates are available upon request. Claims for missing issues must be made within six months of our publication (mailing) date. Please address all your requests regarding orders and subscription queries to: Elsevier Science B.V., Journal Department, P.O. Box 211, 1000 AE Amsterdam, Netherlands. Tel.: (+31-20) 485 3642; Fax: (+31-20) 485 3598. Customers in the USA and Canada wishing information on this and other Elsevier journals, please contact Journal Information Center, Elsevier Science Inc., 655 Avenue of the Americas, New York, NY 10010, USA, Tel. (+1-212) 633 3750, Telefax (+1-212) 633 3764.

Abstracts/Contents Lists published in Analytical Abstracts, Biochemical Abstracts, Biological Abstracts, Chemical Abstracts, Chemical Titles, Chromatography Abstracts, Current Awareness in Biological Sciences (CABS), Current Contents/Life Sciences, Current Contents/Physical, Chemical & Earth Sciences, Deep-Sea Research/Part B: Oceanographic Literature Review, Excerpta Medica, Index Medicus, Mass Spectrometry Bulletin, PASCAL-CNRS, Referativnyi Zhurnal, Research Alert and Science Citation Index.

US Mailing Notice. *Journal of Chromatography A* (ISSN 0021-9673) is published weekly (total 52 issues) by Elsevier Science B.V., (Sara Burgerhartstraat 25, P.O. Box 211, 1000 AE Amsterdam, Netherlands). Annual subscription price in the USA US$ 5389.00 (US$ price valid in North, Central and South America only) including air speed delivery. Second class postage paid at Jamaica, NY 11431. **USA POSTMASTERS**: Send address changes to *Journal of Chromatography A*, Publications Expediting, Inc., 200 Meacham Avenue, Elmont, NY 11003. Airfreight and mailing in the USA by Publications Expediting.

See inside back cover for Publication Schedule, Information for Authors and information on Advertisements.

0021-9673/95/$09.50

Printed in the Netherlands

CONTENTS

(Abstracts/Contents Lists published in Analytical Abstracts, Biochemical Abstracts, Biological Abstracts, Chemical Abstracts, Chemical Titles, Chromatography Abstracts, Current Awareness in Biological Sciences (CABS), Current Contents/Life Sciences, Current Contents/Physical, Chemical & Earth Sciences, Deep-Sea Research/Part B: Oceanographic Literature Review, Excerpta Medica, Index Medicus, Mass Spectrometry Bulletin, PASCAL-CNRS, Referativnyi Zhurnal, Research Alert and Science Citation Index)

(Continued overleaf)

Contents (continued)

SHORT COMMUNICATIONS

Column Liquid Chromatography

BOOK REVIEW

JOURNAL OF CHROMATOGRAPHY A

VOL. 689 (1995)

JOURNAL OF CHROMATOGRAPHY A

INCLUDING ELECTROPHORESIS AND OTHER SEPARATION METHODS

ELSEVIER

Amsterdam – Lausanne – New York – Oxford – Shannon – Tokyo

0021-9673/95/$09.50

ELSEVIER

Journal of Chromatography A, 689 (1995) 1

JOURNAL OF CHROMATOGRAPHY A

Publisher's Note

We are pleased to announce that Colin Poole, Department of Chemistry, Imperial College of Science, Technology and Medicine, South Kensington, London, UK, will join the team of Editors of the *Journal of Chromatography A*, as per 1 January 1995.

Professor Poole's research interests are primarily in the application of gas, liquid, thin-layer and supercritical fluid chromatographic techniques to problems of a diverse nature; sample preparation technology; and chemometric analysis.

Without doubt, the appointment of Professor Poole to the Board of Editors will help the journal in maintaining and expanding its role in the field of separation science. We wish him every success and much personal satisfaction in this position.

SSDI 0021-9673(94)01149-4

ELSEVIER

Journal of Chromatography A, 689 (1995) 3–12

JOURNAL OF CHROMATOGRAPHY A

Amphiphilic agarose-based adsorbents for chromatography Comparative study of adsorption capacities and desorption efficiencies

Sven Oscarsson[a,b,*], Dalila Angulo-Tatis[b], Grigoriy Chaga[a], Jerker Porath[c]

[a]*Biochemical Separation Centre, Uppsala University, Box 577, S-751 23 Uppsala, Sweden*

[b]*Department of Chemical Engineering, Mälardalen University, Box 325, S-631 05 Eskilstuna, Sweden*

[c]*Department of Biochemistry, Life Sciences West, University of Arizona, Tucson, AZ 85721, USA*

First received 13 April 1994; revised manuscript received 1 September 1994

Abstract

A number of hydrophobic derivatives attached to cross-linked agarose were studied as protein adsorbents. Differences in the adsorption and desorption behaviour were determined as functions of type and concentration of selected salts. Whereas octyl- and phenyl-Sepharose adsorb serum albumin preferentially, pyridyl-S-agarose shows a much stronger preferential affinity for IgG in the presence of high concentrations of lyotropic salts, such as sulphates. In contrast to pyridyl-S-agarose, a large portion of proteins remained fixed to octyl- and phenyl-Sepharose after extensive washing with 1 *M* NaOH.

1. Introduction

Hydrophobic adsorbents have several applications in the field of biology and medicine for the isolation of proteins. The factors involved in hydrophobic interaction and hydrophobic affinity chromatography have been extensively studied [1–8]. Not only the nature of the adsorbent, but also the concentration and chemical nature of the salt solutions employed for salt-promoted adsorption or elution affect the results.

Two different theories have been proposed to explain the effect of solvent additives on the binding of proteins in hydrophobic affinity chromatography: the preferential protein solvent interaction theory by Arakawa [9] and the surface tension theory proposed by Melander and Horváth [10]. Measurement of the preferential protein solvent interactions gives a measure of the change in the chemical potential of the proteins induced by the addition of co-solvents [11,12], while the surface tension effect studied by Melander and Horváth applies to the cavity theory developed by Sinanoğlu and co-workers [13,14].

With the introduction of thiophilic interaction chromatography [15], our interest has been refocused on the parameters governing protein adsorption. Electrically neutral ligands containing delocalized π-electrons interact selectively with surface-located amino acid side-groups that are

* Corresponding author. Address for correspondence: Biochemical Separation Centre, Uppsala University, Box 577, S-751 23 Uppsala, Sweden.

0021-9673/95/$09.50
SSDI 0021-9673(94)00857-4

rich in π-electrons (indolyl, etc.) according to our working hypothesis.

Are π,π-complexation and hydrophobic interactions synergistic in their adsorption effects? In an attempt to clarify some of these effects, we have measured the adsorption capacities and desorption efficiencies for serum proteins in the presence of different salts and at different salt concentrations.

2. Experimental

2.1. Chemicals and materials

NaOAc, Na_2SO_4, K_2SO_4, NH_4OAc and butylglycidyl ether were purchased from Fluka (Buchs, Switzerland) and NaCl and $NaBH_4$ from Merck (Darmstadt, Germany). Trisma base was obtained from Sigma (St. Louis, MO, USA). Sepharose 4B, octyl-Sepharose, phenyl-Sepharose and octylglycidyl ether were gifts from Pharmacia BioProcess Technology (Uppsala, Sweden). NaOH was purchased from EKA Nobel (Surte, Sweden), mercaptopyridine from Aldrich (Steinheim, Germany) and ethanol from Svensk Sprit (Stockholm, Sweden). All deuterated solvents used for NMR analyses were purchased from Glaser (Germany). Serum samples mixed from 50 different patients to obtain a serum pool were purchased from Uppsala University Hospital. Gels for electrophoresis were from Pharmacia Biotech (Uppsala), Sweden.

2.2. Determination of dynamic capacity

The serum sample was adjusted to 0.5 *M* K_2SO_4 by adding solid salt and 0.1 *M* Tris–HCl buffer (pH 7.5), resulting in 11.5 mg/ml of protein. A column (3 × 1 cm I.D.) filled with the respective adsorbent was equilibrated with 0.5 *M* K_2SO_4–0.1 *M* Tris buffer (pH 7.5). The protein solution was loaded on the column at a flow-rate of 0.64 ml/min until the protein concentration in the eluate was the same as that in the applied sample. Dynamic capacity was determined by the method of Winzor [16].

2.3. Calculation methods for determination of dynamic capacity

The dynamic capacities were calculated by using the equation

$$\text{Dynamic capacity} = [(V_x - V_0)/V_t)]P \quad (1)$$

where V_0 is the volume of the voids between the particles in the bed, V_t the total bed volume and V_x is the volume of protein solution added to the column to achieve an eluate protein concentration corresponding to 50% P, where P is the protein concentration of the aplied sample, V_t = 2.35 ml and P = 11.5 mg/ml, as determined by amino acid analysis.

2.4. Determination of salt-dependent adsorption capacity

In order to achieve high reproducibility, an optimized programme for adsorption, desorption and rinsing of the adsorbent was executed by means of a programmable fast protein liquid chromatography (FPLC) system. Serum was diluted with 0.1 *M* Tris-HCl buffer (pH 7.5) to a protein concentration of 13.6 mg/ml in the presence of the salt to be studied. A column (3 × 1 cm I.D.) packed with the respective adsorbent was equilibrated with the salt dissolved in the 0.1 *M* Tris buffer. A 1-ml volume of sample was loaded on the column at a flow-rate of 0.64 ml/min, followed by 15 ml of the equilibration buffer. A 10-ml volume of 0.1 *M* Tris buffer was passed through the column at a flow-rate of 0.64 ml/min. Finally, the gel was rinsed with 0.1 *M* NaOH when pyridine-S-agarose was used or with 20% (v/v) ethanol in deionized water for the other adsorbents. The procedure described above was repeated at 75% and 50% of the original salt concentrations in addition to the 100% concentration.

2.5. Recovery studies

These studies were performed in the same manner as the salt-dependent adsorption capacity measurements. However, following the elution with 0.1 *M* Tris buffer, the adsorbents were

eluted with 30% ethylene glycol, then rinsed with 0.1 *M* NaOH or 1 *M* NaOH. The amount of protein eluted from the column on excluding salt from the elution buffer was determined by amino acid analysis. The content of human serum albumin (HSA) in the fractions collected during recovery studies was determined by a conventional radioimmunodiagnostic technique. The content of immunoglobulin G (IgG) was determined by a nephelometric technique using the array protein system (Beckman Instruments, Fullerton, CA, USA) at the Department of Clinical Immunology, Uppsala University Hospital. The amount of protein that remained on the adsorbent after rinsing with sodium hydroxide was measured by amino acid analysis on hydrolysed samples. Sepharose 6B was used to investigate the influence of the matrix without any ligands.

2.6. Preparation methods for gels

Pyridyl-S-derivatized gels were prepared according to Oscarsson [17]. Different degrees of substitution of butyl, phenyl and octyl groups on agarose were obtained by varying the concentrations of the respective substances, the reaction time and the reaction temperature.

Preparation of phenylagarose

Sepharose 4B was cross-linked and activated by adding 25 ml of 4 *M* NaOH to 50 g of suction-dried gel (prewashed with deionized water) under stirring followed by 0.35 g of $NaBH_4$; 25 ml of epichlorohydrin were added continuously over 1 h to a final volume of 50 ml. After 20 h at room temperature, the gel was rinsed with deionized water on a sintered-glass filter followed by addition of x g of phenol, 0.34 g of $NaBH_4$ and y ml of NaOH of a certain concentration for a specified reaction time and temperature according to Table 1 (phenylagarose).

Preparation of butylagarose

Sepharose 6B was crosslinked and activated by adding 25 ml of 1 *M* NaOH under stirring to 25 g of suction-dried gel (prewashed with deionized water) followed by 0.35 g of $NaBH_4$ and 4 ml of epichlorohydrin. After reaction for 30 min at room temperature, the gel was rinsed with deionized water on a sintered-glass filter followed by addition of x ml of butyl glycidyl ether, 0.17 g of $NaBH_4$ and y ml of NaOH of a certain concentration and during a specified reaction time and temperature according to Table 1 (butylagarose).

Preparation of octylagarose

Octyl glycidyl ether was used as reagent and x ml were added to the reaction mixture followed by 0.17 g $NaBH_4$ and y ml of NaOH according to Table 1. Otherwise the conditions were the same as for butylagarose.

2.7. Hydrolysis of gels for determination of the degree of substitution by NMR

A 20-mg amount of the respective freeze-dried adsorbent was hydrolysed by adding approximately 2 ml of 20% (v/v) deuterated hydrochloric acid (^2HCl) to an NMR tube and heating the tube at 70°C for 2–3 min. After cooling, the solvent was evaporated and deuterated dimethyl sulphoxide (DMSO) was added to the tube for analysis.

2.8. Other methods

Standard proton NMR spectra were obtained by use of a 200-MHz NMR spectrometer (Varian, Palo Alto, CA, USA). Amino acid analyses were performed according to Spackman et al. [18]. All analyses of elements were performed with an NA 1500 automatic nitrogen, carbon and sulphur analyser (Carlo Erba, Milan, Italy).

3. Results

3.1. Dynamic adsorption capacities

The total amount of protein loaded on to the column was approximately two thirds of the maximum dynamic capacity for the respective adsorbent. The maximum dynamic capacities in K_2SO_4 solutions for phenyl-, octyl- and pyridyl-

Table 1
Conditions for the preparation of phenyl-, octyl- and butylagarose with different degrees of substitution

Adsorbent	Degree of substitution (μmol/g)	Amount of phenol (g)	NaOH (ml)	Reaction time (h)	Temperature (°C)
Phenylagarose	220	6	50 (1 *M*)	24	22–25
	366	10	50 (1 *M*)	24	22–25
	923	4	50 (2 *M*)	6	40
	1066	10	50 (2 *M*)	10	22–25
		Octylglycidyl ether (ml)			
Octylagarose	9	2	10	20	22–25
	20	6	25	20	22–25
	48	10	25	20	22–25
	65	10	25	20	40
	93	10	25	20	60
		Butylglycidyl ether (ml)			
Butylagarose	67	5	25 (4 *M*)	20	22–25
	134	20	25 (4 *M*)	20	22–25
	300	30	50 (4 *M*)	6	40
	546	25	50 (1 *M*)	5	70

S-agarose were found to be 28.4, 23.5 and 21.00 mg of protein per ml of wet gel, respectively. This corresponds to a respective degrees of substitution of 1400, 48 and 1028 μmol/g freeze-dried adsorbent.

3.2. Salt-dependent adsorption capacities

To facilitate our discussion we introduce a parameter that we call the "salt-dependent adsorption capacity" (SAC). SAC is defined as the percentage of the protein adsorbed that can be released from the adsorbent by omitting the salt from the elution buffer.

The effect of the type of salt on the capacity to adsorb serum proteins was studied for four different adsorbents in the presence of five types of salts at one or more salt concentrations. The selected degree of substitution for each gel was 1400 μmol/g freeze-dried adsorbent for phenyl-Sepharose, 48 μmol/g for octyl-Sepharose, 923 μmol/g for pyridyl-S-agarose and 300 μmol/g for butylagarose.

As demonstrated in Fig. 1, pyridyl-S-agarose has the same or a higher SAC for adsorbing proteins than most of the other hydrophobic adsorbents for all the salts studied. When sodium acetate was used in the 1–2 *M* concentration range, SAC ranged from 26.8 to 42.8% of the total applied protein. The corresponding values for phenyl-Sepharose were in the range 13.5–22.9%. Octyl-Sepharose adsorbed smaller amounts of serum proteins compared with butylagarose (see Fig. 1a).

In 0.2–0.6 *M* Na_2SO_4 the SAC values for pyridyl-*S*-agarose were found to be in the range 10.6–40.8% whereas these values for butyl-, octyl- and phenyl-Sepharose were 1.9–16, 0.3–28.8 and 8.7–31.8%, respectively (see Fig. 1b). In 0.75–3 *M* ammonium acetate the SAC values

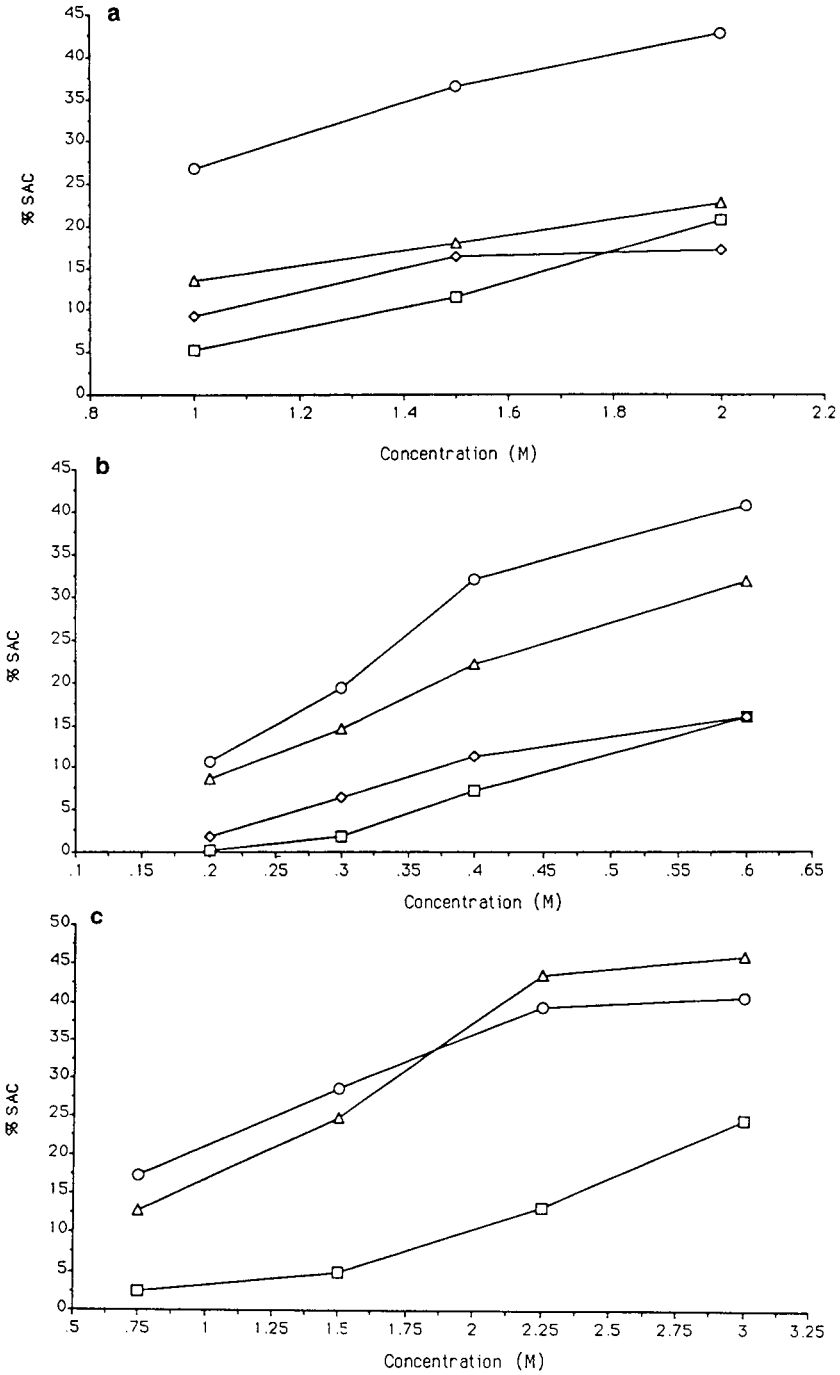

Fig. 1. (a) Percentage of material eluted from a column (3 × 1 cm I.D.) on changing the concentration of NaOAc in the elution buffer (SAC). The protein solution was loaded on the column in the presence of respective salt and salt concentration with a flow-rate of 0.64 ml/min. The protein was eluted at various concentrations of NaOAc in 0.1 *M* Tris buffer (pH 7.5). □ = octyl-Sepharose; ◇ = butylagarose; ○ = pyridyl-S-agarose; △ = phenyl-Sepharose. (b) As (a) except that Na_2SO_4 was used instead of NaOAc. (c) As (a) except that NH_4Cl was used instead of NaOAc.

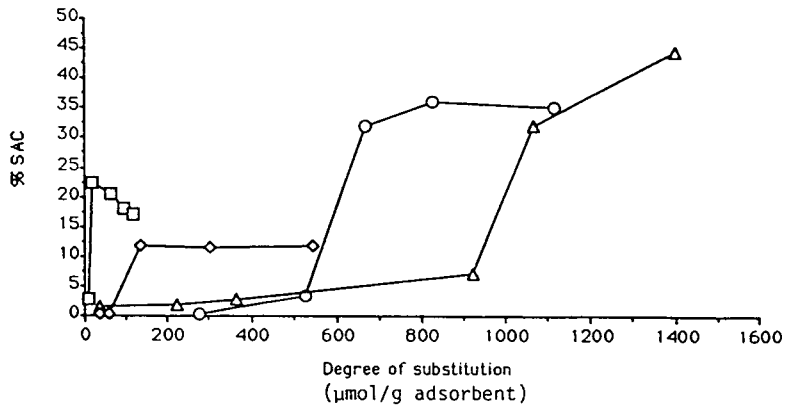

Fig. 2. SAC as a function of the degree of substitution of the ligand (μmol/g adsorbent). Column dimensions, flow-rate and symbols as in Fig. 1. Sample: 0.2 ml of serum diluted with 0.1 *M* Tris buffer (pH 7.5) to a total volume of 1.0 ml. K_2SO_4 was added to a final concentration of 0.5 *M*. Solvent: 0.1 *M* Tris–HCl (pH 7.5) containing 0.5 *M* K_2SO_4. Elution: 0.1 *M* Tris–HCl (pH 7.5).

for pyridyl-S-agarose were found to be in the range 17.2–40.9% whereas for octyl-Sepharose SAC was 1.02–24.7% and for phenyl-Sepharose 12.7–46.3% (see Fig. 1c).

3.3. SAC as a function of degree of substitution

As shown in Fig. 2, maximum capacity was reached at a lower degree of substitution for long aliphatic apolar groups than for a short group. Thus, the degrees of substitution for reaching saturation values were 150 and 20 μmol/g dry gel for butylagarose and octyl-Sepharose, respectively. More than 650 μmol of mercaptopyridine per gram of carbohydrate were required to attain the plateau value for pyridyl-S-agarose, whereas for phenyl-Sepharose a plateau value was not reached even at a degree of substitution as high as 1400 μmol/g carbohydrate.

3.4. Desorption efficiency as a function of the degree of substitution

Fig. 3 illustrates the fraction of protein remaining on the adsorbent after omitting salt from the buffer, as determined by amino acid

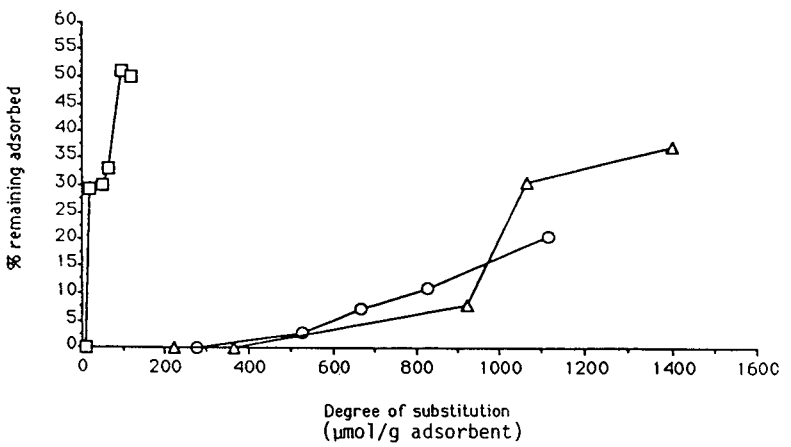

Fig. 3. Percentage of applied protein remaining on the adsorbents after omission of salt (0.5 *M* K_2SO_4) from the solvent. Conditions as in Fig. 2; symbols as in Fig. 1.

analysis. It was found that 2.7–20.7% of the proteins applied on the pyridine-S-adsorbent were virtually irreversibly adsorbed when the degree of substitution was in the range 500–1115 μmol/g adsorbent. The corresponding values for phenyl-Sepharose were 8.1–34.6% at a degree of substitution between 923 and 1400 μmol/g and 29.3–50.0% for octyl-Sepharose when the degree of substitution was 20–116 μmol octyl groups/g dry adsorbent.

3.5. Recovery studies

To obtain more complete information about the recoveries from the different adsorbents, we determined (1) the percentage of the applied proteins that passed through the column, (2) those which were eluted with omission of salt from the elution buffer and (3) those which were eluted with ethylene glycol included in the buffer. Only K_2SO_4 and NaCl as adsorption promoters were studied (see Table 2). Yields between 93 and 110% were obtained as determined by measuring A_{280} and amino acid analyses. The efficiency of 0.1 and 1 *M* NaOH solution in removing proteins adsorbed from the pyridine-S-gel was determined by amino acid analyses. For pyridine-S-agarose, 0.5–1% of the total applied protein remained adsorbed after rinsing the adsorbent with ethylene glycol followed by 0.1 *M* NaOH. The corresponding values were 25% for octyl-Sepharose, 8.3% for phenyl-Sepharose and <1% for butylagarose.

As much as 4.7–5.3% of the applied proteins remained adsorbed on the gel even after treatment of phenyl-Sepharose with 1 *M* NaOH; the corresponding level for octyl-Sepharose was 19.2–21.1%. Pyridyl-S-agarose stands out as a far superior adsorbent; only 0.3–0.4% of applied proteins remained adsorbed after treatment with 1 *M* NaOH.

3.6. Adsorption capacities for IgG and HSA on respective adsorbent

The amounts of HSA and IgG were determined in the fractions obtained after omission of salt from the buffer (operation 2, Table 3). The results clearly show the differences in specificity for HSA and IgG.

Table 2
Recovery studies on serum proteins

Operation[a]	Octyl-Sepharose (48 μmol/g)[b]		Butylagarose (300 μmol/g)[b]		Sepharose 6B		Phenyl-Sepharose (1400 μmol/g)[b]		Pyridyl-S-agarose (1028 μmol/g)[b]	
	K_2SO_4	NaCl	K_2SO_4	NaCl	K_2SO_4	NaCl	K_2SO_4	NaCl	K_2SO_4	NaCl
1	50.2	44.1	87.2	83.4	96.7	92.0	26.8	21.2	56.4	48.0
2	11.6	27.2	6.5	9.6	0.7	3.3	47.3	59.4	31.5	35.0
3	11.7	6.2	1.3	0.8	<1	1.6	12.6	10.0	7.9	5.2
4	0.8	7.1	1.0	0.6	<1	<1	1.9	0.5	3.0	7.2
5	25.0	25.7	0.4	0.7			8.3	6.1	1.4	0.9
Total adsorbed[c]	49.1	66.3	9.2	10.4	0.7	4.9	70.1	76	43.8	48.3
Yield (%)	99.3	110.4	96.4	93.8	97.4	96.9	96.9	97.2	100.2	96.3

Recoveries are given as a percentage of the amount of protein applied.

[a] 1 = Proteins non-adsorbed from 1 ml of serum [diluted 1:5 with 0.1 *M* Tris buffer (pH 7.5)] in the presence of 0.5 *M* K_2SO_4 or 3 *M* NaCl. 2 = Desorption of proteins from the respective adsorbent by omitting salt from the elution buffer. 3 = Desorption of proteins by elution with 30% (v/v) ethylene glycol. 4 = Proteins remaining after rinsing of the adsorbent with 0.1 *M* NaOH. 5 = Amino acid analysis of proteins left on the gel.

[b] Degree of substitution of adsorbent with ligand.

[c] Total adsorbed is the sum of the figures from operations 2, 3, 4 and 5 and gives information about the total amount of protein which was adsorbed on the respective adsorbent. The amount of proteins passing through in operations 1–4 was determined from A_{280} values.

Table 3
Amounts of human IgG and HSA in the fractions obtained when proteins were desorbed from the adsorbents by omitting salt from the elution buffer

Material	Octyl-Sepharose (48 μmol/g)[a]		Butylagarose (300 μmol/g)[a]		Phenyl-Sepharose (1400 μmol/g)[a]		Pyridyl-S-agarose (1028 μmol/g)[a]	
	K_2SO_4	NaCl	K_2SO_4	NaCl	K_2SO_4	NaCl	K_2SO_4	NaCl
Human IgG (μg)	–[b]	360	200	–[b]	1900	1800	1570	1380
HSA	1200	1650	330	30	6000	6050	15	24

[a] Degree of substitution of adsorbent with ligand.
[b] Below the detection limit.

4. Discussion

This study was carried out to evaluate the effect of different salts on protein adsorption on amphiphilic agarose-based adsorbents and to test the effectiveness of different methods of protein desorption. The adsorbents compared are not purely hydrophobic, which is why we use the term "amphiphilic" to indicate the complexity of the adsorption involved in the chromatographic process. Serum was chosen as a model for both capacity and selectivity studies. This selection makes the evaluation more complicated, but at the same time more informative, since serum contains proteins with a wide range of physicochemical characteristics.

We determined the salt-dependent adsorption capacities, i.e. how much of the adsorbed proteins becomes released from the adsorbent on omitting salt from the buffer solution. The determination of dynamic capacity gave valuable, but not complete, information about the efficiency of the chromatographic process, as illustrated by our results. The dynamic capacity was nearly the same for octyl-, phenyl- and pyridyl-S-agarose, but the salt-dependent adsorption capacity differed among these gels. These results reflect differences in desorption efficiencies and selectivity characteristics of the adsorbents. The salt-dependent adsorption capacity was high for pyridyl-S-agarose. The results of the studies on the effect of different salts show that, for most of the salts investigated, the proteins remain on the phenyl and octyl gels after omitting salt from the elution buffer. Effective rinsing of the adsorbent is extremely important, particularly when the adsorbent will be reused. Therefore, we investigated use of ethylene glycol followed by 0.1 or 1 *M* NaOH for elution. Even after treatment with 1 *M* NaOH, a large amount of protein remained adsorbed on octyl-Sepharose and phenyl-Sepharose. In contrast, the pyridyl-S-agarose adsorbent under the same conditions eluted with high efficiency.

These observations reveal a serious weakness in the commercially available hydrophobic adsorbents for bioprocessing where washing with 1 *M* NaOH is a standardized stripping method. There is substantial risk of contamination of fractions when reusing the adsorbent. In addition, the adsorption behaviour can be drastically changed when a protein-covered hydrophobic adsorbent is reused and drastic reductions in adsorption capacity and protein selectivity can occur.

We know from earlier investigations [17,19] that HSA is preferably adsorbed on alkyl ether adsorbents and IgG on pyridyl-S-agarose in the presence of K_2SO_4 or NaCl. This difference was quantified by determination of the total amount of IgG and HSA in those fractions that contained proteins released on deleting salt from the elution buffer. According to these results (see Table 3), a large amount of HSA was adsorbed on both phenyl- and octyl-Sepharose compared with pyridyl-S-agarose. The difference in selec-

tive behavior for IgG and HSA of the different gels strongly indicates that specific interactions occur, especially in the case of pyridyl-S-agarose. However, the side-groups in the proteins involved in the interactions remain unknown.

In order to optimize the downstream processes, the relationship between the salt-dependent adsorption capacity and the efficiency of the desorption of proteins as a function of the degree of substitution with ligands has to be known. From the data in Figs. 2 and 3, we can conclude that, for the pyridyl-S-adsorbent, in the presence of potassium sulphate, the optimum relationship between high salt-dependent adsorption capacity and good desorption efficiency will be obtained at a substitution degree of 650–700 μmol/g of pyridine thioether groups. Under these conditions, the salt-dependent adsorption capacity for serum proteins is 32–35% and only 5–7% remains on the gel after omission of the salt. For octyl-Sepharose the optimum degree of substitution is 20 μmol of alkyl groups, which gives 23% SAC with 29–30% of protein remaining on the gel. The corresponding values for phenyl-Sepharose at a ligand concentration of 1400 μmol/g dried adsorbent are 45% SAC and 36–38% of serum proteins remaining on the gel on omitting salt from the buffer.

The values obtained for butylagarose were too few to be included in Fig. 3. However, from studies performed on butylagarose with a degree of substitution corresponding to 300 μmol/g adsorbent, the SAC value was 11% with 2–3% of the protein remaining on the gel. To compensate for the low capacity for butylagarose, the length of the carbon chain or the bed size must be increased. Increasing the chain length of the ligands will decrease the desorption efficiency.

5. Conclusions

The commercially available hydrophobic interaction chromatography (HIC) adsorbents octyl- and phenyl-Sepharose, are too hydrophobic to be ideal for downstream processes, as too much protein remains on the column after omitting salt from the elution buffer. Even after rinsing the adsorbents with sodium hydroxide the amount of protein remaining on the gel is unacceptable. Use of the less hydrophobic butylagarose will not improve the situation because the capacity of this adsorbent is too low. It is surprising that these undesirable properties have not previously been brought to the general attention of users. New types of less hydrophobic adsorbents need to be developed that can fulfil the demand for a high salt-dependent adsorption capacity and at the same time maintain a high desorption efficiency. Pyridyl-S-agarose is superior in several respects to the conventional adsorbents used for hydrophobic interaction chromatography, but it differs in some respects in its affinity properties. The influence of different salts on the type of proteins adsorbed to respective adsorbents is under investigation.

Acknowledgements

We are grateful to our sponsors, County Administration of Södermanland, Nyköping, Sweden (S.O.) and National Institutes of Health (GM 45832), Bethesda, MD, USA (J.P.). We also thank Dr. Joy Winzerling for valuable linguistic suggestions.

References

[1] B.H.J. Hofstee, *Anal. Biochem.*, 52 (1973) 430.
[2] J. Porath, L. Sundberg, N. Fornstedt and I. Olsson, *Nature*, 245 (1973) 465.
[3] S. Hjertén, J. Rosengren and S. Påhlman, *J. Chromatogr.*, 101 (1974) 281.
[4] S. Kochwa, M. Brownell, R.E. Rosenfield and L.R. Wassermann, *J. Immunol.*, 99 (1966) 981.
[5] R.A. Rimerman and G.W. Hatfield, *Science*, 182 (1973) 1268.
[6] C.R. Geren, S.C. Magee and K.E. Ebner, *Arch. Biochem.*, 172 (1976) 149.
[7] W. Norde, F. MacRitchie, G. Nowicka and I. Lycklema, *J. Colloid Interface Sci.*, 112 (1986) 447.
[8] A.J. Alpert, *J. Chromatogr.*, 359 (1978) 325.
[9] T. Arakawa, *Arch. Biochem. Biophys.*, 248 (1986) 101.
[10] W. Melander and C. Horváth, *Arch. Biochem. Biophys.*, 183 (1977) 200.

[11] T. Arakawa and S.N. Timasheff, *Methods Enzymol.*, 114 (1985) 49.
[12] T. Arakawa and S.N. Timasheff, *Biochemistry*, 29 (1990) 1924.
[13] O. Sinanoğlu and S. Abdulnur, *Fed. Proc. Fed. Am. Soc. Exp. Biol.*, 24, No. 2, Part III (1965) 12.
[14] O. Sinanoğlu, in B. Pullman (Editor), *Molecular Associations in Biology*, Academic Press, New York, 1968, p. 427.
[15] J. Porath, F. Maisano and M. Belwe, *FEBS Lett.*, 185 (1985) 306.
[16] D.J. Winzor, *J. Chromatogr.*, 597 (1992) 67.
[17] S. Oscarsson, *Acta Univ. Ups., Compr. Sum. Ups. Diss. Fac. Sci.*, No. 218 (1989).
[18] D.H. Spackman, S. Moore and W.H. Stein, *Anal. Chem.*, 30 (1958) 1190.
[19] S. Oscarsson and J. Porath, *J. Chromatogr.*, 499 (1990) 235.

ELSEVIER

Journal of Chromatography A, 689 (1995) 13–21

JOURNAL OF CHROMATOGRAPHY A

High-performance liquid chromatography of alditols with indirect photometric detection

Anne-Marie Dona*, Jean-François Verchère

Unité de Recherche Associée 500 du C.N.R.S., Université de Rouen, Faculté des Sciences, 76821 Mont-Saint-Aignan, France

First received 12 July 1994; revised manuscript received 14 October 1994

Abstract

Alditols were determined in aqueous solution using a novel indirect photometric technique as a post-column detection method. It allowed the use of the common UV detector for these transparent analytes. The method is based on the decrease of absorbance ($\lambda = 347$ nm) due to the competitive complexation of molybdate by the chloranilate ion (coloured complex) and an alditol (colourless complex). The experimental conditions were defined in a preliminary study which related the sensitivity for each analyte to the formation constant of its molybdate complex. D-Glucose, which forms a weak complex, does not interfere. The method was applied to the HPLC determination of mixtures of alditols with separation on a calcium column. The calibration curves are linear in the concentration range 0–100 $mg \cdot l^{-1}$. It demonstrates that indirect photometric detection may be used for the selective determination of specified analytes, in contrast with its usual application as a universal detection technique.

1. Introduction

Alditols are polyols obtained by reduction of the corresponding aldoses and ketoses. Their general formula is $HOCH_2-(CHOH)_{n-2}-CH_2OH$. Important industrial alditols are those with $n = 5$ or 6, namely xylitol, D-mannitol and D-glucitol that are used as additives and anti-crystallising agents in the food industry, especially in "sugar-free" products [1]. Mixtures of D-mannitol and D-glucitol (known as sorbitol) are manufactured by hydrolysis of sucrose to D-glucose and D-fructose followed by subsequent hydrogenation.

The determination of alditols in foodstuffs containing natural aldoses is requested for control of food quality. Mixtures of carbohydrates in aqueous solutions are easily separated by liquid chromatography [2] using anion-exchange resins in OH form or cation-exchange resins in Ca^{2+} [3,4], Pb^{2+} or Ag^{+} [5] form. Grafted amino or amino-propyl columns [6] may also be used. Such separations are often performed in borate buffer, since borate ions form complexes of different stabilities, depending on the configuration of the alditols [7]. In every case, the detection of carbohydrates presents a real problem, since classical techniques like refractive index or UV absorbance measurements below 200 nm are of low selectivity [8].

Conductimetric detection has been employed for chromatography in borate medium, because the borate complexes of alditols are strongly

* Corresponding author.

0021-9673/95/$09.50
SSDI 0021-9673(94)00981-3

acidic [9,10]. Pulsed amperometric detection [11] is a general method for all carbohydrates which requires an expensive apparatus. Whereas UV–visible photometric detection is not suitable for the direct determination of carbohydrates, it may be used after derivatization [8]. An interesting post-column derivatization method is based on the fast formation of a ternary Cu^{2+}–NH_3–carbohydrate complex [12]. In this work, we attempted to approach the problem of photometric detection in the indirect way [13,14] by provoking the "bleaching" of a coloured complex in response to the presence of an alditol. Such a process involves competitive complexation of a metal ion by an auxiliary ligand (forming an absorbing compound) and by an alditol forming a stronger, non-absorbing, complex.

Molybdenum (VI) was chosen as the complex-forming metal because the MoO_4^{2-} molybdate ion forms stable, colourless anionic complexes with carbohydrates L [15–19] in acidic solution. These species are dinuclear, (Mo:L = 2) and their structures have been determined by NMR studies [20–22] and crystal structure determinations [23,24]. Their stabilities are strongly dependent on the relative configurations of the hydroxyl groups of the ligand [22,25–27], alditols forming more stable complexes than aldoses [28,29].

Chloranilate (the ion of 2,5-dichloro-3,6-dihydroxy-1,4-benzoquinone, H_2C) was selected as the complex-forming auxiliary ligand, because this delocalized ion (Fig. 1a and 1b) possesses high molar absorbances in the UV and the visible spectrum, a high chemical stability, and an appreciable solubility in water. These properties are associated with interesting analytical potentialities that have received numerous applications [30], including indirect spectrophotometry [31]. The chloranilate ion C^{2-} is known to form a highly coloured 1:1 complex with molybdenum (VI) [32–34] (Fig. 1c). Finally, in the pH range 4–5, the molybdate–chloranilate complex was weaker than molybdate–alditol complexes (Fig. 1d), making the ligand-exchange process thermodynamically favorable.

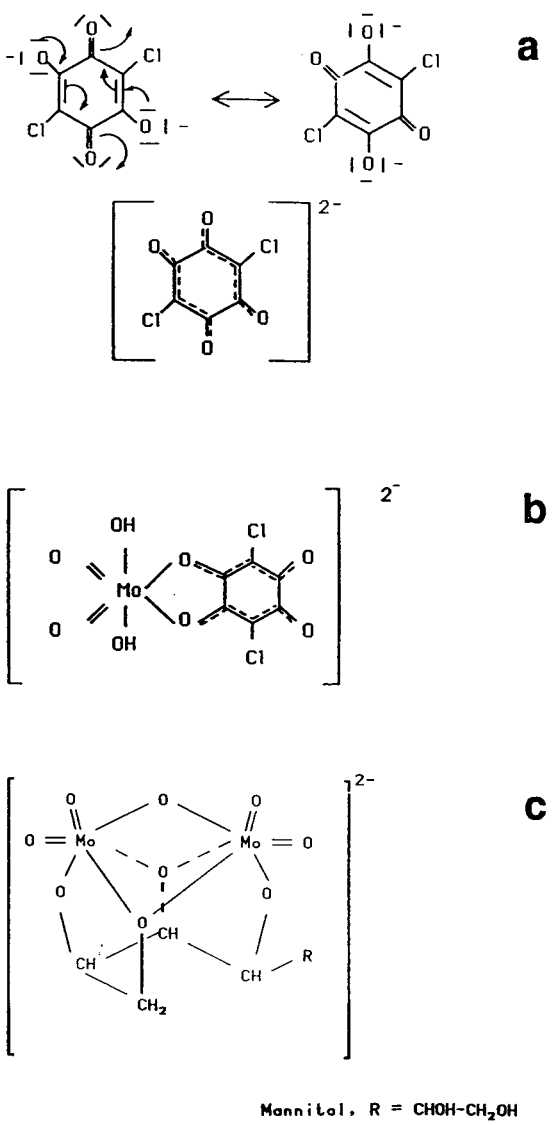

Fig. 1. Structures of (a) the chloranilate ion, (b) the (1,1,2) molybdate–chloranilate complex and (c) the (2,1,2) dimolybdate–mannitol complex. R = CHOH–CH_2OH.

2. Theory: principle of the indirect photometric detection of alditols

The analytical reaction is based on the competitive complexation of molybdate by chlorani-

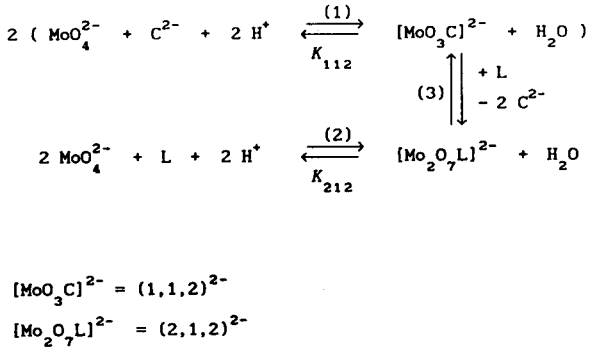

Fig. 2. Scheme of the competitive complexation of the molybdate ion by the chloranilate ion (C^{2-}, reaction 1) and an alditol (L, reaction 2). The overall analytical reaction is the ligand-exchange process of reaction 3.

late and an alditol as shown in Fig. 2. If the concentrations and pH are adjusted so that the alditol complex is more stable than the sacrificial chloranilate complex, the overall reaction is completely shifted to the formation of the alditol complex [reaction (3) in Fig. 2]. The optimal conditions of formation of the molybdate–chloranilate complex were determined in the following way. In order to use cells with optical path length $l = 1$ mm, the concentration of chloranilate was fixed at $5 \cdot 10^{-4}$ M. The ratio of concentrations $[MoO_4^{2-}]/[C^{2-}] = 2$ was chosen in order to increase the initial proportion of the sacrificial complex. A comparison of the curves of variation of absorbance versus pH for the molybdate–chloranilate complex, before and after partial decomposition by a model alditol (D-mannitol was used), showed that the maximum decrease of absorbance (at $\lambda = 347$ nm) occurred near pH 4.7. As this value is close to the pK of acetic acid, we eventually decided to use a 1:1 acetate buffer of pH 4.60.

In an alditol-free solution, the formation of the (1,1,2) molybdate–chloranilate complex may be written:

$$MoO_4^{2-} + C^{2-} + 2H^+ \rightleftarrows (1,1,2)^{2-} \qquad (1)$$

In the presence of an alditol L, equilibrium (1) is shifted backwards, in response to the formation of the (2,1,2) molybdate–alditol complex:

$$2MoO_4^{2-} + L + 2H^+ \rightleftarrows (2,1,2)^{2-} + 3H_2O \qquad (2)$$

The equilibrium constant for reaction (2) is represented by K_{212} and defines the formation constant [22] of the complex.

According to overall reaction (3) in Fig. 2, when an alditol was added to a solution of the molybdate–chloranilate complex, a decrease of absorbance at 347 nm and an increase of absorbance at 318 nm were simultaneously observed (Fig. 3). The variations were due to the dissociation of the (1,1,2) molybdate–chlorani-

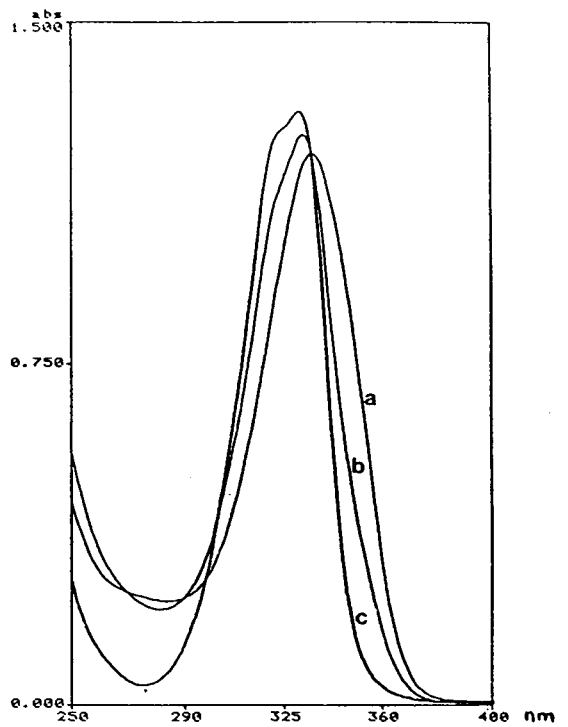

Fig. 3. UV Spectra of (a) the initial molybdate–chloranilate complex, (c) the final mixture of free chloranilate and alditol complex and (b) an intermediate stage with ca. 50% reaction at pH 4.60 (acetate buffer). Optical path length $l = 1$ mm. Analytical concentration of chloranilic acid, $c_T = 5 \cdot 10^{-4}$ M, and of disodium molybdate, $c_{Mo} = 1 \cdot 10^{-3}$ M.

late complex (Fig. 3, a) to form the colourless molybdate–alditol complex and free chloranilate ion (Fig. 3, c). When the reaction was not complete, an intermediate spectrum was obtained (Fig. 3, b). The observation of the isosbestic point at $\lambda = 335$ nm showed that no other species were involved in the analytical reaction.

3. Experimental

3.1. Reagents

All chemicals were of analytical-reagent grade and were used without further purification. A stock solution of molybdate–chloranilate complex in acetate buffer (pH = 4.60) was prepared by mixing in the following order: sodium hydroxide (0.1 *M*), chloranilic acid (Fluka, puriss, $5 \cdot 10^{-4}$ *M*), acetic acid (0.2 *M*), and sodium molybdate (10^{-3} *M*). It was finally diluted to the required concentration with purified (Millipore) water. This solution could be kept for one month at room temperature if protected from light.

For HPLC, the stock solution of the sacrificial complex was prepared as described above, but the concentration of chloranilic acid ($2.5 \cdot 10^{-4}$ *M*) and sodium molybdate ($5 \cdot 10^{-4}$ *M*) were modified in order to ensure the reading of a peak intensity close to 1 with the absorbance detector.

For discontinuous indirect photometric titration, the introduction of analytes into 100 cm^3 of the above solution was made from aliquots of solutions of alditols (typically 10–50 $g \cdot l^{-1}$), using a Gilson micropipette ($V_{max} = 2$ cm^3). Interfering substances were added in solid form. For *HPLC*, the solutions of alditols (1 $g \cdot l^{-1}$) were prepared by weighing and dilution in purified water.

3.2. Apparatus

After waiting for 5 min for the equilibration of temperature, absorbance measurements were performed at $\lambda = 347$ nm and 318 nm on a Kontron Uvikon 860 spectrophotometer equipped with quartz cells (path length $l = 1$ mm). The temperature was fixed at 25.0 ± 0.3°C by a water bath and a pump. The pH values were measured with a Hanna pH meter and a combined glass electrode.

The HPLC apparatus is schematically represented in Fig. 4 and included two pumps (Perkin Elmer, series 10). The carrier (water) is transported by the first pump P1 and the molybdate–chloranilate complex reagent by the second pump P2. Absorbance measurements were performed with a Spectra-Physics UV detector (Spectra 100) equipped with a fixed 6-mm path length cell, and operated at 347 nm. The separations of alditols were realised on a Phenomenex column (Rezex Cal., monosaccharide) containing an ion-exchange resin in Ca^{2+} form. This column was heated to 85°C in a Prolabo oven (Stabitherm). The reaction coil (Teflon) was 230 cm long and the volume of the injection loop was 50 μl. The samples were injected into the chromatographic system with a 100-μl syringe (Hamilton).

For the comparison with refractometric detection, we used the same column fitted with a Varian RI-4 refractometer, with minimal changes in the chromatographic conditions, except for the injection loop (100 μl).

All chromatograms were recorded and treated on a microcomputer, using laboratory-made software. The flow rates were 0.5 cm^3/min for pump P1 and 0.4 cm^3/min for pump P2. The absorbance before injection had a value close to 1 that was compensated to zero before injecting the sample.

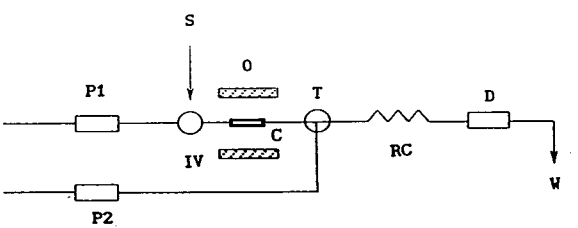

Fig. 4. Schematic diagram of the manifold for HPLC experiments. P_1 = pump for carrier (water), P_2 = pump for the molybdate–chloranilate complex reagent, IV = injection valve (sample volume, 50 μl), S = sample, C = analytical column, O = oven (t, 85°C), T = mixing tee, RC = reaction coil, D = UV detector, W = waste.

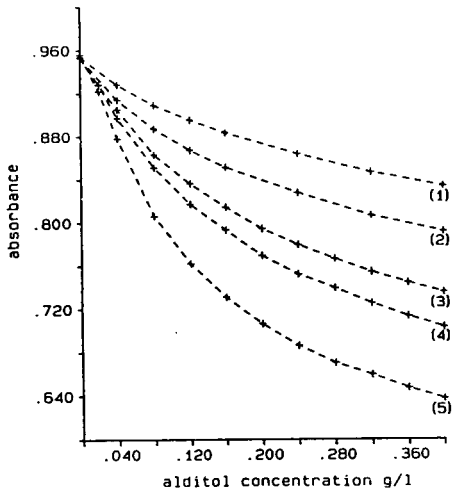

Fig. 5. Variations of the absorbance ($\lambda = 347$ nm) of the molybdate–chloranilate reagent with addition of alditols (1) xylitol, (2) D-arabinitol, (3) D-glucitol, (4) D-mannitol and (5) galactitol at pH 4.60 (acetate buffer). Optical path length $l = 1$ mm. Analytical concentration of chloranilic acid, $c_T = 5 \cdot 10^{-4}$ M, and of disodium molybdate, $c_{Mo} = 1 \cdot 10^{-3}$ M.

4. Results and discussion

4.1. Validation of the indirect photometric procedure

Determination of alditols at pH 4.60

The method was first applied to the determination of alditols by discontinuous indirect photometric titration. When aliquots of a solution of alditol are added to a buffered solution (pH = 4.60) of the molybdate–chloranilate complex, the dissociation of the sacrificial complex due to the formation of the alditol complex, according to reaction (3) in Fig. 2, induces a decrease of absorbance at 347 nm and an increase at 318 nm that were monitored. Fig. 5 represents the variations of absorbance at 347 nm versus the concentration of five analytes: galactitol, D-mannitol, D-glucitol, D-arabinitol and xylitol. The reproducibility of the absorbance measurements was better than 1%. These plots define calibration curves for the determination of each alditol in aqueous solution. A noteworthy feature of the method is that each analyte responds in a specific way, depending on the formation constant of its molybdate complex. The relative positions of the curves are related to the stabilities of the complexes (Table 1) defined by their formation constants [22]. For aldoses in the same concentration range, horizontal response plots were obtained, indicating that they would not interfere in the determination of alditols. This agrees with the low values of the formation constants of the molybdate complexes of aldoses [28,29].

Sensitivity and limits of detection

The sensitivity (S) was defined as the slope of the initial linear part of the plot of absorbance versus the concentration of alditol, and was calculated at 347 and 318 nm for each alditol (Table 1). For all alditols, the ratio S_{347}/S_{318} had

Table 1
Formation constants of the molybdate complexes (log K_{212}), sensitivities (S) and limits of detection (LOD) for the alditols

	Galactitol	D-Mannitol	D-Glucitol	D-Arabinitol	Xylitol
log K^a_{212}	17.30	16.87	16.75	16.34	16.00
S_{347} ($l \cdot g^{-1}$)	1.88	1.28	1.14	0.83	0.56
S_{318} ($l \cdot g^{-1}$)	1.19	0.76	0.71	0.53	0.34
S_{347}/S_{318}	1.58	1.68	1.61	1.57	1.65
$LOD_{347} \cdot 10^2$ ($g \cdot l^{-1}$)	1.05	1.6	1.75	2.4	3.6
$LOD_{318} \cdot 10^2$ ($g \cdot l^{-1}$)	1.7	2.6	2.8	3.8	5.9

[a] K_{212} is the equilibrium constant [29] for the formation of the (2,1,2) molybdate–alditol–proton complex. The reagent is a solution of the chloranilate ($c_T = 5 \cdot 10^{-4}$ M)–molybdate ($c_{Mo} = 1 \cdot 10^{-3}$ M) complex at pH 4.60 (acetate buffer). The sensitivity is defined (see text) by the ratio of the decrease of absorbance at 347 nm or the increase of absorbance at 318 nm, using 1-mm cells, versus the concentration of alditol. The limit of detection was calculated from the standard deviation for absorbance, $3\sigma = 0.02$.

a constant value close to 1.6, showing excellent agreement between the measurements at both wavelengths.

Under our standard conditions, the initial absorbance at 347 nm of the molybdate–chloranilate complex was 0.95 + 0.02 for $l = 1$ mm, from ten replicate determinations. Hence, the limit of detection (LOD) was defined as $LOD = 0.02/S$. LOD values for the five alditols are given in Table 1. The higher sensitivity was found for galactitol. The lower sensitivity was that for xylitol (almost 3 times lower than for galactitol) that forms the weakest complex. At 347 nm, $1.05 \cdot 10^{-2}$ g·l^{-1} of galactitol can be detected ($1.7\ 10^{-2}$ g·l^{-1} at 318 nm). The mean ratio LOD_{347}/LOD_{318} is close to 0.6.

Interferences

Because the determination of alditols is generally required for biological samples and food control, the possible interferences of common inorganic anions: sulphate, nitrate, chloride and phosphate ions ($c = 10$ g·l^{-1}) were examined at $\lambda = 347$ nm (Table 2). The highest interference is due to the phosphate ion which decreases the absorbance by 20%. On the other hand, sulphate, nitrate and chloride ions interfere weakly, as the decrease of absorbance is at most equal to 2%.

Organic acids and hydroxy acids like oxalic [26,35,36], tartaric [37] and citric [38] acids, that are known to form stable molybdate complexes, interfered significantly. The strongest interference is due to oxalic acid that dissociates the molybdate–chloranilate complex more readily than any alditol. Since the final objective of this work was to apply the indirect photometric method to the post-column detection of alditols after high-performance liquid chromatography on an ion-exchange resin in Ca^{2+} form, such interferences were not considered a serious drawback, because these anions would react with Ca(II) ions sequestered in the analytical column and therefore must be removed prior to analysis with an anion-exchange resin treatment. Thus, inorganic or organic anions are not expected to be present in the chromatographic samples.

Table 2
Interferences of neutral biomolecules and inorganic ions

Interferent	$c = 4$ g·l^{-1}	$c = 10$ g·l^{-1}
D-Glucose	0.8	2.1
D-Xylose	1.4	2.9
D-Ribose	6.2	–
D-Mannose	6.3	–
Urea	–	0.5
Sulphate	–	1.4
Nitrate	–	1.8
Chloride	–	2.0
Phosphate	12.5	20.1

Reported values indicate the decrease (in %) of the absorbance ($\lambda = 347$ nm) of a solution of the chloranilate ($c_T = 5 \cdot 10^{-4}$ *M*)–molybdate ($c_{Mo} = 1 \cdot 10^{-3}$ *M*) complex at pH 4.60 (acetate buffer) in the presence of the specified concentration of interferent (optical path length 1 mm).

Consequently, the interferences of neutral biomolecules were examined in more detail, as such compounds would not be removed by the preliminary exchange-resin treatment. Urea interferes less than inorganic anions. Four aldoses were examined: D-glucose, D-xylose, D-ribose and D-mannose (Table 2). At a concentration of 4.0 g·l^{-1}, D-glucose and D-xylose interfere weakly, as they decrease the absorbance by 1 to 2%, but D-ribose and D-mannose decrease the absorbance by more than 6%. It agrees with the relative order of stability of their molybdate complexes: D-mannose > D-ribose > D-xylose > D-glucose [28,29].

However, since the concentrations of aldoses (4.0 g·l^{-1}) used in the interference experiments were considerably higher than the concentrations of alditols (0.01–0.40 g·l^{-1}), the alditols may be determined in this concentration range without interference of aldoses, even with D-mannose and D-ribose in moderate amounts. This result is in agreement with a report describing the polarimetric determination of D-mannitol and D-glucitol [39] in the form of their molybdate complexes, that possess enhanced optical rotation [15]. It was found that D-glucose did not interfere, as would be expected because of the weakness of its molybdate complex [29].

The proposed indirect photometric method is fast and simple. However, because each alditol decreases the absorbance of the reagent with a

specific sensitivity, the method is not suitable for the determination of mixtures of alditols.

4.2. High-performance liquid chromatography of alditols

Mixtures of alditols were analyzed by HPLC, using a cation-exchange resin in Ca^{2+} form, heated at 85°C. We examined the applicability of indirect photometry as a post-column detection method. In principle, the effluent is mixed with a stream of the sacrificial complex and the reaction takes place in the reaction coil. Finally, the absorbance is measured by the UV detector. The elution of each alditol would then give rise to a negative peak at $\lambda = 347$ nm. Advantages would be the use of a very common detector and a partial selectivity, since only compounds that can complex molybdate would be detected.

Retention times and relative peak heights

The same five alditols were studied: galactitol, D-mannitol, D-glucitol, D-arabinitol and xylitol, and were injected as pure samples for standardization or in binary mixtures. Measurements made in triplicate showed that the retention times had similar values for pure alditols or in mixtures. The mean results are summarized in Table 3, together with the Fischer projections of the alditols. Most couples of alditols are eluted with time intervals higher than 30 s and are well separated except xylitol/D-glucitol and D-mannitol/D-arabinitol that give only one peak.

Table 3
Retention times and Fischer formulas of the five alditols

Alditol	Formula	Retention time[a]
Galactitol	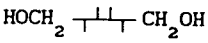	24 min 45 s
D-Mannitol	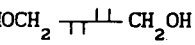	21 min 35 s
D-Glucitol	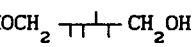	26 min 00 s
D-Arabinitol	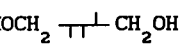	22 min 00 s
Xylitol	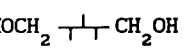	25 min 30 s

[a] Accuracy ± 15 s. Conditions as in Experimental Section.

Table 4
(h) for various alditols

Alditol	h
Galactitol	0.269
D-Mannitol	0.210
D-Glucitol	0.147
D-Arabinitol	0.082
Xylitol	0.048

Relative peak height h is given in absorbance units at $\lambda = 347$ nm. Conditions as in Experimental Section. Injection: 50 μl of aqueous solution of alditol ($c = 1.00\ g \cdot l^{-1}$).

The peak heights obtained for the injection of solutions of alditols ($c = 1.00\ g \cdot l^{-1}$) are compared in Table 4. The values obtained in four independent determinations did not differ by more than 1%. The response order is similar to that found in the preliminary study and agrees with the relative stabilities of the corresponding molybdate complexes. It means that a specific calibration curve must be drawn for every alditol present in the chromatographic mixture.

Separation and determination of mixtures of galactitol and D-glucitol

The retention times of galactitol and D-glucitol differ by more than 1 min (Table 3) and these alditols are eluted as two peaks that slightly overlap (Fig. 6). However, the separation was reasonably complete, since we verified that the same peak intensities were found when the compounds were injected separately, or as mixtures. The calibration curves are linear in the 0–0.10 $g \cdot l^{-1}$ concentration range. Higher concentrations may be determined either by direct reading on the calibration curves, or after suitable dilution.

The sensitivities were defined as the slopes of the linear portion of the calibration curves and are given in Table 5. The limits of detection obtained with the UV detector are given in Table 6, together with those for the refractometric detector which was currently used in the laboratory. The limit of detection in the indirect photometric mode is 2 to 7 times smaller than with refractometric detection, although the volume of injection loop was doubled in the case of

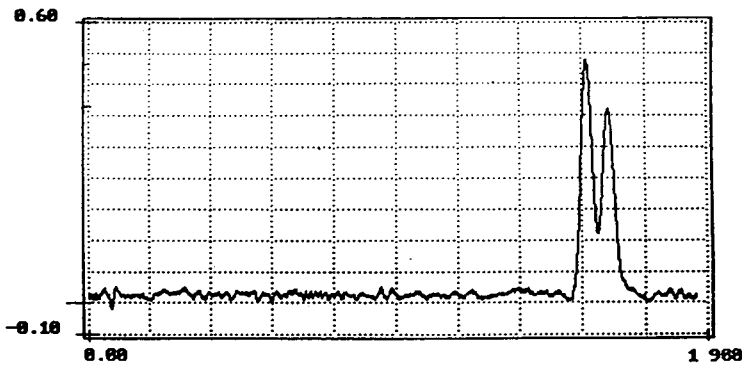

Fig. 6. Chromatogram of an equimolar mixture of galactitol and D-glucitol with indirect photometric detection ($\lambda = 347$ nm). The peak height is higher for galactitol (eluted first) because of the larger sensitivity. The signal input was reversed in order to show positive deviations. Vertical axis: arbitrary absorbance units. Horizontal axis: time (190 s/square).

Table 5
Sensitivities (S) for the chromatographic determination of galactitol and D-glucitol

	Galactitol	D-Glucitol
S ($l \cdot mol^{-1}$)	143.9	56.5
S ($l \cdot g^{-1}$)	0.79	0.31

Peak heights are in absorbance units. $\lambda = 347$ nm. Conditions as in Experimental Section.

refractometric detection. Moreover, the limit of detection is the same for galactitol and D-glucitol with refractometric detection, whereas the limit of detection is related to the stability of the alditol–molybdate complex in the case of photometric detection, which is particularly advantageous for galactitol.

Table 6
Comparison of the detection limits of refractometric and photometric detection in the HPLC separation of galactitol and D-glucitol

Mode of detection	Refractometric	Photometric[a]
Volume injected (μl)	100	50
Galactitol	$5 \cdot 10^{-4}$ M	$7 \cdot 10^{-5}$ M
D-Glucitol	$5 \cdot 10^{-4}$ M	$2.5 \cdot 10^{-4}$ M

[a] Indirect photometry at $\lambda = 347$ nm, according to the proposed method.

Interferences

Since the analytical column should not be supplied with samples containing ions that would react with calcium ions, no interference can arise from inorganic or organic anions that must be removed from the samples by a preliminary treatment with an anion-exchange resin. Among possible interfering sugars, we checked that the ubiquitous glucose did not interfere, first by injecting solutions ($c = 2$ $g \cdot l^{-1}$) of D-glucose alone, that did not produce a noticeable signal, and then by injecting mixtures of D-glucitol and D-glucose, that gave a single signal equal to that for D-glucitol alone. It demonstrates that the method is useful for food control, as alditols introduced as additives may be determined in the presence of natural sugars, without prior separation.

5. Conclusion

The present method employing a solution of the molybdate–chloranilate complex as the coloured reagent offers a new mode of indirect photometric detection for alditols in the presence of aldoses. The selectivity of the determination is due to the sensitivity of the ligand-exchange reaction to the configuration of the analyte. Its accuracy compares favourably with that of refractometry index detection.

References

[1] P.J. Sicard, in G.G. Birch and K.J. Parker (Editors), *Nutritive Sweeteners*, Applied Science, London, 1982, p. 145.
[2] S.C. Churms, *J. Chromatogr.*, 500 (1990) 555.
[3] M.R. Ladish and G.T. Tsao, *J. Chromatogr.*, 166 (1978) 85.
[4] L.E. Fitt, S. Hassler and D.E. Just, *J. Chromatogr.*, 187 (1980) 381.
[5] H.D. Scobell and K.M. Brobst, *J. Chromatogr.*, 212 (1981) 51.
[6] R. Schwarzenbach, *J. Chromatogr.*, 117 (1976) 206.
[7] K. Larsson and O. Samuelson, *Carbohydr. Res.*, 50 (1976) 1.
[8] M.F. Chaplin, in M.F. Chaplin and J.F. Kennedy (Editors), *Carbohydrate Analysis, a Practical Approach*, IRL Press, Oxford, 1986.
[9] T. Okada and T. Kuwamoto, *Anal. Chem.*, 58 (1986) 1375.
[10] T. Okada, *Anal. Chem.*, 60 (1988) 1336.
[11] W.R. LaCourse and D.C. Johnson, *Carbohydr. Res.*, 215 (1991) 159.
[12] G.K. Grimble, H.M. Barker and R.H. Taylor, *Anal. Biochem.*, 128 (1983) 422.
[13] H. Small and T.E. Miller Jr, *Anal. Chem.*, 54 (1982) 462.
[14] J.F. Verchère and A.M. Dona, *Analusis*, 20 (1992) 437.
[15] N.K. Richtmyer and C.S. Hudson, *J. Am. Chem. Soc.*, 73 (1951) 2249.
[16] E.J. Bourne, D.H. Hutson and H. Weigel, *J. Chem. Soc.*, (1960) 4252.
[17] E.J. Bourne, D.H. Hutson and H. Weigel, *J. Chem. Soc.*, (1961) 35.
[18] H.J.F. Angus and H. Weigel, *J. Chem. Soc.*, (1964) 3994.
[19] W. Voelter, E. Bayer, R. Records, E. Bunnenberg and C. Djerassi, *Chem. Ber.*, 102 (1969) 1005.
[20] M. Matulova, V. Bilik, and J. Alföldi, *Chem. Papers*, 43 (1989) 403.
[21] M. Matulova and V. Bilik, *Chem. Papers*, 44 (1990) 703.
[22] S. Chapelle, J.F. Verchère and J.P. Sauvage, *Polyhedron*, 9 (1990) 1225.
[23] J.E. Godfrey and J.M. Waters, *Cryst. Struct. Commun.*, 4 (1975) 5.
[24] B. Hedman, *Acta Cryst.*, B33 (1977) 3077.
[25] L. Petterson, *Acta Chem. Scand.*, 26 (1972) 4067.
[26] M. Mikesova and M. Bartusek, *Collect. Czech. Chem. Commun.*, 43 (1978) 1867.
[27] E. Mikanova and M. Bartusek, *Scr. Fac. Sci. Nat. Univ. Purk. Brun.*, 11 (1981) 451.
[28] J.F. Verchère and S. Chapelle, *Polyhedron*, 8 (1989) 333.
[29] J.P. Sauvage, S. Chapelle, A.M. Dona and J.F. Verchère, *Carbohydr. Res.*, 243 (1993) 293.
[30] J.M. Poirier and J.F. Verchère, *Talanta*, 26 (1979) 341.
[31] A.M. Dona and J.F. Verchère, *Analyst*, 116 (1991) 533.
[32] W.F. Lee, N.K. Shastri and E.S. Amis, *Talanta*, 11 (1964) 685.
[33] J.F. Verchère, *J. Chem. Research*, (1978) (S) 178, (M) 2216.
[34] J.F. Verchère and J.M. Poirier, *J. Inorg. Nucl. Chem.*, 42 (1980) 1514.
[35] E.S. Johansen and O. Jöns, *Talanta*, 31 (1984) 743.
[36] J.J. Cruywagen, J.B. Heyns and R.F. van de Water, *J. Chem. Soc. Dalton Trans.*, (1986) 1857.
[37] J.J. Cruywagen, J.B. Heyns and E.A. Rohwer, *J. Chem. Soc. Dalton Trans.*, (1990) 1951.
[38] J.J. Cruywagen and R.F. van de Water, *Polyhedron*, 5 (1986) 521.
[39] M. Hamon, C. Morin and R. Bourdon, *Anal. Chim. Acta*, 46 (1969) 255.

ELSEVIER

Journal of Chromatography A, 689 (1995) 23–30

JOURNAL OF CHROMATOGRAPHY A

High-performance liquid chromatographic resolution of amino acid enantiomers derivatized with fluorescent chiral Edman reagents

Toshimasa Toyo'oka[a,*], Yi-Ming Liu[b]

[a]*Department of Analytical Chemistry, School of Pharmaceutical Sciences, University of Shizuoka, 52-1 Yada, Shizuoka 422, Japan*

[b]*Division of Environmental Chemistry, National Institute of Health Sciences, 1-18-1 Kamiyoga, Setagaya-ku, Tokyo 158, Japan*

First received 25 July 1994; revised manuscript received 12 October 1994

Abstract

The fluorescent chiral Edman reagents, 4-(3-isothiocyanatopyrrolidin-1-yl)-7-nitro-2,1,3-benzoxadiazole [*R*(−)- and *S*(+)-NBD-PyNCS] and 4-(3-isothiocyanatopyrrolidin-1-yl)-7-(N,N-dimethylaminosulfonyl)-2,1,3-benzoxadiazole [*R*(−)- and *S*(+)-DBD-PyNCS], have been utilized for the resolution of amino acid enantiomers as diastereomeric derivatives. These reagents react with amino acid enantiomers in the presence of base catalyst (triethylamine, 1-azabicyclo[2.2.2]octane and 1,8-diazabicyclo[5.4.0]-7-undecene) to produce the corresponding thiocarbamoyl-amino acid diastereomers under the mild reaction conditions of 55°C for 10 min. The resulting derivatives are relatively stable, not only in alkaline reaction solution but also in acidic medium, with no measurable conversion to the thiohydantoin derivatives. The reactivities of both enantiomers of the derivatization reagents with the amino acid enantiomers (L- and D-isoleucine) are comparable. The fluorescence properties (maximal wavelengths and intensities) of the thiocarbamoyl-amino acid derivatives are dependent upon the solvents in the medium. Some amino acids labeled with the proposed reagents are efficiently resolved by an ODS column with water–acetonitrile containing 0.05% trifluoroacetic acid. The R_s values are in the ranges 3.57–0.55 (13 amino acids) for the diastereomers obtained with NBD-PyNCS, and 2.57–0.68 (14 amino acids) for those with DBD-PyNCS. The R_s values obtained from neutral and/or aromatic amino acids are larger than those of basic and acidic amino acids.

1. Introduction

The resolution of amino acid enantiomers has been widely investigated because of their commercial significance and ease of availability. Amino acids are used primarily by the pharmaceutical and food industries. In many cases, the L-isomers of the corresponding amino acids are required by these industries because only L-isomers are used as natural nutrients for the human body. Therefore, the determination of optical purity is important for the manufacture of amino acids. Optically pure amino acids are also required for the syntheses of several chiral reagents, catalysts and physiologically active substances including bioactive peptides and antibiotics. Although peptides and proteins in mammals are composed of L-amino acids, racemiza-

* Corresponding author.

0021-9673/95/$09.50
SSDI 0021-9673(94)00978-3

tion may alter modify the biological activity. The racemization reactions of amino acids have also been used to estimate the age of fossil bones and teeth. Consequently, highly effective resolution of amino acid enantiomers is an important subject.

Chromatographic techniques such as gas chromatography (GC) [1,2] and high-performance liquid chromatography (HPLC) [3,4] can be employed for the resolution of racemates. A great number of methods, which involve both the direct method with a chiral stationary phase (CSP) column and an indirect method requiring derivatization with chiral reagents, have been developed for resolving amino acids racemates [5]. HPLC has emerged as an important tool for this purpose because of its good reproducibility and efficiency for a wide range of compounds. Although chiral separations of amino acids by the direct methods with CSP columns are quite popular, the indirect methods which involve derivatization steps with chiral reagents are also receiving considerable attention. The introduction of chromophores may enhance both the detection and the resolution. Some derivatization reagents such as 2,3,4,6-tetra-O-acetyl-β-D-glucopyranosyl (GITC) [6] and *R*-α-methylbenzyl isothiocyanate (*R*-AMBI) [7] have been developed for chiral separation of amino acids. Adequate separations of these labels were obtained by reversed-phase chromatography, but the sensitivities seem to be insufficient to trace level detection in real samples. A major advantage of the indirect HPLC method with fluorescence detection is the possibility of excellent sensitivity due to the properties of the derivatization reagent. The combinations of *o*-phthalaldehyde (OPA) and various chiral thiols (e.g. N-acetyl-L-cysteine, Boc-L-cysteine, etc.) are frequently used for derivatization and separation of amino acid enantiomers as fluorescence compounds [8–10]. However, for some applications the isoindole derivatives produced from OPA/thiols do not have adequate stability [11,12].

In a previous paper [13], we reported the syntheses of the novel fluorescence Edman-type reagents, i.e. *S*(+)- and *R*(−)-enantiomers of 4 - (3 - isothiocyanatopyrrolidin - 1 - yl) - 7 - nitro-2,1,3-benzoxadiazole (NBD-PyNCS) and 4-(3-isothiocyanatopyrrolidin - 1 - yl) - 7 - (N,N - dimethylaminosulfonyl) - 2,1,3 - benzoxadiazole (DBD-PyNCS). These reagents have been demonstrated as useful for the resolution of various amines including β-blocking drugs. This paper deals with the investigations of the derivatization conditions for amino acids, the fluorescence properties of the resulting thiocarbamoyl-amino acid, and the separation by reversed-phase chromatography of the diastereomers derived from the reactions of some amino acids with the chiral Edman reagents.

2. Experimental

2.1. Materials and reagents

S(+)- and *R*(−)-NBD-PyNCS and *S*(+)- and *R*(−)-DBD-PyNCS were synthesized as described previously [13]. Both enantiomers of amino acids were obtained from Sigma (St. Louis, MO, USA). 1-Azabicyclo[2.2.2]octane (quinuclidine) and 1,8-diazabicyclo[5.4.0]-7-undecene (DBU) were purchased from Nacalai Tesque (Kyoto, Japan). Trifluoroacetic acid (TFA), acetonitrile, and water were of HPLC grade (Wako). All other chemicals were of analytical-reagent grade and were used without further purification.

2.2. HPLC

The HPLC system consisted of two LC-9A pumps (Shimadzu) and an SCL-6B system controller (Shimadzu). Sample solutions were injected with a SIL-6B auto injector (Shimadzu). The analytical column was an Inertsil ODS-80A (150 × 4.6 mm I.D., 5 μm) for reversed-phase chromatography (GL Sciences, Tokyo, Japan). The columns were maintained at 40°C with a CTO-6A column oven (Shimadzu). A Shimadzu RF-550 fluorescence monitor equipped with a 12-μl flow cell was employed for the detection. The excitation and emission wavelengths were fixed at 490 and 530 nm for the derivatives of

amino acids with NBD-PyNCS, and at 460 and 540 nm for those with DBD-PyNCS. The peak areas obtained from the fluorescence monitor were calculated with a C-R4A Chromatopac (Shimadzu). All mobile phases were de-gassed with an on-line degasser (DEGAS; Shodex, Tokyo, Japan). The flow-rate of the eluent was 1.0 ml/min.

2.3. Derivatization procedure for amino acids

A 10-μl volume of the reagent [5 mM $R(-)$- or $S(+)$-enantiomer] in acetonitrile and 10 μl of amino acid enantiomers (1 mM of each enantiomer) in acetonitrile–water (1:1) containing 2% triethylamine (TEA) were mixed in a 1.5-ml mini-vial (GL Sciences). The vials were tightly capped and heated at 55°C with a dry heat block for 10 min. Then 480 μl of 1 M acetic acid (AcOH) in acetonitrile–water (1:1) were added to the reaction mixture to stop the derivatization reaction. The acidic solution was diluted ten times with acetonitrile and then 5 μl of the solution was injected into the column. The reagent blanks without amino acids were also treated in the same manner.

The capacity factor (k'), separation factor (α) and the resolution value (R_s) were calculated from the equations $k' = (t_R - t_0)/t_0$, $\alpha = k'_2/k'_1$ and $R_s = 2(t_{R2} - t_{R1})/(w_1 + w_2)$, where t_R, t_{R1} and t_{R2} are the peak retention times, t_0 is the retention time of an unretained compound (void volume of the column) ($t_0 = 1.27$ min) and w_1 and w_2 are the widths of the bases formed by triangulation of the peaks.

2.4. Fluorescence properties of the reagents and their derivatives

For the fluorescent spectra measurements, 20 μl of the acid solutions of the D-tyrosine derivatives, obtained from recommended procedures, were injected onto the column and the peak corresponding to the thiocarbamoyl-amino acid derivative was collected downstream from the detector (ca. 2-ml portion). The eluent collected in the tube was evaporated under reduced pressure, and then a small quantity of acetonitrile was added to dissolve the residue. Equal volumes of the solution was added to portions of 2 ml of various solvents, and maximal wavelengths (excitation and emission) and relative fluorescence intensities (RFIs) were measured with a fluorescence spectrophotometer. Fluorescence properties of the chiral reagents themselves were also measured at 2 μM concentration without chromatographic separation.

3. Results and discussion

Fig. 1 shows the derivatization reaction of amino acids with the chiral fluorescent Edman reagents, NBD-PyNCS and DBD-PyNCS. The reaction proceeds in alkaline medium to produce corresponding thiocarbamoyl-amino acids.

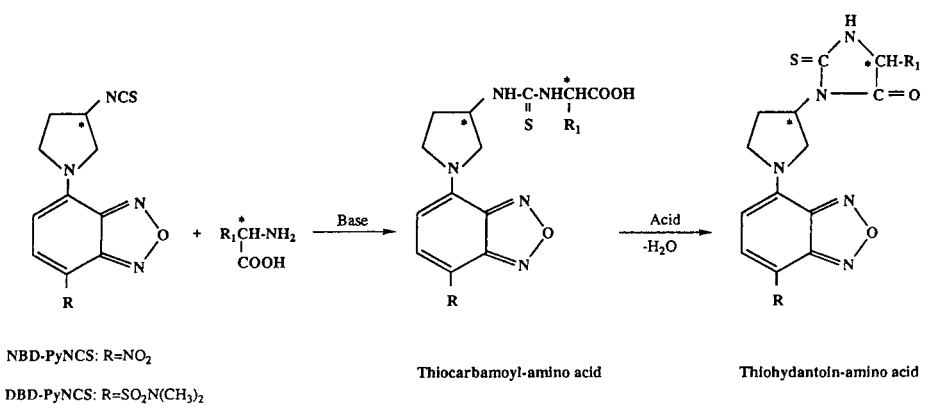

Fig. 1. Reaction of amino acids with optically active fluorescent Edman reagents.

Thiocarbamoyl-amino acids, produced with Edman reagents like phenylisothiocyanate (PITC), are converted to corresponding thiohydantoin derivatives in strong acid solution [14,15]. In the case of the thiocarbamoyl-amino acids derived from NBD-PyNCS and DBD-PyNCS, however, no such conversion was found with 1 *M* acetic acid which was added to the reaction mixture to stop the derivatization reaction. When hydrochloric acid at the same concentration level was used for the termination of the derivatization reaction, no substantial differences were observed on the chromatograms. Furthermore, no degradation of the derivatives is observed as compared with both chromatograms before and after storage for more than 24 h at 5°C. The fluorescent derivatization reagents in neutral acetonitrile solution are stable for at least 3 weeks at 5°C and 1 week at room temperature. It is noteworthy that the reagents are sufficiently stable to retain the –NCS functional group in the acidic solution, even after heating at 50°C for 3 h. In contrast, the –NCS functional group of previously reported Edman reagents decompose to produce the corresponding $-NH_2$ compounds in strong acidic medium [16]. The results suggest that the reagents and the derivatives are relatively stable in the acidic medium. Good stability of the reagents and the derivatives is an important property for a useful reagent for trace quantities of amino acids.

Some parameters affecting the derivatization reaction were studied to select optimal conditions. Alkaline solution is essential for the derivatization with Edman-type reagents; therefore, the effect of base catalyst on the derivatization was examined with tryptophan and isoleucine. These amino acids were selected as the representatives of aromatic and aliphatic amino acids, respectively. As shown in Fig. 2, three organic bases —TEA, DBU and quinuclidine— gave similar yields of the derivatives. The low yields with $NaHCO_3$ may be due to the poor nucleophilic properties of the inorganic salt. Although TEA, DBU and quinuclidine are equally effective as catalysts for the derivatization, TEA was selected for the derivatization

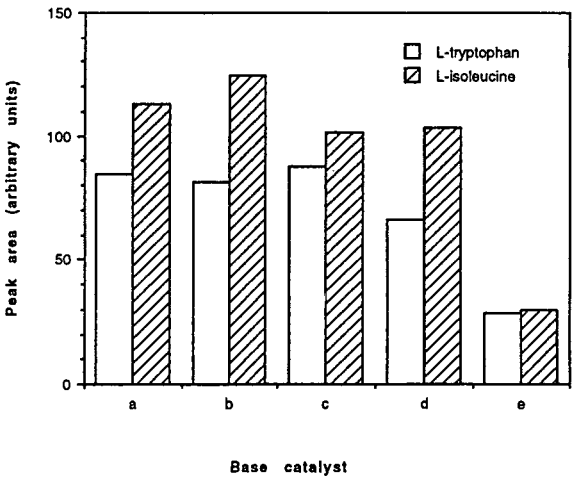

Fig. 2. Comparison of base catalysts for the derivatization of amino acids with *R*(−)-NBD-PyNCS. a = 0.5% TEA; b = 0.5% quinuclidine; c = 0.5% DBU; d = 0.05 *M* borate buffer (pH 10); e = 0.5 *M* $NaHCO_3$ buffer (pH 9.5).

because of its ready availability. With respect to the concentration of TEA, similar results were observed in the range from 0.5 to 3% (Fig. 3); however, concentrations higher than 3% reduced the production of the thiocarbamoyl-amino acid derivatives. Therefore, 1% TEA was selected in the following experiments. Fig. 4 shows the influence of the reagent concentration on the derivatization. The peak areas were almost constant at reagent-to-analyte ratios in excess of 5.

Immediate reaction is generally more likely to

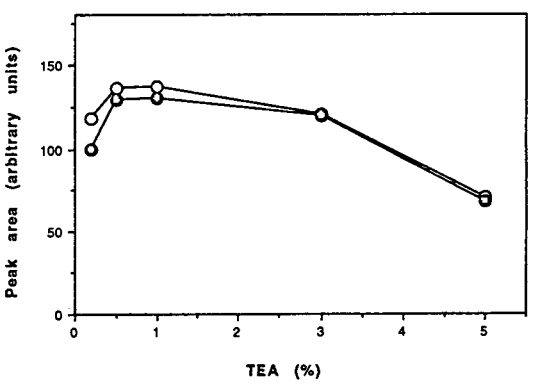

Fig. 3. Effect of TEA concentration on the derivatization with *R*(−)-NBD-PyNCS. ○ = L-Tryptophan; ● = L-isoleucine.

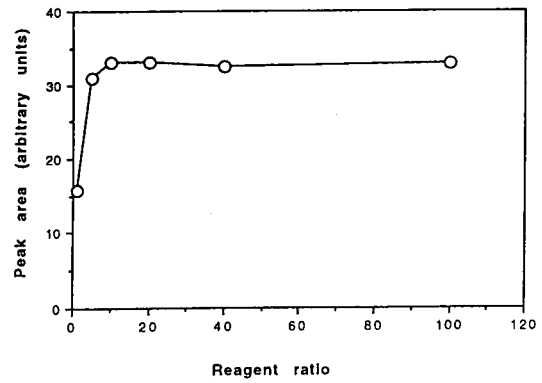

Fig. 4. Effect of *R*(−)-NBD-PyNCS concentration on the derivatization of L-isoleucine.

yield preferable highly reproducible results than a very slow reaction. In addition, the chiral derivatization reagents must react at similar rates with both enantiomers. Big differences in reaction rate will yield uncertain results, especially in the detection of trace quantities. The reactivity of the reagent was evaluated with both enantiomers of isoleucine. Fig. 5 shows the time courses of the derivatization reaction with *R*(−)-NBD-PyNCS. The reactions were essentially complete after 10 min at 55°C. Judging from both curves, the reaction rates seem to be comparable for both enantiomers of NBD-PyNCS. The reaction of amino acids with DBD-PyNCS is considered to be essentially the same as those with NBD-PyNCS, since the effect of

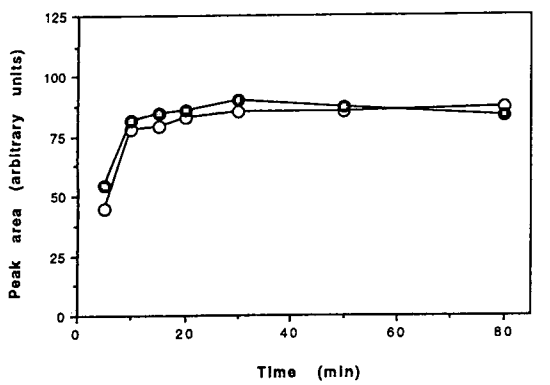

Fig. 5. Time courses of the derivatization reaction with *R*(−)-NBD-PyNCS at 55°C in the presence of 1% TEA. ○ = L-Isoleucine; ● = D-isoleucine.

the functional groups ($-NO_2$ and SO_2NMe_2) at 4-position in the benzofurazan structure would be expected to be negligible. Because the derivatization reaction occurs at a site well removed from the 4-position [17,18]. Based upon the above observations, derivatization at 55°C for 10 min in water–acetonitrile (1:1) in the presence of 1% TEA is recommended for the preparation of diastereomers of the amino acid enantiomers.

Table 1 shows the maximum fluorescent wavelengths (excitation and emission) and the RFIs of the tyrosine derivatives. The fluorescence properties of the derivatives are dependent upon the solvent in the medium. The maximal excitation and emission wavelengths appear to be dependent on the strength of hydrophobicity of the solvents as suggested by the shift towards blue with increasing hydrophobicity of the medium. On the other hand, the fluorescence intensity is not so easily explained and differs in each solvent. The RFIs of the derivatives with NBD-PyNCS and DBD-PyNCS are higher in aprotic organic solvents (AcOEt and CH_2Cl_2, etc.) than in protic solvents such as methanol and ethanol. The fluorescence maxima (excitation and emission wavelengths) and the fluorescence intensities were almost the same as those with and without 0.1% TFA in water–acetonitrile. Essentially the same fluorescence characteristics were also obtained with the reagent themselves (data not shown); therefore, the fluorescence seems to be due to the benzofurazan structure of the reagents.

The separation of the enantiomers of 18 amino acids, which are usually found in acid hydrolysates of peptides, enzymes and proteins, was tried by reversed-phase HPLC after derivatization with the chiral fluorescent reagents. In the present experiments, column temperature at 40°C was selected to obtain reproducible results of retention time of the derivatives. The capacity factor (k'), separation factor (α) and resolution value (R_s) for each pair of the thiocarbamoyl-amino acids derived from *R*(−)-NBD-PyNCS and *R*(−)-DBD-PyNCS are listed in Tables 2 and 3. The diastereomers derived from neutral and/or aromatic amino acids were well resolved

Table 1
Fluorescence properties of tyrosine derivatives with the reagents in various solvents

Solvent	With DBD-PyNCS			With NBD-PyNCS		
	Excitation (nm)	Emission (nm)	RFI	Excitation (nm)	Emission (nm)	RFI
CH_3CN–water (1:1)	458	540	13.5	488	528	36
CH_3CN	458	541	100	480	525	100
MeOH	459	536	33	475	525	56
EtOH	460	537	40	475	525	43
DMF	464	541	99	485	530	75
Acetone	458	536	132	475	521	100
AcOEt	456	532	120	470	520	200
n-Hexane	436	515	131	450	508	172
CH_2Cl_2	456	528	127	470	512	194

MeOH = Methanol; EtOH = ethanol; DMF = dimethylformamide; AcOEt = ethyl acetate; RFI = relative fluorescence intensity.

by reversed-phase HPLC with water–acetonitrile containing TFA as the eluent. However, the resolution of the basic amino acid derivatives was inadequate with this solvent mixture. Attempts to resolve acidic amino acids such as asparagic acid and glutamic acid were also unsuccessful. The extent of separation varies with different amino acids and the derivatization reagents, NBD-PyNCS and DBD-PyNCS. The difference of R_s values with DBD-PyNCS is smaller than that with NBD-PyNCS (ca. 2.57–0.68 versus ca. 3.57–0.55). Therefore, DBD-PyNCS appears to be a superior reagent than NBD-PyNCS for the resolution of amino acids. When $R(-)$-isomers of the reagents are used as the derivatization reagents, the diastereomers of D-amino acids are eluted faster than those of L-amino acids. Opposite elution order is ob-

Table 2
Enantiomeric separation of amino acids after derivatization with $R(-)$-NBD-PyNCS

Amino acid	k'		α	R_s	Eluent
	D-Isomer	L-Isomer			
Alanine	10.71	11.19	1.05	0.55	a
Cystine	3.34	4.03	1.21	1.13	e
Isoleucine	10.94	12.30	1.12	1.78	c
Leucine	5.61	6.29	1.12	1.04	d
Lysine	7.91	9.13	1.15	1.65	d
Methionine	6.37	6.92	1.09	0.97	c
Norleucine	12.17	13.75	1.13	1.85	c
Proline	4.87	6.06	1.20	1.50	b
Phenylalanine	12.52	14.90	1.19	3.57	c
Threonine	7.77	8.25	1.06	0.71	a
Tryptophan	5.95	7.05	1.18	1.54	d
Tyrosine	9.20	10.00	1.09	1.20	b
Valine	6.11	6.81	1.12	1.62	c

Eluents: CH_3CN–water mixtures containing 0.05% TFA. CH_3CN contents: a = 25%; b = 30%; c = 35%; d = 40%; e = 45% (v/v).

Table 3
Enantiomeric separation of amino acids after derivatization with $R(-)$-DBD-PyNCS

Amino acid	k'		α	R_s	Eluent
	D-Isomer	L-Isomer			
Alanine	4.61	4.96	1.08	0.85	c
Cystine	4.28	5.39	1.26	1.85	e
Histidine	4.03	4.39	1.09	0.68	a
Isoleucine	7.95	9.40	1.18	2.29	d
Leucine	8.02	9.31	1.16	2.04	d
Lysine	7.11	8.24	1.16	2.06	e
Methionine	4.93	5.51	1.12	1.45	d
Norleucine	5.17	5.98	1.16	1.72	e
Proline	5.61	6.15	1.10	1.48	c
Phenylalanine	13.09	13.95	1.07	2.29	e
Threonine	6.46	7.03	1.09	1.06	b
Tryptophan	6.12	8.42	1.38	2.57	e
Tyrosine	5.96	6.54	1.10	0.93	c
Valine	10.40	10.96	1.05	1.87	c

Eluents: CH_3CN–water mixtures containing 0.05% TFA. CH_3CN contents: a = 25%; b = 30%; c = 35%; d = 40%; e = 45% (v/v).

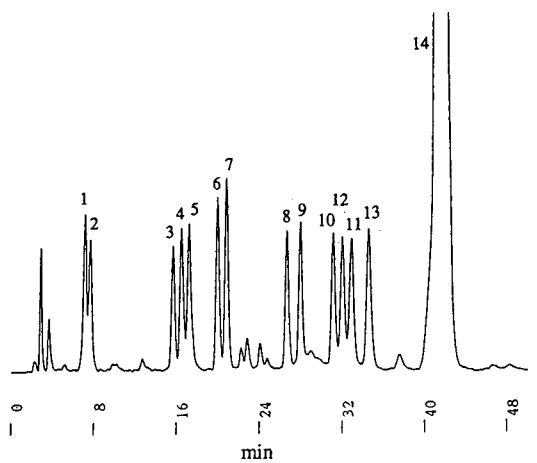

Fig. 6. Chromatograms of thiocarbamoyl-amino acid diastereomers derived from $R(-)$-DBD-PyNCS. Peaks: 1 = D-histidine; 2 = L-histidine; 3 = glycine; 4 = D-threonine; 5 = L-threonine; 6 = D-proline; 7 = L-proline; 8 = D-valine; 9 = L-valine; 10 = D-leucine; 11 = L-leucine; 12 = D-tryptophan; 13 = L-tryptophan; 14 = $R(-)$-DBD-PyNCS. Each peak except the reagent is corresponding to 20 pmol. Eluents: (A) water containing 0.05% TFA; (B) acetonitrile containing 0.05% TFA; isocratic elution of A–B (75:25) for 5 min, linear gradient elution from A–B (75:25) to A–B (60:40) for 20 min, and then isocratic elution of A–B (60:40) for 25 min. Other HPLC conditions are given in the Experimental section.

served with use of $S(+)$-isomers of the reagents. Fig. 6 shows a separation by reversed-phase chromatography of the thiocarbamoyl-amino acids formed from $R(-)$-DBD-PyNCS. A sole peak corresponding to glycine derivative appeared in the chromatogram because there is no asymmetric carbon in the glycine structure. Each pair of the other amino acids tested were clearly separated by the linear gradient elution with water–acetonitrile containing 0.05% TFA. The largest peak (ca. 41 min) observed in the chromatogram is the unreacted reagent; while other small peaks seem to be caused by impurities in the analytes. The total analysis of the enantiomers of 18 amino acids, which are usually produced by acid hydrolysis of polypeptides, are under study in our laboratory.

4. Conclusions

Amino acid enantiomers derivatized under the mild reaction conditions with DBD-PyNCS and NBD-PyNCS enantiomers are separated by the reversed-phase chromatography. The resulting thiocarbamoyl-amino acids exhibit good stability

and strong fluorescence at long wavelengths. The sensitivity of the proposed methods with NBD-PyNCS and DBD-PyNCS is almost comparable with the reported methods using OPA/thiols and Edman-type reagents. However, our methods offer superior resolution of amino acid enantiomers and simplicity of the operation. In addition, the stability of the derivatives is better than that of the derivatives with OPA/chiral thiol. The excitation maxima at around 488 nm for the thiocabamoyl-amino acids with NBD-PyNCS is suitable for the determination with argon-ion laser-induced fluorescence detection [19,20]; whereas those with DBD-PyNCS are detectable at ca. fmol–amol range with peroxyoxalate chemiluminescence detection [21]. Hence, the proposed methods with DBD-PyNCS and NBD-PyNCS may serve for enantiomeric quantification of chiral amino acids in real samples. Chiral sequence analysis of peptides and proteins might be another important application, as described in the previous paper [13]. As well as the determination of antipodo enantiomer in each amino acid, the sequence analysis of polypeptides is currently in progress.

Acknowledgement

The authors thank Dr. C.R. Warner, Food and Drug Administration in Washington DC, USA, for reviewing the manuscript.

References

[1] T. Nambara and J. Goto, *Bunseki Kagaku*, 23 (1974) 704.
[2] V. Schurig and H.P. Nowotny, *Angew. Chem., Int. Ed. Engl.*, 29 (1990) 939.
[3] A.M. Krstulovic (Editor), *Chiral Separation by HPLC*, Ellis Horwood, Chichester, 1989.
[4] M. Zief and L.J. Crane (Editors), *Chromatographic Chiral Separation*, Marcel Dekker, New York, 1988.
[5] R. Bhushan and S. Joshi, *Biomed. Chromatogr.*, 7 (1993) 235.
[6] T. Kinoshita, Y. Kasahara and N. Nimura, *J. Chromatogr.*, 210 (1981) 77.
[7] J. Gal and A.J. Sedman, *J. Chromatogr.*, 314 (1984) 275.
[8] R.H. Buck and K. Krummen, *J. Chromatogr.*, 387 (1987) 255.
[9] S. Einarsson, S. Folestadd and B. Joseffson, *J. Liq. Chromatogr.*, 10 (1987) 1589.
[10] T. Takeuchi, T. Niwa and D. Ishii, *J. High Resolut. Chromatogr. Chromatogr. Commun.*, 11 (1988) 343.
[11] K. Imai and T. Toyo'oka, in R.W. Frei and K. Zech (Editors), *Selective Sample Handling and Detection in High-Performance Liquid Chromatography*, Part A (*Journal of Chromatography Library*, Vol. 39A), Elsevier, Amsterdam, 1988, p. 209.
[12] H. Lingeman, W.J.M. Underberg, A. Takadate and A. Hulshoff, *J. Liq. Chromatogr.*, 8 (1985) 789.
[13] T. Toyo'oka and Y.-M. Liu, *Analyst*, (1994) in press.
[14] R.L. Heinrikson and S.C. Meredith, *Anal. Biochem.*, 136 (1984) 65.
[15] K. Muramoto, H. Kamiya and H. Kawauchi, *Anal. Biochem.*, 141 (1984) 446.
[16] O. Imakyure, M. Kai, T. Mitsui, H. Nohta and Y. Ohkura, *Anal. Sci.*, 9 (1993) 647.
[17] T. Toyo'oka, M. Ishibashi, T. Terao and K. Imai, *Analyst*, 118 (1993) 759.
[18] T. Toyo'oka, Y.-M. Liu, N. Hanioka, H. Jinno, M. Ando and K. Imai, *J. Chromatogr. A*, 675 (1994) 79.
[19] T. Toyo'oka, M. Ishibashi and T. Terao, *J. Chromatogr.*, 625 (1992) 357.
[20] T. Toyo'oka, Y.-M. Liu, N. Hanioka, H. Jinno and M. Ando, *Anal. Chim. Acta*, 285 (1994) 343.
[21] T. Toyo'oka, M. Ishibashi and T. Terao, *J. Chromatogr.*, 627 (1992) 75.

ELSEVIER

Journal of Chromatography A, 689 (1995) 31–38

JOURNAL OF CHROMATOGRAPHY A

Trace analysis of impurities in 3′-azido-3′-deoxythymidine by reversed-phase high-performance liquid chromatography and thermospray mass spectrometry

Arkan Almudaris, David S. Ashton, Andrew Ray and Klara Valko*

Department of Physical Sciences, Wellcome Research Laboratories, Langley Court, Beckenham, Kent BR3 3BS, UK

First received 12 July 1994; revised manuscript received 21 September 1994

Abstract

An analytical method has been developed for the detection of trace amounts of impurities in 3′-azido-3′-deoxythymidine referred to herein as AZT (Zidovudine). A sample extract was preconcentrated by normal-phase high-performance liquid chromatography (HPLC) with subsequent on-line reversed-phase HPLC–thermospray mass spectrometry (TSP-MS). During the sample extraction and concentration step, carried out by semipreparative normal-phase chromatography, the preliminary separation of the impurities from the AZT takes place. The organic solvent (dichloroethane–acetonitrile, 40:60) is evaporated from the collected fractions and the compounds are redissolved in a smaller volume of the reversed-phase mobile phases for a further degree of concentration. The collected fractions are then subjected to reversed-phase HPLC–TSP-MS. The influence of acetonitrile concentration and pH on the reversed-phase separation together with the sensitivity of the TSP-MS detection have been examined to maximise detection levels. The 3′-azido-3′-deoxy-5′-O-tritylthymidine, triphenyl methanol and 3′-chloro-3′-deoxythymidine, which are route-indicative impurities formed during the synthesis can be detected in the 50–100 ppb (w/w) range.

1. Introduction

3′-Azido-3′-deoxythymidine (AZT) is the active ingredient in the antiretroviral product manufactured and marketed by the Wellcome Foundation under the trademark Retrovir. AZT has an activity against human immunodeficiency virus (HIV) [1–3] and Retrovir is approved for the treatment of patients with acquired immune deficiency syndrome (AIDS) and AIDS-related complex (ARC) [4–7]. For the study of the plasma and urine concentrations of AZT and its metabolites several reversed-phase HPLC assay methods have been developed [8–10]. The mobile phase compositions applied ranged from 6 to 15% (v/v) acetonitrile in various buffers (phosphate or ammonium acetate with pH 2.7 to 4.5) and have been used to separate the peaks of interest from other endogenous compounds. As our purpose was to develop a method for the detection of route indicative impurities, present at very low concentration (below 0.0005%) in AZT, a single reversed-phase procedure without preconcentration could not be applied. The compounds of interest are more hydrophobic than AZT, and therefore they elute with longer

* Corresponding author.

SSDI 0021-9673(94)00920-1

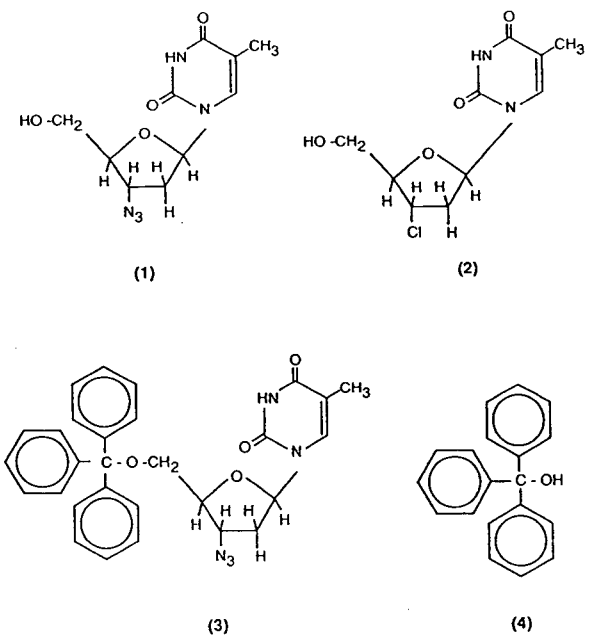

Fig. 1. Chemical structures of the compounds investigated. **1** = 3′-Azido-3′-deoxythymidine (AZT); **2** = 3′-chloro-3′-deoxythymidine (Cl-thymidine); **3** = 3′-azido-3′-deoxy-5′-O-tritylthymidine (trityl-AZT); **4** = triphenyl methanol.

retention times on reversed-phase columns. This is disadvantageous for low level detection. A volatile buffer such as ammonium acetate should be present in the mobile phase for thermospray (TSP) buffer ionisation. The involatile phosphate buffer cannot be used with this technique.

In this paper an analytical method is described by which approximately 10 ppb (w/w) amounts of synthetic route indicative impurities of AZT (Fig. 1) can be detected for purposes of patent protection.

2. Materials and methods

The compounds investigated (**1–4** in Fig. 1) were synthesized by the Wellcome Foundation (UK). Their purity was checked by chemical analysis and chromatography. The acetonitrile was purchased from Romil Chemicals (Loughborough, UK) and was of Super Purity Solvent grade ("190 far UV"). The 1,2-dichloroethane used was HPLC grade and was obtained from Rathburn (Walkerburn, UK). The ammonium acetate and acetic acid were HPLC grade and obtained from Fisons (Loughborough, UK) and BDH (Poole, UK), respectively.

2.1. Sample preparation and preconcentration by normal-phase chromatography

The required amount of AZT either as bulk powder or as a pharmaceutical product (e.g. a tablet or the contents of a capsule) was weighed into a scintillation vial to obtain 600 mg stated amount of AZT; 20 ml of extraction solvent was then added to the vial ("the sample extraction vial"). Another 20 ml of extracting solvent in another scintillation vial was subjected to the same procedures to provide an extraction blank. The extracting solvent was acetonitrile–1,2-dichloroethane (60:40, v/v). This solvent mixture was used as the mobile phase in the normal-phase chromatography. Both vials were placed on a mechanical shaker for 30 min. The 600 mg of AZT are soluble in the 20 ml of extraction solvent but the pharmaceutical product can contain additional insoluble components. After centrifuging both vials for 30 min at 2500 rpm (1500 *g*), the supernatant liquid from the sample extraction vial was removed and transferred into another vial. The contents of both vials, i.e. the sample extraction vial and extraction blank vial, were concentrated under a stream of dry nitrogen. From the sample extraction vial the AZT component continuously precipitated as the solvent volume was decreased. When approximately 4 ml of solvent remained, the sample extraction vial was centrifuged again for 10 min at 2500 rpm (1500 *g*), and the supernatant liquid transferred to another vial. This concentration was continued until approximately 200 μl of solvent remained in both vials. The contents of the sample extraction vial were then filtered using a Millex-HV_{13} 0.45-μm filter (Millipore, Bedford, MA, USA). A 150-μl volume of the extraction blank, followed by 150 μl from the sample extraction were injected into the normal-phase HPLC system.

Two Waters (Division of Millipore, Milford, MA, USA) 510 pumps with automated gradient

controller were used together with a Waters 712 WISP autosampler and Waters 490E programmable multiwavelength detector. The column temperature was maintained at 30°C using an oven unit obtained from Jones Chromatography (Hengoed, UK). The semipreparative Zorbax Sil, 250 × 9.4 mm column was purchased from DuPont (Wilmington, DE, USA) and the silica guard column (10 mm × 4.6 mm) was purchased from Anachem (Luton, UK). The (NP) mobile phase was acetonitrile–1,2-dichloroethane (60:40, v/v), the same as the extracting solvent, with a flow-rate of 2.5 ml/min. The detection was carried out at 265 nm UV with sensitivity 0.05 absorbance unit full scale (AUFS) range. Quantitative evaluations of the chromatograms according to the UV absorbance were made by a Multichrom data acquisition and analysis system (VG Data Systems, Altrincham, UK). The fractions corresponding to the triphenyl methanol, 3′-azido-3′-deoxy-5′-O-tritylthymidine (trityl-AZT) and 3′-chloro-3′-deoxythymidine (Cl-thymidine) were collected manually in scintillation vials. Fractions were collected after injection of the mobile phase as a machine blank (150 μl); the extraction blank (150 μl); followed by the sample extraction (150 μl). The fractions collected were blown down to dryness and redissolved in 200 μl of acetonitrile–water (60:40) (the triphenyl methanol and the trityl-AZT fractions) or acetonitrile–water (8:92) (Cl-thymidine fractions).

2.2. RP-HPLC–mass spectrometry method with TSP ionisation

The redissolved fractions were transferred to autosampler vials, and 100 μl from each vial injected into the HPLC–mass spectrometry (MS) system. A Hewlett-Packard (Waldbronn, Germany) Model 1050 pump unit, ultraviolet detector and the autosampler were used. The reversed-phase column was a Zorbax C_{18} (150 × 4.6 mm) (DuPont). The mobile phase flow-rate was 1.0 ml/min and the column temperature was 30°C. The triphenyl methanol and the trityl-AZT fractions were analyzed by acetonitrile–water (60:40, v/v) with 0.1 *M* ammonium acetate (pH 7), while the Cl-thymidine was analyzed by acetonitrile–water (8:92, v/v) with 0.1 *M* ammonium acetate (pH 3.5; adjusted by concentrated acetic acid). The effluent was monitored by UV at 265 nm and also by a TSP interface to a Fisons (Manchester, UK) VG-TRIO-1000 mass spectrometer. Positive TSP buffer ionisation was applied for the detection of triphenyl methanol detected as a triphenylmethyl cation $(C_6H_5)_3C^+$ (*m/z* 243), and the Cl-thymidine detected as a protonated molecular ion $(M+H)^+$ (*m/z* 261), while the trityl-AZT was detected as a deprotonated molecular ion $(M-H)^-$ *m/z* 508. The TSP conditions were: source temperature 230°C; nozzle temperature was 225°C for the measurements of triphenyl methanol and the trityl-AZT and 235°C for the Cl-thymidine. The repeller voltage was 165 V throughout.

3. Results and discussion

Typical HPLC–UV chromatograms, obtained from normal-phase chromatography of the standard compounds and for the sample extract are shown in Fig. 2. The large peak on the chromatogram of the sample extract (Fig. 2D) corresponds to AZT. The advantage of this normal-phase chromatography is that two of the compounds to be detected are eluted before the AZT peak. The peak of the Cl-thymidine cannot be detected because it is overlapped by the large AZT peak. The typical retention times and the fractions cut are summarized in Table 1. It can be seen that the target impurities are present at a very low level. For example the trityl-AZT peak in the sample extract corresponds to approximately 100 ng of compound injected.

At this stage of the method the most important achievement is the elimination of the AZT from the fractions containing triphenyl methanol and trityl-AZT (fractions B and D, respectively). Unfortunately the fraction containing Cl-thymidine (fraction F) still contains a reasonable amount of AZT. Therefore, this fraction needs to be further separated by the reversed-phase chromatography.

An important criterion of the reversed-phase

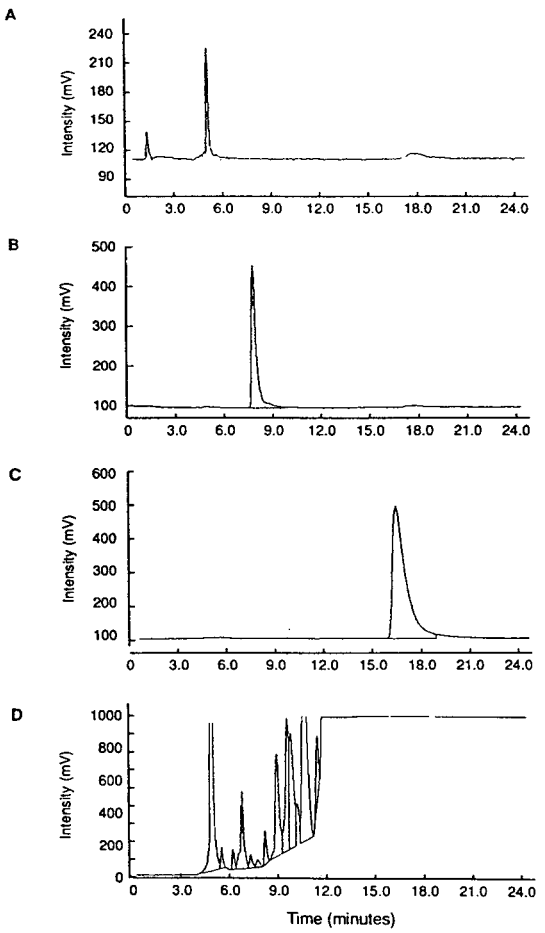

Fig. 2. Typical chromatograms of 1.5 μg injected amount of triphenyl methanol (A), 1.5 μg injected amount of trityl-AZT (B), 1.5 μg Cl-thymidine (C) and the sample extraction of six Retrovir capsules (D). Chromatographic conditions: column: Zorbax Sil 250 × 9.4 mm with silica guard column (10 × 4.6 mm); mobile phase: acetonitrile–1,2-dichloroethane (60:40, v/v); flow-rate: 2.50 ml/min; temperature 30°C; detection: UV at 265 nm.

HPLC–TSP-MS method development is to use mobile phases which give short retention times (preferably less than 10 min) and consequently stronger signals in single ion monitoring without loss of chromatographic resolution. It is also important to have ammonium acetate present to facilitate TSP buffer ionisation. When the mobile phase contains more than 65% acetonitrile it forms an immiscible solution with the aqueous ammonium acetate. Therefore the acetonitrile concentration must be kept lower.

To enhance the detection and sensitivity with the separation of the compounds of interest, their retention behaviour has been investigated on the reversed-phase column by varying the acetonitrile and the ammonium acetate concentrations with the pH. The plots obtained of the log k' values against the acetonitrile concentration at pH 7 for the compounds can be seen in Fig. 3. The triphenyl methanol and the trityl-AZT can be easily separated, even their retention order can be changed. The separation of AZT from the Cl-thymidine is more difficult. The resolution of the two peaks could not be increased by changing the acetonitrile concentration as can be seen in Fig. 3. The separation of the AZT from the Cl-thymidine has also been investigated as a function of mobile phase pH (Fig. 4). It can be seen that by decreasing the mobile phase pH, the retention times of the compounds decreased significantly, due to protonation of the molecules. This allowed a decrease in the acetonitrile concentration, and improved resolution was achieved. Further, the sensitivity of the TSP single ion monitoring at m/z 261 of the Cl-thymidine doubled at a pH below its pK_b.

Fig. 5 shows the retention dependence of triphenyl methanol and trityl-AZT on pH and ammonium acetate concentration by using 60% acetonitrile as organic modifier in the mobile phase. It can be seen that the ammonium acetate concentration shows more influence on the retention of the compounds than the pH. The sensitivity of the TSP-MS for single ion monitoring in the case of triphenyl methanol and trityl-AZT did not increase significantly. Therefore the neutral pH and the commonly used 0.1 M ammonium acetate concentration was selected.

On the basis of the results presented in Figs. 3–5 the typical chromatograms obtained by the optimized mobile phases are shown in Fig. 6.

3.1. Detection limit

The detection limit of the three compounds was determined by injecting progressively less of

Table 1
Typical retention times and the fractions cut from the normal-phase chromatography

Fraction	Time (min)	Compound	Retention time (min)
A	0–4.5	Blank	
B	4.5–5.8	Triphenyl methanol (**4**)	5.0
C	5.8–7.3	Blank	
D	7.3–8.7	Trityl-AZT (**3**)	8.0
E	8.7–13.0	Blank	
F	13.0–17.0	Cl-Thymidine (**2**)	16.0
G	17.0–20.0	AZT (**1**)	17.8

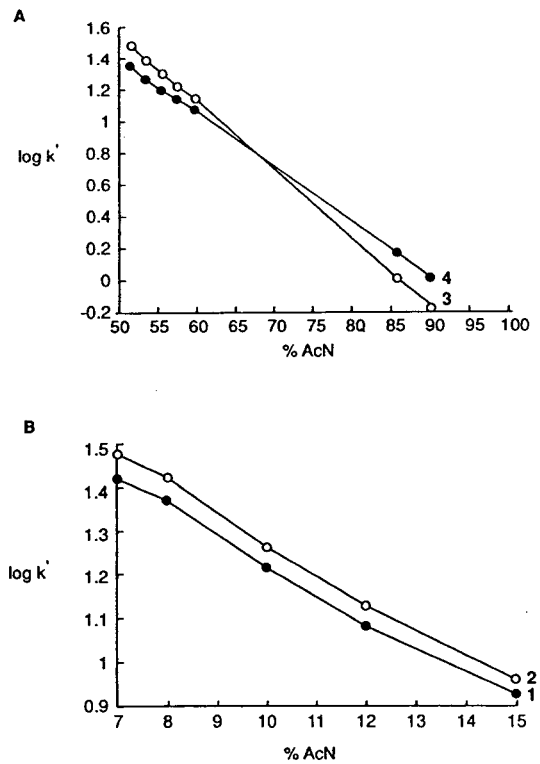

Fig. 3. Plots of the log k' values as a function of the acetonitrile (AcN) concentration of (A) triphenyl methanol (**4**) and trityl-AZT (**3**) and (B) AZT (**1**) and Cl-thymidine (**2**). The mobile was a mixture of acetonitrile and water.

each until the signal-to-noise ratio decreased to 3. By UV detection at 265 nm with a sensitivity range of 0.05 AUFS the detection limits of the triphenyl methanol, trityl-AZT and the Cl-

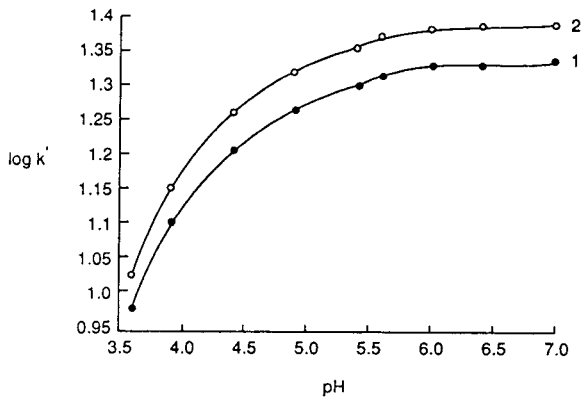

Fig. 4. Plot of the log k' values as a function of mobile phase pH for Cl-thymidine (**2**) and AZT (**1**). The mobile phase was acetonitrile–0.1 *M* ammonium acetate buffer (8:92, v/v).

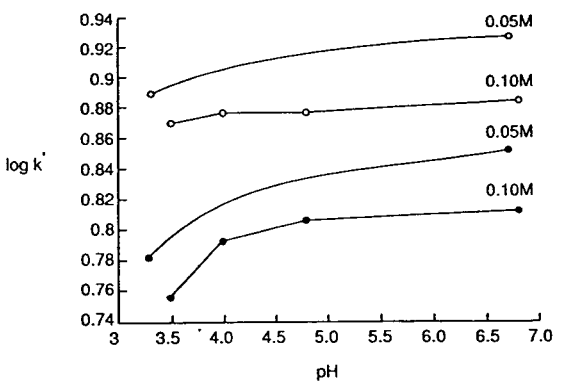

Fig. 5. The retention parameters (log k') of triphenyl methanol (●) and trityl-AZT (○) as a function of the pH and the ammonium acetate concentration of the mobile phase. The mobile phase was acetonitrile–0.05 or 0.10 *M* (as indicated) ammonium acetate solution (60:40, v/v) and pH.

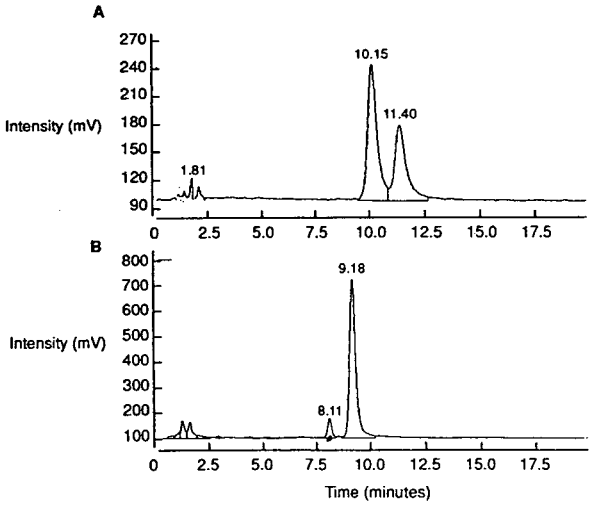

Fig. 6. The optimized separation of (A) Cl-thymidine and AZT and (B) triphenyl methanol and trityl-AZT by reversed-phase chromatography. Column: Zorbax C_{18} 150 × 4.6 mm; flow-rate: 1.0 ml/min; detection: UV at 265 nm. Mobile phases: (A) acetonitrile–0.1 *M* ammonium acetate pH 4 (8:92); (B) acetonitrile–0.1 *M* ammonium acetate pH 7 (60:40, v/v). Injected samples: (A) 210 ng AZT and 16 ng Cl-thymidine, (B) 200 ng triphenyl methanol and 300 ng trityl-AZT.

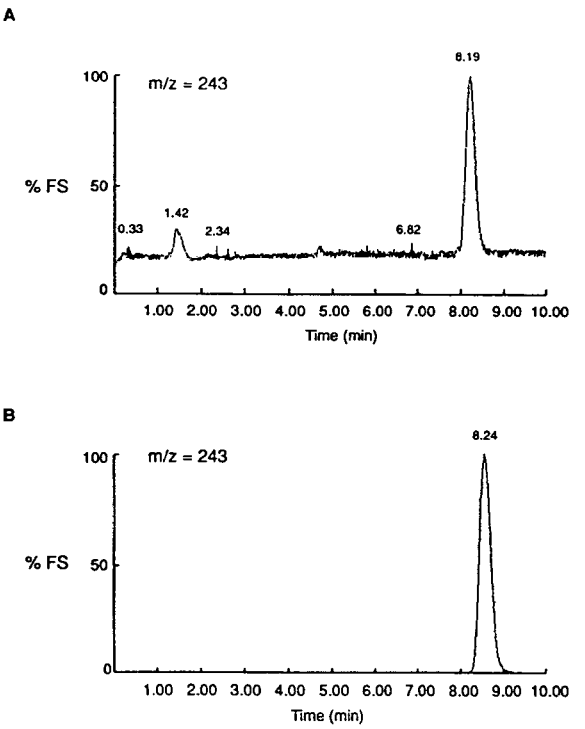

Fig. 7. The reconstructed RP-HPLC–TSP-MS ion chromatograms of 10 ng triphenyl methanol standard (A) and the corresponding sample extraction fraction B (B). HPLC–TSP-MS conditions: Zorbax C_{18} 150 × 4.6 mm column; acetonitrile–water (60:40) with 0.1 *M* ammonium acetate; 1.0 ml/min flow-rate.

thymidine were 10, 1 and 5 ng, respectively. However by TSP-MS single ion monitoring of the peaks the detection limits of the compounds were lower. Figs. 7–9 show the reconstructed ion chromatograms of the triphenyl methanol, trityl-AZT and Cl-thymidine obtained by injecting standards and corresponding sample extraction fractions onto the reversed-phase HPLC–TSP-MS.

3.2. Recovery study

The method presented here is not intended to be quantitative as our purpose was only to detect the synthetic route-indicative impurities. However a recovery study was carried out to reveal the steps where substantial loss of compound could occur and to determine the lowest amount of impurities which can be detected by the method. Substantial loss of impurities can be supposed during the concentration step prior to the normal-phase chromatography. Slow precipitation of AZT during the evaporation stage could co-precipitate the compounds of interest. Further loss (approximately 25%) can be expected by injecting 150 μl from the 200 μl concentrated solutions. The recovery of the compounds from the collected fractions after blowing down completely the acetonitrile–1,2-dichloroethane (60:40, v/v) (mobile phase) and redissolving in the reversed-phase mobile phase was measured for the trityl-AZT and Cl-thymidine. The study was carried out with 625 ng amount of each compound. The recovery of trityl-AZT was 94.8 ± 4.2%, while the recovery of the more polar Cl-thymidine was only 76.0 ± 2.2%.

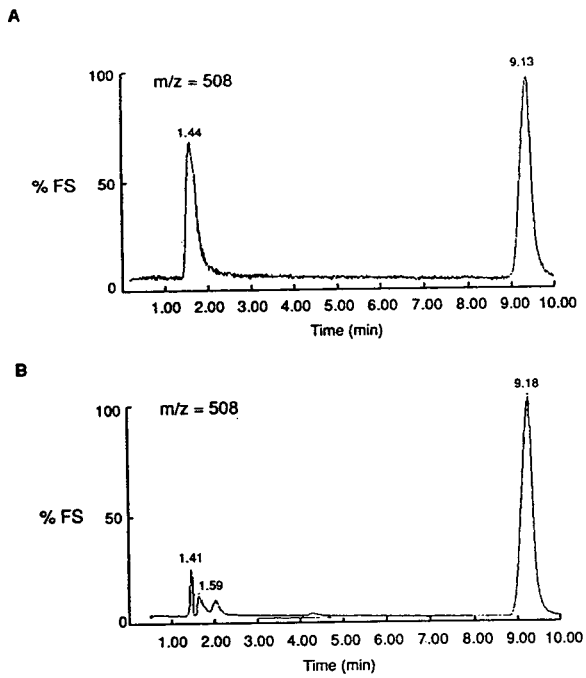

Fig. 8. The reconstructed RP-HPLC–TSP-MS ion chromatograms of 10 ng of trityl-AZT standard (A) and the corresponding sample extraction fraction D (B). The peak at 1.44 min is a pulse caused by injection. Its size is a result of the autoscaling the small sample peak. HPLC conditions as in Fig. 7.

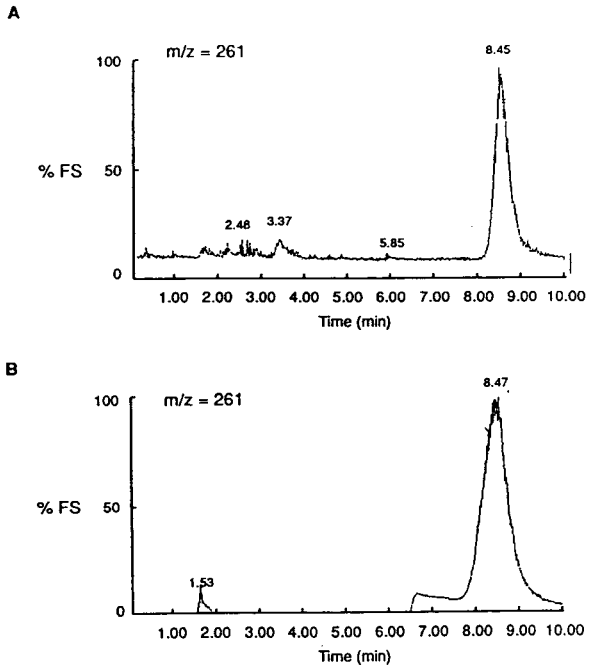

Fig. 9. The reconstructed RP-HPLC–TSP-MS ion chromatograms of 10 ng Cl-thymidine standard (A) and the corresponding sample extraction fraction F (B). The small "hump" before the main peak at 8.47 min is a fragment ion from the large amount of AZT present in this fraction. HPLC–TSP-MS conditions: Zorbax C_{18} 150 × 4.6 mm column; acetonitrile–water (8:92, v/v) with 0.1 *M* ammonium acetate; 1.0 ml/min flow-rate.

The recovery of the triphenyl methanol, trityl-AZT and Cl-thymidine without the presence of AZT was studied by extraction from a solution containing 12.0 ng of each compound. The detected amount of each compound was 1.2 ng triphenyl methanol and 1.0 ng of trityl-AZT. Cl-Thymidine was not detected in this experiment. The efficiency of the recovery by this method is therefore approximately 10% for trityl-AZT and triphenyl methanol and lower for Cl-thymidine. Assuming a significant loss by co-precipitation of the compounds in the precipitating AZT and another 50% loss by injecting of 100 μl from the 200 μl for the HPLC–TSP-MS the method allows us to detect and prove the identity of the route indicative impurities present in the range 50–100 ppb.

In conclusion a very sensitive and selective method has been developed for the detection of route indicative impurities present in AZT formulations. After separating the compounds from the AZT on a normal-phase semipreparative column, the isolated fractions were subjected to reversed-phase TSP-MS analysis. Although it is not a quantitative method it enables detection of the compounds in the 50–100 ppb range.

References

[1] H. Mitsuya, K.J. Weinhold, P.A. Furman, M.H. St. Clair, S. Nusinoff Lehrman, R.C. Gallo, D. Bolognesi, D.W. Barry and S. Broder, *Proc. Natl. Acad. Sci. U.S.A.*, 82 (1985) 7096.

[2] P.A. Furman, J.A. Fyfe, M.H. St. Clair, K. Weinhold, J.L. Rideout, G.A. Freeman, S. Nusinoff Lehrman, D.P. Bolognesi, S. Broder, H. Mitsuya and D.W. Barry, *Proc. Natl. Acad. Sci. U.S.A.*, 83 (1986) 8333.

[3] H. Nakshima, T. Matsui, S. Harada, N. Kobayashi, A. Matsuda, T. Ueda and N. Yamamoto, *Antimicrob. Agents Chemometr.*, 30 (1986) 933.

[4] R.E. Chaisson, J.P. Allain, M. Leuther and P.A. Volberding, *N. Engl. J. Med.*, 315 (1986) 1610.

[5] M.A. Fischl, D.D. Richman, M.H. Grieco, M.S. Gottlieb, P.A. Volberding, O.L. Laskin, J.M. Leedom, J.E. Groopman, D. Mildvan, R.T. Schooley, G.G. Jackson, D.T. Durack, D. King and the AZT Collaborative Working Group, *N. Engl. J. Med.*, 317 (1987) 185.

[6] H.C. Lane, H. Masur, J.A. Kovacs, R. Walker, S. Carleton, T. Folks and A.S. Fauci, *Clin. Res.*, 35 (1987) 480A.

[7] R. Yarchoan, R.W. Klecker, K.J. Weinhold, P.D. Markham, H.K. Lyerly, D.T. Durack, E. Gelmann, S. Nusinoff Lehrman, R.M. Blum, D.W. Barry, G.M. Shearer, M.A. Fischl, H. Mitsuya, R.C. Gallo, J.M. Collins, D.P. Bolognesi, C.E. Myers and S. Broder, *Lancet*, i (1986) 575.

[8] J.D. Unadkat, S.S. Crosby, J.P. Wang and C.C. Hertel, *J. Chromatogr.*, 430 (1988) 420.

[9] S.S. Good, D.J. Reynolds and P. De Miranda, *J. Chromatogr.*, 431 (1988) 123.

[10] R.M. Ruprecht, A.H. Sharpe, R. Jaenisch and D. Trites, *J. Chromatogr.*, 323 (1990) 371.

ELSEVIER

Journal of Chromatography A, 689 (1995) 39–43

JOURNAL OF CHROMATOGRAPHY A

High-performance liquid chromatographic determination of vanadium in crude petroleum oils using bis(salicylaldehyde)tetramethylethylenediimine

Muhammad Y. Khuhawar*, Shah Nawaz Lanjwani, Ghulam Q. Khaskhely

Institute of Chemistry, University of Sindh, Jamshoro, Sindh, Pakistan

First received 16 February 1994; revised manuscript received 30 June 1994

Abstract

A method was developed for the complexation and solvent extraction of the oxovanadium(IV) complex of bis(salicylaldehyde)tetramethylethylenediimine(H_2SA_2Ten) in chloroform. The complex was eluted from a normal-phase high-performance liquid chromatographic (HPLC) column using chloroform or chloroform–1,2-dichloroethane–acetonitrile (78:17:5) as eluent. The detection limit for vanadium was 2.5 ng per injection. The method was applied to the determination of vanadium in crude petroleum oils in the range 0.47–0.54 μg/g oil. Copper and nickel could also be extracted simultaneously, and there was complete separation between copper, nickel and vanadium using HPLC conditions. A coin containing copper, nickel and vanadium was analysed.

1. Introduction

A number of methods have been reported for the determination of vanadium in crude oils, including atomic absorption [1], inductively coupled plasma atomic emission [2] and radioisotope X-ray fluorescence spectrometry [3], flow-injection analysis [4], neutron activation analysis [5] and gas chromatography (GC) [6]. High-performance liquid chromatographic (HPLC) methods are interesting because of the ease of separation and the capability for the simultaneous determination of a number of metal ions, using a suitable complexing agent.

A number of complexing reagents have been used for the HPLC separation of vanadium from cobalt, iron, chromium, nickel, copper, palladium, aluminium and zinc [7–13]. Some of the complexing reagents used are 8-hydroxyquinoline [14,15], 2 - (5 - bromo - 2 - pyridylazo) - 5 -diethylaminophenol [13], 2 - (3,5 - dibromo - 2-pyridylazo) - 5 - diethylaminophenol [10,16], 2,2′ - dihydroxyazobenzene [11,17], 2 - (8-quinolylazo) - 5 - N,N - diethylaminophenol [12] and 4 - (2-pyridylazo)resorcinol [18,19]. Normal-phase [14], reversed-phase [12–15] and ion-pair reversed-phase [9–11,16] modes have been used. Vanadium has been determined in rain and sea water and airborne particles [12,13,15].

The reagent bis(salicylaldehyde)tetramethylethylenediimine [2,3 - dimethyl - 2,3 - N,N′ - butanebis (salicylaldimine)] (H_2SA_2Ten) has been used for the determination of copper and nickel using GC and normal-phase HPLC [14]. The copper and nickel were extracted as metal chelates in toluene from aqueous solution. How-

* Corresponding author.

0021-9673/95/$09.50
SSDI 0021-9673(94)00613-X

ever, using the specified conditions vanadium was not extracted from the aqueous phase. Dilli and Patsalides [6] used bis (acetylpivalylmethane) ethylenediimine for the GC determination of vanadium in crude oils by derivatization in methanol, followed by solvent extraction in carbon disulphide. A slightly modified method of Dilli and Patsailides [6] was used in this work for the HPLC determination of vanadium using H_2SA_2Ten as complexing agent. HPLC methods reported for the determination of vanadium involved derivatization and elution of vanadium as vanadium(V) [9–18]. Recently, vanadium(IV) and vanadium(V) have been separated using 4-(2-pyridylazo)resorcinol as chelating agent by reversed-phase HPLC [19], but the present work was based on the separation and determination of vanadium(IV) from copper(II) and nickel(II) using solvent extraction and normal-phase HPLC.

2. Experimental

H_2SA_2Ten reagent was prepared by heating together salicylaldehyde and 2,3-dimethyl-2,3-aminobutane in a 2:1 molar ratio. Its copper(II), nickel(II) and oxovanadium(IV) chelates were prepared by refluxing together an equimolar solution of copper(II) acetate, nickel(II) acetate or vanadium(IV) sulphate in methanol and the reagent for 15–30 min as reported previously [20,21]. Elemental analyses, carried out by Elemental Micro Analysis (Devon, UK) agreed with the expected values [20].

A Hitachi Model 655A liquid chromatograph connected with a variable-wavelength UV monitor, a Rheodyne Model 7125 injector and a Hitachi D2500 chromatointegrator was used.

A silica gel 100 (5 μm) column (200 × 4.6 mm I.D.) (Hewlett-Packard) and a column (250 × 4 mm I.D.) packed with LiChrosorb Si 100 (5 μm) were used.

Acetic acid (glacial), sulphuric acid (95–98%), nitric acid (65%), ammonia solution (35%) and perchloric acid (69%) (Merck) were used.

2.1. Solvent extraction of vanadium

Sulphur dioxide was passed through solutions containing different amounts of vanadium (0–250 μg) for 30 s, then glacial acetic acid (0.5 ml) and 35% ammonia solution (0.5 ml) were added. The contents were heated gently on an oil-bath and most of the solvent was evaporated. The residue was dissolved in ethanol (5 ml) and 2 ml of H_2SA_2Ten reagent solution (1.0% w/v in ethanol) were added. The contents were warmed at 60–70°C for 15 min and transferred into a separating funnel containing water (20 ml). Chloroform (5 ml) was added and the contents were mixed well. The layers were allowed to separate and the organic layer was collected. An aliquot (5 μl) of the extract was injected on to the column (200 × 4.6 mm I.D.) and the complex was eluted with chloroform at a flow-rate of 0.9 ml/min followed by UV detection at 300 nm.

2.2. Simultaneous extraction of copper, nickel and vanadium

Through an aliquot of solution (1–5 ml) containing copper, nickel and vanadium (0–150 μg) was bubbled sulphur dioxide for 30 s, then glacial acetic acid (0.5 ml) and 35% ammonia solution (0.5 ml) were added. Most of the solvent was evaporated on an oil-bath and the same extraction procedure as in Section 2.1 was followed. The extract (5 μl) was injected on to the column (250 × 4 mm I.D.) packed with LiChrosorb Si 100 and the complexes were eluted with 1,2-dichloroethane–chloroform–acetonitrile (78:17:5, v/v/v) at a flow-rate of 0.9 ml/min, followed by UV detection at 270 nm.

2.3. Determination of vanadium in crude oils

To crude oil samples (5–30 g) obtained from the Khaskhely, Lashari and Thora oil fields located in the south Indus Basin near Hyderabad, Sindh, Pakistan, were added 95–98% sulphuric acid (10 ml), 65% nitric acid (20 ml), and perchloric acid (4 ml). The contents were heated gently, then more nitric acid was added

until the solution became clear. The solution was concentrated to 1–2 ml and the volume was adjusted to 10 ml with water. A 5–10 ml volume of the solution was taken and the same procedure as in Section 2.1 was followed.

2.4. Determination of copper and nickel in a coin

To a coin (25 pasia) (2.321 g) was added hydrochloric acid (25 ml) and the mixture was heated gently. More hydrochloric acid (25 ml) was added until the solution became clear. The solution was concentrated to 1–2 ml and the volume was adjusted to 100 ml with water. A 0.1 ml volume of the solution was taken and the procedure as in Section 2.2 was followed.

3. Results and discussion

The reagent H_2SA_2Ten reacts selectively with vanadium(IV) to form a complex, SA_2TenVO (Fig. 1). Therefore, sulphur dioxide was bubbled through the solution to reduce vanadium(VI) to vanadium(IV). The reagent failed to extract vanadium(IV) from aqueous solution. Therefore, prederivatization was carried out in ethanol. Oxovanadium(VI) acetate is more soluble in ethanol, so acetic acid was added to the solution, before heating the solution to dryness, in order to convert oxovandium(IV) sulphate into oxovanadium(IV) acetate. Using these conditions with a heating time of 15 min, followed by extraction in chloroform, the transfer of vanadium from the aqueous to the organic phase was quantitative. This was checked by extracting

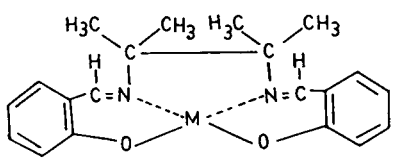

M= Cu,Ni,VO

Fig. 1. Formula of metal chelates.

250–2000 μg of vanadium(IV) in chloroform (5 ml) and measuring the absorbance of the solution at 598 nm spectrophotometrically. A linear calibration graph was obtained that obeyed Beer's law. This extraction procedure was used for the determination of vanadium at trace levels using HPLC with UV detection.

The vanadium chelate was easily eluted from the silica gel 100 column (200 × 4.6 mm I.D.) with chloroform, giving a symmetrical peak with a retention time of 3.60 min. The excess of the reagent eluted with a retention time of 3.00 min and did not interfere with the determination of vanadium (Fig. 2). The response of the detection at 300 nm was checked by injecting 5 μl of extracts of different concentrations and measuring the average peak height ($n = 3$). A linear calibration graph was obtained in the range 0–250 μg of vanadium. The detection limit measured as three times the background noise was 2.5 μg of vanadium in 5 ml, corresponding to 2.5 ng of vanadium per injection.

Test solutions containing different amounts of vanadium were also analysed and relative error

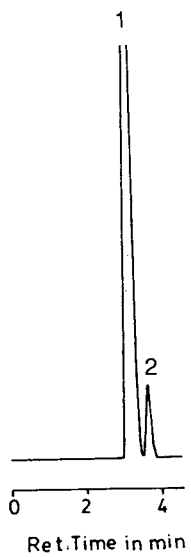

Fig. 2. HPLC separation of (1) reagent and (2) oxovanadium complex. Column, silica gel 100 (200 × 4.6 mm I.D.); eluent, chloroform; flow-rate, 0.9 ml/min; detection, UV at 300 nm.

was found to be 0–4.1%. The vanadium concentrations in the crude petroleum oils obtained from Khaskhely, Lashari and Thora oil fields were found to be in the ranges 0.54, 0.50 and 0.47 μg/g, respectively, with relative standard deviations of 4–10%.

When the extraction procedure was checked for the simultaneous extraction and subsequent HPLC determination of copper, nickel and vanadium, it was interesting that the use of sulphur dioxide to reduce vanadium(VI) to vanadium(IV) did not prevent the derivatization of copper and nickel. The optimum separation between copper, nickel and vanadium on the column (250 × 4 mm I.D.) packed with LiChrosorb Si 100 was obtained when the complexes were eluted isocratically using chloroform–1,2-dichloroethane–acetonitrile (78:17:5, v/v/v) at a flow-rate of 0.9 ml/min with UV detection at 270 nm (Fig. 3). Linear calibration graphs for the simultaneous determination of copper, nickel and vanadium were obtained in the range 0–150 μg, with correlation coefficients (r) of 0.999, 0.988 and 0.986 for vanadium, nickel and copper, respectively.

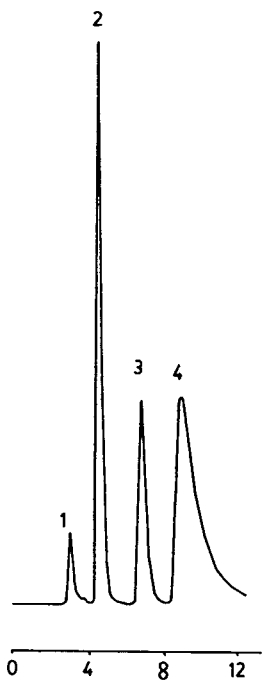

Fig. 3. HPLC separation of (1) reagent and (2) vanadium, (3) nickel and (4) copper chelates. Column, LiChrosorb Si 100 (250 × 4 mm I.D.); eluent, 1,2-dichloroethane–chloroform–acetonitrile (78:17:5); flow-rate, 0.9 ml/min; detection, UV at 270 nm.

The reagent H_2SA_2Ten also reacts with cobalt(II) and iron(II) to form coloured complexes. Their effect on the determination of copper, nickel and vanadium was checked at a level of 1000 μg of cobalt and iron. The cobalt(II) and iron(II) chelates were not eluted from the column and did not interfere in the determination of copper, nickel and vanadium.

Finally, a coin was analysed for its contents of copper, nickel and vanadium. The copper and nickel concentrations were found to be 40.9 ± 0.9% and 8.6 ± 0.5% ($n = 3$, 95% confidence level), respectively. The coin sample solution was also spiked with vanadium (50 μg) to check the simultaneous extraction and determination of vanadium and the relative error was 5%.

References

[1] F.J. Langmyhr and U. Aadalen, *Anal. Chim. Acta*, 115 (1980) 365.
[2] J.L. Fabec and M.L. Ruschak, *Anal. Chem.*, 57 (1985) 1853.
[3] M. Alvarez, J. Alvarado, A.R. Cristiano, L.M. Marco and M.M. Perez, *J. Radioanal. Nucl. Chem.*, 144 (1990) 327.
[4] R. Forteza, M.T. Oms, J. Cardenas and V. Carda, *Analusis*, 18 (1990) 491.
[5] Z. Ding, Z. Chai, J. Fu, C. Sheng, Q. Lin and D. Wu, *Hijishu*, 13 (1990) 203.
[6] S. Dilli and S. Patsalides, *Anal. Chim. Acta*, 128 (1981) 109.
[7] G. Nickless, *J. Chromatogr.*, 313 (1984) 129.
[8] X. Zhang and C. Lin, *Fenxi Huaxue*, 16 (1988) 122.
[9] C. Ohtsuka, H. Wada, T. Ishizuki and G. Nakagawa, *Anal. Chim. Acta*, 223 (1989) 339.
[10] Y. Yuan and Y. Wang, *Talanta*, 36 (1989) 777.
[11] H. Hoshino, K. Nakano and T. Yotsuyanagi, *Analyst*, 115 (1990) 133.
[12] J. Miura, H. Hoshino and T. Yotsuyanagi, *Anal. Chim. Acta*, 233 (1990) 121.
[13] Y. Zhao and C. Fu, *Anal. Chim. Acta*, 230 (1990) 23.
[14] L.H.J. Lajunen, E. Eijarvi and T. Kenakkala, *Analyst*, 109 (1984) 699.

[15] H. Ohashi, N. Uehara and Y. Shiji, *J. Chromatogr.*, 539 (1991) 225.
[16] Y. Zhao and C. Fu, *Analyst*, 116 (1991) 621.
[17] E. Kancko and T. Yotsuyanagi, *Biomed. Res. Trace Elem.*, 1 (1990) 231.
[18] X. Ming, Y. Wu and G. Schwedt, *Fresenius J. Anal. Chem.*, 342 (1992) 556.
[19] S.J. Tsai and S.J. Hsu, *Analyst*, 119 (1994) 403.
[20] M.Y. Khuhawar and G.Q. Khaskheli, *J. Chem. Soc. Pak.*, 13 (1991) 10.
[21] D.F. Averill and R.F. Broman, *Inorg. Chem.*, 17 (1978) 3389.

ELSEVIER

Journal of Chromatography A, 689 (1995) 45–61

JOURNAL OF CHROMATOGRAPHY A

Polarization, relaxation and unrestrictedly linear response in a bipolar, constant-frequency electron-capture detector☆

Hameraj Singh, Brian Millier, Walter A. Aue*

Department of Chemistry, Dalhousie University, Halifax, Nova Scotia B3H 4J3, Canada

First received 21 June 1994

Abstract

To investigate *bipolar* constant-frequency regimes in the electron-capture detector (ECD), a "tripulser" was built. The tripulser was able to generate unit sequences of up to three pulses, individually defined as to width, amplitude and relative position, with 600 ns to 1 s and 0 to 250 V definition ranges. On a commercial ^{63}Ni two-chamber ECD (Tracor), the high-frequency region of bipolar pulsing (ca. 10 to 100 kHz) was explored. The detector showed clear polarization–relaxation (PR) effects within time spans (on the order of 10^{-5} s) that were commensurate with the theoretical mobility of electrons. Speculative evidence was found to suggest that PR kinetics, as driven by particular bipolar pulse sequences, resulted in changes to the (heterogeneous) charged-particle distribution and effectively allowed higher than usual concentrations of electrons (and cations) to exist in the ECD. Based on this evidence, a bipolar, constant-frequency drive was developed that, when tested on the Tracor ECD, showed good analytical performance. Most important (and in contrast to the behavior of any other unipolar constant-frequency mode) the bipolar (Tracor) ECD yielded strictly *linear* calibration curves —starting from the detection limit ($5 \cdot 10^{-18}$ mol/s of α-1,2,3,4,5,6-hexachlorocyclohexane at $S/N_{p\text{-}p} = 2$), over three orders of magnitude, all the way to an amount of analyte that totally exhausted the baseline current.

1. Introduction

It seems obvious that "polarization" (electrical inhomogeneity, the development of space charges) must take place inside the electron-capture detector (ECD) when a constant or temporary external voltage is imposed across the cell. The grounds for assuming that internal polarization occurs on a significant scale are many; and they are both experimental and theoretical in nature.

One experimental example is provided by the impedance to current flow in the two possible field directions. (In this study, "regular field" refers to the conventional situation in which the externally imposed voltage makes the radioactive foil the cathode, while "reversed field" makes the foil the anode —regardless of which electrode is at ground potential.) The current flows in the two possible field directions —given the same voltage drop, of course— differ greatly [1,2]. Thus the ECD can serve as a (not quite perfect) half-wave rectifier. If so, it must possess internal cell potentials (space charges) that preferentially hinder the flow of electrons in one, i.e. the reversed-field, direction.

One theoretical example is provided by the ab

* Corresponding author.

☆ Part of doctoral thesis of H.S.

0021-9673/95/$09.50
SSDI 0021-9673(94)00900-7

initio calculation of spatially and temporally resolved charged-particle concentrations and corresponding potential gradients in a simulated parallel-plate ECD driven by bipolar square waves [3]. This calculation clearly demonstrated that under reversed-field conditions electrons are trapped in a (positive) potential well. The well is situated close to the radioactive foil and its behaviour can be easily followed over the whole frequency range up to 50 kHz [3,4]. Regardless of the mechanism of impedance, however, it seems self-evident that the charged-particle distribution must become polarized when an external voltage is switched on, and that it must relax when that voltage is switched off.

Our interest in the process of polarization and relaxation ("PR") has several roots. The main one is this: because the ECD acts as a rectifier, it can be driven by directionally alternating (bipolar) voltages. In the simplest case, household current will do [5]. This mode of operation differs from the initial d.c. and all following, unipolar-pulsed ECD drives of the literature [6–16]. We call the detector, when driven by alternating voltages in sine or square-wave form, the a.c. ECD [17].

To our knowledge, the a.c. ECD has seen only minor, if indeed any, practical use in analytical laboratories. It is, however, a perceptually most interesting device. Indeed, based on the classical theory of electron capture one would argue that it should not work at all. In fact, it works quite well [4,5,17].

How does the polarization phenomenon tie in with sinusoidal or square-wave a.c. drives? Thus: When the imposed voltage switches direction, the polarization of the charged-particle distribution inside the ECD cell must follow suit. How much time does that take? Can the time necessary to achieve a sizable extent of polarization ever become comparable to the pulse repetition time of the drive? If it does, will the performance of the a.c. ECD become dependent on the kinetics of polarization?

Since the fastest reasonable type of polarization relates to electrons, and since the a.c. ECD uses drive regimes of up to ca. 10^6 Hz, the question appears justified. After all, at voltages and other conditions typical of the a.c. ECD, unimpeded electrons drift through nitrogen at about 10^5 cm/s [18]. That would suggest that somewhere in the 10^4 to 10^6 Hz range —the numbers depend on the construction of the detector, the nature of the radioisotope and the carrier gas, the imposed voltage and temperature, the existing contamination, etc., etc.— polarization kinetics could become dominant.

But what about relaxation? Under, say, a square-wave a.c. drive, the full regular-field voltage switches on immediately after the full reversed-field voltage switches off, and vice versa. The polarization adjusts accordingly: it finds no time for relaxation. To allow the ECD the time to dissipate the generated space charges requires pulse-free periods. (These intervals between pulses are conventionally characterized as being "field-free" in the ECD literature; however, the latter term will not be used here to avoid confusing the externally imposed voltage with the resulting but, in space and time, different and variable internal field.)

Thus, appropriately spaced pulses could be profitably employed to induce and test PR effects by time-integrated observation. In the simplest case that approach could answer some obvious questions. For instance: does a positive pulse preceding a negative pulse influence the current flow and response of the ECD? If so, does it make any difference how close the two pulses come? What about a negative pulse preceding a positive pulse? Aside from their potential analytical utility, the answers to these questions may also fill one of the several large gaps that still remain in our understanding of the ECD.

The only "practical" ECD use of bipolar pulsing has, to our knowledge, been proposed by Simon and Wells [19] for the *constant*-current mode. These authors describe their technical approach, mechanistic objectives, and practical results as follows: "The bipolar pulse consists of an initial extraction pulse, followed immediately by a reversed biased pulse. . . . The action of the bipolar pulser is to reverse the displacement of the ions due to the initial extraction pulse to their original position, thus minimizing the collection of anions. . . . The most notable effect of the bipolar pulser is to linearize the response of

the ECD at high sample concentrations . . . " [19].

Working under rather different conditions and toward a different goal, Warden et al. [20] found that "a bipolar pulse wave form [which] contains a positive-going pulse of amplitude and duration equal to the usual negative-going pulse which precedes it . . . had no measurable affect on the standing currents or on the responses at all pulse frequencies".

Given the vagaries arising from different ECD constructions, operational modes and mechanistic theories, the reader may well question the wisdom of using *repetitive* pulse sequences. Could the PR process not be probed by monitoring the current flow during and after a *single* pulse? The literature experiment closest related to this question was carried out by Gobby et al. [21]. It used an atmospheric-pressure ionization source for mass spectrometry (API-MS), with the source resembling an ECD. The mass spectrometer monitored the flow of cations and anions through a pinhole.

The —to our knowledge— only single-pulse experiment with electrons in a (more or less) conventional ECD was carried out by Lovelock and Watson [22]. It was designed to answer the question whether electrons were drifting unimpeded through the cell or whether their drift speed was influenced by ambipolar diffusion (cf. [15]). The former was reported to be the case.

Lovelock and Watson's report proved tantalizing to us, not the least because of its fairly obvious potential extension to, say, a probing of electron, cation and anion movements in the ECD under various drive modes. Apart from being of fundamental interest, such a probe could yield much-needed information on the chemical nature of peaks for, say, confirmation purposes; it could introduce selectivity among compounds of similar electron-capture cross-section for, say, more reliable analysis; and it could provide mechanistic details for, say, solving some of the design problems under which the ECD still labors. Being bereft of technical details, however, this lone report of singly-pulsed ECD operation could unfortunately not be reproduced by the modest means at our disposal.

To wit, our current was extremely low, the required temporal resolution was very high, and the capacitance of the cell seriously interfered [3]. Although a ragged feature vaguely resembling Lovelock and Watson's "electron pulse" [22] could finally be obtained; and although that feature was, very approximately, of the expected magnitude (charge), mobility, and also reactivity toward molecular oxygen (in other words, air injections wiped it out), our data were still of decidedly inferior quality. More importantly, an attempt to monitor the arrival of *positive* ions produced an equally ragged feature of exactly the same charge, mobility, shape and chemical reactivity as the "electron pulse" (an "image current"?) [3].

Single-pulse measurements of temporally resolved charged-particle flow were therefore discontinued and replaced by the —technique-wise more straightforward, though interpretation-wise more ambiguous— measurements of time-integrated currents resulting from multiple-pulse drives in a conventional ECD. For these measurements, the prototype of a microprocessor-controlled square-wave pulse generator [3] was constructed as a graduate course project.

Its use demonstrated that a positive (reversed-field) pulse, when it *preceded* a negative pulse by less than about 20 μs, did reduce the detector current. The reduction in current was not (or at least was not predominantly) due to a reversed-field current. Rather, it was judged to be due to a polarization that, as long as it persisted, opposed the transport of electrons to the collecting electrode during the subsequent regular-field pulse [3].

For the objectives of the present paper, a more user-friendly, bipolar pulse generator of greater speed, power and versatility had to be developed. We boldly called it the "tripulser".

2. Experimental

The tripulser[1] (Fig. 1 shows its block diagram) was a laboratory-built microprocessor-based square-wave pulse generator capable of repeat-

[1] Researchers interested in the tripulser are invited to contact B.M. for details.

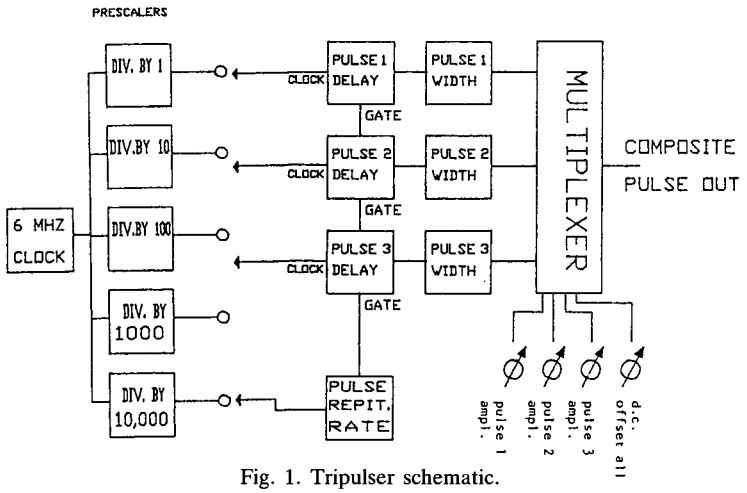

Fig. 1. Tripulser schematic.

ing a unit sequence comprised of up to three individually defineable pulses. The sequence repetition rate, as well as the delay time and width of each of the pulses within a given sequence, were entered on a key pad by the operator before each experiment. Time periods could vary from the upper limit of 1 s down to the (in practice achievable) resolution of 600 ns. All timing parameters were defined in response to prompts that appeared, prior to starting the experiment, on a terminal connected to the pulser through an RS-232 serial data link.

The polarity and amplitude of the individual pulses, as well as the d.c. offset, were controlled by potentiometers built into the tripulser. The overall attainable amplitude range was 250 V (e.g., up to + / − 125 V for equal-sized bipolar pulses, or up to + or −250 V for unipolar pulses), subject to a slew rate of 150 V/μs and the condition that pulses not overlap.

The tripulser circuit could be triggered by an external pulse generator that thus controlled, and was therefore able to vary, the pulse sequence's repetition rate during the experiment. (Note that, in contrast, the pulse widths, delays, polarities and amplitudes could be changed only if the experiment was interrupted; this precluded the use of any of the latter parameters as operationally active criteria in, say, a feedback circuit.)

The tripulser's output was always connected to the ECD's *foil*: a "negative" pulse therefore imposed a "regular" field, a "positive" pulse a "reversed" field across the cell.

The gas chromatograph with ^{63}Ni ECD was a Tracor Model 550; it had been used in our laboratory for about two decades. The column was a 100 × 0.2 cm I.D. borosilicate tube packed with 5% OV-101 on Chromosorb W AW, 100–120 mesh (i.e. of particle diameters between 150 and 125 μm, approximately); the 35 ml/min carrier gas and the 50 ml/min purge gas were "prepurified"-grade nitrogen, further freed of oxygen and water by passage through heated zirconium sponge (gas purifier; Supelco, Bellefonte, PA, USA).

For the frequently used test analyte α-1,2,3,4,5,6-hexachlorocyclohexane —an inactive isomer of the well-known insecticide lindane (which is the γ isomer)— the temperatures used were: injector 250, column 150, transfer line port 270 and detector 300°C. (Note that these altogether conventional GC–ECD conditions are mentioned here for the record only; similar results could have been obtained from a great variety of analytes under a wide range of conditions.)

α-1,2,3,4,5,6-Hexachlorocyclohexane was purchased from ICN Labs. (Irvine, CA, USA) and used without further purification. The solvent hexane was "distilled-in-glass, non-UV" grade from Caledon Labs. (Georgetown, Ontario,

Canada); it was distilled again from calcium hydride under a stream of nitrogen prior to each *high*-sensitivity experiment (cf. [23]).

The continued performance level of the ECD was tested from time to time in the —historically oldest, instrumentally simplest and diagnostically most revealing— d.c. mode. Scanning its current–voltage profile ascertained that the detector had not been contaminated —or that it had not otherwise suffered changes in its vital characteristics— by and during the experiments. (No significant changes were found during this study).

The ECD output current was amplified by the built-in Tracor electrometer and displayed on a Linear Instruments strip chart recorder and/or a Fluke 75 multimeter. The performance of the tripulser was monitored by a 60 MHz oscilloscope (Model 2215A; Tektronix, Beaverton, OR, USA) and/or a frequency meter (DFC 100 multifunction counter; JDR Instruments, 2233 Samaritan Drive, San Jose, CA 95124, USA).

3. Results and discussion

It may be well to start with two simple and general evaluations to set the stage and, in the process, define some parameters for the more specialized experiments to follow.

3.1. First general evaluation: what do the current profiles look like?

The most telling characteristics of pulsed ECDs are their current–frequency profiles. Fig. 2 shows three such profiles, presented for easier viewing in both semilog (left) and linear (right) form. Note that the specific shape of profiles can depend on the amplitude —and, if pulse-free intervals occur, the width— of the pulses. Each of the regular-field pulses used in this experiment (which exert at least −75 V for 6 μs) would, by the tenets of the classical ECD theory (e.g. [14]), be strong enough to clear the cell of electrons.

The first profile uses a straightforward square-wave *a.c.* (no pulse-free intervals) [17]; the second a *unipolar* negative drive (identical with

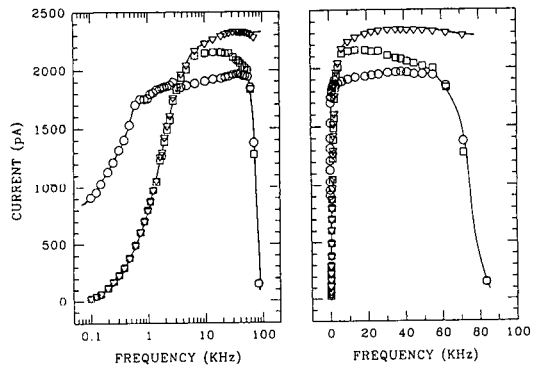

Fig. 2. Current profiles for comparison of a.c. (○), unipolar pulsed (▽) and bipolar pulsed (□) square-wave drives. Pulse width (unipolar and bipolar): 6 μs. Pulse amplitude: a.c. and bipolar + / − 75 V; unipolar −75 V. Bipolar pulses follow one another at equal intervals. Maximum d.c. current: 2.88 nA. Left plot: semilogarithmic; right plot: linear.

the secondmost popular ECD mode [6–11]); the third a *bipolar* (temporally symmetric) pulse sequence. Interestingly, but in hindsight predictably, there exist two separate locations in the plot where two (though not the same two) of the three profiles join.

At low frequencies, it is the two intermittently pulsing regimes whose profiles join. In other words, the positive pulse of the bipolar regime is ineffectual in this region. And this makes sense: its reversed-field current is only a minute fraction of the regular-field current, and the system has more than enough time to relax between pulses. At *very* low frequencies, both current profiles must obviously drop to zero.

The a.c. profile, in contrast, does not: a very heavy 75 V are *continually* imposed in one direction or the other. As the frequency reduces to extremely low values —i.e. as the alternating "d.c." stretches of opposing polarity grow longer and longer, the instrument will show correspondingly alternating regular-field and reversed-field d.c. currents, provided the pulse width is significantly longer than the time constant of electrometer and recorder [24]. If the pulse width is significantly shorter, the instrument will show only the *difference* between the two currents. (The current shown in the 0.1–1 kHz range is of the latter type. Since the regular-field

current is still considerably larger than the reversed-field current even at a continuous 75 V, and since the two pulses have the same length, the profile straightens out at very low frequencies: it approaches a current level that is slightly lower than half the conventional d.c. current at −75 V.)

At medium frequencies, the bipolar regimes reach slightly different "plateau" regions. The left-side rise to the plateau is essentially governed by the recombination ($M^+ + e^-$) rate. The two pulsing regimes reach somewhat higher plateaus than the a.c. regime; a consequence of the heavier a.c. regime's higher reversed-field current. Further explanations on a.c. drive behaviour in this region have been given earlier [7,25] and, being of little importance to this study, need not be repeated here.

At high frequencies, it is the a.c. and the bipolar pulsed profiles that join and jointly drop to zero. (The unipolar pulsed profile, in contrast, must continue on to a level identical with the −75 V *d.c.* current [17].) This again makes sense: The bipolar pulses are starting to approach each other closely (at 83 kHz they would theoretically merge); thus they are beginning to resemble an a.c. regime. And the a.c. negative pulse becomes too short in that region to drive even perfectly unimpeded electrons across the cell to the collecting anode [17]. As a consequence, electrons may "oscillate" [4] under a high-frequency a.c. regime (until they recombine with positive ions, are captured by analyte molecules, or collide with some conductive structure). The two profiles join and start to drop from the plateau at about 15 μs repetition time (a time that obviously depends on the chosen voltage).

It should be mentioned that the term "oscillation" is used here in a partly metaphoric sense —though physical oscillation of electrons is calculable for an idealized ECD system, it has never been experimentally observed in a real one. (The fact that the electrometer registers no current does not necessarily mean that no current flows: its time constant of about a tenth of a second renders the electrometer opaque to a.c. above ca. 10 Hz, and the instrument can thus register only the net (d.c.) flow of charges.)

Even the concepts of "oscillation" and "PR" intertwine in that region. Whether one or the other is used at this stage depends mainly on the extent to which one sees electrons as being trapped in potential wells, or as being merely impeded, or as being allowed to travel freely back and forth; and whether one sees them as migrating to the collecting anode within one or within several pulse periods. Although there is a physical side to the difference between the two concepts and terms, there is also a semantic one —and the experiments, so far, permit description through either. (We consider such concepts to be more valuable for suggesting new than for explaining old research.)

3.2. Second general evaluation: where could polarization occur?

The second general evaluation we wish to include here was initially conducted to demonstrate the practical use of *three* pulses (the first experiment used only two) and also to check how large the integrated voltage would have to be in order to (apparently) sweep the cell free of electrons. Only as an afterthought did we pose the question what —if anything— should happen if two pulses were to change their *relative positions* within a given sequence. Several experiments were thus run at different combinations of voltage and pulse width. Fig. 3 shows two of these: there the pulses are 100 V high and 2 or 5 μs wide.

The "stationary" part of the pulse sequence resembles bipolar pulsing at 5 kHz, i.e. at a repetition rate of 200 μs. Positive and negative "stationary" pulses strike evenly every 100 μs, while a "mobile" negative pulse strikes in the available intervals. In Fig. 3, the "delay" time of the mobile pulse, i.e. its position in the repeating sequence, is drawn as the abscissa. Fig. 3 also provides a largely self-explanatory schematic of the three pulses. As in the schematics of some later figures, the first pulse of the *subsequent* pulse packet is deliberately included, in order to better represent the *whole* duration of the unit sequence and more meaningfully portray *all* temporal relationships between pulses.

The "mobile" negative pulse ("2") is moved from a position closely following the starting

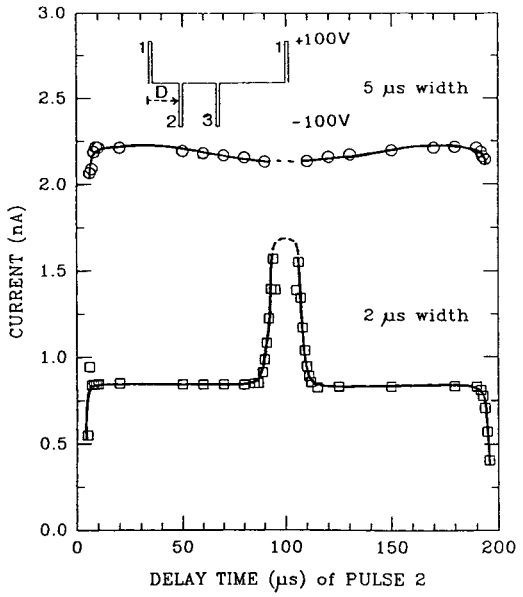

Fig. 3. Current profiles from a bipolar, triple-pulse drive, showing PR effects from +/−, −/− and −/+ pulse approaches. Pulse width: 2 or 5 μs. Pulse 1: +100 V, 1 μs delay; pulse 2: −100 V, variable delay; pulse 3: −100 V, 100 μs delay. Pulse sequence repeats every 200 μs. D = Delay time.

positive pulse ("1") to a position closely preceding, then closely succeeding the center negative pulse ("3"), to a position closely approaching the starting positive pulse (again "1") of the next sequence. That means that the mobile negative pulse will, inter alia, strike just before and just after both positive and negative stationary pulses.

What makes Fig. 3 so interesting —and what we did not fully anticipate— are these four close encounters. Their interesting aspects are most clearly conveyed by the low-current 2-μs profile —i.e. the profile of a system in which *both* recombination *and* collection of ionic species claim significant fractions of the available charge (or, using the conventional description, in which the pulses are too weak to clear the cell of electrons). In all four cases in which one pulse gets close to the next, the otherwise fairly constant current level is being severely disturbed. In each case the disturbance occurs within (very approximately) 8 μs. (Again, this is roughly comparable to the time it would take unimpeded electrons to traverse most of the ECD cell.)

This disturbance appears to be consistent, no matter whether the two pulses involved in the particular encounter are of the same or of the opposite polarity, and no matter which pulse leads and which follows. We first direct our attention to the center of the picture, where the mobile negative pulse gets close to the stationary negative pulse.

If two 2-μs negative pulses get very close to each other, we can expect them to act like one 4-μs pulse. (Although the pulser does not allow pulses to overlap or even touch, it can, of course, be used to produce an analogous 2-pulse bipolar series consisting of a 2-μs positive starting pulse and a 4-μs negative central pulse, in order to verify that the system behaves according to expectation.) But why does the mobile pulse, when it is *not* close to its centrally located companion —i.e. when it strikes somewhere else in the freely accessible regions from roughly 10 to 80 and 120 to 190 μs delay time— have so much *less* effect on the current?

The only explanation for this is that the two negative pulses, when spaced far enough from one another, allow the system to relax in the intervening time. In physical terms, this could be envisioned as a process in which some of the electrons, having been pushed by the first negative pulse into the channel leading to the anode —but not far enough through to be immediately collected— are both pulled back (by the positive space charge they left behind) and pushed back (by their own negative space charge) before the second negative pulse strikes.

However, if the second negative pulse should strike *immediately* after the first, the electrons can not be pushed/pulled back but are rather given another push forward to the anode for collection. Since collection, when it occurs, is irreversible, closely spaced negative pulses (with no relaxation intervening) collect a larger current than widely spaced ones do.

If the result of closely spaced pulses of equal (negative) polarity is a relative increase in current, the experiment shows that the result of closely spaced pulses of opposite polarity is a relative decrease. Mechanistically, however, the

precipitous current decrease at the edges of Fig. 3 seems to make no sense —unless one were to invoke a substantial increase in reversed-field current, i.e. an a.c. contribution that the d.c. electrometer could not sense. But this is most unlikely to happen and we do not believe that it does. Rather, we believe that an increasing fraction of electrons simply fail to be collected under these circumstances.

But why should electrons fail to be collected just because a positive pulse struck very shortly before or after the negative pulse? The result seems particularly puzzling in the latter case: since it is the negative pulse that pushes electrons toward collection, and since collection is final, what conceivable difference could a subsequently occurring positive pulse make? It was this mechanistic question, plus the (in hindsight) potential analytical importance of the system, that enticed us to investigate the topic in greater experimental detail.

3.3. A closer look at PR regions

To define and explore the regions in which PR occurs, a simple bipolar regime was set up in which the two pulses were of equal width and amplitude. The (collecting) negative pulse was perceived as "stationary", the (disturbing) positive pulse as "mobile". The positive pulse could thus exert its influence on the negative pulse either by closely following or by closely leading it. The resulting current profiles from four such regimes, which differ only in their + / − 10, 20, 50 and 100 V pulse amplitudes, can be found in Fig. 4. (Several more regimes were tested and behaved similar to the ones shown. The additional horizontal line in each graph indicates the current level found by applying the negative pulse only.)

At low voltages, the current drops dramatically when the "disturbing" positive pulse closely leads or follows the "collecting" negative pulse. Fig. 5 shows an estimate (using the first and last data points from Fig. 4) of the percent current remaining when the positive pulse follows (" − / + ", left side of Fig. 4) or leads (" + / − ", right side of Fig. 4) the negative pulse. In two of the

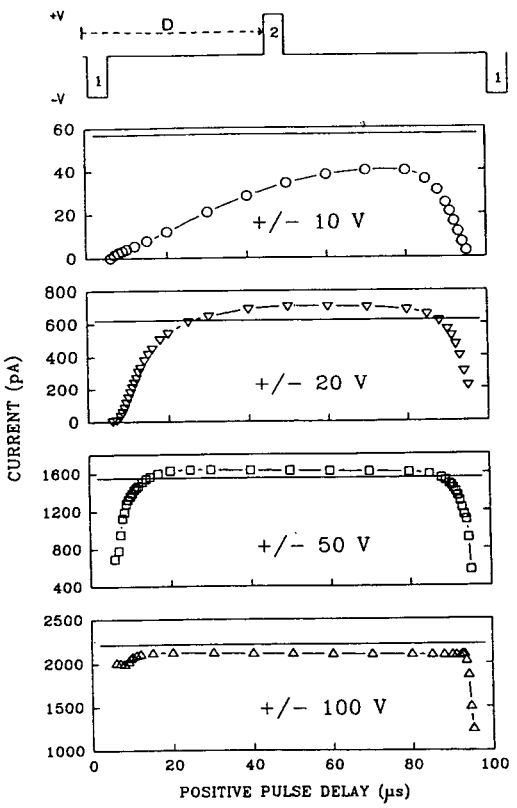

Fig. 4. Current profiles from a bipolar, dual-pulse drive, showing polarization/relaxation effects from close − / + and + / − pulse approaches. Pulse width: 5 μs; pulse amplitude: + / − 10, 20, 50 or 100 V. Negative pulse delay: 1 μs; positive pulse delay: variable. Pulse sequence repeats every 100 μs. The horizontal line indicates the corresponding unipolar (negative pulses only) current level. Maximum d.c. current: 2.88 nA. D = Delay time.

former cases, the current profile actually runs smack into zero: a surprisingly strong showing for a polarization effect.

3.4. First pulse configuration: negative leads positive

How can a complete or even a partial current reduction be rationalized? If we consider first the left side of the graphs shown in Fig. 4 —i.e. where the negative pulse *leads* the positive pulse— the only reasonable explanation that we can think of is that the electrons were transported from the polarizing foil chamber into the

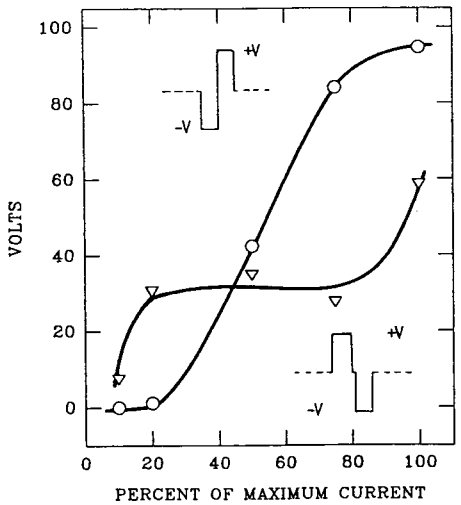

Fig. 5. Approximate current, expressed as percent of maximum, which remains during −/+ and +/− pulse encounters. Data from Fig. 4 (plus one additional point).

central channel and on into the collecting-electrode chamber, but that they did not actually reach the anode during the negative pulse. (The fact that the Tracor ECD has a two-chamber construction with the anode, similar to the foil, being of relatively large and cylindrical shape [26], may have benefitted the experiment. It certainly supports the assumed scenario: the imposed-field gradient must be quite steep through the channel but quite gentle in its approach to the two electrodes.)

If no positive pulse were to follow, some of the electrons, driven by their own negative space charge in the essentially unipolar environment of the collection chamber, would migrate to the collecting electrode. Some might also return through the boron nitride channel to the foil chamber, being pushed this way by their own negative space charge in the collection chamber, and being pulled there by the net positive, much slower dissipating space charge of the plasma.

If, however, the positive pulse should hit before the system has had time to thus relax, *most* of the electrons would be forced to return to the foil chamber (to wait there for recombination or for the arrival of the next negative pulse). It seems obvious, however, that this process can come into its own only if the pulses are so weak that they are barely able to force the electrons from the plasma into the channel: this should therefore occur at conditions of low voltage and correspondingly low overall current. Under these conditions, the concentrations of cations and electrons must be close to their steady-state maximum in the foil chamber.

If, on the other hand, the pulses are strong enough to drive most electrons right into the anode —where they are irreversibly collected— then the subsequent positive pulse can no longer reverse the electron flow. This should occur at conditions of high voltage and correspondingly high overall current. Figs. 4 and 5 are in essential agreement with this push/pull scenario.

3.5. Second pulse configuration: negative follows positive

We can now consider the "right side" of the graphs shown in Fig. 4, where the negative pulse *follows* the positive pulse. Here we can assume that the positive pulse merely polarizes the charge distribution in the foil chamber, since it is too weak to push larger numbers of cations into the collection chamber and electrons into the foil. (This assumption is strongly supported by the huge difference in impedance between reversed-field and regular-field operation in the Tracor ECD [1,2], as well as by response results to come.

If the subsequent negative pulse then strikes before the system has had time to relax, it would need double strength to overcome the polarization *and* push the electrons through the channel into the collection chamber. Since the two pulses are of matched amplitude in each experiment, one would expect this effect to be less dependent on voltage. Figs. 4 and 5 bear this out.

3.6. Third pulse configuration: positive in the middle

The speculations above provide a reasonable answer to the riddle of the current that disappeared at the left and right sides of the Fig. 4 plots, but they still do not address the outright

paradox of the current in the middle. The paradox is this: in the cases of + / − 20 and + / − 50 V pulsing, the bipolar current is *larger* than the negative unipolar current. How can the latter, which is driven by negative pulses, *increase* when *oppositely* directed positive pulses are added? And, no, the effect is not an electronic artifact, and neither is it negligible: the bipolar regime, with the positive pulses striking right between the negative pulses, collects 13 and 5% more current at + / − 20 and 50 V, respectively, than the corresponding unipolar regime of negative pulses only. But why?

The only "explanation" we can give here is, admittedly, speculative. It involves the highly concentration-sensitive *second*-order recombination reaction, e.g.

$$N_4^+ + e^- \rightarrow 2N_2$$

This reaction is fundamental to the ECD and, in conjunction with the activity of the radioactive foil, determines the maximum possible concentration of electrons in the (clean) ECD [25,27]. Although electron concentrations are often by custom (really: by necessity) calculated on the "stirred reactor" model, it is obvious that the distribution of ion pairs in the ECD is heterogenous over long stretches (detector dimensions), owing to the short, roughly exponential distribution of ion pairs generated by ^{63}Ni βs. In other words, a relatively thin layer of relatively dense plasma lines the radioactive foil in the case of ^{63}Ni [28], and the situation is even more extreme in the case of ^{3}H [29].

Therefore, any process that polarizes (pulls opposite charges apart) and/or homogenizes (evens out charge concentrations across the cell) will result in a shorter- or longer-term decrease in the highly concentration-sensitive, overall rate of recombination, i.e. it will allow overall higher charged-particle concentrations to exist. And this is, of course, what the positive pulse does: it pulls electrons toward and pushes cations away from, the radioactive foil. The resulting increase in the overall electron concentration allows a larger current to be later collected. Note that the largest observed increase in current as a percentage of the total (about 13%), seems roughly commensurate with the relaxation time as a percentage of the repetition time (the former being estimated from the left- and right-side descent of the + / − 20 V profile in Fig. 4).

That the process is voltage dependent is experimentally obvious. But why in this manner? To answer we first need to consider the location, concentration and fate of charged particles under a unipolar pulse regime.

At a very *low* voltage, the current is also very low. That means that few charged particles (ion pairs) are collected; most simply recombine. The physical position of cations changes little, i.e. their time-averaged spatial distribution closely approximates the spatial distribution of ionization events. The concentration of charged particles is close to the maximum possible; i.e. it is close to that of the steady state of ion-pair generation vs. ion-pair recombination. In other words, recombination proceeds close to its highest attainable rate. (We recognize that some of the statements above and below are tautologous; however, we need to set the stage for discussions to follow.)

At a very *high* voltage, the current is close to its maximum. Most charged particles are collected; very few recombine. The average cation position lies between the place of generation and the place of collection (the foil). The cation sheath is thus contracted (compared to low- or no-voltage conditions). The concentration of charged particles is low, and so is the rate of recombination. (In this context, note that the repetition time is more than an order of magnitude shorter than the time the system needs to establish steady state [3].)

Let us now disturb these charged-particle distributions with a pulse: first at the very low, then at the very high voltage setting.

At the very *low* voltage setting —which is dominated by ion-pair generation and distribution— the effect of the disturbing pulse on the overall plasma distribution must be minimal. (The rate of ion-pair generation is far higher than the rate of ion-pair collection.) In contrast, the disturbing pulse affects the collection process much more strongly. Electrons that do not make it to the electrode while the negative pulse is on, have a high chance of recombining with the

greater number of wider distributed cations (all in comparison with the high-voltage regime). When the time allowed for relaxation is too short (left and right side of Fig. 4, + / − 10 V), the number of collected electrons (the current) is thus severely curtailed. The effect is so strong and spreads so far in time that the bipolar current stays below the unipolar current even in the middle of the plot.

At the very *high* voltage setting —which is dominated by ion pair collection— the effect of the disturbing pulse on the charged-particle distribution could be strong and that should decrease the recombination rate. However, the recombination rate is already at a very low level (the rate of ion-pair collection is close to the rate of ion-pair generation). Thus the effect must remain small. Single negative pulses are, however, now strong enough to drive electrons right into the anode. This is an irreversible process that preempts any subsequent relaxation. The regions of close pulse approaches (left and right side of Fig. 4, + / − 100 V) become therefore much less pronounced. Thus the bipolar current should be close to the unipolar current in the middle of the plot. However, because of its high voltage, the positive pulse also collects a small but significant *reverse* current that, monitored through the slow electrometer, makes the bipolar current appear smaller than the unipolar one.

At *intermediate* voltage settings, finally, the numbers of collected ion pairs is very roughly comparable to the number of recombined ion pairs. The system is not dominated by either a close-to-maximum recombination rate as in the low-voltage case, nor by a close-to-maximum collection rate as in the high-voltage case. This gives the positive pulse the chance to disturb the charged-particle distribution enough to depress the recombination rate, without exerting too much counterproductive influence on current collection from the (now higher) overall concentration of charged particles.

3.7. Current profiles under PR conditions

Similar information, accepting of similar explanations, is shown in the next three figures. These figures offer, however, a more complete database and a more convenient picture for use in the later studies of response. Fig. 6 shows the percentage of maximum bipolar vs. unipolar current with other conditions as in Fig. 4. The region where the former exceeds the latter is rather prominent: it leaves little doubt about the existence of a current paradoxically strengthened by pulses that oppose it.

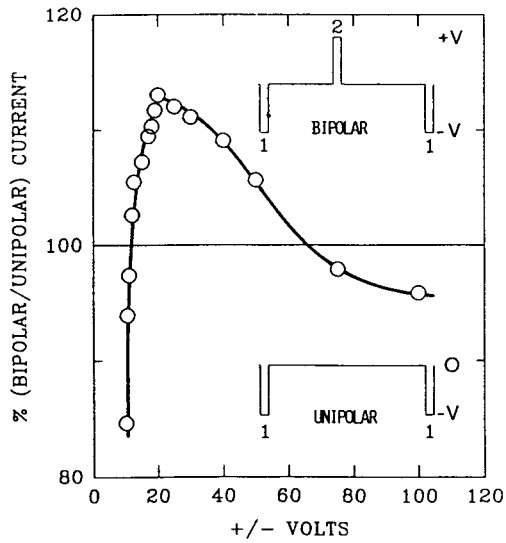

Fig. 6. Maximum current from a bipolar drive, expressed as percent of (negative) unipolar-drive current, as dependent on pulse amplitude. Pulse width: 5 μs. Pulse sequence repeats every 100 μs.

Figs. 7 and 8 show how the strength of the positive pulse influences the current under various circumstances: Fig. 7 in terms of positive-pulse *width* (with similar amplitudes for positive and negative pulses); Fig. 8 in terms of positive-pulse *amplitude* (for three different levels of negative-pulse strength). Note the relative position of the maxima in Fig. 7, which roughly conforms to expectations based on the value of the time-integrated positive voltage. Note also in Fig. 9 that the (negative) low-level current strengthens (thus showing the discussed paradoxon from a different angle), while the high-level current weakens, as the amplitude of the positive pulse increases. Figs. 6–8 are, of course, consistent with the data of, and explanations for, Figs. 4 and 5.

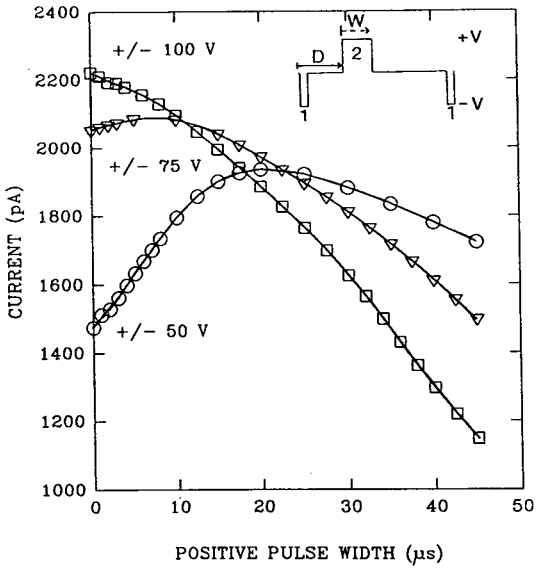

Fig. 7. Current profiles from a bipolar drive, showing the effect of increasing positive pulse width at three voltage levels. Pulse amplitudes + / − 50, 75 or 100 V. Pulse 1: negative, delay 1 μs, width 5 μs; pulse 2: positive, delay 30 μs, width variable. Pulse sequence repeats every 100 μs.

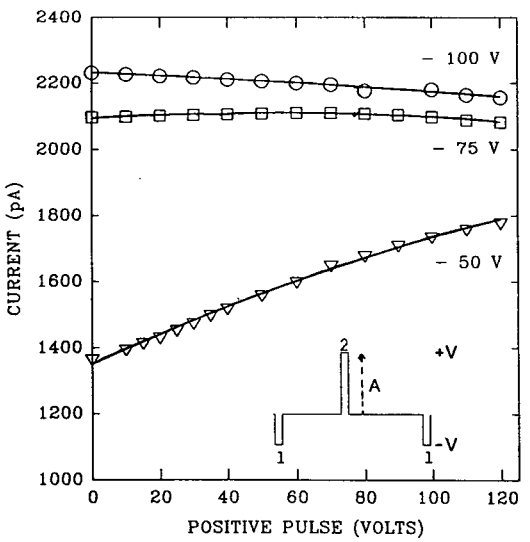

Fig. 8. Current profiles from a bipolar drive, showing the effect of increasing positive-pulse amplitude at three negative-pulse voltage levels. Pulse width 5 μs. Pulse 1: amplitude −50, 75 or 100 V, delay 1 μs; pulse 2: amplitude variable, delay 50 μs. Pulse sequence repeats every 100 μs.

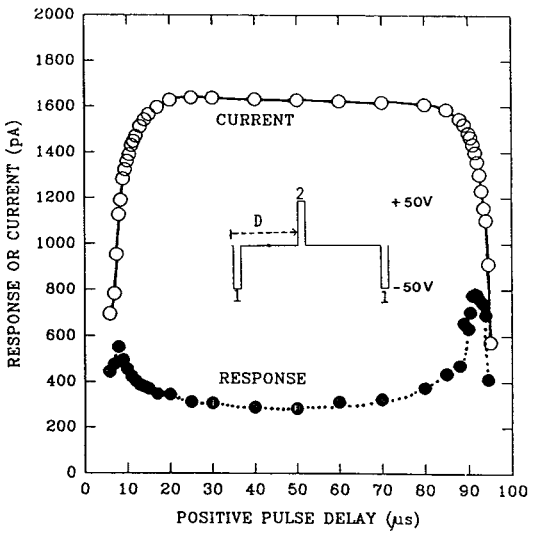

Fig. 9. Current and (inverted) response profiles from a bipolar drive, showing the effect of positive-pulse position (delay time). Pulse amplitude: + / − 50 V, pulse width: 5 μs. Pulse sequence repeats every 100 μs, i.e. the repetition frequency is 10 kHz. Analyte: 5 pg α-hexachlorocyclohexane.

3.8. Response profiles under PR conditions

We now have accumulated the necessary understanding of the system's behavior when analyte is absent: it allows us to proceed to the more difficult situation that arises when analyte is present. Two relevant circumstances come to mind.

First, since response to analyte in a constant-frequency regime represents the vertical distance between "baseline" and "peak" current profiles, it is usually strongest where the current profile shows the steepest slope. This would suggest that the best-responding regions should be those where the positive pulse moves close to the negative one (the extreme left and right sides in the graphs of Fig. 4).

Second, from what has been said before, it appears likely that a bipolar system could "store" a higher overall concentration of electrons in the cell than the conventional unipolar one. This is important in terms of linearity. If we formally assume that the rate of the analyte's electron-capture reaction, e.g.

$$A + e^- \rightarrow A^-$$

is proportional to the response seen on the recorder, then an analyte depleting the electron concentration will cause the calibration curve to become non-linear.

Although this is readily apparent from first principles, it is difficult to formulate in a quantitative manner because of the periodic and —in its temporal consequences for ion concentrations and space charges inside the ECD— poorly understood mechanics of current collection. Operating within the first 5% of standing current is often thought to assure the analyst linear range. (This rule-of-thumb presumes, inter alia, that each single pulse is strong enough to collect all free electrons.) An earlier simulation of ours for such a case yielded indeed a value of about 3 to 4%. Using approximately $10^{1/2}$% of the standing current thus lets the analyte stay below 10% deviation from linearity for "homogeneous" kinetics [27]; yet we believe this not to be applicable to the relatively large and heterogeneous two-chamber Tracor ECD. Some detectors like the Tracor ECD clearly do much better: linear ranges up to a third or a even a half of the standing current can be observed. Obviously, however, such excessive behavior has been difficult to reconcile with presumed ECD kinetics.

From an analytical viewpoint, if a bipolar ECD really allows the average electron concentration to rise above that of a comparable unipolar ECD, then the former may have the chance to produce a longer linear range. Or, from a mechanistic viewpoint, if the linear range of a particular calibration curve should indeed turn out to be longer than usual, then this may indicate a higher-than-expected electron concentration inside the ECD.

Fig. 9 shows the by now familiar current profile, together with the corresponding response profile as obtained by repeatedly injecting 5 pg of a strong electron capturer. Expectedly, the response profile shows maxima both on the left and on the right side of the plot (wherever the current profile steeply descends). The right-side response maximum, with the positive pulse preceding the negative one, is usually the stronger of the two —not surprisingly so in light of the earlier discussions— and it is therefore used for all later figures.

The process of a positive (i.e. reversed-field) pulse striking just *before* the negative one, has, to our knowledge of the published literature, never before been investigated for mechanistic —never mind analytical— reasons. Investigating it would, indeed, seem to make little sense if the investigator happened to believe that electrons move unimpeded at all times and that negative pulses remove all electrons from the system: If the leading positive pulse skimmed electrons off the top before the following negative pulse has had a chance to herd them to the anode, the standing current would drop —and so would the response. Even if the positive pulse had no such effect, what good would it do to use it?

3.9. ECD diagnostics and performance characteristics in the PR realm

At the delay time of maximum response —i.e. with a pattern of bipolar pulses roughly optimized for the 10 kHz repetition frequency— current and response of the system were measured for different voltage levels. The strangely familiar looking result is shown in Fig. 10. What makes it look familiar is, of course, its resemblance to conventional current–voltage curves for d.c. and unipolar-pulsed ECD modes. The maximum of the response curve occurs at the "knee" position of the current curve; and we expect —though we have not ascertained— that it would move slightly to the right with larger amounts of analyte, in analogy to d.c. ECD behavior (e.g. [1], Fig. 8).

It seems reasonable to suspect that this response is *hyper*coulometric; meaning that e/m, the ratio of (apparently) captured electrons to analyte molecules, exceeds unity. To confirm this suspicion, the right-side ordinate offers a (hyper)coulometric ratio scale. Note that the hypercoulometric ratio, as defined here, is easily determined on a single peak from a single ECD, by dividing the peak's area in faradays (moles of electrons) by the moles of analyte injected. (This "hypercoulometric ratio", as we have been

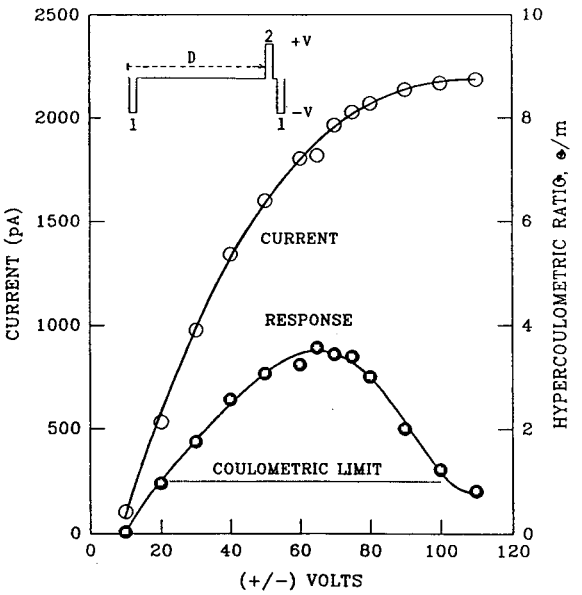

Fig. 10. Current and (inverted) response profiles from a bipolar drive at the + / − (right side) response maximum, showing the effect of pulse amplitude. Pulse width: 5 μs. Pulse 1: negative, delay 1 μs; pulse 2: positive, delay 93 μs. Pulse sequence repeats every 100 μs, i.e. frequency = 10 kHz. Analyte: 5 pg α-hexachlorocyclohexane.

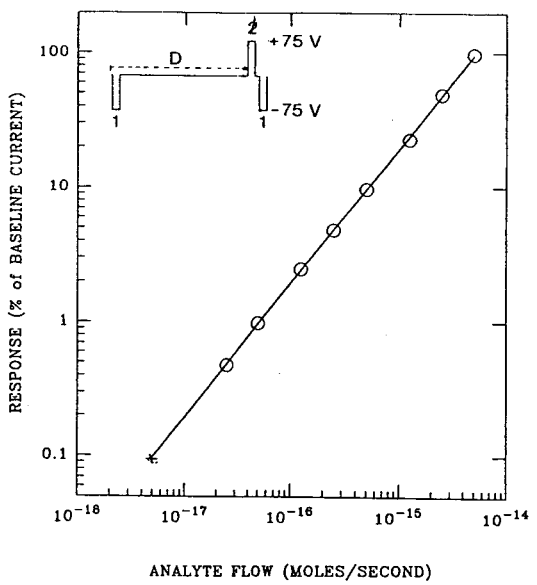

Fig. 11. Calibration curve of α-1,2,3,4,5,6-hexachlorocyclohexane from a constant-frequency (10 kHz) bipolar drive, at the + / − (right side) response maximum. Pulse amplitude + / − 75 V, pulse width 5 μs. Pulse 1: negative, delay 1 μs; pulse 2: positive, delay 93 μs. The lowest point is extrapolated; it marks the $S/N_{p\text{-}p} = 2$ detection limit. Extrapolate farther down to an ordinate value of ca. 0.03 for the $S/\sigma = 3$ detection limit.

[1,27,30] using the term, differs —in principle and in practice— from the "hypercoulometric ratio" or "hypercoulometry factor" used in the interesting work of Lasa et al. [31,32], which relates to the behavior of *two* ECDs connected in series.)

The hypercoulometric response of this study, i.e. e/m ≈ 3.5 by our definition, is better than any *bipolar* result obtained so far [4,7]; although it is still dwarfed by the e/m ≈ 50 of a d.c. system run under elevated pressure on the same detector [33].

The calibration curve prevailing at these hypercoulometric conditions is shown in Fig. 11. It is drawn at precisely unity slope; demonstrating thereby that the response remains linear over the *entire* standing-current range. The line starts at about 0.1% of standing current at the extrapolated $S/N_{p\text{-}p} = 2$ detection limit. [$N_{p\text{-}p}$ is the peak-to-peak noise of the baseline with drift and spikes excluded, at an resistance–capacitance (RC) filter time constant of about 1 s.] The detection limit for α-1,2,3,4,5,6-hexachlorocyclohexane, at the $S/N_{p\text{-}p} = 2$ definition, is typically about $2 \cdot 10^{-14}$ g or $5 \cdot 10^{-18}$ mol/s (divide these numbers by about 3 [34] to obtain the $S/\sigma = 3$ detection limit).

The detection limits, while more than adequate, are however far less important and certainly much less surprising than the perfect linearity shown by Fig. 11. The actual peaks, some of which are reproduced in Fig. 12, look strangely cropped: the recorder pen rose straight to the zero-current line where it banked off as sharply as if it had hit the end of the recorder range (which, of course, it did not).

Even at less favorable pulsing conditions, a large degree of linearity is maintained. For instance, if a delay time of 7 μs is chosen (corresponding to the *left*-side maximum of Fig. 9, but otherwise conforming to the conditions of Fig. 11), the linearity extends to about 80% of

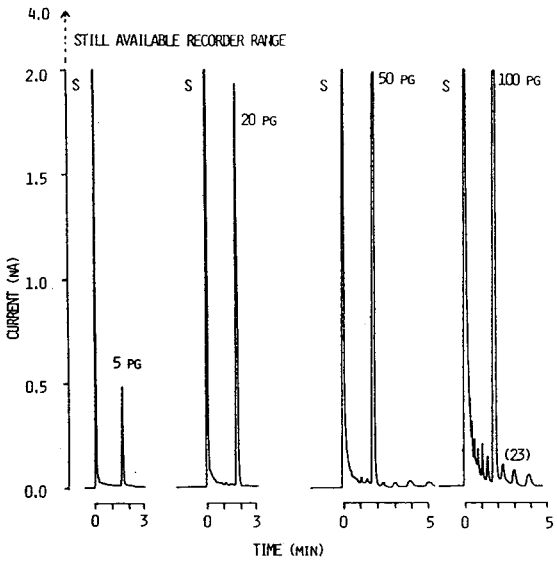

Fig. 12. Chromatograms obtained during measurement of the upper calibration range (Fig. 11) and beyond, of 5–100 pg of α-1,2,3,4,5,6-hexachlorocyclohexane as indicated, using a constant-frequency bipolar drive and showing the total consumption of the standing current in mid-recorder range. The additional peaks, which appear strongest in the right-side chromatograms, are oxidation products of the solvent (S) hexane (cf. [23]).

standing current; if a delay time of 50 μs is chosen (corresponding to the middle of Fig. 9), the linearity still reaches about 70%.

3.10. Some further speculations

It is therefore reasonable to speculate —in view of earlier considerations dealing with the kinetic order of electron capture— that there must exist in the bipolar ECD a "storage facility" for, and hence an unexpectedly high concentration of, electrons (as always, of course, accompanied by cations). Only then can the overall second-order electron-capture reaction appear, as it does in Fig. 11, in the pseudo-first-order form of a calibration curve that is linear right up to the point where the electron current is completely exhausted. If our speculation is correct, then indeed the main role of the positive pulse is to help "store" electrons in the system.

It may be argued that this evidence of a vastly extended linearity only appears so convincing because "linearity" traditionally refers to the *standing* (baseline) current —and standing currents vary greatly, of course, among the various (optimized) ECD modes. So, to buttress the evidence for extended linearity, we have calculated the linear ranges of three ECD modes not only as percentages of their individual standing currents, but also as percentages of the total number of electrical charges generated, i.e. of the "*maximum* d.c. current". The results are shown in Table 1.

In Table 1, the d.c. and unipolar-pulse driven electron-capture linearities appear relatively similar when listed as fractions of the maximum d.c. current; the bipolar-pulsed electron-capture linearity, in contrast, extends over twice that range —in fact until it can no longer be physically measured. This suggests that the positive pulse does indeed allow the regime to "store" a higher than usual concentration of electrons. We speculate that it does so by inducing a temporary spatial distribution that protects some electrons from being collected and that, at the same time, protects some electrons from being neutralized by cations. Note that recombination is a second-order reaction, which is highly sensitive to (local) changes in concentration.

The numbers of Table 1 indicate also —if kinetic linearity principles obtain— that some "storage"-like effect occurs even in d.c. and pulsed unipolar systems. To pursue this argument further would, however, take us beyond the objectives of this study. It should also be pointed out in this context (as well as in the

Table 1
Current-related linear ranges in the tractor ECD

Polarisation mode[a]	Linearity as % of:	
	Maximum d.c. current	Baseline current
d.c.	28	34
Pulsed unipolar	34	47
Pulsed bipolar	(68)[b]	100

[a] All constant voltage, constant frequency.
[b] Baseline current limited.

general context of ECD characteristics and performance) that different commercial ECDs are of very different construction and that, therefore and so far, the described behavior patterns and trends *should be considered valid only for the two-chamber Tracor ^{63}Ni ECD*. Furthermore, we squeezed the analytical figures-of-merit from a squeaking clean (though two-decades old) ECD. If —for purpose of simulating ECD performance in, say, a typical pesticide residue laboratory— our detector had been given daily loads of dirty samples, it might have proved less obliging.

Whether and to what extent PR effects can be found and used in other detectors; and whether, perhaps, new detector constructions could maximize and capitalize on such PR, is at present an open question. The perfect linearity found in the Tracor ECD is, of course, very interesting —but its linear range, a full three orders of magnitude, may still be less than that of a good *constant*-current system. One particular constant-current system has, in fact, been coaxed to respond linearly over almost six (!) orders of magnitude [35]. On the other hand, most constant-current systems produce far shorter linear ranges (cf. [11]) and, in addition, are wont to cause a non-linearity problem with strong capturers (e.g. [22]). To our experience, and judging from explanations of the phenomenon advanced so far, this problem should not occur in the bipolar-pulsed, constant-frequency system of this study.

On strictly formal grounds, and over much of the calibration range, the unipolar *constant-current* system could be said to achieve linearity by rationing the supply of electrons to the capture reaction. The bipolar *constant-frequency* system, on the other hand, achieves the same purpose —or so we speculate— by supplying electrons in excess. Of course, to have available an excess of electrons also benefits response, as the clearly hypercoulometric performance and the related, quite respectable detection limit demonstrate.

Acknowledgements

We thank Professor D.R. Arnold for agreeing to donate a spare terminal, and the National Science and Engineering Research Council of Canada for continuing to support our research.

References

[1] W.A. Aue and S. Kapila, *J. Chromatogr.*, 188 (1980) 1.
[2] K.W.M. Siu and W.A. Aue, *J. Chromatogr.*, 392 (1987) 143.
[3] A.W. McMahon, *Ph.D. Thesis*, Dalhousie University, Halifax, 1987.
[4] A.W. McMahon and W.A. Aue, *Mikrochim. Acta*, III (1988) 11.
[5] K.W.M. Siu and W.A. Aue, *J. Chromatogr.*, 268 (1983) 273.
[6] A. Zlatkis and C.F. Poole (Editors), *Electron Capture* (*Journal of Chromatography Library*, Vol. 20), Elsevier, Amsterdam, 1981.
[7] M. Dressler, *Selective Gas Chromatographic Detectors* (*Journal of Chromatography Library*, Vol. 36), Elsevier, Amsterdam, 1986.
[8] E.D. Pellizzari, *J. Chromatogr.*, 98 (1974) 323.
[9] W.A. Aue and S. Kapila, *J. Chromatogr. Sci.*, 11 (1973) 255.
[10] E.P. Grimsrud, in H.H. Hill and D.G. McMinn (Editors), *Detectors for Capillary Chromatography*, Wiley, New York, 1992, Ch. 5.
[11] J. Connor, *J. Chromatogr.*, 200 (1980) 15.
[12] E.P. Grimsrud, *Mass Spectr. Rev.*, 10 (1992) 457.
[13] S.O. Farwell, D.R. Gage and R.A. Kagel, *J. Chromatogr. Sci.*, 19 (1981) 358.
[14] W.E. Wentworth, E. Chen and J.E. Lovelock, *J. Phys. Chem.*, 70 (1966) 445.
[15] M.W. Siegel and M.C. McKeown, *J. Chromatogr.*, 122 (1976) 397.
[16] A. Neukermans, W. Kruger and D. McManigill, *J. Chromatogr.*, 235 (1982) 1.
[17] W.A. Aue, K.W.M. Siu and S.S. Berman, *J. Chromatogr.*, 395 (1987) 335.
[18] J.L. Pack and A.V. Phelps, *Phys. Rev.*, 121 (1961) 798.
[19] R. Simon and G. Wells, *J. Chromatogr.*, 302 (1984) 221.
[20] S.W. Warden, R.J. Crawford, W.B. Knighton and E.P. Grimsrud, *Anal. Chem.*, 57 (1985) 659.
[21] P.L. Gobby, E.P. Grimsrud and S.W. Warden, *Anal. Chem.*, 52 (1980) 473.
[22] J.E. Lovelock and A.J. Watson, *J. Chromatogr.*, 158 (1978) 123.
[23] E.R. Rohwer, G.-C. Chen and A.J. Hassett, *J. High Resolut. Chromatogr.*, 16 (1993) 561.
[24] K.W.M. Siu, S.S. Berman and W.A. Aue, *J. Chromatogr.*, 391 (1987) 433.
[25] K.W.M. Siu, S. S. Berman and W.A. Aue, *J. Chromatogr.*, 408 (1987) 53.
[26] *Manual, Electron Capture Detector*, Tracor, Austin, TX, 1972.

[27] W.A. Aue, K.W.M. Siu, D. Beauchemin and S.S. Berman, *J. Chromatogr.*, 500 (1990) 95.
[28] K.W.M. Siu and W.A. Aue, *Can. J. Chem.*, 65 (1987) 1012.
[29] A.W. McMahon and W.A. Aue, *Mikrochim. Acta*, II (1987) 91.
[30] W.A. Aue and S. Kapila, *J. Chromatogr.*, 112 (1975) 247.
[31] J. Lasa, I. Sliwka and B. Drozdowicz, *Chromatographia*, 32 (1991) 248.
[32] J. Lasa, B. Drozdowicz and I. Sliwka, *Chromatographia*, 38 (1994) 304.
[33] S. Kapila and W.A. Aue, *J. Chromatogr.*, 118 (1976) 233.
[34] X.-Y. Sun, H. Singh, B. Millier, C.H. Warren and W.A. Aue, *J. Chromatogr. A*, 687 (1994) 259.
[35] J.J. Baum and C. Josias, presented at the *27th Pittsburgh Conference, Cleveland, OH, March 1976*, abstract 437.

ELSEVIER

Journal of Chromatography A, 689 (1995) 63–68

JOURNAL OF CHROMATOGRAPHY A

High-precision gas chromatography–combustion isotope ratio mass spectrometry at low signal levels

Keith J. Goodman, J. Thomas Brenna*

Division of Nutritional Sciences, Cornell University, Ithaca, NY 14853, USA

First received 30 August 1994; revised manuscript received 7 October 1994

Abstract

Precision and accuracy of gas chromatography–combustion isotope ratio mass spectrometry are investigated for sample levels down to about 5 pmol C in fatty acid methyl ester mixtures spanning 1000-fold in concentration. Precision and accuracy of isotope ratios diverge rapidly for conventional summation methods, and become unusable below 30 pmol material on column. At lower levels, mean isotope ratios were statistically different from reference values indicating bias as well as poor precision. In contrast, curve fitting, using the exponentially modified Gaussian line shape, gives improved precision for most peaks and useful results down to 3 pmol. The curve-fitting algorithm was also less sensitive to signal integration time than the summation method. These data indicate that curve fitting may be the method of choice for integration of noisy data when high-precision isotope ratios are desired.

1. Introduction

High-precision gas [1,2] (or liquid [3,4]) chromatography–combustion isotope ratio mass spectrometry (xC–C-IR-MS) for analysis of C or N isotopes [5,6] is gaining importance across many areas of natural science [7]. These techniques facilitate the analysis of individual compounds at very small sample sizes, with precision levels approaching that of conventional dual inlet [8]. Most applications take advantage of these improved parameters, as well as the capability to rapidly obtain high-precision compound-specific results without cumbersome chemical separation prior to analysis (e.g. Refs. [9–11]). However, a wide variety of applications require the analysis of complex mixtures, inevitably involving overlapping peaks. We previously reported that the conventional summation integration algorithm produces systematic bias at degrees of overlap as low as 10% valley, even for compounds of well matched isotope ratio (e.g. $\Delta\delta^{13}C < 0.5$) [12]. Most notably, this bias is observed while high precision is maintained. Further, isotope ratios for minor components (< 10 ng) are seldom calculated because of overlaps and the well known difficulties in defining peak start/stop in low signal-to-noise ratio (S/N) cases. This is true even though high-precision results ($\delta^{13}C < 0.5$) can be achieved for sub-ng sample sizes under ideal circumstances [8].

We have recently shown that curve fitting can be effective in recovering accurate isotope ratios from severely overlapping peaks while preserving high precision [12]. Curve-fitting methods are known to be more resilient to low S/N than

* Corresponding author.

0021-9673/95/$09.50
SSDI 0021-9673(94)00969-4

summation algorithms, where peak definition is most difficult [13–15]. Analysis of low levels by GC–C-IR-MS is of particular interest for tracer studies where precision as poor as $\delta^{13}C < 100$ is useful for detecting enriched metabolites [2]. We report here a systematic study comparing curve fitting to conventional summation for well-resolved small sample injections over four orders of magnitude in single GC–C-IR-MS chromatograms.

2. Experimental

2.1. Instrumentation

A Varian 3400 GC system interfaced to a Finnigan MAT 252 high-sensitivity gas isotope ratio mass spectrometer via a combustion interface was used for this study. The instrument was operated at an accelerating potential of 8 kV and a source pressure of $2 \cdot 10^{-6}$ Torr (1 Torr = 133.322 Pa). Briefly, the effluent of the capillary column is directed to a combustion furnace held at 850°C and loaded with CuO as a source of O_2. Combustion products are dried and pass through an open split prior to entrance to the IR-MS ion source. CO_2 is monitored continuously at m/z 44, 45 and 46 with three dedicated faraday cups and associated electronics. Asymmetric peak shapes are commonly observed because of the numerous connections and changes in capillary diameter between the GC column and the mass spectrometer. Details of the system can be found elsewhere [2].

A fatty acid methyl ester (FAME) standard mixture was separated on a J & W (Folsom, CA, USA) DB-23 capillary column, (30 m × 0.32 mm I.D., 0.25 μm film). Carrier flow through the GC column was 45 cm/s He (99.999 + %), with in-line O_2 and H_2O traps. Fatty acid standards were obtained from Sigma (St. Louis, MO, USA) and were 99 + % pure by GC analysis. Hexane (Fisher Optima grade) was used whenever solvent was necessary, and samples were stored in glass vials with Teflon-lined caps. The test mixture was composed of methyl pentadecanoate (Me15:0), methyl heptadecanoate (Me17:0), methyl octadecanoate (Me18:0) and methyl heneicosanoate (Me21:0) at concentrations of about 0.16, 1.6, 16 and 160 ng/μl, respectively. Injections of 0.5 μl of this mixture were made in splitless injection mode. A second, equimolar mixture of these compounds (0.2 μg/μl each) was prepared and analyzed separately to establish reference isotope values for each compound.

The vendor-supplied data acquisition system collects a signal from each mass channel simultaneously for adjustable integration times. At the conclusion of an integration period, a counter is queried, zeroed, and restarted, giving a >99% duty cycle. Any particular integration time is a tradeoff between noise per data point and faithful reproduction of lineshape. Longer integration times improve S/N for each data point, but distort lineshape. This distortion can be important for accurate curve fits, as well as for precise definition of peak start/stop for summation. The test mixture was analyzed using integration times of 0.25, 0.125 or 0.0625 s to investigate the effect of this parameter on summation and on curve-fitting peak integration approaches. Four or five replicates were made at each integration time.

2.2. Data processing

The vendor-provided software "ISODAT" (Finnigan MAT, Bremen, Germany) was used to process the data by the summation method. A review of this software has been published recently [16]. Slope sensitivity (SS) for peak start/stop definition is set by the user. A rolling five-point linear least squares fit is applied to the chromatogram, with peak start defined when the slope exceeds the SS; stops are defined as the point beyond the peak where the slope falls below the absolute value of the SS. SS settings chosen to detect strong peaks and reject spurious noise-related peaks do not satisfactorily detect very small peaks, while settings used to detect small peaks are overly sensitive to noise. Therefore, two separate settings for slope sensitivity were compared, SS = 0.8 mV/s for higher level detection which has performed satisfactorily in

routine applications in our laboratory over the last three years, and SS = 0.1 mV/s for low detection. Other workers report SS = 1 mV/s as satisfactory for routine analyses [8].

The commercial program Peakfit (Jandel Scientific) was used for all curve fitting. Previously, we evaluated several functions for use with GC–C-IR-MS peaks [12]. The well-known exponentially modified Gaussian (EMG) function, constructed as the mathematical convolution of the Gaussian and exponential functions [15], accurately reproduces the line shapes as long as the column is not overloaded and appears to work particularly well for low signal levels. It was used exclusively in this work. Each set of four or five chromatograms for each integration time were processed with the SS = 0.8, SS = 0.1, and curve-fit methods.

As in previous work, we calculate high-precision isotope ratios according to the following:

$$\delta 45 = \left(\frac{R_{SPL} - R_{PDB}}{R_{PDB}}\right) \times 1000 \quad (1)$$

where R_X is the ratio of integrated areas for the m/z 45 to 44 channels, SPL and PDB refer to the sample and the international standard PeeDee Belemnite, respectively, international standard with $R_{PDB} = 0.0112372$. This expression does not take into account the contribution of $^{12}C^{16}O^{17}O$ to the m/z 45 signal, which is small and in the case of GC–C-IR-MS is nearly constant. Areas are obtained by either fitting the m/z 44 and 45 channels or using the summation methods. No outliers were excluded from this data set.

Tests of statistical differences of means were performed using the t-distribution at the 95% confidence level [17].

3. Results and discussion

A representative chromatogram is presented in Fig. 1, and plotted in semilog format so that the four orders of magnitude peak intensities and background noise levels are discernable. Peak intensities above baseline range from about 2 mV for the smallest, earliest eluting peak to a high of

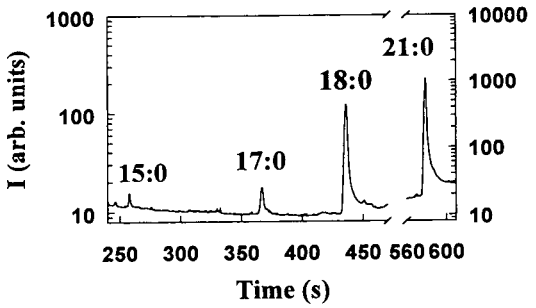

Fig. 1. GC–C-IR-MS chromatogram of the FAME test mixture plotted in semilog format.

500 mV for the most abundant but broader, latest eluting peak. There is a significant amount of chemical noise near the intensity of the smallest peak, which corresponds to 0.1% of the largest peak, Me21:0. As all FAMEs in the mixture are 99 + % pure, contaminants at this level entering the test mixture with Me21:0 are expected. Signal outputted in volts by the data system was converted to current, and peak area in nA s was calculated and used for comparison.

Deviations from reference values in $\delta 45$ units (‰) are presented in Figs. 2–4 for the individual determinations of FAMEs at the three integration times investigated. The abscissa represents signal area and is approximately logarithmic, although points have been offset horizontally for illustrative purposes. Both summation methods diverge more rapidly than the fitted data as sample size decreases for all integration times. Performance of the summation methods degrades significantly at 63 ms integration time compared with the 125 and 250 ms case. In contrast, the curve-fit performance did not degrade significantly at the lower integration time. At 200 and 2000 nA s, precisions were best at 63 ms integration time, while the lower signal levels gave slightly better results at 250 ms integration time.

Precisions for the higher SS are superior to those for the lower SS at all levels. At the lowest signal level investigated, the SS = 0.8 summation method failed to detect peaks reliably while the SS = 0.1 method produced highly inaccurate and imprecise ratios. The summation results are also seen to deviate substantially from the reference

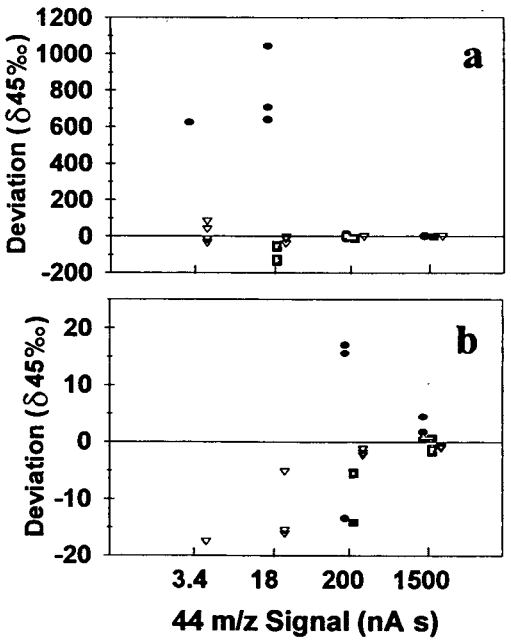

Fig. 2. δ45 deviations from reference values for 63 ms integration rate using the three different integration methods: □ = SS 0.8 mV/s; O = SS 0.1 mV/s; ▽ = curve fit. Points for SS = 0.8 mV/s and fitted data are offset their actual signal level for illustrative purposes. Data of a is plotted in b with expanded ordinate.

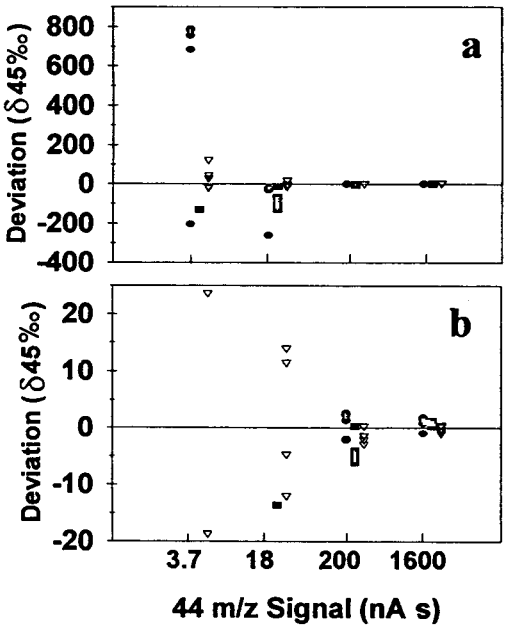

Fig. 3. δ45 deviations from reference values for 125 ms integration rate. Symbols as in Fig. 2.

levels. This observation is consistent with our previous report, and may also explain inaccuracy observed for highly enriched material at low sample levels [18]. In fact, S.D.s improve with shorter integration time for the strongest signal level.

Summary data of δ45 values are presented in Table 1, tabulated using average signal levels (in nA s), along with reference values from the equimolar mixture. Precisions (S.D.) for the reference values were all $\delta^{13}C < 0.4$ which are consistent with our routine measurements under nearly ideal GC–C-IR-MS conditions. The SS = 0.8 method detected only one peak at the lowest level across all integration times. Precisions and accuracy for the curve-fit data are superior for all but one cell.

Accuracy was assessed by statistically testing mean deviations for equivalence with zero. All of the 20 nA s deviations for the SS = 0.8 method were significantly different from zero, indicating systematic shifts in measured isotope ratio

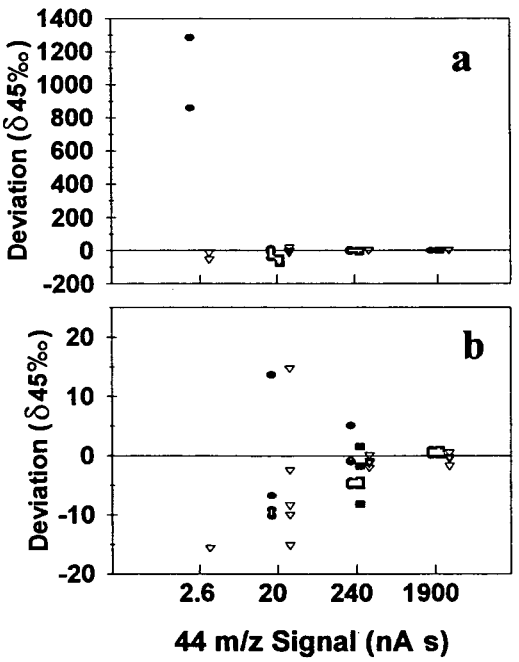

Fig. 4. δ45 deviations from reference values for 250 ms integration rate. Symbols as in Fig. 2.

Table 1
δ45 (Mean ± standard deviation)

	Average area (nA s)	δ45			
		63 ms	125 ms	250 ms	Reference
SS = 0.8 mV/s	3	(No peaks)	−156.65 ± (n = 1)	(No peaks)	−26.98 ± 0.36
	20	−126.7 ± 45.3[a]	−119.7 ± 46.2[a]	−102.1 ± 15.9[a]	−34.17 ± 0.17
	200	−27.59 ± 4.34[a]	−23.91 ± 2.47	−23.43 ± 3.64	−19.95 ± 0.27
	2000	−30.82 ± 1.16	−29.18 ± 0.42	−29.39 ± 0.46	−29.88 ± 0.23
SS = 0.1 mV/s	3	598.3 ± (n = 1)	534.3 ± 430.0[a]	1046 ± 301	−26.98 ± 0.36
	20	763.3 ± 216.2[a]	−107.9 ± 105.0	−45.69 ± 21.3	−34.17 ± 0.17
	200	−13.51 ± 17.2	−19.51 ± 2.30	−21.15 ± 4.01	19.95 ± 0.27
	2000	−28.05 ± 1.88	−64.91 ± 80.14 (−29.08 ± 1.27)[b]	−29.31 ± 0.40	−29.88 ± 0.23
Curve fit	3	−10.19 ± 54.03	0.93 ± 57.69	−63.18 ± 29.03	−26.98 ± 0.36
	20	−53.43 ± 14.85	−36.50 ± 14.72	−38.50 ± 11.52	−34.17 ± 0.17
	200	−21.65 ± 0.56[a]	−21.57 ± 1.18	−21.05 ± 0.75	−19.95 ± 0.27
	2000	−30.82 ± 0.14	−30.24 ± 0.59	−30.40 ± 0.82	−29.88 ± 0.23

[a] Statistically different from reference value ($p < 0.05$).
[b] Mean and error for SS = 0.1 mV/s (2000 nA s) excluding one aberrant determination.

for signal levels below 200 nA s using this method. The SS = 0.1 method showed significant differences for only the 63 ms integration time, but gave very large errors for all but the 250 ms integration time. At the 3 nA s level, where the higher SS failed to detect peaks, the SS = 0.1 method produced large errors ($\delta^{13}C > 300$) and statistically different mean isotope ratios. In contrast, only one of twelve fitted means is different from the reference values (63 ms, 200 nA s) at 95% confidence.

The relatively high quality of the curve-fitted data at low levels prompted investigation of the preservation of peak area with decreasing sample size, for quantitative analysis. Graded solutions of pure Me17:0 in hexane were injected at levels from about 10 pmol to 500 nmol C. Areas for the *m/z* 44 signal were obtained by each of the calibration methods and summary data are plotted in Fig. 5, in log–log format. Peak areas below about 1 nmol are not accessible in our version of the vendor software and so are not presented. The SS = 0.8 method parallels the curve-fit method to 1 nmol, while the SS = 0.1 method diverges, with slopes and S.D.s for the two methods of $6 \cdot 10^{-3} \pm 6 \cdot 10^{-6}$ ($r^2 > 0.999$) and $5 \cdot 10^{-3} \pm 20 \cdot 10^{-6}$ ($r^2 < 0.99$), respectively. The curve-fit method provides good linearity down to 10 pmol, with slope and S.D. of $5 \cdot 10^{-3} \pm 6 \cdot 10^{-6}$ ($r^2 > 0.999$) over this range.

The Finnigan MAT 252 instrument is specified to operate at an absolute sensitivity of 1000 CO_2 molecules/ion detected, and typically attains this

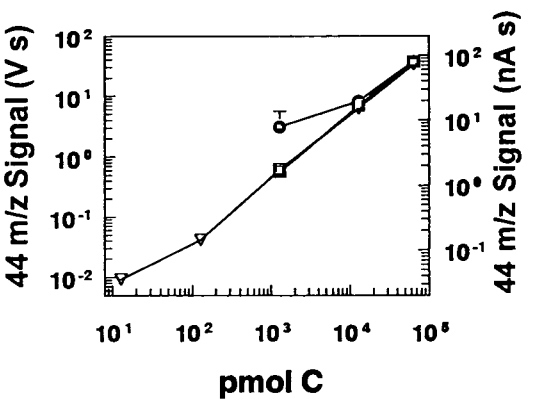

Fig. 5. Calibration curve showing the relationship of integrated area to mass of Me17:0 injected on-column for all three integration methods. □ = SS 0.8 mV/s; ○ = SS 0.1 mV/s; ▽ = curve fit.

level. For such an instrument, the 2000 nA s area would be produced with about 5 nmol C entering the combustion furnace, while the 3 nA s level would be attained with 5 pmol C. It should be emphasized that these detection limits are based on molar C content, and so are largely independent of the analyte molecular mass for most organic molecules of biomedical interest. These data indicate that curve fitting produces useful isotope ratios at this level of total analyte.

4. Conclusions

For tracer applications, a cutoff for "high precision" can be defined as an error of $\delta^{13}C = 100$ (S.D.), which corresponds to 0.1% in absolute terms and to the practical limit of organic mass spectrometers operated in selected ion mode (SIM) [2]. The SS = 0.1 mV/s detected peaks at levels below the SS = 0.8 mV/s method, but produced S.D.s greater than $\delta^{13}C = 100‰$ in most cases at the lower levels. SS = 0.1 did perform better for the largest integration time and lowest signal, further suggesting that the summation methods require a minimum S/N for adequate performance. For this reason, it appears that the higher value for SS is appropriate when using the summation method, as it detects peaks down to levels at which high precision is obtained. In cases where very small peaks must be detected by summation, consecutive data points can be summed to improve S/N per data point, with a lower SS then applied to the resulting chromatogram.

At all levels, curve-fitting produced satisfactory precision and accuracy, and was nearly immune to the choice of integration time. It was the only method that produced useful isotope ratios at the lowest levels. It also gives linear response over the entire usable dynamic range and so is also suitable for quantitative analysis. Our previous results showed that curve fitting satisfactorily recovers aberrant isotope ratios derived from overlapping peaks [12]. Together, these studies indicate that curve fitting may be the method of choice for integrating peaks in high-precision chromatography applications where complex mixtures are commonly encountered.

Acknowledgements

This work was supported by NIH grant GM49209. K.J.G. acknowledges predoctoral support from NIH training grant DK07158.

References

[1] D.E. Matthews and J.M. Hayes, *Anal. Chem.*, 50 (1978) 1465–1473.
[2] K.J. Goodman and J.T. Brenna, *Anal. Chem.*, 64 (1992) 1088–1095.
[3] R.J. Caimi and J.T. Brenna, *Anal. Chem.*, 65 (1993) 3497–3500.
[4] R.J. Caimi and J.T. Brenna, *J. Mass Spectrom.*, (1995) in press.
[5] D.A. Merritt and J.M. Hayes, *J. Am. Soc. Mass Spectrom.*, 5 (1994) 387–397.
[6] T. Preston and C. Slater, *Proc. Nutr. Soc.*, 53 (1994) 363–372.
[7] J.T. Brenna, *Acc. Chem. Res.*, (1994) in press.
[8] D.A. Merritt and J.M. Hayes, *Anal. Chem.*, 66 (1994) 2336–2347.
[9] S. Tissot, S. Normand, R. Guilluy, C. Pachiaudi, M. Beylot, M. Laville, R. Cohen, R. Mornex and J.P. Riou, *Diabetologia*, 33 (1990) 449–456.
[10] Z.K. Guo, A.H. Luke, W.P. Lee and D. Schoeller, *Anal. Chem.*, 65 (1993) 1954–1959.
[11] Y. Khalfallah, S. Normand, S. Tissot, C. Pachiaudi, M. Beylot and J.P. Riou, *Biol. Mass Spectrom.*, 22 (1993) 707–711.
[12] K.J. Goodman and J.T. Brenna, *Anal. Chem.*, 66 (1994) 1294–1301.
[13] A.H. Anderson, T.C. Gibb and A.B. Littlewood, *J. Chromatogr. Sci.*, 8 (1970) 640–646.
[14] A.H. Anderson, T.C. Gibb and A.B. Littlewood, *Anal. Chem.*, 42 (1970) 434–440.
[15] N. Dyson, *Chromatographic Integration Methods*, Royal Society of Chemistry, Cambridge, UK, 1990.
[16] M.P. Ricci, D.A. Merritt, K.H. Freeman and J.M. Hayes, *Org. Geochem.*, 21 (1994) 561–571.
[17] G.W. Snedecor and W.G. Cochran, *Statistical Methods*, Iowa State Univ. Press, Ames, IA, 1989.
[18] K.J. Goodman and J.T. Brenna, presented at the *41st Annual ASMS Conference on Mass Spectrometry and Allied Topics, San Francisco, CA, 1993*, abstracts, pp. 738a–738b.

ELSEVIER

Journal of Chromatography A, 689 (1995) 69–76

JOURNAL OF CHROMATOGRAPHY A

Evaluation of different injection techniques in the gas chromatographic determination of thermolabile trace impurities in a drug substance

Silke Klick

Analytical Chemistry, Astra Hässle AB, S-431 83 Mölndal, Sweden

First received 30 March 1994; revised manuscript received 19 August 1994

Abstract

A gas chromatographic method for the determination of an epoxide in a drug substance was validated. Hot splitless injection of the sample extract was identified as a critical step with unsatisfactory repeatability. Therefore, the gas chromatographic procedure was re-evaluated using an instrument equipped with an on-column inlet and a split–splitless inlet with a programmable column head pressure. Further, the re-evaluated method also included the determination of the corresponding chlorohydrin that might occur as a reaction product of the epoxide. Three different sets of parameters were chosen: splitless injection using the same parameters as were used in the validation experiments, splitless injection with a high initial column head pressure and cool on-column injection. Generally, the precision of repeated injections of standard solutions and of the analysis of spiked sample extracts was improved using the newer instrument. On-column injection gave the best results in terms of both precision and absolute peak areas. The limits of detection and quantification for the overall method were 0.09 and 0.29 μg/g, respectively, for the epoxide and 0.09 and 0.31 μg/g, respectively, for the chlorohydrin. On hot splitless injection the chlorohydrin formed the epoxide, and also losses of the epoxide were observed. Owing to a shorter residence time in the hot injector block, a high initial column head pressure could successfully reduce the degradation of the analytes. However, the precision was not improved because of occasional leakage of the septum immediately after injection, which resulted in uncontrolled losses and discrimination.

1. Introduction

Epoxides are potentially toxic, mutagenic and carcinogenic agents. The presence of ethylene oxide residuals in food stuffs and pharmaceuticals is regulated by the authorities in many countries owing to its known carcinogenic potential in humans. The limit is typically 1 ppm. In drug substances any epoxide that might be present must be regarded as a toxic impurity although it might be less reactive than ethylene oxide. The concentration should be kept as low as possible, and a limit will usually be included in the specification of the particular drug substance. Individual identification and specific test methods are then required. The analytical test method must be validated especially for selectivity and limits of detection and quantification.

The epoxide H 137/89 [*p*-cyano(epoxypropoxy)benzene], is involved in the synthesis of Almokalant, an antiarrhythmic drug in the clinical phase of investigation. A validated analytical method was needed for its determination in the region of 1 μg/g, which was close to the ex-

0021-9673/95/$09.50
SSDI 0021-9673(94)00801-9

pected limit of quantification. Further, there was interest in determining, with the same method, the corresponding chlorohydrin H 240/18 [*p*-cyano(3 - chloro - 2 - hydroxypropoxy)benzene], which is a possible reaction product of H 137/89. Chemical structures are presented in Fig. 1.

The limits of detection and quantification in trace analysis with chromatographic methods depend on the selectivity and precision of the method and on the performance of the chromatographic system. The method to be applied for the determination of the epoxide and chlorohydrin was capillary gas chromatography using a non-polar methylsilicone as the stationary phase. Epoxide and chlorohydrin were extracted from the main compound by liquid–liquid extraction with dichloromethane. Almokalant has a pK_a value of 7.8 and can be kept in the aqueous phase by adding an excess of phosphoric acid. During validation of the method for the determination of epoxide, splitless injection turned out to be a critical step for the method precision, and thermodegradation was considered as a reason. The method was therefore re-evaluated using a second gas chromatographic system equipped with an on-column inlet and a split–splitless inlet with programmable column head pressure. Cool on-column injection is regarded as the "smoothest" injection technique as the sample enters the column without previous volatilization and at low initial temperature. Hence it is the method of choice for thermolabile samples [1,2], provided that the sample is sufficiently clean, to avoid interfering matrix effects. In splitless injection pressure programming can reduce the residence time of the vaporized sample in the hot injection port and hence thermodegradation can be minimized [3]. In this work, different gas chromatographic methods were tested and optimized. In order to find the most suitable method for the determination of both substances, parts of the validation experiments were repeated and the results from different gas chromatographic methods were compared.

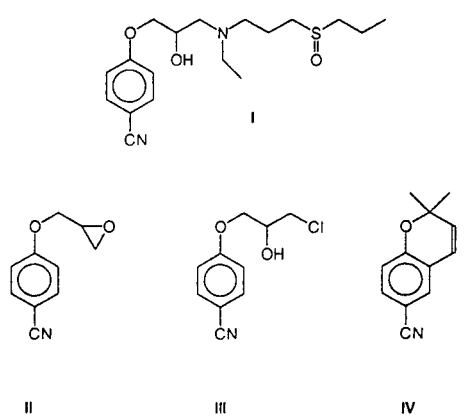

Fig. 1. Structural formulae of Almokalant (I), epoxide H 137/89 (II), chlorohydrin H 240/18 (III) and the internal standard (IV).

2. Experimental

A solution of about 4 μg/ml H 254/89 (6-cyano-2,2-dimethyl-2*H*-1-benzopyran, Fig. 1) in dichloromethane was prepared and used as an internal standard solution. Working standard solutions of epoxide H 137/89 and chlorohydrin H 240/18 were prepared from stock standard solutions by dilution with the internal standard solution. The sample (0.95–1.05 g of Almokalant) was weighed into a vial equipped with a Teflon-lined screw-cap and spiked with an appropriate amount of the standard solutions. A 3.00-ml volume of internal standard solution and 3.00 ml of 1 *M* phosphoric acid were added and the vial was shaken vigorously for 5 min and centrifuged for 5 min at about 2500 rpm (ca. 800 *g*). The upper phase was removed and 3.00 ml of 0.1 *M* phosphoric acid were added. The vial was shaken again for 5 min. After centrifugation, the upper phase was removed and the organic phase was transferred into another vial where it was dried over about 5 mg of anhydrous sodium sulfate. Standard solutions and sample extracts were injected into the gas chromatograph.

The validation experiments were performed using a Hewlett-Packard HP 5790 gas chromatograph equipped with a capillary column split–splitless injector. The gas chromatographic parameters were as follows: column, 25 m × 0.32

mm I.D. fused-silica capillary column coated with 0.52-μm cross-linked methylsilicone (Hewlett Packard Ultra 1); temperatures, injector 200°C, detector 280°C, oven initial temperature 40°C (held for 2 min), increased at 12°C/min to 270°C (held for 5 min); carrier gas, helium at 2.0 ml/min (0.71 bar); splitting ratio, 1:15; detector auxiliary gas, nitrogen at 35 ml/min; and detector gases, hydrogen at 35 ml/min and air at 240 ml/min.

The second instrument was a Hewlett-Packard HP 5890 Series II gas chromatograph equipped with a flame ionization detector, a capillary column split–splitless injector and an on-column injector. The same column was used but it was coupled to a 5 m × 0.32 mm I.D. fused-silica capillary retention gap. Detector gases and detector temperatures were the same as described above. The initial carrier gas (helium) flow-rate was 1.8 ml/min and the column head pressure was 0.69 bar. The temperature programmes were similar in all methods used.

The sample was injected manually, either splitless or on-column, with a 10-μl syringe with a removable fused-silica needle. For splitless injections, deactivated, straight glass liners, 79 mm × 4 mm I.D., with a small plug of deactivated glass-wool were used. The glass-wool was positioned about half way down the liner. The syringe needle length was 50 mm and it placed the sample at or slightly above the glass-wool plug. Injection of 2-μl samples, needle volume included, was performed using the hot needle technique. The plunger was pushed down rapidly and the needle was withdrawn from the inlet immediately after injection. This is regarded as the most reproducible manual injection technique.

3. Results and discussion

3.1. Validation experiments

The described method was validated with respect to chromatographic selectivity, linearity, recovery, precision and limits of detection and quantification. The chlorohydrin was not included in the validation experiments.

A chromatogram of a sample spiked with 10 μg/g of epoxide run on the HP 5790 gas chromatograph is shown in Fig. 2. An unspiked blank sample was prepared in the same manner. The dichloromethane extract was reduced to *ca.* 1 ml by blowing with nitrogen and injected into the gas chromatograph. The blank was free of detectable concentrations of the epoxide.

The recovery of the epoxide in spiked samples of Almokalant was studied at three concentration levels between 1 and 10 μg/g. Samples of 1.00 ± 0.05 g were weighed and spiked with standard solution. The extraction was performed according to the method described above and the concentration of the epoxide in the organic phase was calculated. An extraction yield of

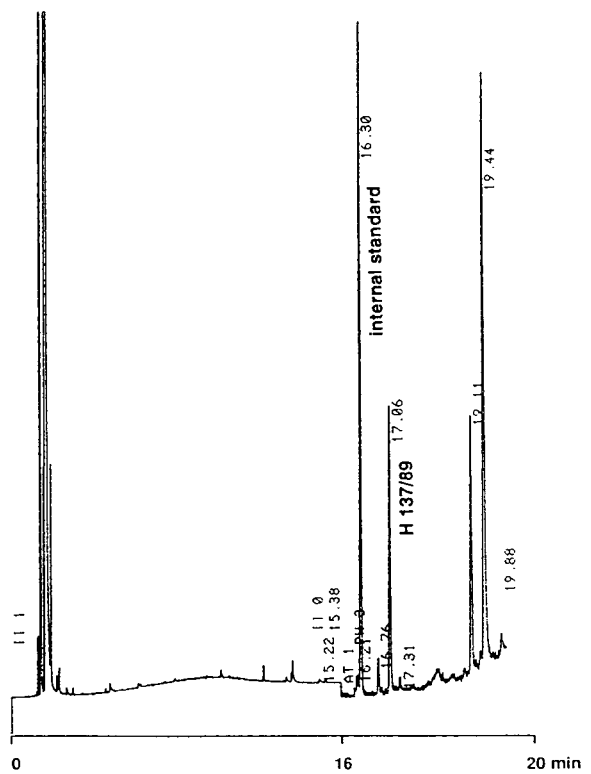

Fig. 2. Chromatogram of a sample of Almokalant spiked with 10 μg/g of epoxide H 137/89 and run on the HP 5790 gas chromatograph.

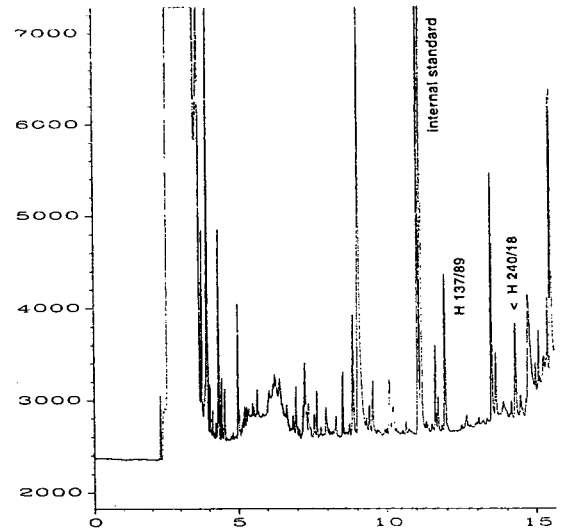

Fig. 3. Chromatogram of a sample of Almokalant spiked with 1 μg/g of epoxide H 137/89 and chlorohydrin H 240/18 and injected on-column on to the HP 5890 Series II gas chromatograph. Time scale in min. Values on the *y*-axis in pA.

88.5% was obtained as the percentage of added epoxide that could be recovered in the organic phase.

The repeatability of the method was determined at a concentration close to the limit of quantification. Five samples of Almokalant were spiked with epoxide stock standard solution to give a final concentration of about 1 μg/g. These samples were also used as the lowest concentration level for the determination of the extraction yield. The peak-area ratios of epoxide and internal standard were calculated for the five samples. The relative standard deviation of the peak area ratio of epoxide and internal standard was 9.2%.

The method limit of detection (MLD) was defined as the concentration (μg/g) giving a peak-area ratio of the epoxide to the internal standard equal to three times the standard deviation of the peak-area ratio of a concentration slightly above the expected limit of quantification. The limit of quantification was defined as the concentration (in μg/g) giving a peak-area ratio of the epoxide to the internal standard equal to ten times the standard deviation of the peak area ratio of a concentration slightly above the expected limit of quantification (according to Taylor [4]). Based on the data obtained in the precision experiments, the method limit of detection was 0.3 μg/g and the limit of quantification was 0.9 μg/g.

The extraction step was studied in more detail in a number of additional experiments. Three samples were spiked with the same amount of epoxide (*ca.* 10 μg/g) and extracted in different ways. One sample was shaken manually for 5 min and the other two were shaken with a shaking apparatus at 350 rpm for 5 min and for 30 min, respectively. The sample shaken for 30 min showed a slightly lower recovery (80.2%) than the samples shaken for 5 min. This may be a result of hydrolysis of the epoxide. Manual shaking or use of a shaking apparatus had no effect on the extraction yield. Further, the extractability of the internal standard from dichloromethane to phosphoric acid was tested in the presence of the sample matrix. About 1 g of Almokalant was weighed and 3 ml of the internal standard solution were added. After addition of 3 ml of 1 *M* H_3PO_4, the vial was shaken vigorously for 5 min and the phases were separated by centrifugation. The aqueous phase was transferred to a new vial and shaken with 3 ml of dichloromethane without internal standard for 5 min. The dichloromethane phase was injected into the gas chromatograph. No internal standard was detectable. Hence the internal standard was not likely to be extracted into the aqueous phase during sample work-up.

3.2. Re-evaluation

Although the validated limit of quantification was sufficient, the precision of the method was not satisfactory. A number of experiments were carried out in order to find the critical parameters. However, removal of the glass-wool from the glass liner, changing the glass liner, variation of the injector temperature (180 and 220°C), variation of the splitless time and injection of 1 μl instead of 2 μl did not improve the precision of repeated injections of standard solutions of either epoxide or chlorohydrin. It was obvious from the above experiments that the chloro-

hydrin was subject to thermodegradation and formed epoxide by release of HCl. The peak shape indicated that no degradation occurred on the column so that the sample introduction system seemed to be the place of degradation, for example, as a result of active sites within the injection system or simply by heat [2,5]. It was also observed that the absolute peak areas in some instances varied by more than 10% relative standard deviation. Therefore, the gas chromatographic process was re-evaluated using a newer instrument (HP 5890 Series II gas chromatograph) equipped with both a capillary column split–splitless injector and an on-column injector, and electronic pressure programming of the column head pressure. Additionally, determination of the chlorohydrin H 240/18 in Almokalant was included in the method.

Three different methods were tested:

(I) (splitless). Similar parameters as described above for the HP 5790 instrument, splitless injection.

(II) (electronic pressure programming, EPP). A high inlet pressure during injection (2.2 bar, 30 s) in order to obtain a high inlet-flow rate and thus reduce possible thermal decomposition of the sample during splitless injection.

(III) (cool on-column injection). The instrument parameters were similar to those in methods I and II.

The use of a retention gap in the re-evaluation experiments did not influence the peak shape; it was merely used in order to protect the column from contamination by the sample extracts injected on-column. In the on-column experiments epoxide and chlorohydrin were determined in the same run whereas in the splitless experiments epoxide and chlorohydrin were run separately. The precision of the injection was determined from repeated injections of standard solutions containing 5 μg/ml of epoxide or chlorohydrin. The precision of the overall method was tested as described above with repeated samples spiked with epoxide or chlorohydrin at the 1 μg/g level. However, in the re-evaluation experiments no epoxide- and chlorohydrin-free Almokalant batch was available. The available batch contained 0.54 μg/g of epoxide and 0.69 μg/g of chlorohydrin, determined with the on-column method. The true concentration levels of the spiked samples are therefore about 1.5 μg/g of epoxide and 1.7 μg/g of chlorohydrin. For the same reason, the extraction yield of the chlorohydrin could not be determined and was suggested to be 100%. As the same blank was used for all re-evaluation experiments, this did not influence the final results. The results are summarized in Table 1 and compared with the results obtained from the HP 5790 gas chromatograph. A chromatogram of a sample of Almokalant spiked with 1 μg/g of epoxide and chlorohydrin and injected on column is shown in Fig. 3.

Using similar parameters on the HP 5790 and 5890 instruments, the relative standard deviation of repeated splitless injections of the epoxide was improved considerably on the HP 5890 and the relative standard deviation of the overall method could be lowered from 9.2 to 2.6%. According to the manufacturer, the pneumatic systems are identical for the two instrument models. However, an important difference in injector design is the insulation between injector block and column oven. In the older instrument a temperature gradient could develop along the hot injector owing to insufficient insulation from the cooler oven. Condensation of higher boiling components in the lower part of the injector could result in a lower precision in sample transfer. In the HP 5890 instrument the injector insulation was improved and an aluminium cap was installed which additionally prevents heat exchange between the two compartments of the gas chromatograph (information from Hewlett-Packard, Stockholm, Sweden).

Injection of the chlorohydrin standard solutions showed that it degraded during injection and formed epoxide. As can be seen in Table 2, on normal splitless injection (method I) 26% of the injected chlorohydrin formed epoxide. A higher inlet pressure during injection, shortening the residence time of the vaporized sample in the injection block, decreased the formation of epoxide to 9%. With an increase in the inlet temperature from 200 to 230°C, epoxide formation increased to 37%. A chromatogram of this sample is shown in Fig. 4. In contrast, no epoxide formation from a pure chlorohydrin

Table 1
Comparison of different methods for the determination of the epoxide H 137/89 and the chlorohydrin H 240/18 in Almokalant

GC model (method)	Epoxide				Chlorohydrin			
	R.S.D.$_{inj}$ (%)	R.S.D.$_{met}$ (%)	LOD (μg/g)	LOQ (μg/g)	R.S.D.$_{inj}$ (%)	R.S.D.$_{met}$ (%)	LOD (μg/g)	LOQ (μg/g)
HP 5790 (splitless)	3.7 ($n = 7$)	9.2 ($n = 5$)	0.3	0.9	–	–	–	–
HP 5890 (I, splitless)	0.39 ($n = 3$)	2.6 ($n = 5$)	0.13	0.42	6.7 ($n = 3$)	3.1 ($n = 5$)	0.17	0.56
HP 5890 (II, EPP)	0.32 ($n = 3$)	4.3 ($n = 5$)	0.22	0.72	3.8 ($n = 3$)	6.9 ($n = 5$)	0.35	1.2
HP 5890 (III, on-column)	0.19 ($n = 3$)	1.8 ($n = 5$)	0.09	0.29	0.64 ($n = 3$)	2.1 ($n = 5$)	0.09	0.31

R.S.D.$_{inj}$ = Relative standard deviation of the peak-area ratio of the epoxide (chlorohydrin) to the internal standard for repeated injection of a standard solution (5 μg/ml); R.S.D.$_{met}$ = relative standard deviation of the peak-area ratio of epoxide (chlorohydrin) to the internal standard in repeated samples spiked with 1 μg/g of epoxide or chlorohydrin; LOD = limit of detection; LOQ = limit of quantification.

standard was observed during on-column injection. The dependence on injector temperature and residence time in the injector block of the chlorohydrin peak area can also be seen in Table 3, where absolute peak areas are compared.

Although the thermolability of the chlorohydrin is more obvious, a slight thermolability of the epoxide is also indicated from the absolute peak areas shown in Table 3. Compared with the on-column method the peak areas of the epoxide are decreased by between 6.5 and 17%, depending on the method, whereas the differences in internal standard peak areas between on-column and splitless methods are considerably lower.

Table 2
Formation of epoxide from chlorohydrin standard with different methods on the HP 5890 gas chromatograph

Method	Epoxide formed (%)[a]
I (splitless)	26 (injector temp. 200°C)
	37 (injector temp. 230°C)
II (EPP)	9
III (on-column)	0

[a] Percentage of chlorohydrin injected that has been converted into epoxide.

The losses of chlorohydrin during splitless injection cannot be explained only by epoxide formation since the amount epoxide recovered is lower than the corresponding loss of chlorohydrin compared with on-column injection. A possible

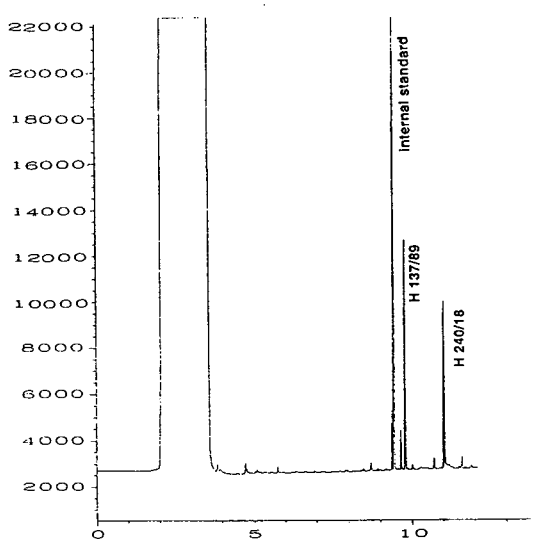

Fig. 4. Chromatogram of a standard solution of chlorohydrin H 240/18 injected on to the HP 5890 instrument at an injector temperature of 230 instead of 200°C used in method I. The epoxide H 137/89 was formed from the injected chlorohydrin in the hot injector block and corresponds 37% of the chlorohydrin. Scales as in Fig. 3.

Table 3
Absolute areas ± relative standard deviations of internal standard, epoxide and chlorohydrin peaks obtained from repeated injections of standard solutions using different methods

Method	Epoxide		Chlorohydrin	
	Area internal standard	Area epoxide	Area internal standard	Area chlorohydrin
I (splitless)	31 519 ± 4.1% ($n = 3$)	32 010 ± 4.7% ($n = 3$)	30 329 ± 4.6% ($n = 3$)	11 637 ± 5.5% ($n = 3$)
II (EPP)	33 127 ± 3.5% ($n = 3$)	34 922 ± 3.7% ($n = 3$)	32 826 ± 3.5% ($n = 3$)	23 638 ± 1.8% ($n = 3$)
III (on-column)	32 310 ± 0.61% ($n = 3$)	37 333 ± 0.75% ($n = 3$)	32 310 ± 0.61% ($n = 3$)	28 882 ± 0.94% ($n = 3$)

reason is the formation of degradation products other than epoxide, adsorption in the injection system, which might affect both epoxide and chlorohydrin, or any kind of discrimination. If discrimination occurs it will affect the relative response of the chlorohydrin more than that of the epoxide, as the latter has a retention time closer to that of the internal standard.

The use of a high initial column head pressure was very effective in decreasing chlorohydrin losses during splitless injection, and absolute peak areas of the chlorohydrin peak could be more than doubled by using this technique. The loss relative to on-column injection was 18%, compared with 60% with normal initial pressure. However, problems occurred owing to septum leaks that occurred occasionally and resulted in severe discrimination. Changing the septum did not immediately improve the injection and the system seemed to be very sensitive to factors such as the type of septum used, the number of injections made through the same septum, the tightness of the septum retainer nut and the speed at which the syringe needle was withdrawn from the injection port. Samples for which a septum leak was observed were re-injected. An automatic injector might improve this type of problem.

On-column injection is known to improve precision and accuracy and to eliminate problems resulting from discrimination [2]. Comparing the different methods, on-column injection gave best results in terms of both precision and absolute peak areas. Hence, the method limits of detection and the limits of quantification could be lowered. When chlorohydrin is present in the sample it will form epoxide on splitless injection and therefore on-column injection is required in order to produce reliable results.

4. Conclusions

Generally, the precision of the injection and of the overall method was improved considerably using the HP 5890 instrument. The reason might be improved insulation between the injector and the gas chromatograph oven. High initial inlet pressure during injection, effective in decreasing thermodegradation of the chlorohydrin, did not improve the precision. The increased pressure led to occasional leakage of the septum immediately after injection, which resulted in uncontrolled losses and discrimination.

The results indicate that the chlorohydrin and, to a minor extent, the epoxide suffer from thermal degradation and/or adsorption in the hot injector block during splitless injection, which results in poor precision. Consequently, the best results regarding precision and limits of detection and quantification were obtained by using cool on-column injection. When chlorohydrin is present in the sample it will form epoxide on splitless injection and hence on-column injection becomes the method of choice.

References

[1] H.-M. Müller and H.-J. Stan, *J. High Resolut. Chromatogr.*, 13 (1990) 759.
[2] K. Grob, *Classical Split and Splitless Injection in capillary GC*, Hüthig, Heidelberg, 2nd ed., 1988, pp. 176–188.
[3] P.L. Wylie, K.J. Klein, M.Q. Thompson and B.W. Hermann, *J. High Resolut. Chromatogr.*, 15 (1992) 763.
[4] J.K. Taylor, *Quality Assurance of Chemical Measurements*, Lewis, Chelsea, MI, 1987, p. 79.
[5] H. Husmann, G. Schomburg, K.-D. Müller, H.P. Nalik and G. von Recklinghausen, *J. High Resolut. Chromatogr.*, 13 (1990) 780.

ELSEVIER

Journal of Chromatography A, 689 (1995) 77–84

JOURNAL OF CHROMATOGRAPHY A

Gas chromatographic separation of bile acid 3-glucosides and 3-glucuronides without prior deconjugation on a stainless-steel capillary column

Takashi Iida[a,*], Shinnosuke Tazawa[a], Tamaaki Tamaru[a], Junichi Goto[b], Toshio Nambara[b]

[a]*College of Engineering, Nihon University, Koriyama, Fukushima 963, Japan*
[b]*Pharmaceutical Institute, Tohoku University, Aobayama, Sendai 980, Japan*

First received 21 June 1994; revised manuscript received 5 September 1994

Abstract

A method for the gas chromatographic (GC) separation of the 3-glucoside and 3-glucuronide conjugates of bile acids without the necessity for a hydrolytic step is described. The bile acid glycosides were derivatized to their complete methyl ester trimethylsilyl (Me-TMS) or methyl ester dimethylethylsilyl (Me-DMES) ether derivatives, which in turn were chromatographed on an inert and thermostable stainless-steel capillary column, Ultra ALLOY-1 (HT), coated with a thin film (0.15 μm) of chemically bonded and cross-linked dimethylsiloxane. They exhibited a single peak of the theoretical shape without any accompanying peaks due to thermal decomposition, even at oven temperatures of 320–330°C. Excellent GC separation of isomeric bile acid glycosides was achieved by the combined use of suitable derivatives and column. This method, which does not need the prior deconjugation of the glycosidic moiety, could be usefully applied to biosynthetic and metabolic studies of bile acids in biological materials.

1. Introduction

In recent years, considerable attention has been directed to the biosynthesis and metabolism of bile acids in connection with hepatobiliary diseases. Particular interest has been focused on the physiological significance of the glycosidic conjugates of bile acids. Bile acid glucuronides, one of the earliest known glycosidic conjugates, have been reported to exist in various human biological fluids [1–4]. In addition to bile acid glucuronides, analogous glucosides [5–8] and N-acetylglucosaminides [9,10] have recently been identified as novel bile acid conjugates in human urine.

Gas chromatography (GC) is a powerful tool for the profile analysis of bile acids in biological specimens. Prior to GC analysis, glycoside-conjugated bile acids and amidated bile acids with glycine or taurine and/or sulphated bile acids are conventionally hydrolysed to their unconjugated forms, which are then converted into suitable volatile derivatives, because they are comparatively polar and lack volatility [11]. However, deconjugation has several drawbacks, because it loses information about the type and site of conjugation and has the possibility of producing artifacts by inefficient hydrolysis.

* Corresponding author.

0021-9673/95/$09.50
SSDI 0021-9673(94)00860-4

Therefore, a reliable method for the direct GC determination of these conjugated bile acids without need for prior deconjugation is urgently required.

We have been investigating the direct GC analysis of conjugated bile acids without the necessity for a hydrolytic step, and previous papers have demonstrated that GC of glycine- [11–14] and glucoside-conjugated [6,8] bile acids is possible. In addition, the recent successful use of a new type of a metal capillary column, Ultra ALLOY, for the separation of alcohols, amines and triglycerides prompted us to examine this column in the analysis of bile acid conjugates [15]. It has been reported that the performance of this column is superior to those of fused-silica and aluminium-clad fused-silica capillary columns with respect to inertness, thermal stability and mechanical strength under high temperature and vibration.

In continuation of an ongoing programme of GC analyses of conjugated bile acids, we report here a method for the direct GC determination of 3-glucoside and 3-glucuronide conjugates of bile acids without prior deconjugation. For the purpose of comparison, the corresponding unconjugated and glycine-conjugated bile acids were also analysed under the same GC conditions.

2. Experimental

2.1. Materials and reagents

The following abbreviations of compounds are used: LCA = lithocholic acid (**1**); CDCA = chenodeoxycholic acid (**2**); UDCA = ursodeoxycholic acid (**3**); DCA = deoxycholic acid (**4**); CA = cholic acid (**5**); glyco-LCA = glycolithocholic acid (**6**); glyco-CDCA = glycochenodeoxycholic acid (**7**); glyco-UDCA = glycoursodeoxycholic acid (**8**); glyco-DCA = glycodeoxycholic acid (**9**); glyco-CA = glycocholic acid (**10**); LCA 3-Glc. = lithocholic acid 3-glucoside (**11**); CDCA 3-Glc. = chenodeoxycholic acid 3-glucoside (**12**); UDCA 3-Glc. = ursodeoxycholic acid 3-glucoside (**13**); DCA 3-Glc. = deoxycholic acid 3-glucoside (**14**); CA 3-Glc. = cholic acid 3-glucoside (**15**); LCA 3-GlcA. = lithocholic acid 3-glucuronide (**16**); CDCA 3-GlcA. = chenodeoxycholic acid 3-glucuronide (**17**); UDCA 3-GlcA. = ursodeoxycholic acid 3-glucuronide (**18**); DCA 3-GlcA. = deoxycholic acid 3-glucuronide (**19**); CA 3-GlcA. = cholic acid 3-glucuronide (**20**).

Almost all of the unconjugated bile acids (**1–5**) and their corresponding glycine (**6–10**), glucoside (**11–15**) and glucuronide (**16–20**) conjugates were from our laboratory collection, which include new and natural bile acid 3-glucosides [16] and 3-glucuronides [17] recently synthesized in these laboratories. UDCA 3-GlcA. (**18**) was kindly supplied by Tokyo Tanabe (Tokyo, Japan).

The silylating reagents, N-trimethylsilylimidazole (TMSI) and N,N-dimethylethylsilylimidazole (DMESI), were obtained from Tokyo Kasei Kogyo (Tokyo, Japan). All solvents used were of analytical-reagent grade.

2.2. Derivatization

Ethereal diazomethane was prepared with a Wheaton generator using N-methyl-N′-nitro-N-nitrosoguanidine as methyl donor. The diazomethane solution (0.5 ml) was added to a solution of the bile acid glycoside (ca.0.5 mg) in methanol (50 μl) in a reaction vial, and the mixture was allowed to stand at room temperature for 1 h. After the excess reagent and solvent had been evaporated under a stream of nitrogen, silylating reagent (50 μl, TMSI or DMESI) was added to the residue and the mixture was heated at 60°C for 1 h in a Reacti-Therm (Pierce, Rockford, IL, USA). An aliquot of the derivatized sample solutions [methyl ester trimethylsilyl (Me-TMS) ether or methyl ester dimethylethylsilyl (Me-DMES) ether] diluted with benzene (200 μl) was injected into the GC system together with internal standards (C_{32} and C_{44}).

2.3. Gas chromatography

A Shimadzu GC-14A gas chromatograph equipped with a flame ionization detector and data processing system (Shimadzu Chromatopac

C-R6A) was used. It was fitted with an Ultra ALLOY-1 (HT) stainless-steel capillary column (30 m × 0.25 mm I.D.) coated with a thin film (0.15 μm) of chemically bonded and cross-linked dimethylsiloxane (equivalent to 400-HT) and operated under the following conditions: carrier gas (helium) flow-rate, 0.7 ml/min; purge gas flow-rate, 20 ml/min; make-up gas flow-rate, 60 ml/min; injection method, split (1:50) or splitless; injector temperature, 330°C; detector temperature, 350°C; column temperature, either isothermal, 320°C for Me-TMS ethers or 330°C for Me-DMES ethers, or programmed, raised from 280 to 290°C at 4°C/min, held for 7 min, and then raised to 330°C at 2°C/min for Me-TMS ethers, or raised from 260 to 300°C at 2°C/min, held for 3 min, and then raised to 330°C at 2°C/min for Me-DMES ethers. The metal capillary column was purchased from Frontier Lab. (Koriyama, Japan).

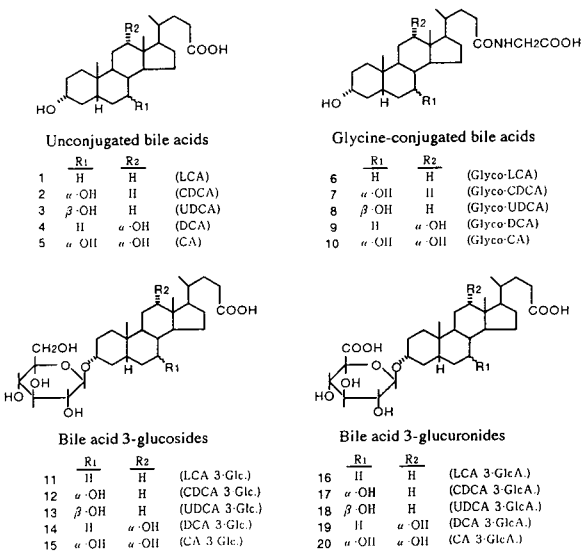

	R_1	R_2	
1	H	H	(LCA)
2	α-OH	H	(CDCA)
3	β-OH	H	(UDCA)
4	H	α-OH	(DCA)
5	α-OH	α-OH	(CA)
6	H	H	(Glyco-LCA)
7	α-OH	H	(Glyco-CDCA)
8	β-OH	H	(Glyco-UDCA)
9	H	α-OH	(Glyco-DCA)
10	α-OH	α-OH	(Glyco-CA)
11	H	H	(LCA 3-Glc.)
12	α-OH	H	(CDCA 3-Glc.)
13	β-OH	H	(UDCA 3-Glc.)
14	H	α-OH	(DCA 3-Glc.)
15	α-OH	α-OH	(CA 3-Glc.)
16	H	H	(LCA 3-GlcA.)
17	α-OH	H	(CDCA 3-GlcA.)
18	β-OH	H	(UDCA 3-GlcA.)
19	H	α-OH	(DCA 3-GlcA.)
20	α-OH	α-OH	(CA 3-GlcA.)

Fig. 1. Structures of compounds **1–20**.

3. Results and discussion

The structures of bile acid 3-glucosides [LCA 3-Glc. (**11**), CDCA 3-Glc. (**12**), UDCA 3-Glc. (**13**), DCA 3-Glc. (**14**) and CA 3-Glc. (**15**)] and 3-glucuronides [LCA 3-GlcA. (**16**), CDCA 3-GlcA. (**17**), UDCA 3-GlcA. (**18**), DCA 3-GlcA. (**19**) and CA 3-GlcA.(**20**)] examined in this study are shown in Fig. 1. For the purpose of comparison, the GC behaviour of the corresponding unconjugated (**1–5**) and glycine-conjugated (**6-10**) bile acids was also studied.

The four groups of the bile acids (**1–20**) were examined in a study of the two classes of derivatives and the column chosen. The free unconjugated and conjugated bile acids were converted into their methyl esters in both the sugar and steroidal side-chain moieties with ethereal diazomethane. The resulting bile acid methyl esters were then derivatized to their complete Me-TMS and Me-DMES ethers using TMSI and DMESI, respectively, as silylating agents of hydroxyl groups. All four groups of the bile acids including the glucoside and glucuronide conjugates were readily converted into the corresponding methyl ester silyl ethers under the mild conditions described under Experimental.

When the Me-TMS and Me-DMES ether derivatives of the bile acid glycosides were chromatographed on a stainless-steel capillary column of Ultra ALLOY-1 (HT), coated with a thin film (0.15 μm) of chemically bonded and cross-linked dimethylsiloxane, they exhibited a single peak of the theoretical shape without any accompanying peaks due to thermal decomposition in the column, even at oven temperatures of 320–330°C. In addition, the retention data (see below) for UDCA 3-Glc. (**13**), DCA 3-Glc. (**14**) and CA 3-Glc. (**15**) agreed well with those reported by Marschall and co-workers [6,8], demonstrating the thermal stability of these compounds. This result has considerable advantages; the avoidance of a hydrolytic step for the glycosidic linkages would prevent inefficient hydrolysis and provides direct information about the site of conjugation by GC. Further, the use of a thermostable metal capillary column has an advantage over a fused-silica column [8]; the analysis time for the same compounds is much shortened at relatively high temperatures, suggesting that the successful analysis of more polar and high-boiling compounds is possible.

The combined use of suitable derivatives and a column giving a sharp GC peak also proved to

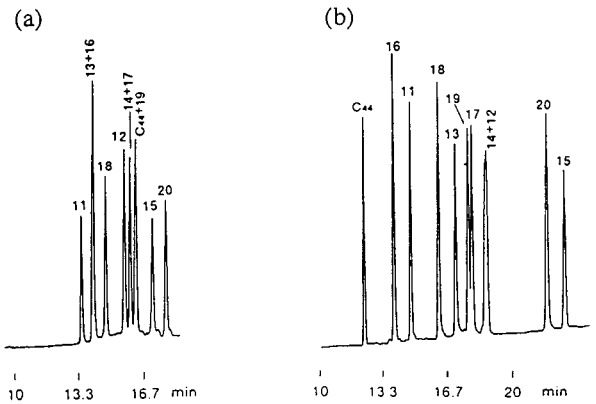

Fig. 2. Capillary GC of a mixture of the ten glucoside and glucuronide conjugates of bile acids as their (a) Me-TMS and (b) Me-DMES ether derivatives. GC conditions, isothermal (see text). Peaks: 11 = LCA 3-Glc.; 12 = CDCA 3-Glc.; 13 = UDCA 3-Glc.,; 14 = DCA 3-Glc.; 15 = CA 3-Glc.; 16 = LCA 3-GlcA.; 17 = CDCA 3-GlcA.; 18 = UDCA 3-GlcA.; 19 = DCA 3-GlcA.; 20 = CA 3-GlcA.

be well suited for the separation of isomeric glycosides. Fig. 2 shows typical chromatograms of a mixture of the ten bile acid 3-glucosides and 3-glucuronides measured under isothermal GC conditions at 320 or 330°C. As can be seen, the five glucosides were completely resolved as their Me-TMS ethers on the metal capillary column, emerging in the order LCA 3-Glc. (**11**), UDCA 3-Glc. (**13**), CDCA 3-Glc. (**12**), DCA 3-Glc. (**14**), CA 3-Glc. (**15**). The corresponding glucuronides on this column exhibited the same elution order: LCA 3-GlcA. (**16**), UDCA 3-GlcA. (**18**), CDCA 3-GlcA. (**17**), DCA 3-GlcA. (**19**), CA 3-GlcA. (**20**). (Two variants of the glycosidic conjugate pairs, **13** vs. **16** and **14** vs. **17**, overlap under the isothermal GC conditions examined.) The Me-DMES ether derivatives of each of the two groups of the glycosidic conjugates followed a similar elution order, except for the two isomeric pairs **12** vs. **14** and **17** vs. **19**, which differed from those observed for the corresponding Me-TMS ethers: **11**, **13**, **12** = **14**, **15**; **16**, **18**, **19**, **17**, **20**.

Table 1 shows the retention data of all twenty unconjugated and conjugated bile acids observed for the two classes of derivatization products on an Ultra ALLOY-1 (HT) column. Retention data were expressed as the relative retention time (RRT) and methylene unit (MU) values; RRT was expressed relative to an appropriate derivative of DCA 3-GlcA. (**19**) and MU was determined using C_{30}–C_{50} *n*-alkanes [18]. The MU values were calculated by the cubic expression of approximate polynomial expression methods (see below). The $\Delta[Um]_{D-T}$ values [19], which were defined as the differences in the MU values between the Me-DMES and Me-TMS ethers for the same compound on this column, are also listed in Table 1.

As expected, the Me-DMES ether derivatives always gave longer retention times than the corresponding Me-TMS ethers, owing to the heavier ethyl groups. In order to clarify further the general features of the four groups of bile acids, the correlation of MU values between the Me-TMS and Me-DMES ether derivatives for the same compound was expressed graphically. As shown in Fig. 3, the plots afforded a regression line with good linearity, expressed as $y = 0.837x + 4.05$ ($r = 0.991$, $n = 20$). The correlation implies that if either the MU value of the Me-TMS or Me-DMES ether of an unknown bile acid is known, the three groups of bile acids (unconjugates and glycine and glycoside conjugates) can be easily characterized by applying the regression line.

Our previous GC studies on various unconjugated [19–21] and glycine-conjugated [13,14] bile acids as their ester silyl ether derivatives revealed that in general the addition of hydroxyl groups in the steroid molecules produces nearly consistent increases in the $\Delta[Um]_{D-T}$ values. On the basis of the finding, it is deduced from the $\Delta[Um]_{D-T}$ data shown in Table 1 that the $\Delta[Um]_{D-T}$ values for mono-, di- and trihydroxylated bile acid 3-glucosides are approximately 3.1, 4.0 and 5.1 and those for 3-glucuronides are approximately 2.3, 3.4 and 4.4, respectively. The corresponding values for unconjugated and glycine conjugated compounds are in good agreement with those reported in previous papers [13,19]. As the increment of the above units is essentially independent of the other structural characteristics, the determination of the $\Delta[Um]_{D-T}$ value for an unknown bile acid 3-glycoside affords a useful method not only for

Table 1
RRT and MU values of the Me-TMS and Me-DMES ether derivatives of unconjugated compounds and glycine, glucoside and glucuronide conjugates of bile acids

Type	No.	Compound	Ml-TMS		Me-DMES		$\Delta[Um]_{D-T}$[a]
			RRT	MU	RRT	MU	
Unconjugated	**1**	LCA	0.18	31.51	0.22	32.45	0.94
	2	CDCA	0.208	32.37	0.29	34.31	1.94
	3	UDCA	0.22	32.70	0.31	34.69	1.99
	4	DCA	0.20	32.15	0.28	33.97	1.82
	5	CA	0.214	32.55	0.35	35.60	3.05
Glycine conjugates	**6**	Glyco-LCA	0.45	37.60	0.50	38.74	1.14
	7	Glyco-CDCA	0.51	38.44	0.60	40.51	2.07
	8	Glyco-UDCA	0.54	38.82	0.62	40.86	2.04
	9	Glyco-DCA	0.49	38.09	0.58	40.06	1.97
	10	Glyco-CA	0.51	38.44	0.68	41.71	3.27
Glucoside conjugates	**11**	LCA 3-Glc.	0.83	42.45	0.83	45.58	3.13
	12	CDCA 3-Glc.	0.97	43.61	1.05	47.59	3.98
	13	UDCA 3-Glc.	0.87	42.78	0.96	46.85	4.07
	14	DCA 3-Glc.	0.98	43.75	1.05	47.59	3.84
	15	CA 3-Glc.	1.05	44.29	1.22	49.40	5.11
Glucuronide conjugates	**16**	LCA 3-GlcA.	0.87	42.78	0.79	45.08	2.30
	17	CDCA 3-GlcA.	0.98	43.75	1.01	47.26	3.51
	18	UDCA 3-GlcA.	0.91	43.12	0.92	46.40	3.28
	19	DCA 3-GlcA.	1.00	43.89	1.00	47.16	3.27
	20	CA 3-GlcA.	1.10	44.60	1.23	49.01	4.41

RTT was expressed relative to the methyl ester sily ether derivatives of DCA 3-GlcA. (**19**). MU was calculated by a polynomial method (see text).
[a] Differences in the MU values between Me-DMES and Me-TMS ether derivatives for the same compound.

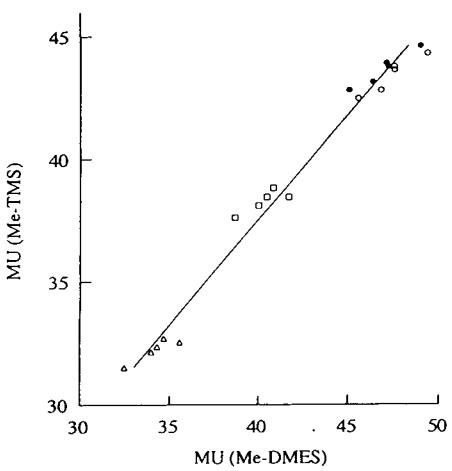

Fig. 3. Correlation in the MU values between the corresponding Me-TMS and Me-DMES ether derivatives. △ = Unconjugated compounds; ● = glucuronide conjugates; ○ = glucoside conjugates; □ = glycine conjugates, $y = 0.837x + 4.05$ ($r = 0.991$, $n = 20$).

estimating the number of hydroxyl groups in the aglycone moiety, but also for differentiating the two variants of sugar moieties.

In Table 2, the differences in the MU values

Table 2
$\Delta[Um]_{Glc.-GlcA.}$ values[a] observed for 3-glycoside conjugates of bile acids

3-Glycoside conjugate of	Me-TMS	Me-DMES
LCA	−0.33	0.50
CDCA	−0.14	0.33
UDCA	−0.34	0.45
DCA	−0.14	0.43
CA	−0.31	0.39

[a] Differences in the MU values between analogous bile acid 3-glucoside and 3-glucuronide for the same derivative.

between analogous bile acid glucosides and glucuronides [e.g., CA 3-Glc. (**15**) vs. CA 3-GlcA. (**20**)] for the same derivative are expressed in terms of $\Delta[Um]_{Glc.-GlcA.}$ values; a negative value denotes that the retention time of a glucoside conjugate is shorter than that of the corresponding glucuronide. The Me-TMS ether derivatives always show the negative $\Delta[Um]_{Glc.-GlcA.}$ values. On the other hand, the reverse relationship (positive $\Delta[Um]_{Glc.-GlcA.}$ values) was observed on changing from Me-TMS to Me-DMES ether derivatives. As the two glycosidic pairs differ from each other only in the number of hydroxyl groups present in the sugar moieties (four for glucosides and three for glucuronides), the above significant correlation can be reasonably explained as a result of the retarding effect on the retention times due to the DMES group and is therefore useful for identifying the structure of the sugar moieties.

Fig. 4 illustrates typical chromatograms for the simultaneous analysis of a mixture of fifteen unconjugated and glycine- and glucuronide-conjugated bile acids as their Me-TMS and Me-DMES ethers measured under temperature-programmed GC conditions (see Experimental). As can be seen, this column provided clean separations of the three groups of the bile acids with short analysis times (for example, 7 min for unconjugated compounds, 15 min for glycine conjugates and 30 min for glucuronide conjugates as their Me-TMS ethers). In particular, the Me-DMES ether derivatives provide an improved resolution not only of each of the three groups of unconjugated and conjugated bile acids but also of the individual isomers in each group. In addition, the general order of elution in each group of unconjugated and conjugated bile acids for the Me-DMES ethers was related to the number of hydroxyl groups in the aglycone moiety: mono-, di, trihydroxylated.

The detection limits of these compounds were found to be in the range 3–5 ng (by the splitless injection method) with a signal-to-noise ratio of 5:1. These chromatographic responses may be much improved by measuring the GC-selected ion monitoring in GC–MS [22].

Table 3 shows the MU values [18] of bile acid 3-glycoside Me-DMES ethers obtained under two isothermal and temperature-programmed GC conditions and with two calculation methods (approximate linear and polynomial expressions). As a result, the coefficients of variation relative standard deviations (R.S.D.) of the

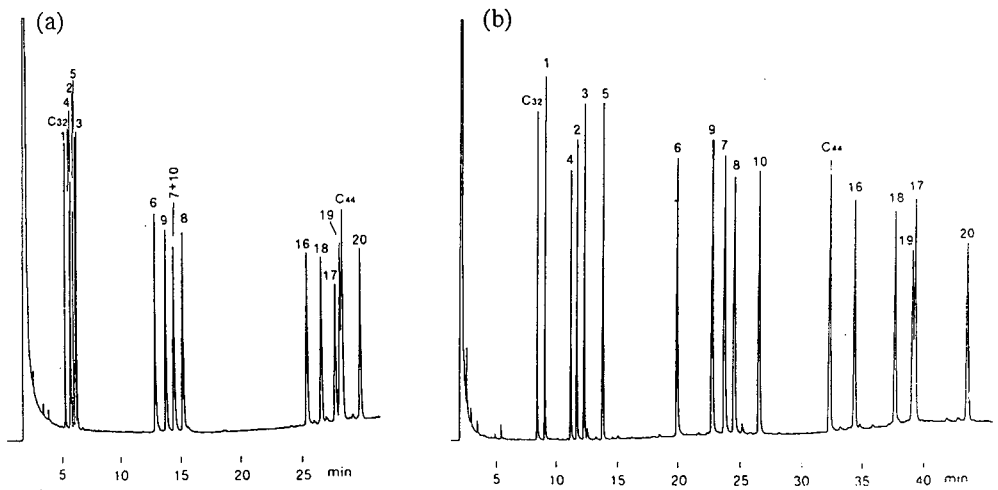

Fig. 4. Capillary GC (temperature programmed) of a mixture of the fifteen unconjugated compounds and glycine and glucuronide conjugates of bile acids as their (a) Me-TMS and (b) Me-DMES ether derivatives. Peaks: 1 = LCA; 2 = CDCA; 3 = UDCA; 4 = DCA; 5 = CA; 6 = glyco-LCA; 7 = glyco-CDCA; 8 = glyco-UDCA; 9 = glyco-DCA; 10 = glyco-CA; 11–20 as in Fig. 2.

Table 3
MU values calculated by approximate linear and cubic expression methods

Compound	Linear expression		$\Delta[Um]_{\lvert Iso.-Prog.\rvert}$ [a]	Cubic expression		$\Delta[Um]_{\lvert Iso.-Prog.\rvert}$ [a]
	Isothermal[b]	Programmed[c]		Isothermal[d]	Programmed[e]	
LCA 3-Glc.	45.49	45.62	0.13	45.53	45.58	0.05
CDCA 3-Glc.	47.42	47.32	0.10	47.54	47.59	0.05
UDCA 3-Glc.	46.69	46.70	0.01	46.77	46.85	0.08
DCA 3-Glc.	47.42	47.32	0.10	47.54	47.59	0.05
CA 3-Glc.	49.20	48.78	0.42	49.40	49.40	0.00
LCA 3-GlcA.	45.02	45.18	0.16	45.04	45.08	0.04
CDCA 3-GlcA.	47.11	47.04	0.07	47.21	47.26	0.05
UDCA 3-GlcA.	46.26	46.32	0.06	46.32	46.40	0.08
DCA 3-GlcA.	47.01	46.96	0.05	47.11	47.16	0.05
CA 3-GlcA.	48.82	48.48	0.34	49.00	49.01	0.01

The samples were measured as Me-DMES ether derivatives.
[a] Differences in the MU values between isothermal and temperature-programmed GC conditions.
[b] $y = -2.66 + 0.76 \times 10^{-1}x$ ($n = 27$, R.S.D. = 0.50%).
[c] $y = -2.48 + 0.74 \times 10^{-1}x$ ($n = 27$, R.S.D. = 1.11%).
[d] $y = -3.15 + 1.08 \times 10^{-1}x - 0.67 \times 10^{-3}x^2 - 0.04 \times 10^{-4}x^3$ ($n = 27$, R.S.D. = 0.19%).
[e] $y = -2.53 + 0.57 \times 10^{-1}x + 1.04 \times 10^{-3}x^2 - 0.14 \times 10^{-4}x^3$ ($n = 27$, R.S.D. = 0.13%).

linear and cubic expressions obtained were 0.50% (isothermal) and 1.11% (programmed) ($n = 27$) and 0.19% (isothermal) and 0.13% (programmed) ($n = 27$), respectively, indicating a higher reliability of the latter expression. It is also evident from Table 3 that in general the differences in the MU values between isothermal and temperature-programmed GC conditions by applying a cubic expression, defined as $\Delta[Um]_{\lvert Iso.-Pro.\rvert}$ values, are much smaller than those obtained by applying a linear expression. Accordingly, the MU values of comparatively polar and high-boiling compounds such as bile acid glycosides may be calculated by using a polynomial equation.

In conclusion, the 3-glucoside and 3-glucuronide conjugates of bile acids have been successfully separated by GC without need for the prior deconjugation. The combined use of a suitable derivative and a stainless-steel capillary column, Ultra ALLOY-1 (HT), chemically bonded and cross-linked with dimethylsiloxane, provided excellent GC characteristics and separations of isomeric bile acid glycosides as their methyl ester silyl ether derivatives with relatively short analysis times. The retention data reported here provide an insight into the structural elucidation of these biologically important bile acid glycosides, and the method may have the ability to determine simultaneously unconjugated and glycine-, glucoside- and glucuronide-conjugated bile acids in biological fluids without prior group separation and deconjugation.

Acknowledgements

We are grateful to Dr. C. Watanabe, Frontier Lab., for his helpful advice on the use of the stainless-steel capillary column. Thanks are also due to Tokyo Tanabe for the generous supply of ursodeoxycholic acid 3-glucuronide. This work was supported in part by a Grant-in-Aid for Scientific Research from the Ministry of Education, Science and Culture of Japan.

References

[1] P. Back, K. Spacznsky and W. Gerok, *Hoppe-Seyler's Z. Physiol. Chem.*, 355 (1974) 749.
[2] P. Back, *Hoppe-Seyler's Z. Physiol. Chem.*, 357 (1976) 212.
[3] A. Almé and J. Sjövall, *J. Steroid Biochem.*, 13 (1980) 907.
[4] J. Goto, K. Suzaki, M. Ebihara, T. Nambara and A. Masu, *J. Chromatogr.*, 345 (1985) 241.
[5] H. Matern, S. Matern and W. Gerok, *Proc. Natl. Acad. Sci. U.S.A.*, 81 (1984) 7036.

[6] H.-U. Marschall, B. Egestad, H. Matern and J. Sjövall, *FEBS Lett.*, 213 (1987) 411.
[7] H.-U. Marschall, G. Green, B. Egestad and J. Sjövall, *J. Chromatogr.*, 452 (1988) 459.
[8] H. Wietholtz, H.-U. Marschall, R. Reuschenbach, H. Matern and S. Matern, *Hepatology*, 13 (1991) 656.
[9] H.-U. Marschall, B. Egestad, H. Matern, S. Matern and J. Sjövall, *J. Biol. Chem.*, 264 (1989) 12989.
[10] H.-U. Marschall, H. Matern, H. Wietholtz, B. Egestad, S. Matern and J. Sjövall, *J. Clin. Invest.*, 89 (1992) 1981.
[11] J.M. Street and K.D.R. Setchell, *Biomed. Chromatogr.*, 2 (1988) 229.
[12] T. Iida, T. Itoh, K. Hagiwara, F.C. Chang, J. Goto and T. Nambara, *Lipids*, 24 (1989) 1053.
[13] T. Iida, T. Tamaru, F.C. Chang, J. Goto and T. Nambara, *Biomed. Chromatogr.*, 6 (1992) 4.
[14] T. Iida, T. Tamaru, F.C. Chang, J. Goto and T. Nambara, *J. Chromatogr.*, 558 (1991) 451.
[15] C. Watanabe, M. Morikawa, K. Sato, Y. Takayama and R. Freeman, in *14th International Symposium on Capillary Chromatography*, 1992, p. 6.
[16] J. Goto, K. Suzaki and T. Nambara, *Chem. Pharm. Bull.*, 28 (1980) 1258.
[17] T. Iida, S. Nishida, Y. Yamaguchi, M. Kodake, F.C. Chang, T. Niwa, J. Goto and T. Nambara, *J. Lipid Res.*, in press.
[18] W.J.A. VandenHeuvel, W.L. Gardiner and E.C. Horning, *Anal. Chem.*, 36 (1964) 1550.
[19] T. Iida, T. Momose, T. Tamura, T. Matsumoto, J. Goto, T. Nambara and F.C. Chang, *J. Chromatogr.*, 389 (1987) 155.
[20] T. Iida, I. Komatsubara, F.C. Chang, J. Goto and T. Nambara, *J. Chromatogr.*, 537 (1991) 345.
[21] J. Goto, Y. Teraya, T. Nambara and T. Iida, *J. Chromatogr.*, 585 (1991) 281.
[22] J. Goto, K. Watanabe, H. Miura, T. Nambara and T. Iida, *J. Chromatogr.*, 388 (1987) 379.

ELSEVIER

Journal of Chromatography A, 689 (1995) 85–96

JOURNAL OF CHROMATOGRAPHY A

Sodium dodecyl sulfate capillary electrophoresis of proteins in entangled solutions of poly(vinyl alcohol)

Ernesto Simò-Alfonso[a,1], Monica Conti[a], Cecilia Gelfi[b], Pier Giorgio Righetti[a,*]

[a]*Faculty of Pharmacy and Department of Biomedical Sciences and Technologies, University of Milan, Via Celoria 2, Milan 20133, Italy*

[b]*ITBA, CNR, Via Ampère 56, Milan, Italy*

First received 19 July 1994; revised manuscript received 5 September 1994

Abstract

A novel polymer network is described for efficient sieving of sodium dodecyl sulfate (SDS)–protein complexes: poly(vinyl alcohol) (PVA; average M_r 133 000). The entanglement threshold of these solutions was found to be at 3% (w/v) PVA. Solutions from 4 to 6% PVA offer excellent resolution in the 14 400–94 000 protein molecular mass interval. Ferguson plot analysis showed that the separation is indeed based on mass discrimination, as it should in SDS electrophoresis, with extrapolated (at 0% polymer) limit values of mobility for all particles in the range $(2.34–2.87) \cdot 10^{-8}$ m^2 V^{-1}s^{-1}. The advantages of PVA are full transparency in the UV region down to 200 nm and extremely low viscosities (e.g., a 5% PVA solution has a viscosity 25 times greater than that of buffer at 30°C). A unique wall effect was found, by which, on decreasing the inner diameter of the capillary from 75 to 25 μm, the apparent entanglement threshold was shifted to extremely dilute PVA solutions, since in 25-μm capillaries efficient sieving was obtained below 1% PVA, i.e., at concentrations well below the entangled regime. It is hypothesized that residual, free silanols present (even in a coated capillary) act as nucleation sites for H-bond formation and aggregation of free PVA molecules.

1. Introduction

In 1983, Hjertén [1] was the first to demonstrate the use of capillaries filled with gels while separating the components of bovine serum albumin. Later, Cohen and co-workers [2,3] showed the value of gel-filled capillaries in high-resolution analysis of charged macromolecules by capillary zone electrophoresis (CZE). Typically, for mass evaluation of sodium dodecyl sulfate (SDS)–protein complexes, a polyacrylamide gel was the matrix of choice also in CZE [2–4], but separations in 10–25% HydroLink gels were also reported [5]. However, in contrast to slab-gel techniques, gel-filled capillaries have so far met with only limited success. This is due to a variety of reasons, such as pore-size limitations, formation and trapping of air bubbles during gel polymerization, denaturation and collapse of the matrix due to local overheating, sample trapping and precipitation at the injection port.

Soon chemically cross-linked gels were

* Corresponding author.

[1] On leave of absence from the Departamento de Quimica Analitica, Facultad de Quimica, Universitat de Valencia, 46100 Burjassot, Spain.

0021-9673/95/$09.50
SSDI 0021-9673(94)00862-0

abandoned in favour of viscous solutions of linear (or branched) polymers, according to original observations of De Gennes [6] and Bode [7] that polymer networks, above a critical concentration (the "entanglement threshold") would be efficient in sieving macromolecules. Linear polyacrylamide, as a viscous polymer solution, was soon proposed for mass discrimination of SDS–protein complexes in CZE [8]. Sieving dynamic matrices are immune from the noxious problems of air-bubble formation (which would automatically open the electric circuit in such tiny channels) and from sample precipitation at the injection port. Owing to the lack of a fixed-pore geometry, also very large macromolecules (or aggregates) can open a pore in their wake, while they would inevitably precipitate at the deposition site in cross-linked polyacrylamide gels. This allows repeated use of the same matrix (typically >30 runs). Even on matrix fouling, the viscosity of a 6% polyacrylamide network still allows refilling of the capillary at the normal pressures utilized in CZE for, e.g., sample injection [9]. However, even this solution did not prove optimal. As shown by Ganzler et al. [10], the ideal detection system for proteins in transit in a capillary would be by UV absorption at 214 nm, where the molar absorptivities of proteins are 20–50 times larger than at 280 nm. However, at this low wavelength, polyacrylamide, which also contains amido bonds, absorbs 20–50 times more light than other UV-transparent polymers at comparable concentrations.

A search was therefore started for efficient UV-transparent polymers, ideally also exhibiting low viscosity, so as to allow replacement and refilling even after each run, if needed. Ganzler et al. [10] reported successful SDS runs in two such formulations: a 10% solution of dextran (M_r $2 \cdot 10^6$) and a 3% solution of polyethylene glycol (PEG, average M_r 100 000). The applicability of such an approach was later confirmed by Lausch et al. [11]. Soon, several articles appeared reporting efficient protein sieving in other types of polymers. Thus, Guttman et al. [12] described the use of lower M_r dextrans (M_r 72 000, 10% branching, at a 15% concentration) and of polyethylene oxide (PEO, typically a 3% solution of average M_r 100 000). They also studied the influence of temperature on the sieving effect in SDS–protein complexes and found the best separations at 50°C (in dextrans, whereas a deterioration of separation was apparent in the same temperature interval in PEO). Recently, SDS electrophoresis was reported for other types of UV-transparent polysaccharides, such as pullulan [a branched polysaccharide composed of α-(1–6)-linked maltotriose] [13]. Typically, separations were carried out in a 7% polymer solution (having average M_r 50 000–100 000), although good resolution was achieved for proteins standards (in an M_r range from 14 400 to 116 000) from as low as 1% up to 7% pullulan.

In this work, we investigated the possibility of using poly(vinyl alcohol) (PVA, average M_r 133 000) as a dynamic sieving matrix for SDS–protein complexes. This investigation stems from the observation of Righetti and Snyder [14] that the viscosity of PVA solutions could be greatly modulated by adding to this polymer short PEG chains, to the point of forming a thermally reversible gel. The use of PVA has been reported previously by Schomburg's group, but mostly for dynamic coating of bare fused silica [15] and in some attempts at DNA sieving [16]. The same group ultimately rejected the use of PVA, on the grounds of its deterioration on storage due to strong self-aggregation and potential precipitation.

2. Experimental

2.1. Reagents

Poly(vinyl alcohol) (PVA) and hydroxyethylcellulose (HEC) were obtained from Poly-Sciences (Warrington, PA, USA), polyethylene glycol (PEG), SDS, 2-mercaptoethanol and sulfuric acid from Merk (Darmstadt, Germany) and 2-amino-2-methyl-1,3-propanediol (AMPD) and cacodylic acid (CACO) from Sigma (St. Louis, MO, USA). Low-molecular-mass protein standards (α-lactalbumin, M_r 14 400, trypsin inhibitor, M_r 20 100, carbonic anhydrase, M_r 30 000,

ovalbumin, M_r 43 000, bovine serum albumin, M_r 67 000, phosphorylase *b*, M_r 94 000, dextran T-2000, dextran T-500 and dextran T-250 (Dex) were purchased from Pharmacia–LKB (Uppsala, Sweden). Cerium (IV) sulfate tetrahydrate was obtained from Fluka (Buchs, Switzerland) and acrylamide, ammonium peroxodisulfate and N,N,N′,N′-tetramethylethylendiamine (TEMED) from Bio-Rad Labs (Richmond, CA, USA). N-acryloylaminoethoxyethanol (AAEE) was synthesized according to Chiari et al. [17].

2.2. Capillary electrophoresis

CZE was performed with a Waters Quanta 4000 apparatus from Millipore (Milford, MA, USA) and in parallel with a Model 270 A-HT capillary electrophoresis system (Applied Biosystems, Foster City, CA, USA). Capillaries (34 cm × 100–25 μm I.D.) coated by a slight modification of Hjertén's protocol utilizing AAEE as monomer [18] and filled with different types of polymers at various concentrations were used. For separations in dextran polymers the capillaries were additionally coated with Ce^{IV} salts as described by Ganzler et al. [10]. Before sample injection the baseline and current were monitored at 5 kV for 20 min until constant values were reached. The samples were injected at 5 kV for 2 s. The absorbance was monitored at 214 nm.

2.3. Sample preparation

The low-molecular-mass markers were dissolved (to a final concentration of 4 mg/ml) in 100 μl of 60 m*M* CACO–AMPD buffer containing 1% SDS and 1% 2-mercaptoethanol (pH 8.8), heated at 100°C for 5 min and immediately injected. The same buffer was used in all CZE runs, except that the concentration of SDS was lowered to 0.1% and 2-mercaptoethanol was omitted.

2.4. Polymer preparation

PVA and HEC were dissolved in the AMPD–CACO running buffer at 70°C, then sonicated to eliminate air bubbles. PEG and Dex, at various concentrations, were dissolved in AMPD–CACO buffer at room temperature. Polyacrylamide was polymerized in capillaries for 1 h at room temperature. All capillaries were conditioned with separation buffer for 20 min at 5 kV prior to the initial protein separation run.

2.5. Viscosimetry

Viscosity measurements on polymer solutions were performed on a Bohlin VOR rheometer (Bohlin Rheology, Lund, Sweden), with the sample thermostated at 30°C. The shear rate chosen was in the interval 1.86–2.34 s^{-1}. A concentric cylinder measuring system was adopted, with a 14 mm diameter for the inner cylinder and a 15.4 cm diameter for the outer cylinder. Viscosity is expressed in mPa s, the viscosity of water at 25°C being 1 and that of the running buffer being 1.68.

2.6. Calculation of global resolution

The global resolution (R_{sg}) was calculated as the product of each individual resolution divided by the average of individual resolutions. By this method too large differences in individual resolutions are minimized and data are more easily compared. A global resolution as a plain average of individual resolutions could give erroneous data [19].

3. Results

We first evaluated the overall resolution of the six denatured protein markers as a function of the percentage of polymer in the Dex-2000 system of Ganzler et al. [10], and also in shorter dextran chains (M_r 500 000 and 250 000, Dex-500 and Dex-250, respectively). As shown in Fig. 1A, Dex-2000 appears to offer the highest R_{sg} at the lowest concentration. Both Dex-500 and Dex-250 exhibit lower R_{sg} and have to be used at high concentrations, well above the 10% value found to be optimum with Dex-2000 [10]. However, the situation is more complex than that: if

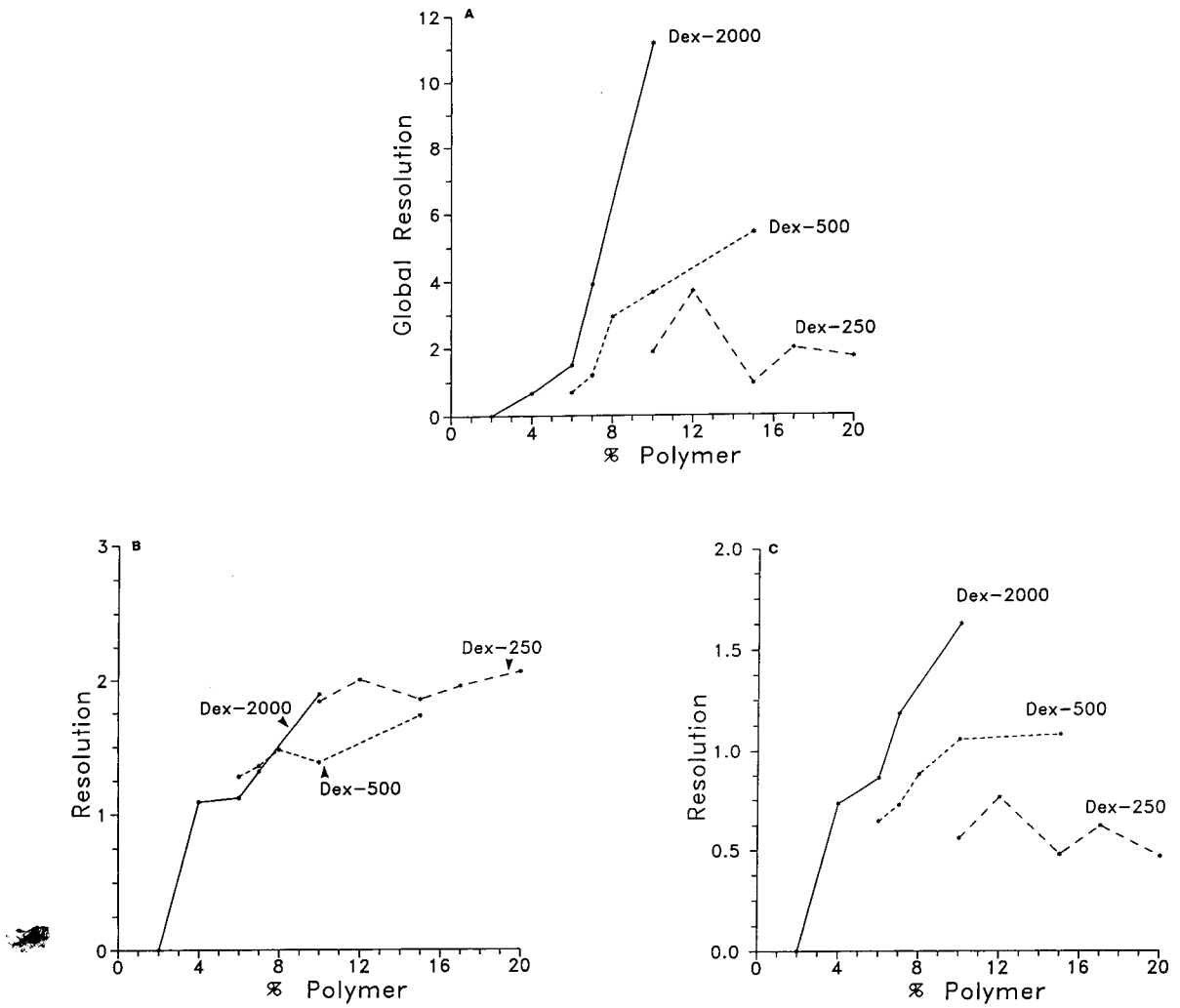

Fig. 1. Resolution vs. percentage of polymer in the separation of six protein markers in three different dextran solutions: Dex-2000, Dex-500 and Dex-250. (A) Global resolution; (B) resolution of an adjacent pair of polypeptide chains of relatively low M_r (14 400 and 20 100); (C) resolution of an adjacent pair of polypeptide chains of relatively high M_r (67 000 and 94 000). Experimental conditions: Waters Quanta 4000; capillary, 34 cm × 75 μm I.D.; buffer, 60 m*M* AMPD–CACO (pH 8.8) in 0.1% SDS; sample load, 5 kV, 2 s (protein concentration 4 mg/ml); run, 8 kV, 11.5 μA. Analogous results were obtained with the Model 270 A-HT capillary electrophoresis system.

we now evaluate resolution in terms of adjacent pairs, it is found that for the smaller proteins (the pair of M_r 14 400 and 20 100), the highest resolution is indeed obtained in the shorter dextran chains (Dex-250; see Fig. 1B). Conversely, if we now evaluate the resolution for the highest M_r pair (67 000 and 94 000), the best performance is again offered by Dex-2000 (Fig. 1C). However, attempts at otpimizing the resolution over the entire analyte M_r range by blending Dex-250 with Dex-2000 in appropriate ratios did not give significant improvements in performance (data not shown).

The 10% Dex-2000 sieving matrix, as proposed by Ganzler et al. [10], was found to offer a good performance coupled with good run repro-

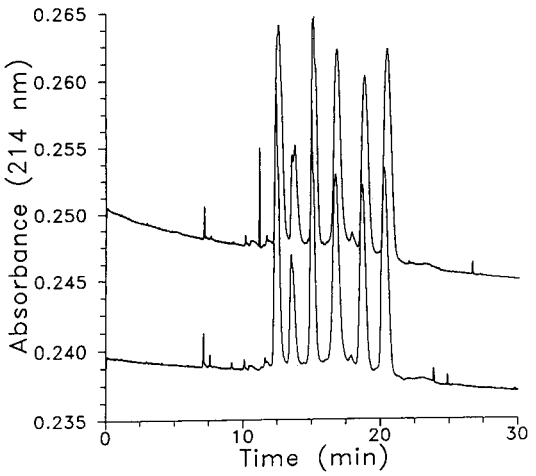

Fig. 2. SDS electropherogram (214-nm readings) of six protein standards. Peaks (from left to right): α-lactalbumin, M_r 14 400; trypsin inhibitor, M_r 20 100; carbonic anhydrase, M_r 30 000; ovalbumin, M_r 43 000; bovine serum albumin, M_r 67 000; phosphorylase *b*, M_r 94 000. Sieving matrix, 10% Dex-2000. All other conditions as in Fig. 1. Two consecutive runs are displayed.

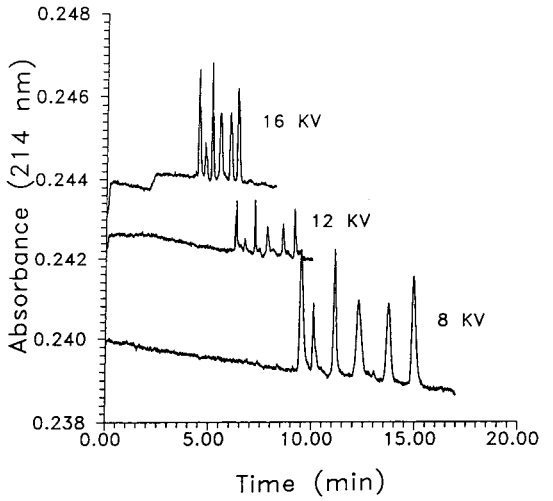

Fig. 3. SDS electropherograms (214-nm readings) of six protein standards. Peaks (from left to right): α-lactalbumin, M_r 14 400; trypsin inhibitor, M_r 20 100; carbonic anhydrase, M_r 30 000; ovalbumin, M_r 43 000; bovine serum albumin, M_r 67 000; phosphorylase *b*, M_r 94 000. Sieving matrix, 4% PVA; capillary, 34 cm × 50 μm I.D. Upper trace, 16-kV run; middle trace, 12-kV run; lower trace, 8-kV run.

ducibility, as shown in Fig. 2. Attempts at using Dex-2000 at concentrations >10% failed for two reasons: the viscosity is too high and the resolution drops markedly (possibly also owing to too long transit times with concomitant peak diffusion; not shown).

We next assessed the performance of PVA as a function of applied voltage at fixed percentage of polymer (4%) and fixed capillary I.D. (50 μm). As shown in Fig. 3, the set of six protein markers is fully resolved at all applied voltages, with baseline resolution even at 16 kV. As expected, at the highest applied voltage the train of peaks is eluted much earlier, between 4 and 8 min. The sieving properties of PVA, however, vary dramatically with concentration. As shown in Fig. 4, when evaluating resolution as a function of polymer concentration, the series of profiles shown, covering the 3–8% interval, suggest a loss of resolution at both ends of the range, with a peak of performance centred at 5–6% polymer. However, while the loss of resolution at the lowest polymer concentration explored (3–4%) is not so pronounced (the six marker peaks are still there), the higher PVA concentration values

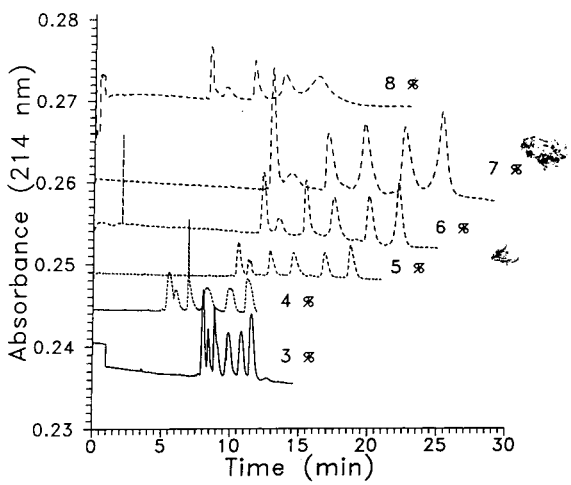

Fig. 4. SDS electropherograms (214-nm readings) of six protein standards. Peaks (from left to right): α-lactalbumin, M_r 14 400, trypsin inhibitor, M_r 20 100; carbonic anhydrase, M_r 30 000; ovalbumin, M_r 43 000; bovine serum albumin, M_r 67 000; phosphorylase *b*, M_r 94 000. Capillary, 34 cm × 75 μm I.D. Sieving matrix (from bottom to top): 3%, 4%, 5%, 6%, 7% and 8% PVA. All other experimental conditions as in Fig. 1.

(7–8%) show a marked decrease in performance, with loss of some analyte peaks and unacceptably high zone spreading.

In order to demonstrate that the separation is based on protein M_r values, we constructed a Ferguson plot with the data in Fig. 4. Ferguson graphs are elaborated by plotting the logarithm of mobility (in $m^2\ V^{-1}\ s^{-1}$) as a function of the concentration of sieving polymer. As shown in Fig. 5, these plots give quasi-linear curves, having a slope (K_R) proportional to the effective molecular surface area and thus, ultimately, to M_r. It is also seen that, when extrapolated to 0% PVA, the mobilities tend to converge to limiting values in the range $\mu = (2.34–2.87)\cdot 10^{-8}$ $m^2\ V^{-1}\ s^{-1}$.

A unique effect of the capillary diameter on resolution is reported in Fig. 6A. Curiously, if one adopts a 75 μm I.D. capillary, the overall resolution is diminished and the R_{sg} peak is shifted at higher PVA values (6% PVA, Fig. 6A). Conversely, when a 50 μm I.D. capillary is utilized, two phenomena are evident: R_{sg} is five

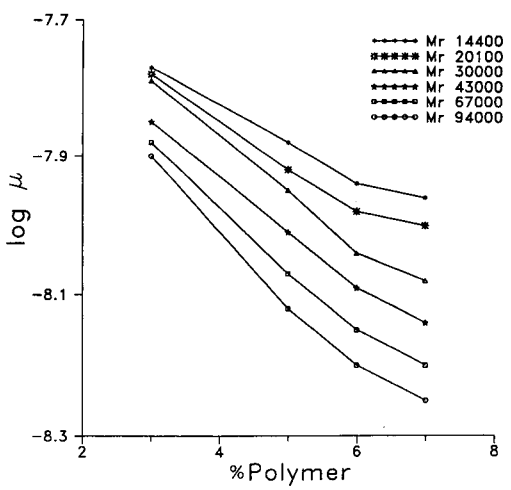

Fig. 5. Ferguson plot analysis of the data in Fig. 4. The peak transit times in Fig. 4 (at different PVA concentrations) are transformed into mobilities (μ, expressed in $m^2\ V^{-1}\ s^{-1}$). Finally, for each M_r marker, the log M_r is plotted against PVA concentration (in the 3–7% range).

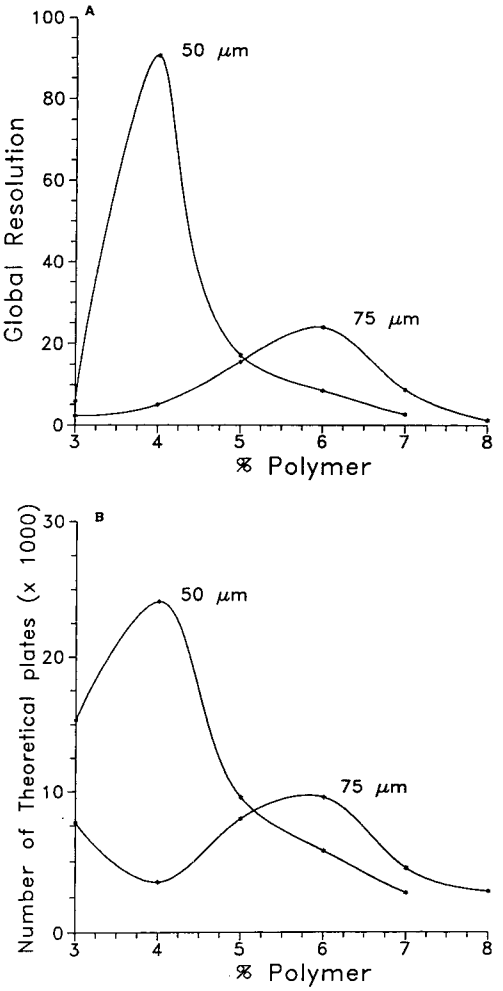

Fig. 6. (A) Global resolution and (B) number of theoretical plates vs. PVA concentration in two different capillaries of 50 and 75 μm I.D.

times higher and the highest resolution is found at much lower PVA concentrations (barely 4%). An even more dramatic effect is found if a 25 μm I.D. capillary is adopted: the highest R_{sg} is found centred below 1% PVA (not shown, owing to difficulties in obtaining a proper UV absorbance signal). This effect is unique, as apparently such separations are obtained well below the entanglement threshold, as will be discussed below. If the results are expressed in terms of

theoretical plate number, analogous data are obtained (Fig. 6B) for the two capillary diameters investigated. Hence it appears that, with PVA solutions, resolution is strongly dependent on some peculiar wall effect (see Discussion). We could exclude temperature effects on R_{sg}, as shown in Fig. 6A, because, at the applied voltage used (8 kV), the temperature difference between the two runs was barely 1°C, as calculated with the aid of the thermal theory and a computer program we have developed for assessing the precise inner temperature in a capillary [20,21].

We finally adopted a 50 μm I.D. capillary, as it represents a good compromise between sensitivity and the "wall effect" reported in Fig. 6A. With this system, we investigated global resolution as a function of increasing PVA concentration and different applied voltages. As shown in Fig. 7, the highest R_{sg} is obtained at 8–12 kV, with a peak centred at relatively low PVA concentration (4%). When the applied voltage is increased to 16 kV, two phenomena become apparent: R_{sg} is substantially lowered and maximum resolution is obtained only at higher PVA concentrations (here slightly above 5%). It should be noted that there are no appreciable viscosity changes, because on going from 8 to 16 kV the temperature increment of the buffer inside the capillary is only 1°C.

In a recent report, Barron et al. [22] described a unique phenomenon occurring in hydroxyethylcellulose (HEC, M_n 90 000–105 000): DNA separations seem to occur at HEC concentrations ($\leq$0.002%) well below the entanglement threshold. Since in principle an SDS-coated portein could behave, in electrophoretic migration, much like a small DNA fragment, we tried to evaluate whether such a phenomenon could apply also in the present instance. We therefore assessed the viscosity of the PVA solutions at progressively higher concentrations. As shown in Fig. 8, departure from linearity occurs at precisely 3% (w/v) polymer concentration. According to Barron et al. [23], this point represents the entanglement threshold. Hence it appears that all SDS–protein separations are only operative above this critical threshold, in agreement with De Gennes' [6] theory. The fact that in describing Fig. 6A and B we have hinted that in a 25

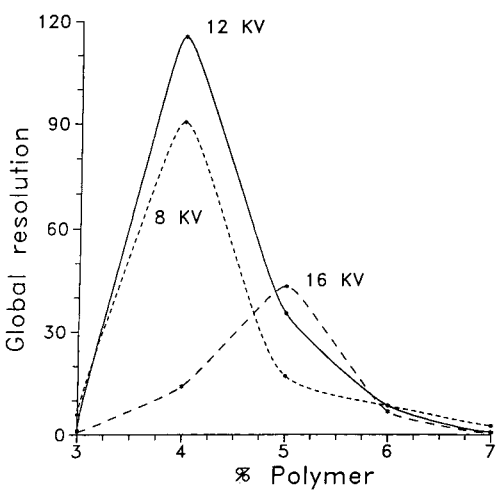

Fig. 7. Global resolution vs. PVA concentration in a 50 μm I.D. capillary as a function of three different applied voltages: 8, 12 and 16 kV.

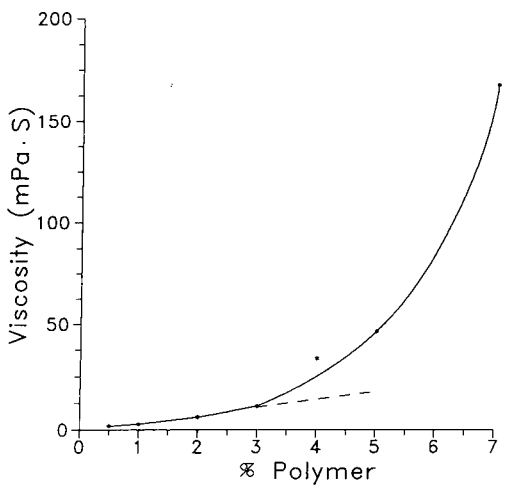

Fig. 8. Viscosity of PVA solutions. The point of departure from the initial linear slope is taken to represent the entanglement threshold (in this case 3% PVA solution). Viscosities measured at 30°C with a Bohlin VOR rheometer.

μm I.D. capillary separations could occur at PVA values as low as 1% is interpreted by us by assuming a completely different mechanism (see Discussion).

4. Discussion

4.1. Use of viscous polymer solutions

As now amply shown in the literature, viscous polymer networks represent a unique solution for proper macromolecular sieving in capillaries, where gel polymerization is besieged by severe problems. For routine operations, the search has been extended to polymers possessing some unique characteristics, such as UV transparency (to as low as 214 nm for peptide bond analysis) and low viscosity, so as to allow refilling even after each run, if needed. The solution proposed by Ganzler et al. [10], of using Dex-2000, satisfies both requirements and appears to work very well in SDS electrophoresis. In a search for other polymers, we propose here PVA, which also is transparent to as low as 200 nm and which also exhibits low viscosity. In fact, at the concentrations routinely used of 4–5% polymer, above the entanglement threshold, the viscosity is extremely low, 25 times higher than that of plain buffer (see Fig. 8). This is very advantageous, as replenishing the capillary after each run does not in fact present any problem, as opposed to polyacrylamide solutions, which are so viscous as to be unyielding to any pumping process above a critical 6% concentration [9,24]. However, such low-viscosity solutions would represent a problem in uncoated capillaries: the electrosmotic pump would quickly push them out of the capillary, thus impairing resolution. Therefore, even though, in principle, in separations of highly negative charged species, such as DNA and SDS-laden proteins, coating of the capillary inner surface would per se not be necessary, it is in fact essential in PVA, dextran and any other low-viscosity polymer solution. In order to enhance reproducibility, we have additionally adopted coating with the novel monomer N-acryloylaminoethoxyethanol, coupling a high hydrophilicity with extreme hydrolytic stability. This coating was found to be stable even up to 200 h of operation at pH 10.5 [17].

4.2. Entanglement threshold

According to De Gennes' theory [6], a fundamental distinction exists between dilute polymer solutions where the coils are separated and more concentrated solutions where the coils overlap. At the overlap threshold, the coils begin to be densely packed and thus begin to entangle. As a result, a kind of a "porous" structure is formed, with a correlation length, or average mesh size, that decreases rapidly with increasing concentration. When biological macromolecules are driven through this meshwork of coils, sieving occurs, much like in a chemically cross-linked gel. Thus, up to the present time, by general consensus, it was believed that sieving in viscous polymer solutions would occur only near and above this entanglement threshold. This view has now been challenged by Barron and co-workers [22,23], who demonstrated that, with DNA fragments, sieving can occur in extremely dilute HEC solutions ($\leq$0.002%), i.e., well below this threshold, set at 0.35% polymer in the case of HEC. In reality, these data can be fully reconciled with De Gennes' theory simply by invoking a "transient entanglement coupling mechanism". A good example is given in ref. [22]: HEC (M_n 90 000–105 000) behaves in solution much like a rigid rod, with a Porod–Kratky radius of gyration (R_g) of 56.5 nm. If, in a dilute HEC solution, one attempts separation, by a sieving mechanism, of a small DNA fragment, say of 118 base pairs (bp) (having an R_g of 35 nm and a contour length of 40 nm, i.e., below the 45-nm persistence length of ds DNA), essentially no entanglement will result between this small DNA and HEC and no sieving will occur. Conversely, if one takes a long restriction fragment (e.g., a 9416 bp DNA, having an R_g of 533 nm, i.e., ten times larger than that of an HEC molecule), it will be this long DNA filament (which, if extended, would have an end to end length of 3201 nm) which will screen a large number of HEC coils and become entangled.

Sieving will thus occur through this transient "entangled" regime. In agreement with this, we have found that in our solutions of PVA coils (which have an average size similar to that of HEC) we could not obtain a satisfactory separation of PCR fragments in the 100–400 bp range. How is it, then, that we can have efficient sieving of proteins in the M_r 14 400–94 000 range? This could be due to two additive mechanisms. First, protein–SDS co-micelles are much larger than a protein filament alone. In addition, PVA chains might have a unique entanglement regime, owing to extensive hydrogen bonding, as explained below.

4.3. Use of Ferguson plots

The Ferguson plot analysis (Fig. 5) is presented at the request of a referee and was not in our original paper. Fortunately, analysis of Fig. 5 could lead to some interesting conclusions. It should first be recalled that, according to the original theory [25], proteins having the same surface charge, but differing in mass, should have different slopes (K_R), but the same y-intercept (corresponding to free mobility, μ). This should be the case for DNA and SDS–protein micelles alike. However, if one analyses most of the Ferguson plots presented in the literature, one can see that, although the K_R values almost always agree with expectations, very rarely does this occur for the y-intercepts. Our data are no exception to this general trend. Going back to Fig. 5, one can see that there are at least three different "intercepts": (a) the smaller molecules (M_r 14 400–30 000), coalesce at 2.2% PVA (at which they exhibit an apparent common value of free mobility of $1.9 \cdot 10^{-8}$ m^2 V^{-1} s^{-1}); (b) larger molecules (M_r 43 000–94 000) coalesce at 1.2% PVA (at which they exhibit the same apparent common value of free mobility of $1.9 \cdot 10^{-8}$ m^2 V^{-1} s^{-1}); finally, if one extrapolates to 0% PVA, all free μ values diverge again, in the range $(2.34–2.87) \cdot 10^{-8}$ m^2 V^{-1} s^{-1}. What is the meaning of all this? We should like to propose two different scenarios, as follows.

(α) The α scenario goes back to the concept of relativity. Perhaps the "entanglement" threshold, so much under debate today, is not really an absolute value, but a relative one. It is an intrinsic property of the polymer solution, per se, but it is a relative value because it depends also on the size of the object to be sieved. Thus, while the "entanglement threshold" of pure PVA, per se, is 3% (see Fig. 8) in reality, for smaller proteins (the M_r 14 400–30 000 group) the solution becomes fully disentangled at 2.2% concentration (where all species exhibit the same free mobility), whereas for larger particles (in our case the M_r 43 000–94 000 polypeptides) the solution is fully disentangled at 1.2% concentration (common μ value).

(β) The β scenario regards the common extrapolated value of μ at 0% PVA (which is anything but common). What is the meaning of this? We have at the moment only one explanation: perhaps it is not completely true that the ratio of protein to SDS (believed to be in general 1:1.4, w/w) is as constant as we believe it to be, but it depends to some extent also on the mass of the protein (exceptions due to the amino acid composition and to prosthetic groups are well known already). If this is true, one can never really expect a single μ value corresponding to the free mobility of the particle under investigation. Of course, one could argue that larger particles experience a greater viscous drag in free solution, so that the free μ value will not be the same, anyhow. However, this can only apply (assuming that the charge-to-mass ratio is constant in protein–SDS micelles) if the shape of such micelles is not the same, whereas in general it is believed that polypeptides swamped by SDS have the same shape, resembling a prolate ellipsoid, with a constant minor axis and a major axis proportional to the length of the polypeptide chain [26].

4.4. Use of different sieving polymers

It is now apparent that different polymers cannot be used interchangeably for DNA and protein separations alike. For example, although HEC has been found to perform extremely well in DNA separations, especially for larger fragments, it did not give any acceptable separation

of protein–SDS complexes in all ranges of concentrations explored (from 0.35% up to 1.5%, i.e., the highest possible concentration compatible with injecting the solution in a capillary). Also PEG (M_n 35 000) did not produce any acceptable result up to 40% concentration. Conversely, polyacrylamide, which is one of the best viscous polymer solutions for DNA separations, also performed very well in sieving SDS–protein co-micelles. However, owing to its very high absorbance, it cannot be proposed as the matrix of choice when monitoring at 214 nm. PVA seems to have a unique behaviour, producing different types of entangled regimes, possibly as a result of a wall effect originating inside the capillary. We have seen, in fact, that on decreasing the capillary I.D. from 75 to 25 μm, the peak resolution is progressively lowered from 6% to 4% PVA to as low as <1% PVA in the narrowest bore explored (25 μm). This unique behaviour (which would seem to contradict the fact that sieving should occur above the entanglement threshold, set at 3% polymer in the case of PVA) might be explained through an observation made by Schomburg and co-workers [16]: "PVA could be subjected to strong self-aggregation by intermolecular interaction between the polymer chains via hydrogen bonding between the hydroxyl groups present in high concentration in the PVA molecule. The hydroxylic character of this molecule also affects the strong adsorptive interaction with the fused-silica surface and therefore the modifying properties of PVA. Ageing of PVA solutions in fused-silica capillaries could probably be initiated and accelerated by the silanol at the silica surfaces. The adsorbed PVA molecules may undergo a conformational rearrangement on the silica surface, which may facilitate the fixation of additional PVA layers on this surface". In agreement with these observations, we found, when attempting to measure the viscosity of PVA solutions directly in a CZE unit, as recently proposed by Bello et al. [27], that in each successive measurement (performed in bare silica capillaries) the viscosity of the same PVA solution increased markedly until complete clogging of the capillary bore occurred. In addition, recent observations suggest that, owing to the high shear rate existing in the double layer, polymer solutions could undergo a transition from a collapsed globule to extended filaments, which would greatly favour their adsorption into the Debye–Hückel layer and potentially facilitate the build-up of successive strata [28]. Hence we believe that the unique sieving properties shown in narrow-bore capillaries (25 μm), by which PVA solutions well below the entanglement threshold can efficiently separate protein–SDS complexes, are indeed an apparent phenomenon: at such a high surface-to-volume ratio, the wall effect becomes very pronounced and probably forces the PVA solution to assume an "entangled" regime. Hence we suggest that the wall, in very narrow-bore capillaries, provides nucleation sites for entanglement of very dilute PVA solutions, forcing them to assume an "entangled" regime (i.e., here the mechanism proposed by Barron et al. does not apply). In agreement with this, Righetti and Snyder [14] have shown that even minute amounts of sodium tetraborate, when added to a 5% PVA solution, can induce a transition from a viscous liquid to a gel phase. For example, in the presence of only 0.1% sodium tetraborate, a 5% PVA solution forms a thermally reversible gel, with a melting point of 50°C. As an additional proof of the formation of extensive hydrogen bonds in PVA solutions, we performed viscosity measurements on 8% PVA solutions as such and in the presence of 6 *M* urea. Whereas the viscosity of 8% PVA alone was 566 mPa s, the viscosity of 8% PVA in the presence of 6 *M* urea (the latter having a viscosity of 1.68 mPa s) was drastically diminished by 40%, down to only 341 mPa s.

5. Conclusions

PVA solutions [in the 4–6% (w/v) range] offer a unique dynamic sieving matrix for SDS electrophoresis. Such solutions are transparent down to 200 nm and have an extremely low viscosity, thus allowing replenishment of the capillary after each run. It is recommended that the capillary inner wall should be coated, not only for suppressing the electrosmotic flow, but also for minimizing the unique ageing and aggregation

phenomenon described above, induced by free silanols at the silica surface. Even in coated capillaries, it is suggested that when using PVA solutions, replenishment is routinely adopted after each run. In the absence of this precaution, separations start to deteriorate after the third run, possibly owing to the fact that, even with the best coating procedure, some silanols are still free and available for interaction.

Acknowledgements

This work was supported in part by grants from the Consiglio Nazionale delle Ricerche (Comitato di Chimica, Progetto Strategico), the Comitato di Medicina e Biologia and the Radius in Biotechnology (ESA, Paris). E, Simò-Alfonso gratefully acknowledges a grant from the Conselleria de Education i Cultura, Generalitat Valencia. We thank Dr. Cerizza (Applied Biosystems, Italy) for the kind loan of the Model 270 A-HT capillary electrophoresis system.

Note added

After this paper had been accepted, and during its revision, we found a few more articles just published dealing with SDS-CZE, which will be briefly mentioned here. Shieh et al. [29] have studied more thoroughly the sieving system composed of polyethylene oxide (PEO)–SDS. They found that, if the capillary is rinsed with 1 *M* HCl between each run, the coating (made of linear polyacrylamide) is stable for more than 400 runs (as a criticism of this, we can add that such strongly acidic conditions will hardly remove traces of contaminant proteins from run to run, as these conditions are precipitating, not solubilizing, for proteins). They also reported relative standard deviations (over 19 runs) of only 0.35–0.45%. We regret, in this paper, the continuing use of the term "gel" for viscous polymer solutions, which can only add to the confusion already existing. With the same PEO–SDS system, Guttman et al. [30], proposed an automated Ferguson plot analysis which can correct for the non-ideal behaviour of glycoproteins and lipoproteins in SDS electrophoresis due to anomalous binding of SDS. The possibility of performing Ferguson plot analysis, in the same PEO–SDS system, was simultaneously and independently proposed by Benedek and Thiede [31].

References

[1] S. Hjertén, in H. Hirai (Editor), *Electrophoresis '83*, Walter de Gruyter, Berlin, 1983, pp. 71–79.
[2] A.S. Cohen and B.L. Karger, *J. Chromatogr.*, 397 (1987) 409–417.
[3] A.S. Cohen, D.R. Najarian, A. Paulus, A. Gutman, A.J. Smith and B.L. Karger, *Proc. Natl. Acad. Sci. U.S.A.*, 85 (1988) 9660–9663.
[4] K. Tsuji, *J. Chromatogr.*, 550 (1991) 823–830.
[5] V. Dolnik and M.V. Novotny, *Anal. Chem.*, 65 (1993) 563–567.
[6] P.G. De Gennes, *Scaling Concepts in Polymer Chemistry*, Cornell University Press, Ithaca, NY, 1979.
[7] H.J. Bode, *Anal. Biochem.*, 83 (1977) 204–210.
[8] A. Widhalm, C. Schwer, D. Blass and E. Kenndler, *J. Chromatogr.*, 546 (1991) 446–451.
[9] M. Chiari, M. Nesi, M. Fazio and P.G. Righetti, *Electrophoresis*, 13 (1992) 690–697.
[10] K. Ganzler, K.S. Greve, A.S. Cohen, B.L. Karger, A. Guttman and N.C. Cooke, *Anal. Chem.*, 64 (1992) 2665–2671.
[11] R. Lausch, T. Scheper, O.W. Reif, J. Schlosser, J. Fleischer and R. Freitag, *J. Chromatogr. A*, 654 (1993) 190–195.
[12] A. Guttman, J. Horvath and N. Cooke, *Anal. Chem.*, 65 (1993) 199–203.
[13] M. Nakatani, A. Shibukawa and T. Nakagawa, *J. Chromatogr. A*, 672 (1994) 213–218.
[14] P.G. Righetti and R.S. Snyder, *Appl. Theor. Electrophoresis*, 1 (1988) 53–58.
[15] M. Gilges, H. Husmann, M.H. Kleemiss, S.R. Motsch and G. Schomburg, *J. High Resolut. Chromatogr.*, 15 (1992) 452–457.
[16] M.H. Kleemiss, M. Gilges and G. Schomburg, *Electrophoresis*, 14 (1993) 515–522.
[17] M. Chiari, C. Micheletti, M. Nesi, M. Fazio and P.G. Righetti, *Electrophoresis*, 15 (1994) 177–186.
[18] M. Chiari, M. Nesi and P.G. Righetti, *Electrophoresis*, 15 (1994) 616–622.
[19] J.R. Torres-Lapasiò, R.M. Villanueva-Camanas, J.M. Sanchis-Mallos, M.J. Medina-Hernández and M.C. García-Alvarez-Coque, *J. Chromatogr. A*, in press.
[20] M.S. Bello, P. de Besi and P.G. Righetti, *J. Chromatogr. A*, 652 (1993) 317–327.

[21] M.S. Bello, P. de Besi and P.G. Righetti, *J. Chromatogr. A*, 652 (1993) 329–336.
[22] A.E. Barron, H.W. Blanch and D.S. Soane, *Electrophoresis*, 15 (1994) 597–615.
[23] A.E. Barron, D.S. Soane and H.W. Blanch, *J. Chromatogr. A*, 652 (1993) 3–16.
[24] M. Chiari, M. Nesi and P.G. Righetti, *J. Chromatogr. A*, 652 (1993) 31–39.
[25] H.R. Maurer, *Disc Electrophoresis and Related Techniques of Polyacrylamide Gel Electrophoresis*, Walte de Gruyter, Berlin, 1971, pp. 8–20.
[26] B.D. Hames, in B.D. Hames and D. Rickwood (Editor), *Gel Electrophoresis of Proteins*, IRL Press, Oxford, 1990, pp. 1–148.
[27] M.S. Bello, R. Rezzonico and P.G. Righetti, *J. Chromatogr. A*, 659 (1994) 199–204.
[28] M.S. Bello, P. de Besi, R. Rezzonico, P.G. Righetti and E. Casiraghi, *Electrophoresis*, 15 (1994) 623–626.
[29] P.C.H. Shieh, D. Hoang, A. Guttman and N. Cooke, *J. Chromatogr. A*, 676 (1994) 219–226.
[30] A. Guttman, P. Shieh, J. Lindahl and N. Cooke, *J. Chromatogr. A*, 676 (1994) 227–231.
[31] K. Benedek and S. Thiede, *J. Chromatogr. A* 676 (1994) 209–217.

ELSEVIER

Journal of Chromatography A, 689 (1995) 97–105

JOURNAL OF CHROMATOGRAPHY A

Fluidified polyacrylamides as molecular sieves in capillary zone electrophoresis of DNA fragments

Cecilia Gelfi[a], Antonia Orsi[b], Fiorella Leoncini[b], Pier Giorgio Righetti[b,*]

[a]*ITBA, CNR, Via Ampère 56, Milan, Italy*

[b]*Faculty of Pharmacy and Department of Biomedical Sciences and Technologies, University of Milan, Via Celoria 2, Milan 20133, Italy*

First received 28 July 1994; revised manuscript received 6 September 1994

Abstract

In order to optimize the separation of DNA fragments, in the 50–500 base pairs (bp) range, a typical size interval of most polymerase chain reaction-amplified DNA chains produced for analysis of genetic diseases, different ways of preparing liquid linear polyacrylamides were evaluated. Standard linear polyacrylamides (PAA), as prepared with typical levels of catalysts (1 μl of pure N,N,N′,N′-tetramethylethylenediamine and 4 μl of 10% peroxodisulfate per ml of gelling solution) at room temperature, have extremely high weight-average molecular mass (M_w) values (in excess of $2 \cdot 10^6$) and can be injected or extruded from a capillary at concentrations above 6% only with great difficulty. The same polyacrylamide, if subjected to mastication by ultrasound at 45 kHz for up to ca. 50 h, exhibits much reduced viscosities (e.g. 700 vs. 3600 mPa s, at 8% concentration) and chain lengths (M_w ca. 550 000) and offers increased resolution in the 50–500 bp interval. However, chain rupture by ultrasound produces charged chains, which migrate out of the capillary under the influence of an electric field, thus impairing resolution. Two other ways have been found to produce uncharged, short chains of very low viscosity: chain termination in 2-propanol by polymerization at 35 and 70°C, respectively. The latter process produces chains of M_w as low as 230 000 (M_n = 55 000; polydispersity = 4.2) with a viscosity of only 350 mPa s for a 10% polymer solution. In the separation of the seventeen DNA fragments of the marker pBR322/HaeIII (ranging in size from 51 to 587 bp), a 6% solution of "short-chain polyacrylamide (PAA)" affords a resolution of 880 000 theoretical plates, vs. 440 000 for "long-chain PAA". In a biological sample of a multiplex Duchenne muscular dystrophy containing eighteen DNA fragments, "short-chain PAA" resolves 17 of them, compared with a pattern of only eleven zones in "long-chain PAA".

1. Introduction

Electrophoretic separation of macromolecules having a constant charge to mass ratio [typically DNA and sodium dodecyl sulfate (SDS)-laden proteins] requires the presence of a sieving gel matrix, in general a polyacrylamide gel for proteins and agarose matrices for DNA [1]. Although slab-gel techniques are now routine in all life-science laboratories, gel-filled capillaries have so far met with only limited success. This is due to a variety of reasons, such as pore-size limitations, formation and trapping of air bubbles during gel polymerization, denaturation and collapse of the matrix due to local overheating, sample trapping and precipitation at the injec-

* Corresponding author.

0021-9673/95/$09.50
SSDI 0021-9673(94)00861-2

tion port. Soon chemically cross-linked gels were abandoned in favour of viscous solutions of linear (or branched) polymers, according to original observations of De Gennes [2] and Bode [3] that polymer networks, above a critical concentration (the "entanglement threshold") would be just as efficient in sieving macromolecules as true gels. Sieving dynamic matrices are immune from the noxious problems of air-bubble formation (which would automatically open the electric circuit in such tiny channels) and from sample precipitation at the injection port. Owing to the lack of a fixed-pore geometry, also very large macromolecules (or aggregates) can open a pore in their wake, while they would inevitably precipitate at the deposition site in cross-linked polyacrylamide gels. This allows repeated use of the same matrix (typically >30 runs).

For DNA separations, modern technologies employ viscous solutions of linear polymers such as polyacrylamide (in the absence of a cross-linker) [4–6], methylcellulose [7,8], hydroxyethylcellulose [9–11], liquefied agarose [12] and hydroxypropylmethylcellulose [13]. For protein analysis, the ideal detection system would be by UV absorption at 214 nm, where the molar absorptivities of proteins are 20–50 times larger than at 280 nm. Thus, a search was started for efficient UV-transparent polymers, ideally also exhibiting low viscosity, so as to allow replacement and refilling even after each run, if needed. Ganzler et al. [14] reported successful SDS runs in two such formulations: a 10% solution of dextran (M_r $2 \cdot 10^6$) and a 3% solution of polyethylene glycol (PEG, average M_r 100 000). The applicability of such an approach was later confirmed by Lausch et al. [15]. Soon, several articles appeared reporting efficient protein sieving in other types of polymers. Thus, Guttman et al. [16] described the use of lower M_r dextrans (M_r 72 000, 10% branching, at a 15% concentration) and of polyethylene oxide (PEO, typically a 3% solution of average M_r 100 000). They also studied the influence of temperature on the sieving effect in SDS–protein complexes and found the best separations at 50°C (in dextrans, whereas a deterioration of separation was apparent in the same temperature interval in PEO). Recently, SDS-electrophoresis was reported for other types of UV-transparent polysaccharides, such as pullulan [a branched polysaccharide composed of α-(1–6)-linked maltotriose] [17]. Typically, separations were carried out in a 7% polymer solution (having average M_r 50 000–100 000), although good resolution was achieved for proteins standards (in an M_r range from 14 400 to 116 000) from as low as 1% up to 7% pullulan.

For DNA analysis, polyacrylamides have proved to have a unique sieving ability, unsurpassed by other types of linear or branched polymers. Unfortunately, under standard polymerization conditions, and in the absence of a cross-linker, long strings (with M_r possibly in the range of a few million) are formed, which results in extremely viscous solutions, unwieldy to any pumping process. We have in fact reported that the concentration limit, for replenishing a capillary, is at around 6% polymer [4]. Above this critical concentration, polyacrylamide has to be polymerized in situ, with all the typical problems connected with radical polymerization: elimination of catalysts, unreacted monomers, etc. In the analysis of polymerase chain reaction (PCR)-amplified products, for the screening of genetic defects, ideally one would want to optimize resolution in a window of DNA sizes ranging from 50 to 500 base pairs (bp) [18,19]. In this size range, one would need much more concentrated polyacrylamides (e.g., 8–10%) for single-base resolution, if needed (although occasionally even 6% polymer solution can afford that). It would therefore be ideal to be able to polymerize low-viscosity polyacrylamides, so as to prepare bulk amounts outside the capillary, purify them by standard means (precipitation in ethanol) and adopt "fill-in and emptying" procedures as needed. In this paper, we propose different methods for achieving this goal.

2. Experimental

2.1. Reagents

Acrylamide tris(hydroxymethylaminomethane) (Tris), ammonium peroxodisulfate and N,N,N',N'-tetramethylethylenediamine (TEMED)

were obtained from Bio-Rad Labs. (Richmond, CA, USA), 3-(trimethoxysilyl)propyl methacrylate (Bind Silane) and poly(ethylene oxide) from Aldrich (Steinheim, Germany) and ethylenediaminetetraacetic acid (EDTA), boric acid, acetic acid and 2-propanol from Merck (Darmstadt, Germany). Fused-silica capillaries (100, 75 and 50 μm I.D., 375 μm O.D.) were obtained from Polymicro Technologies (Phoenix, AZ, USA). The DNA marker pBR322/HaeIII was obtained from Boehringer (Mannheim, Germany).

2.2. Polymer preparations

Linear polyacrylamide of reduced chain length was synthesized by the procedure of Grossman [20], by using 2-propanol as a chain-transfer agent for controlling the molecular mass of the product. Acrylamide (11%) was dissolved in 3% 2-propanol and polymerized at 35 or 70°C in a thermostated bath for 2 h. After extensive dialysis against water, the polymer was lyophilized and dissolved in separation buffer [TBE: 89 m*M* Tris–89 m*M* boric acid–2 m*M* EDTA (pH 8.3)] at different concentrations.

Acrylamide (6%) was polymerized (in the absence of cross-linker) in capillaries overnight at room temperature; the capillaries were then conditioned with separation buffer for 20 min at 100 V/cm.

Mechanically degraded linear polyacrylamide was obtained from 10% polyacrylamide, polymerized overnight at room temperature, subjected to a shearing action, for different times, at 45 kHz (output power 120 W, 25°C) in a sonicator. The viscous matrix causes the molecules to rotate in a clockwise direction. The combined effect of this rotation and the flow of the pervading matrix is to stretch and compress the molecule until chain breaking [21].

2.3. Molecular mass determinations

The number-average (M_n) and weight-average (M_w) molecular masses of the different polymer preparations were determined by gel permeation chromatography (GPC). Samples and standard were run using a Waters Model 590 solvent-delivery system equipped with two Waters Ultrahydrogel linear columns connected in series and with a Waters R401 differential refractometer for peak detection. The injected sample was 100 μl of a 100 mg/ml stock solution, the flow-rate was 0.8 ml/min and the mobile phase was 100 m*M* $NaNO_3$. M_w and M_n of the final products were assessed to be 550 000 for the masticated polyacrylamide (after 47 h of digestion), 230 000 for the polyacrylamide subjected to chain transfer at 70°C and 450 000 for the chain-transfer preparation at 35°C. Five PEO standards were used as calibration markers for GPC, having M_r values of 661 000, 148 000, 73 000, 25 000 and 10 000.

2.4. Capillary electrophoresis

Capillary zone electrophoresis (CZE) was carried out with a Waters Quanta 4000 E apparatus from Millipore (Milford, MA, USA). Capillaries 37 cm long and with different I.D., coated by a slight modification of Hjerten's protocol, utilizing N-acryloylaminoethoxyethanol (AAEE) as monomer [22,23], filled with different viscous polymer solutions, were used. The sample and standard were loaded electrophoretically by applying 100 V/cm for 6 s. Separations were performed at 100 V/cm. Ultraviolet absorbance was monitored at 254 nm. pBR322/HaeIII, covering an 8–587 bp range, and multiplex PCRs in Duchenne muscular dystrophy, covering an 113–547 bp range, were used as markers for evaluating the separation performance.

2.5. Viscosimetry

Viscosity measurements on polymer solutions were performed on a Bohlin VOR rheometer (Bohlin Rheology, Lund, Sweden), with the sample thermostated at 30°C. The shear rate chosen was in the interval 1.86–7.33 s^{-1}. A concentric cylinder measuring system was adopted, with a 14 mm diameter for the inner cylinder and a 15.4 cm diameter for the outer cylinder. Viscosity is expressed in mPa s, the viscosity of water at 25°C being 1.

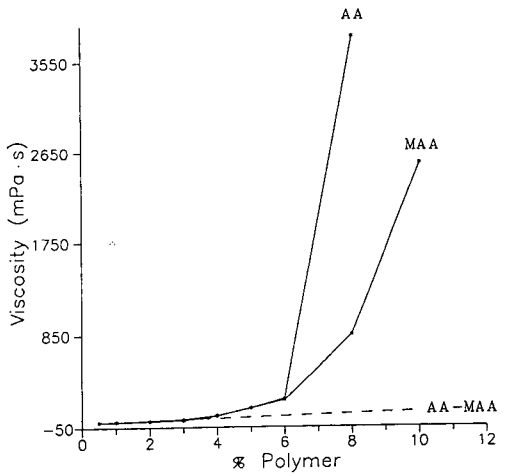

Fig. 1. Viscosity measurements as a function of increasing polymer concentration for conventionally polymerized polyacrylamides (AA) and masticated polyacrylamides (MAA). Measurements performed on a Bohlin VOR rheometer at 30°C. The broken line is an extrapolation of the initial linear slope. In principle, the point of departure from linearity would represent the entanglement threshold, but it is not applicable here owing to the wide range of viscosities explored.

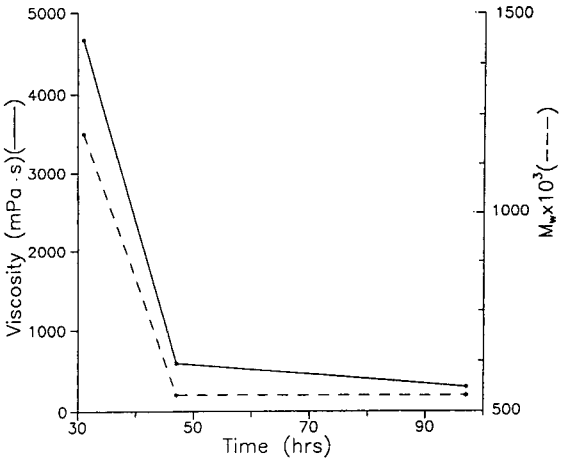

Fig. 2. Kinetics of viscosity (solid line) and M_w (broken line) variations as a function of time of mastication at 45 kHz. Note that, after ca. 50 h of cavitation, no further appreciable viscosity or M_w changes take place.

3. Results

Fig. 1 shows the viscosity, at increasing concentrations, of two different polyacrylamide preparations: a standard sample, as polymerized (AA), and the same sample subjected to mastication with ultrasound for 47 h (MAA). It can be seen that, at low concentrations, both samples appear to exhibit very similar viscosities, with a sharp departure at 6% polymer, where the masticated chains show a dramatic decrease in viscosity (e.g., an 8% solution of MAA gives 849 vs. 3800 mPa s for an equivalent 8% concentration of AA). The point of departure from linearity is generally taken to represent the entanglement threshold [11]. However, here the low-range viscosities could not be explored well at the shear rates utilized, so that we consider that 3% polymer (i.e. the apparent departure from linearity) cannot be taken as a threshold value.

Fig. 2 represents the kinetics of chain rupturing by ultrasound, as followed by viscosity measurements and, in parallel, by assessment of M_w. We have taken as first point a 30-h value since, owing to the limited range of M_r standards we had available and to the high viscosity of undegraded polyacrylamide (in a 10% solution), it was impossible to assess both viscosities and M_w in the starting solutions. However, as a rough estimate of M_w, the starting material exhibited values well above $2 \cdot 10^6$. As expected, viscosity decreases are parallelled by comparable M_w decreases. Mastication appears to reach a plateau after about 50 h ($M_w = 550\,000$; $M_n = 151\,000$; polydispersity = 3.6), after which no substantial decreases in both parameters are experienced. Masticated chains offer a unique increment in the resolution of DNA fragments in the 50–500 bp window we are trying to optimize (not shown); however, after much trial and error, this approach was abandoned, as it seems to produce charged chains, with deleterious effects on the run reproducibility, since the charged polymers migrate out of the separation channel (see Discussion).

In search of other means for reducing chain length and viscosity, we noticed a recent paper by Grossman [20] on polymerization in the presence of chain-transfer agents. We adopted this procedure, in two variants: polymerization

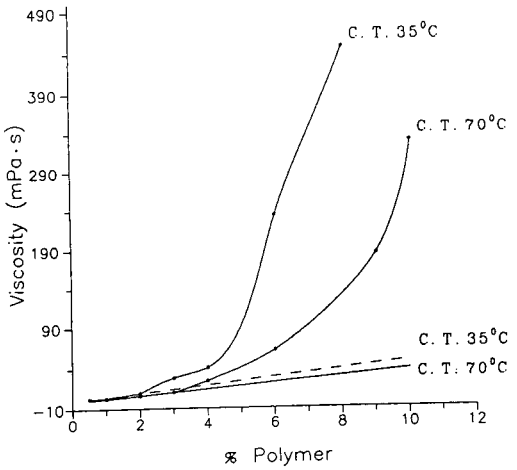

Fig. 3. Viscosity measurements as a function of increasing polymer concentration for polyacrylamides polymerized in the presence of a chain-transfer (C.T.) agent (2-propanol) at 35 and at 70°C. Measurements were performed on a Bohlin VOR rheometer at 30°C. Note that the entanglement threshold, taken as the point of departure from linearity of the experimental viscosity curve, is ca. 1.5% polymer for the reaction at 35°C, but it is at 3% polymer for reaction at 70°C.

at 35 and at 70°C. The results (in terms of viscosity vs. percentage of polymer) are shown in Fig. 3; it is seen that much reduced viscosities can be obtained by chain transfer (C.T.) at 35°C, and even lower if the reaction is conducted at 70°C, as adopted here. As an example, while a 10% solution of masticated chains gives a viscosity of 2540 mPa s, an equivalent solution of polymer produced by chain transfer at 70°C produces a viscosity of only 329 mPa s. These very low viscosities allow easy refilling after each run even at polymer concentrations up to 10%. It is additionally seen (Fig. 3) that the two chain populations exhibit different apparent entanglement thresholds: while this value is ca. 1–1.5% polymer for C.T. at 35°C, it is ca. 3% polymer for C.T. at 70°C. In parallel we examined the decrease in M_w in the two C.T. procedures at the two different temperatures adopted. The final M_w for the lower temperature reaction is centred around 450 000 (M_n = 115 000; polydispersity = 3.9), whereas when adopting the 70°C reaction protocol, the final size of the polyacrylamide chains is centred around M_w 230 000 (M_n = 55 000; polydispersity = 4.2). This explains the still large differences in viscosities between the two chain populations, as plotted in Fig. 3.

The more homogeneous size population of polymers produced by the chain-transfer technique [here called short-chain polyacrylamide (PAA)] should allow a higher resolution of DNA fragments, even at comparable concentrations, as compared with chains polymerized by the standard protocol (long-chain PAA). Fig. 4 compares the patterns obtained when running the DNA standard in long-chain PAA (A) vs. the same concentration (6% polymer) of short chain PAA (B). The substantially increased resolution in the latter system is immediately evident, e.g., the triplet of chains of 458–540 bp is baseline resolved only in the short-chain PAA. The same applies to the quadruplet of chains of 184–234 bp. Additionally, the last fragment, 587 bp, has an unacceptably high width at the base, compared with a much narrower peak width in the short-chain system. When compared with a real biological sample, the differences were even more dramatic. For example in Duchenne muscular dystrophy, we prepared a multiplex PCR of eighteen exons, covering the 50–400 bp range. The long-chain PAA system, even on optimization of all running parameters, could resolve only eleven of the eighteen fragments. The short-chain system proposed here could resolve seventeen of the eighteen DNA fragments (in preparation). In the case of the separation of the DNA marker pBR322/HaeIII (Fig. 4) we evaluated the number of theoretical plates N under the two different experimental conditions, in an electrophoretic run utilizing a 100 μm I.D. capillary. As shown in Fig. 5, long-chain PAA gives an N value of 440 000, as opposed to 880 000 in short-chain PAA. Curiously, however, the resolution is markedly dependent on the capillary diameter, since in a 50 μm I.D. capillary identical resolution is obtained in both instances. This "wall effect", which we have found also in the case of solutions of poly(vinyl alcohol) [24], will be discussed below. In any event, it is not so easy to use, in daily practice, a capillary of only 50 μm I.D., as the signal is too low for a correct evaluation of a

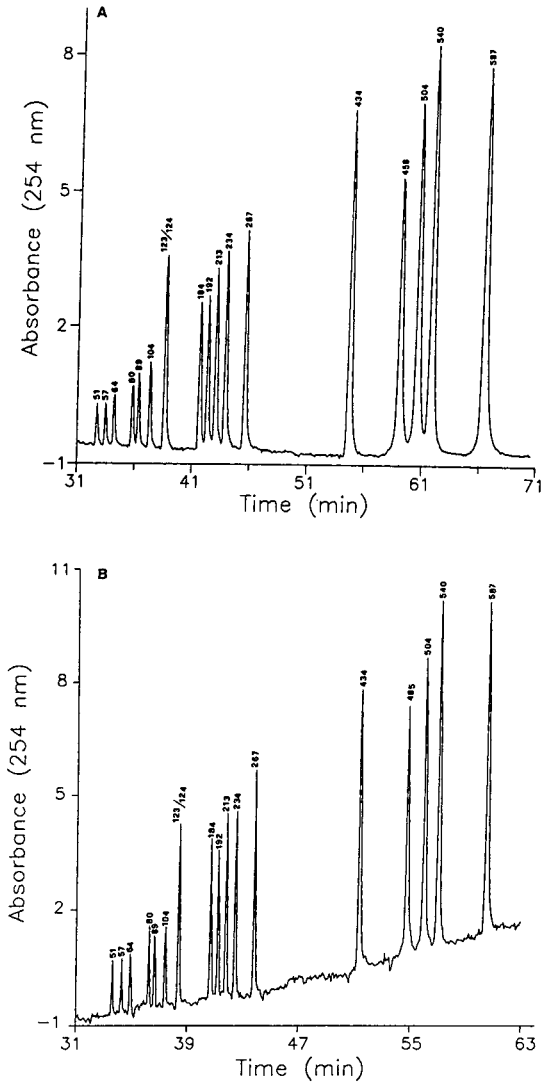

Fig. 4. CZE of DNA marker pBR322/HaeIII in (A) long-chain and (B) short-chain PAA. The standards were loaded electrophoretically by applying 100 V/cm for 6 s. Separations were performed at 100 V/cm in TBE as running buffer and 6% long-chain or short-chain PAA, respectively. Ultraviolet absorbance was monitored at 254 nm. The capillary was 37 cm × 100 μm I.D.

DNA peak when exploiting the natural DNA absorbance at 254 nm, as in the present case (however, it has been suggested that high-sensitivity detectors, such as from Spectra-Physics, etc., can pick up a DNA signal from a 50 μm I.D. capillary). Nevertheless, in general, narrow-bore capillaries can only be used in the laser-induced fluorescence mode, where capillaries as narrow as 5 μm I.D. can be successfully employed [25]. Moreover, in 50 μm I.D. capillaries, pumping in and out long-chain, viscous solutions of polyacrylamide represents a difficult task, as it requires high pressures not available in all CZE units.

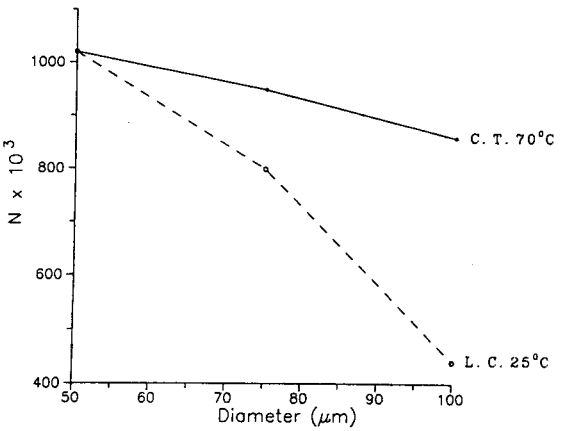

Fig. 5. Evaluation of the number of theoretical plates for the two pBR322/HaeIII separations shown in Fig. 4A and B. L.C. 25°C = long-chain polyacrylamide prepared at 25°C; C.T. 70°C = chain-transfer polymerization at 70°C. The experiments were performed in three different capillaries of 100, 75 and 50 μm I.D. Note how the resolution increases markedly at progressively lower I.D.s.

4. Discussion

4.1. Use of "masticated" chains

The use of mastication (i.e. of cavitation of dilute polymer solutions by ultrasonic radiation) was long ago adopted by the rubber industry for the production of short-chain polymers [26], and is a well standardized procedure. It is based on a chemical reaction (rupture of C–C bonds, in the case of polyacrylamides) induced by direct acquisition of mechanical energy on a molecular scale, and it is conveniently termed a "mechanochemical" reaction. One of the main advantages is that, whereas in thermal degradation of polymers there is an equal probability of scission along the polymer chain, giving a random M_w

distribution, in the process of cavitation non-random scission takes place, producing a much more homogeneous chain size (under optimum conditions approaching the M_w/M_n limit of 1.05) [21]. The reason is that entangled chain structures tend to localize the adsorbed energy in the bonds near the centres of the chain: this non-random rupture restricted to central sections of the molecule leads to a much narrower M_w distribution. It is hypothesized that this concentration of energy near the centre of the molecule is due to the fact that the central region of long molecules in bulk polymer is not able to disentangle sufficiently under shear to dissipate the mechanical work in motion, as instead occurs at the end segments.

On these assumptions, we prepared "long-chain PAA", by standard polymerization conditions, and subjected it to cavitation. The chains obtained after ca. 50 h of mastication indeed exhibited much reduced average lengths and viscosities (see Figs. 1 and 2), but did not offer run reproducibility, although the first few CZE separations offered much increased resolution and N values. We finally understood that chain rupture was accompanied by radical formation at the two new extremities of the shorter chains. In the presence of oxygen, peroxy radicals are formed, which are then terminated by abstraction of hydrogen from the surroundings of the polymer. The end-product of this reaction is the formation of charged carboxylic groups on the ruptured polyacrylamides, which slowly migrate out of the capillary under the electric field. Attempts at quenching this reaction by other means met with limited success. For example, when cavitating under completely anaerobic conditions, no chain degradation took place. Also, the addition of other radical scavengers did not allow proper fluidification of the starting, long-chain polymer solution. Among the different scavengers utilized, we tried also dihydropyrrolamide (a kind gift from Professor Citterio, Milan Polytechnic), known to form a very unreactive radical, shielded by the three methyl groups on the nitrogen, but even this procedure was not satisfactory. We also tried fluidifying the long-chain polyacrylamide by using different frequencies of the ultrasound radiation, up to 20 MHz. However, higher frequencies resulted only in strong heating of the viscous polymer solution, up to boiling, but in no real chain degradation. It turns out that polymer molecules are not stretched enough by higher frequencies to give rise to any sizeable amount of degradation [21]. Owing to all these problems, chain mastication was abandoned in favour of polymerization in presence of chain-transfer agents.

4.2. Use of chain transfer in polyacrylamide production

Grossman's group [20,27,28] has made extensive studies on the use of entangled polymer solutions for DNA separation. Originally, they advocated hydroxyethylcellulose, but the solution finally adopted was the production of short-chain, low-viscosity polyacrylamides obtained by chain termination in the presence of chain transfer agents, such as 2-propanol [20]. Under these polymerization conditions, a final product exhibiting an M_w value of 339 000 was obtained, with a viscosity, for a 6.2% polymer solution, of only 150 cP at 25°C. Although, with these reaction conditions, we also obtained a product with similar physico-chemical properties and electrophoretic performance, in order to optimize further the separation of DNA in the 50–500 bP range, we adopted different polymerization conditions leading to an additional decrease in the viscosity and molecular size of the final product, i.e., reaction in presence of 2-propanol, as a chain transfer agent, but at much higher temperatures (70°C as opposed to room temperature). Under these conditions, our final product exhibits an apparent chain length of M_w 230 000 (M_n 55 000, polydispersity = 4.2) and still lower viscosities for comparable concentrations (barely 80 mPa s for a 6.2% polymer, see Fig. 3). At such low viscosities, we can easily empty and refill capillaries after each run even with a polymer solution of up to 10% concentration. In turn, this produces a drastic increment in resolution in the 50–500 bp DNA size window we wanted to optimize. The idea of using temperature and modulating the catalyst concentration

for varying the average chain length of polyacrylamides was in fact proposed long ago by our group [29–31]. Note that an absolute comparison of M_w between our and Grossman's data cannot be made, since the latter was able to calibrate his column with polyacrylamide standards, whereas we only had PEO available. Thus, wheres he gives an M_w of 339 000 for C.T. at 35°C, under our experimental conditions we obtain, for the same reaction product, an apparent M_w of 450 000. However, on a relative scale, it is clear that C.T. at 70°C generates a product of ca. half size and with a much lower viscosity.

4.3. Optimization of DNA separation according to size windows

It is now clear that, for optimizing DNA separations, one would have not only to select some given polymers (polyacrylamide being the best in our hands), but also to choose the right polymer concentration and appropriate chain length. We therefore consider that the best that can be achieved is the optimization of a given "window" of DNA chain intervals, at which a proper polymer concentration will offer the highest performance. Diluting or concentrating the polymer solution will result in a shift of this optimum window towards higher or lower DNA chain lengths, respectively. This is analogous to SDS electrophoresis, where, for achieving optimum size discrimination over a large protein size interval, one has to resort to a porosity gradient (typically extending from 4% up to 20%T) [32]. At a single polyacrylamide concentration, the range of molecular mass values covered is limited. Although it might be difficult, but not impossible, to fill a capillary with a concentration gradient of sieving linear polymers, for broadening the macrmolecular size interval explored, one would still be faced with the impossibility of using standard CZE units commercially available. In such porosity gradients, where optimum separation will be obtained only by driving DNA fragments of appropriate lengths in selected regions of the gradient, one would have to resort to rigid, stretched and fully transparent capillaries, which could be scanned by a moving detector, as demonstrated long ago by Hjertèn [33].

As a final remark, we observed a strong wall effect in performing separations at progressively lower capillary I.D.s (see Fig. 5), as a result of which resolution in long-chain or short-chain PAA becomes indistinguishable at 50 μm I.D. A similar phenomenon was recently discovered by us when attempting separations of SDS-laden proteins in entangled poly(vinyl alcohol) (PVA) solutions. This phenomenon was attributed to the strong tendency of PVA to form hydrogen bonds not only among the polymer chains in solution, but also with the free silanols on the fused-silica wall [24]. Perhaps a similar type of phenomenon is also operative here as well [note additionally that our capillary is coated with poly(AAEE), which offers a free distal OH group on every other carbon along the chain]. Work is in progress to elucidate these aspects.

Acknowledgements

This work was supported in part by grants from the Consiglio Nazionale delle Ricerche (Comitato di Chimica, Progetto Strategico), the Comitato di Medicina e Biologia and the European Community, Biomed I (No. Gene-93-0018). We are much indebted to Mr. Roberto Coldani (Millipore–Waters, Italy) for help with M_w and M_n assessments.

References

[1] P.G. Righetti, *J. Biochem. Biophys. Methods*, 19 (1989) 1–20.
[2] P.G. De Gennes, *Scaling Concepts in Polymer Chemistry*, Cornell University Press, Ithaca, NY, 1979.
[3] H.J. Bode, *Anal. Biochem.*, 83 (1977) 204–210.
[4] M. Chiari, M. Nesi, M. Fazio and P.G. Righetti, *Electrophoresis*, 13 (1992) 690–697.
[5] M. Chiari, M. Nesi and P.G. Righetti, *J. Chromatogr. A*, 652 (1993) 31–39.
[6] Y.F. Pariat, J. Berka, D.N. Heiger, T. Schmitt, M. Vilenchik, A.S. Cohen, F. Foret and B.L. Karger, *J. Chromatogr. A*, 652 (1993) 57–66.
[7] D.A. McGregor and E.S. Yeung, *J. Chromatogr. A*, 652 (1993) 67–73.

[8] K. Srinivasan, J.E. Girard, P. Williams, R.K. Roby, V.W. Weedn, S.C. Morris, M.C. Kline and D.J. Reeder, *J. Chromatogr. A*, 652 (1993) 83–91.
[9] R.P. Singhal and J. Xian, *J. Chromatogr. A*, 652 (1993) 47–56.
[10] A.E. Barron, D.S. Soane and H.W. Blanch, *J. Chromatogr. A*, 652 (1993) 3–16.
[11] A.E. Barron, H.W. Blanch and D.S. Soane, *Electrophoresis*, 15 (1994) 597–615.
[12] P. Boček and A. Chrambach, *Electrophoresis*, 13 (1992) 31–34.
[13] H.E. Schwartz, K. Ulfelder, J.F. Sunzeri, M.P. Busch and R.G. Brownlee, *J. Chromatogr.*, 559 (1991) 267–274.
[14] K. Ganzler, K.S. Greve, A.S. Cohen, B.L. Karger, A. Guttman and N.C. Cooke, *Anal. Chem.*, 64 (1992) 2665–2671.
[15] R. Lausch, T. Scheper, O.W. Reif, J. Schlosser, J. Fleischer and R. Freitag, *J. Chromatogr. A*, 654 (1993) 190–195.
[16] A. Guttman, J. Horvath and N. Cooke, *Anal. Chem.*, 65 (1993) 199–203.
[17] M. Nakatani, A. Shibukawa and T. Nakagawa, *J. Chromatogr. A*, 672 (1994) 213–218.
[18] C. Gelfi, A. Orsi, P.G. Righetti, V. Brancolini, L. Cremonesi and M. Ferrari, *Electrophoresis*, 15 (1994) 640–643.
[19] M. Nesi, P.G. Righetti, M.C. Patrosso, A. Ferlini and M. Chiari, *Electrophoresis*, 15 (1994) 644–646.
[20] P.D. Grossman, *J. Chromatogr. A*, 663 (1994) 219–227.
[21] F. Bueche, *J. Appl. Polym. Sci.*, 4 (1960) 101–106.
[22] M. Chiari, C. Micheletti, M. Nesi, M. Fazio and P.G. Righetti, *Electrophoresis*, 15 (1994) 177–186.
[23] M. Chiari, M. Nesi and P.G. Righetti, *Electrophoresis*, 15 (1994) 616–622.
[24] E. Simò-Alfonso, M. Conti, C. Gelfi and P.G. Righetti, *J. Chromatogr. A*, 689 (1995) 85–96.
[25] J.H. Wahl, D.R. Goodlett, H.R. Udseth and R.D. Smith, *Anal. Chem.*, 64 (1992) 3194–3196.
[26] W.F. Watson, in M. Fette (Editor), *Chemical Reaction of Polymers*, Vol. XIX, Interscience, New York, 1964, pp. 1085–1111.
[27] P.D. Grossman and D.S. Soane, *J. Chromatogr.*, 559 (1991) 257–266.
[28] P.D. Grossman, T. Hino and D.S. Soane, *J. Chromatogr.*, 608 (1992) 79–83.
[29] C. Gelfi and P.G. Righetti, *Electrophoresis*, 2 (1981) 213–219.
[30] C. Gelfi and P.G. Righetti, *Electrophoresis*, 2 (1981) 220–228.
[31] P.G. Righetti, C. Gelfi and A. Bianchi-Bosisio, *Electrophoresis*, 2 (1981) 291–295.
[32] J. Margolis and K.G. Kenrick, *Anal. Biochem.*, 25 (11968) 347–355.
[33] S. Hjertén, *Chromatogr. Rev.*, 9 (1967) 122–219.

ELSEVIER

Journal of Chromatography A, 689 (1995) 107–121

JOURNAL OF CHROMATOGRAPHY A

Determination by high-performance capillary electrophoresis of alkylaromatics used as bases of sulfonation in the preparation of industrial surfactants☆

P.L. Desbène[a,b,*], C.M. Rony[a,b]

[a]*Laboratoire d'Analyse des Systèmes Organiques Complexes, Université de Rouen, IUT, 43 Rue Saint Germain, 27000 Evreux, France*

[b]*IRFMP, Université de Rouen, 76134 Mont Saint Aignan Cédex, France*

First received 30 January 1994; revised manuscript received 1 August 1994

Abstract

Having previously attempted to determine by high-performance capillary electrophoresis (HPCE) industrial surfactants resulting from the sulfonation of oil fractions (WITCO TRS 10-80), it was decided, because of the complexity of these fractions and of the low resolution obtained, to undertake the analysis by HPCE of mixtures of alkylaromatics used as bases to prepare these compounds. Using a model mixture of alkylbenzenes, including benzene and a series of homologous compounds with alkyl chain lengths of C_1–C_{16}, the conditions of the separation were optimized. It was shown that it is possible to analyse this mixture, with total baseline resolution, in 35 min using simultaneously sodium dodecyl sulfate and an organic co-solvent at high concentrations. These conditions also allow the resolution not only of the alkylated compounds used as the bases for the preparation of industrial alkylbenzenesulfonates (Sulframine ACB and Sulfo TPB) but also the surfactants themselves. It must also be noted that these conditions, transposed to WITCO TRS 10-80, allow for the first time the resolution of this complex mixture.

1. Introduction

Surfactants are amphiphilic compounds, which results in the peculiar properties of these molecules, such as adsorption at interfaces, formation of micelles in solution and the decrease in surface tension. Consequently, these chemicals are often used as wetting or foaming agents, emulsifiers or detergents.

Linear alkylbenzenesulfonates (LAS), which are the main bases of surfactants for domestic use (with a 1.2 million tons a year production, i.e. 24% of the world production of surfactants), have frequently retained the attention of analysts. At first, the distribution of their alkyl chains was determined using gas chromatography. However, this technique requires preliminary conversion of LAS into volatile compounds. This derivatization can be performed via various reactions: desulfonation using acids [1–4], alkaline fusion [5], sulfochlorination [6],

* Corresponding author. Address for correspondence: Laboratoire d'Analyse des Systèmes Organiques Complexes, Université de Rouen, IUT, 43 Rue Saint Germain, 27000 Evreux, France.

☆ Presented at the *6th International Symposium on High Performance Capillary Electrophoresis, San Diego, CA, 31 January–3 February 1994.*

0021-9673/95/$09.50
SSDI 0021-9673(94)00739-X

methylation [7], reduction to alkylthiophenols [8], pyrolysis [9] or acidic pyrolysis [10,11].

In order to avoid the systematic conversion of LAS into volatile compounds, these complex mixtures are now generally determined by a high-performance liquid chromatography, and different chromatographic systems have been proposed. LAS have been determined by reversed-phase partition liquid chromatgraphy, using various stationary phases such as C_{18} [12,13], C_8[13] or C_1 [14] bonded silicas, the mobile phase being in most instances an aqueous solution of sodium perchlorate with methanol [12], acetonitrile [12,13] or tetrahydrofuran [14] as co-solvent. Using such a chromatographic system, with fluorimetric detection, Marcomini and co-workers [15,16] determined LAS at very low concentrations in fluvial waters. On the other hand, the determination of alkylbenzenesulfonates has been also studied either by ion suppression using polymeric stationary phases [17], or by ion-pair chromatography with C_8 [18] or C_{18} [19] bonded silica stationary phases, using tetrabutylammonium or cetrimide as counter ion. Recently, Chen and Pietrzyk [20] separated industrial LAS not only as a function of homologous series, but also as a function of positional isomerism by reversed-phase partition chromatography, using C_{18} bonded silica stationary phase. To achieve this separation, after studying different alkali and alkaline earth metal cations, they used high concentrations of sodium chloride and proceeded to a double elution gradient, increasing the acetonitrile content and decreasing the ionic strength. Unfortunately, these chromatographic techniques, and also ion-exchange chromatography, give disappointing results in the determination of industrial anionic surfactants resulting from the sulfonation of oil fractions [19,21].

Consequently, we considered some years ago studying the determination of alkylbenzenesulfonates by high-performance capillary electrophoresis [22], and also capillary zone electrophoresis (CZE) and micellar electrokinetic chromatography (MEKC). Other workers [23] have studied the separation of sulfate and sulfonate surfactants by isotachtophoresis. Romano et al. [24] analysed an alkylsulfonates mixture by CZE using indirect UV detection.

Although MEKC, in contrast to CZE, allows the resolution of homologous alkylbenzenesulfonates and also of positional isomers [22], the application of this technique to the determination of anionic surfactants resulting from the sulfonation of oil fractions, such WITCO TRS 10-80, is disappointing because of the extreme complexity of these mixtures [22]. As the difficulty is due, at least partially, from the great complexity of the hydrophobic part of the surfactant amphiphilic components, an answer should be sought from the study of the alkylates used as bases for the sulfonation. Consequently, we decided to study the analysis of these raw materials by capillary electrophoresis and more precisely, because of the chemical characteristics of these complex mixtures, by MEKC and, as second step, to apply the operating conditions found to the determination of industrial anionic surfactants.

2. Experimental

2.1. Reagents

The water required for the preparation of buffers was systematically purified by reversed osmosis and filtration using a Milli-RO + Milli-Q system (Millipore, Molsheim, France). The buffer reagents, sodium tetraborate (decahydrate), boric acid and sodium monobasic phosphate, were of analytical-reagent grade from Aldrich, France (La Verpillère, France).Buffers were obtained from concentrated solutions prepared daily, and the pH was controlled systematically before use. Sodium dodecyl sulfate (SDS) was of 99%$^+$ grade from Sigma France (St. Quentin de Fallavier, France). The different organic solvents used, both for the high-performance capillary electrophoresis (HPCE) analyses (i.e., acetonitrile, acetone, methanol and 2-propanol) and for the purification of some samples such as WITCO TRS 10-80 (i.e., chloroform and butanol) were

of RS HPLC grade (Carlo Erba, Rueil Malmaison, France) and were used as received.

2.2. Apparatus

All experiments were carried out on a P/ACE 2100 system (Beckman, Fullerton, CA, USA) monitored by a PS/2 computer (IBM, Greenock, UK) using P/ACE software (Beckman). Data collection was performed with the same software. Samples were loaded by pressure injection (injection time 1 or 2 s) into a fused-silica capillary (57 cm × 50 μm I.D.). UV detection was performed at 214 nm, through the capillary at 50 cm from the inlet. The pH values were measured using a Beckman Model Φ pH meter at the analysis temperature. The electroosmotic flow was systematically determined by injection of methanol or acetone, the migration time of micelle being estimated to 4.5 times the migration time of the electroosmotic flow [25]. Effectively, because of the elution of the most lipophilic alkylbenzenes with the micelle, the direct determination of the micelle migration time was often impossible.

2.3. Samples

The alkylbenzenes used as model molecules were of 99% grade, from Aldrich, and were injected without further purification.

The industrial anionic surfactants studied, i.e., WITCO TRS 10-80, WITCO Sulframine AcB and WITCO Sulfo TPB, and also their bases of sulfonation, linear dodecylbenzene and the tetrapropylbenzene, were kindly furnished by WITCO France (St. Pierre les Elbeuf, France). These industrial compounds were subjected to analysis without further purification, with the exception of WITCO TRS 10-80, which was desalted and dewaxed according to the procedure reported below.

As the raw sample contained some mineral salts, the latter were precipitated by addition of butanol. The desalted product was obtained after filtration and evaporation of the butanol. As this product contains non-sulfonated fractions, it was necessary to eliminate them in order to complete the purification. This was performed using adsorption liquid chromatography on silica. A 2.5 cm I.D. column containing 200 ml of LiChrosorb silica, d_p = 20–50 μm (Merck, Darmstadt, Germany), was used to dewax a 4-g sample of WITCO TRS 10-80. The desalted sample was dissolved in 10 ml of chloroform and was deposited at the column inlet. Waxes were eluted with 300 ml of chloroform. After evaporation of the chloroform, there remained 0.46 g of waxes. The sulfonated fraction was then eluted with methanol. Elution was performed until the total migration of a coloured band corresponding to the polyaromatic fraction. After concentration, 3.48 g of sulfonated compounds remained.

3. Results and discussion

As the alkylaromatic organic matrices used as raw materials for the preparation of industrial anionic surfactants are very complex mixtures of hydrophobic compounds, we first examined the optimization of their analysis by MEKC by studying the electrophoretic behaviour of model molecules.

3.1. Study of the electrophoretic behaviour of model alkylbenzenes in micellar electrokinetic chromatography

The model mixture was composed of alkylbenzenes, including benzene and C_1–C_{16} homologous compounds. We used $Na_2B_4O_7$–NaH_2PO_4 buffer adjusted at pH 9 in order to operate in the presence of an important electroosmotic flow and to obtain fast separations with maximum efficiency.

According to Terabe [25] and Vindevogel and Sandra [26], we examined successively the influence on the resolution of the concentration of SDS, the ratio of organic co-solvents, the ionic strength in the mobile phase and the nature of the organic co-solvent.

Influence of sodium dodecyl sulfate concentration on the resolution of a model mixture of alkylbenzenes

With electrolyte ionic strength kept constant (25 m*M* $Na_2B_4O_7$–50 m*M* NaH_2PO_4 buffer, pH 9) we first studied the influence of the SDS concentration in order to optimize the capacity factors. Effectively, according to Terabe [25] and Vindevogel and Sandra [26], the resolution by time unit is maximum when the capacity factors of the analytes are in the range 0.5–10. As the critical micellar concentration of SDS is 8 m*M* in water at 25°C, we studied an SDS concentration range of 12.5–50 m*M*.

From this series of experiments, it appears that the optimum SDS concentration is 25 m*M*. Effectively, at a higher SDS concentration (50 m*M*), only alkylbenzenes with a chain shorter than three carbons are resolved, the more hydrophobic alkylbenzenes eluting as a poorly resolved signal with too high capacity factors ($k' > 10$). In contrast, with a 25 m*M* concentration of SDS, as reported in Fig. 1, a good resolution in time units is obtained for alkylbenzenes with side-chains of short and medium lengths, with capacity factors of 1.7–4. However, as a result of the relatively narrow separation range, alkylbenzenes with chain lengths longer than C_7 are not resolved. These compounds, which have a great affinity for micelles, elute as a single, broad peak.

However, a lower SDS concentration (12.5 m*M*) does not allow the resolution of alkybenzenes with alkyl chains longer than C_7 to be

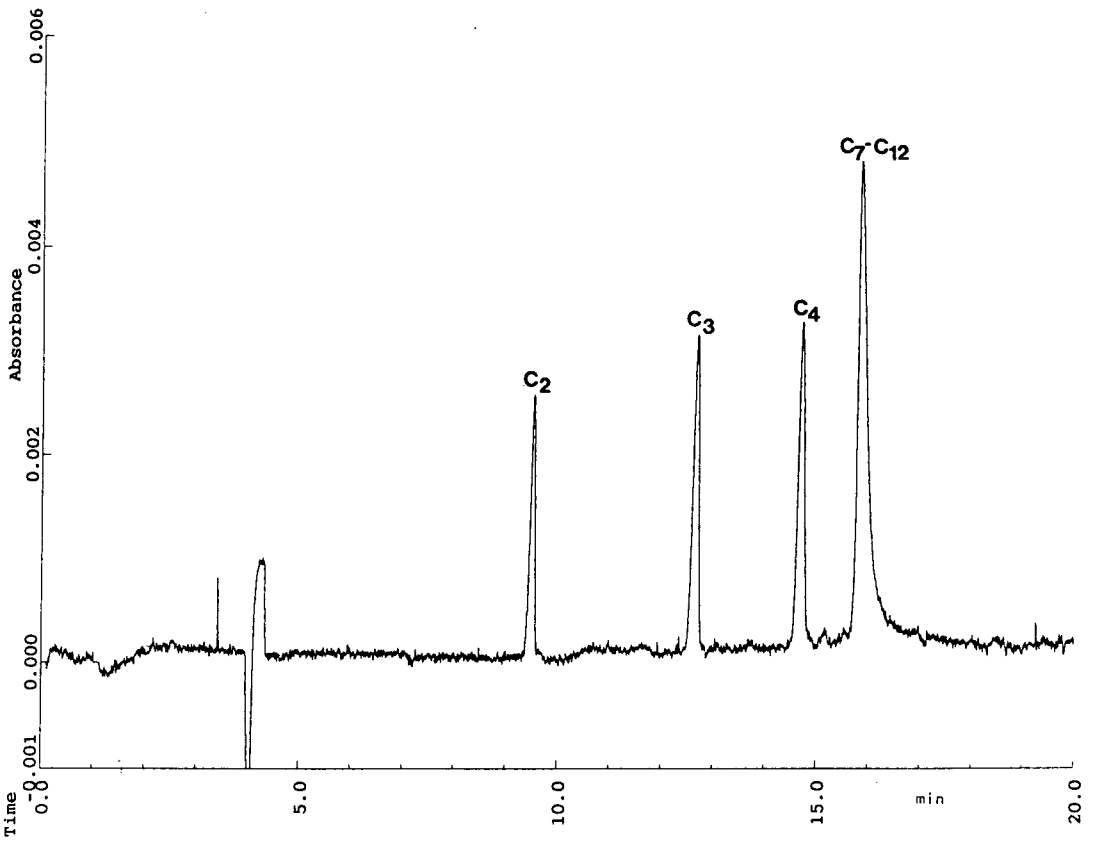

Fig. 1. Influence of SDS concentration on the resolution of a mixture of model alkylbenzenes. Operating conditions: electrolyte, 50 m*M* NaH_2PO_4–25 m*M* $Na_2B_4O_7 \cdot 10H_2O$ buffer (pH 9); [SDS], 25 m*M*; temperature, 30°C; applied voltage, 20 kV; hydrodynamic injection, 1 s; detection at 214 nm.

improved but an important loss of resolution in time units is observed for alkylbenzenes with short chains (C_1, C_2) as their capacity factors become too small.

Consequently, it seems impossible to achieve a satisfactory resolution of alkylbenzenes with alkyl chains lengths greater than C_7 by optimizing only the SDS concentration. As an improvement of the separation can result only from a decrease in the strong interactions between the most hydrophobic compounds and the core of the micelles, we studied in a second step the influence of the addition of a co-solvent on the resolution of our model mixture of alkylbenzenes. Such a strategy was likely to modify the partition coefficients of the solute molecules between the mobile phase and the pseudo-stationary phase, thus allowing the capacity factors to be modified and also the electroosmotic flow velocity and therefore the migration-time window to be changed.

Influence of mobile phase polarity on the resolution of a model mixture of alkylbenzenes

With the SDS concentration kept at the optimum value of 25 m*M*, we studied the influence of increasing the co-solvent concentration on the quality of separation of the model alkylbenzene mixture. We chose acetonitrile as organic co-solvent because of its low viscosity and its relatively high dielectric constant. According to Schwer and Kenndler [27], the electroosmotic flow velocity decreases and the analysis times increase if the viscosity of the electrophoretic medium increases and/or if the dielectric constant of the mobile phase decreases. Consequently, the electroosmotic flow and the electrophoretic system performances will be less perturbed by acetonitrile than by other organic solvents.

A range of acetonitrile concentration of 5–60% was studied in 5% increments. It was found that the addition of small amounts of acetonitrile does not improve the separation of the most hydrophobic compounds (alkylbenzenes with chain lengths between C_7 and C_{12}). A rough separation begins for a concentration of 30% of acetonitrile and an acceptable resolution of the whole alkylbenzene model mixture is obtained with about 45% of acetonitrile (Fig. 2a).

Obviously, for such concentrations of acetonitrile, and in agreement with Bullock [28], there are no more micelles in the electrophoretic medium [29] and under such conditions the different electrophoretic mobilities allowing the separation of alkylbenzenes can result only from hydrophobic interactions between the alkylbenzene molecules and the SDS, i.e., by solvatophoby according to the principle developed by Walbroehl and Jorgenson [30].

However, it must be noted that for such a concentration of acetonitrile in the mobile phase (Fig. 2a), the peak corresponding to phenyldodecane, i.e., the most hydrophobic component of the mixture, appears relatively broad. As this decrease in the efficiency of the system, in the case of the most hydrophobic compounds, could result from the only partial solubility of these compounds in the mobile phase we performed the analysis with a mobile phase containing 50% of acetonitrile. As indicated by Fig. 2b, this mobile phase allows the efficiency of the electrophoretic system to be increased, as the peaks of the most hydrophobic components are clearly narrower in spite of an increase of the analysis time, which results from a noticeable increase in the electroosmotic flow time (t_{eo}), t_{eo} now being 7 min instead of about 6 min previously (Fig. 2a). It is worth noting that under these new operating conditions, baseline resolution is not achieved for all the components of the mixture analysed.

As the resolution seems to increase systematically when the amount of acetonitrile increases, we analysed the model mixture in the presence of a mobile phase containing 60% of acetonitrile. As evidenced by Fig. 2c, two main features appear under these new operating conditions: (i) a new increase in analysis times, resulting from a further decrease in the electroosmotic flow, t_{eo} now being 10 min; and (ii) a general loss of resolution, resulting from insufficient interactions between the analytes and the SDS, as the mobile phase becomes too lipophilic because of the addition of an important amount

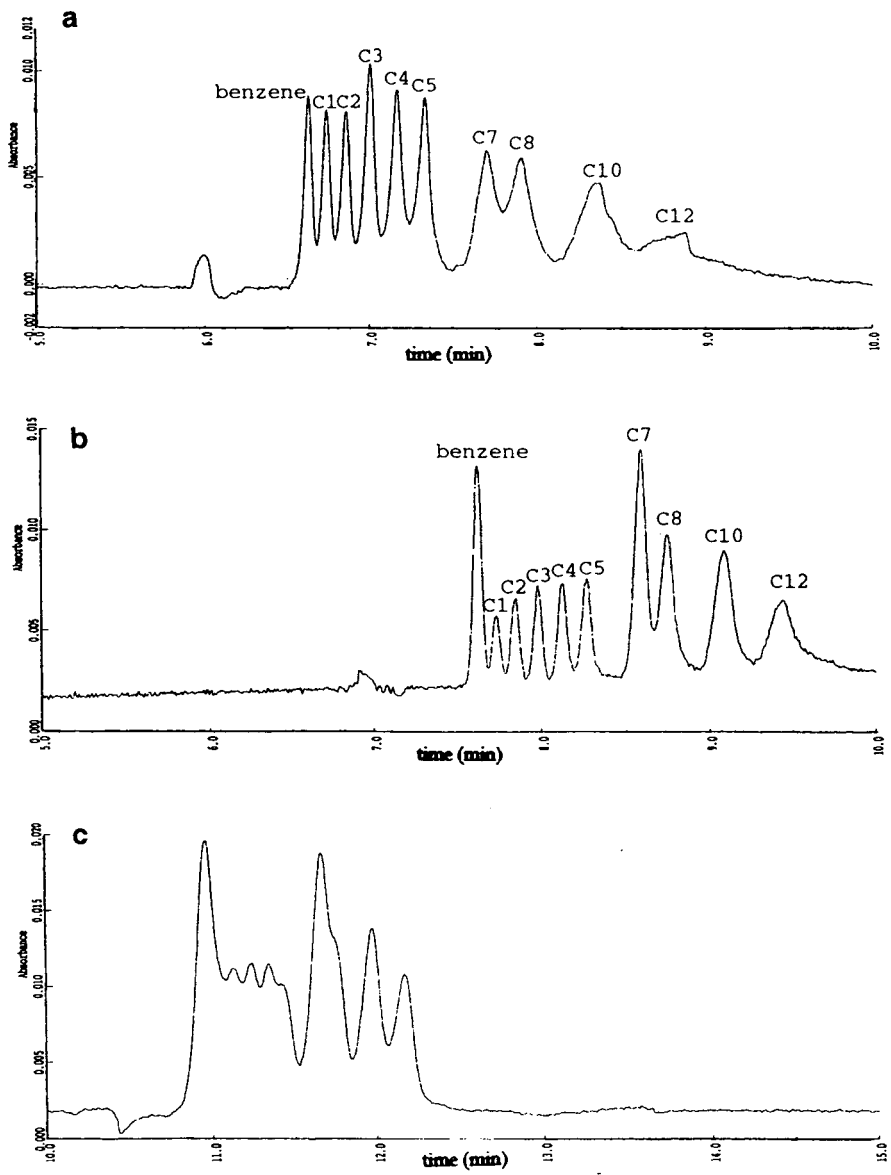

Fig. 2. Influence of the mobile phase polarity on the electrophoretic behaviour of model alkylbenzenes. Operating conditions: electrolyte, 50 m*M* NaH_2PO_4–25 m*M* $Na_2B_4O_7 \cdot 10H_2O$ buffer (pH 9); [SDS], 25 m*M*; temperature, 30°C; applied voltage, 30 kV; hydrodynamic injection, 1 s; detection at 214 nm. Acetonitrile concentration: (a) 45; (b) 50; (c) 60% (v/v).

of acetonitrile. Therefore, the optimum amount of acetonitrile in the mobile phase seems to be around 50%.

After optimizing this parameter, and with the resolution appearing to be almost satisfactory for all the components of the model mixture, we attempted to improve the analysis by increasing the volume of the pseudo-stationary phase.

Influence of the volume of the pseudo-stationary phase on the resolution of a model mixture of alkylbenzenes

Fig. 3 shows the analysis of the model mixture of alkylbenzenes using an electrophoretic system constituted by 50 m*M* NaH_2PO_4–25 m*M* $Na_2B_4O_7$ buffer (pH 9), with 50% of acetonitrile and a 50 m*M* concentration of SDS, i.e., twice the volume of the pseudo-stationary phase used previously. It can be seen that a satisfactory resolution of all the components was obtained for the first time.

In order to improve the resolution in time units, we then studied the influence of the ionic strength of the mobile phase on the electrophoretic behaviour of the model alkylbenzenes.

Influence of ionic strength on the electrophoretic behaviour of the model alkylbenzenes

When the ionic strength of the electrolyte in the mobile phase decreases, the electroosmotic flow velocity increases, resulting in a noticeable decrease in the analysis time [31]. Therefore, we attempted to determine the optimum ionic strength, i.e., that leading to the best compromise between analysis time and resolution.

As evidenced by comparison of Figs. 3 and 4a, a noticeable decrease in the analysis time can be obtained without a loss of resolution if the ionic strength of the mobile phase is ten times smaller. However, the electropherogram obtained under these conditions is characterized by serious noise, in spite of thorough degassing of the electrolyte before analysis. Such a phenomenon was observed previously by Vindevogel and Sandra [32] in studies performed with electrophoretic media containing a high percentage of organic solvent. With the exception of the noise problem, the separation obtained under these ionic strength conditions was satisfactory and 5 m*M* NaH_2PO_4–2.5 m*M* $Na_2B_4O_7$ (pH 9) buffer with an SDS concentration of 50 m*M* appears to be a near-optimum electrolyte.

As a decrease in the noise could only result from a decrease in the acetonitrile concentration in the mobile phase, we decreased the acetoni-

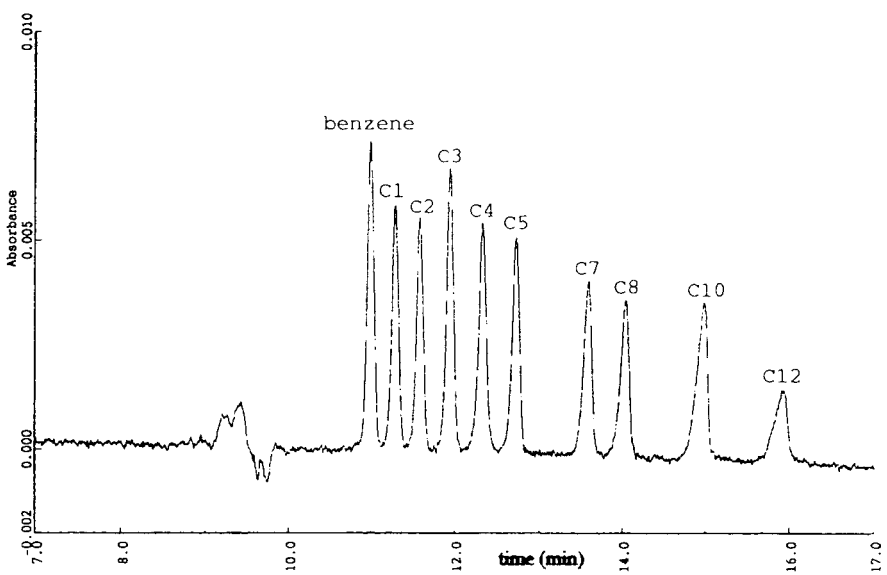

Fig. 3. Influence of an increase in the pseudo-stationary phase volume on the electrophoretic behaviour of model alkylbenzenes. Operating conditions: electrolyte, 50 m*M* NaH_2PO_4–25 m*M* $Na_2B_4O_7 \cdot 10H_2O$ buffer (pH 9); [SDS], 50 m*M*; [CH_3CN], 50% (v/v); temperature, 30°C; applied voltage, 30 kV; hydrodynamic injection, 1 s; detection at 214 nm.

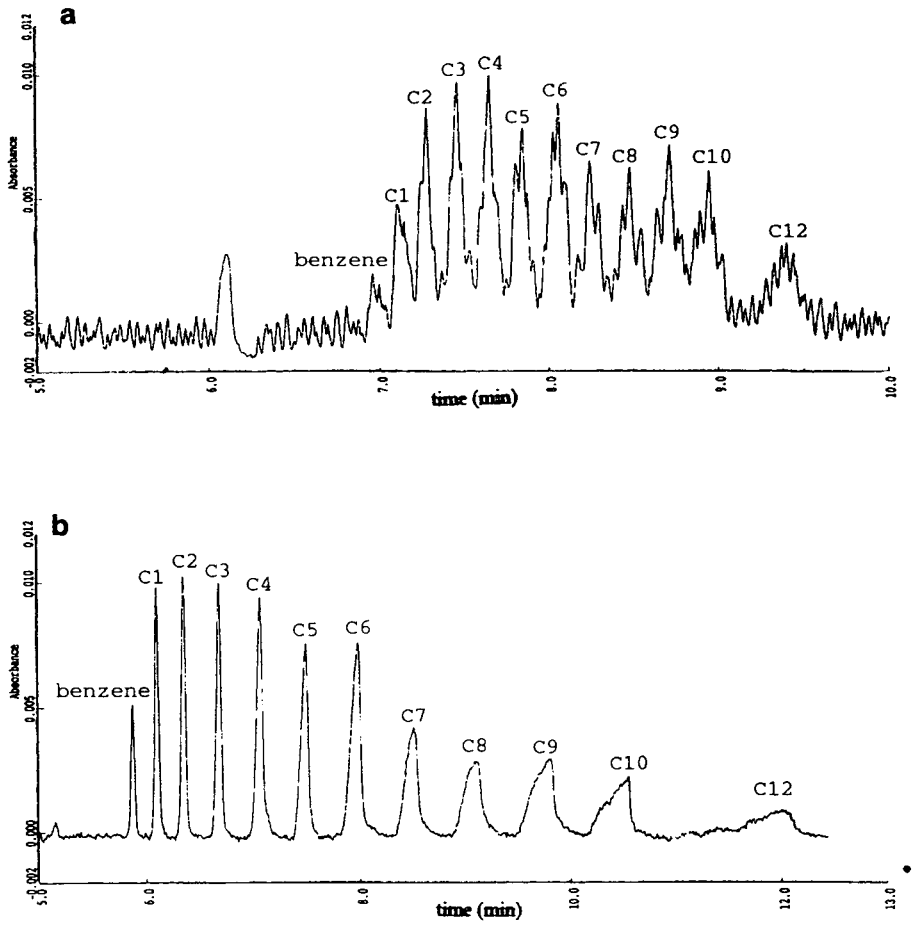

Fig. 4. Influence of the ionic strength of the mobile phase on the electrophoretic behaviour of model alkylbenzenes. Operating conditions: electrolyte, 5 m*M* NaH_2PO_4–2.5 m*M* $Na_2B_4O_7 \cdot 10H_2O$ buffer (pH 9); [SDS], 50 m*M*; temperature, 30°C; applied voltage, 30 kV; hydrodynamic injection, 1 s; detection at 214 nm. Acetonitrile concentration: (a) 50; (b) 40% (v/v).

trile content to 40%. As shown by the Fig. 4b, a satisfactory analysis is then obtained: (i) baseline resolution is obtained for the whole series of homologous alkylbenzenes, from benzene to dodecylbenzene; (ii) the analysis time does not exceed 13 min; and (iii) the signal-to-noise ratio is acceptable under these new conditions and a satisfactory sensitivity is obtained.

The only remaining problem is the unsatisfactory resolution of compounds more hydrophobic than dodecylbenzene. Therefore, with a view to improving the resolution of very hydrophobic compounds, we studied the influence of the nature of the mobile phase organic co-solvent on their electrophoretic behaviour.

Influence of the nature of the organic co-solvent on the resolution of a model mixture of alkylbenzenes

Modification of the chemical structure of the organic co-solvent should result not only in a change in the electroosmotic flow velocity, but also in a change in the electrophoretic system selectivity [25,26]. Therefore, different co-solvents (acetone, tetrahydrofuran, methanol and 2-propanol) were tested.

This comparative study showed that 2-propanol gives a good thermodynamic selectivity, comparable to that obtained with acetonitrile. Moreover, it presents the advantage of being less polar than the latter. Consequently, it allows one to obtain a suitable hydrophobicity of the electrophoretic medium at lower contents than those previously used with acetonitrile, improving considerably the bad detection previously observed with high concentrations of acetonitrile. In contrast, as 2-propanol has a dielectric constant/viscosity ratio lower than that of acetonitrile, its use as a co-solvent results in a decrease in the electroosmotic flow [27] and an increase in the analysis time. It must be noted that this considerable increase in analysis times, more than 30 min in the case of 2-propanol versus 13 min with acetonitrile, is not a real drawback in the present case, as the quality of analysis is considerably improved when 2-propanol is used. Effectively, as shown in Fig. 5, the use of 2-propanol allows for the first time the complete resolution of all the homologous alkylbenzenes with chain lengths of C_1–C_{16} and it is perfectly adapted to the determination of very hydrophobic compounds.

Therefore, we selected 2-propanol as the co-solvent to complete the study, with the following optimum conditions: applied voltage, 30 kV; fused-silica capillary, total length of 57 cm × 50 μm I.D.; mobile phase, 5 m*M* phosphate–2.5 m*M* borax buffer (pH 9) containing 40% of 2-propanol and 50 m*M* SDS; and temperature 30°C. Using these conditions, we analysed industrial mixtures of alkylbenzenes used as bases of sulfonation in the preparation of commercial anionic surfactants and resulting on one hand from the condensation of C_{12}-centred α-olefins on benzene, resulting in a mixture of so-called "linear dodecyl sulfate", and on the other hand from the condensation on benzene of the tetramer of proplyene, giving a mixture of mainly ramified alkylaromatics, "tetrapropylbenzene".

3.2. Application to mixtures of alkylaromatics used as bases of sulfonation during the preparation of industrial surfactants

The electropherograms of these two products are shown in Fig. 6. Unfortunately, there is no fine resolution of either of these two complex

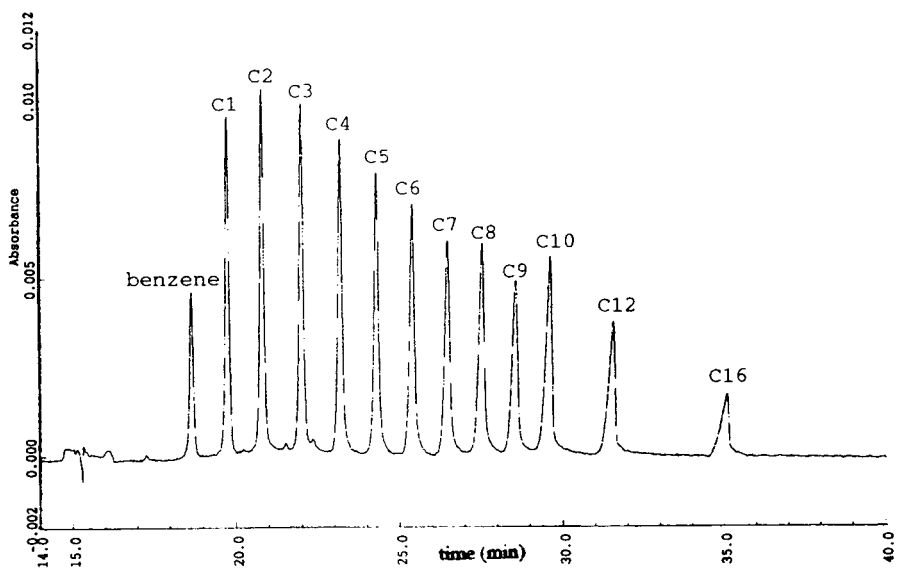

Fig. 5. Analysis of a mixture of model alkylbenzenes by capillary electrophoresis under the optimal conditions: electrolyte, 5 m*M* NaH_2PO_4–2.5 m*M* $Na_2B_4O_7 \cdot 10H_2O$ buffer (pH 9); [SDS], 50 m*M*; [2-propanol], 40% (v/v); temperature, 30°C; applied voltage, 30 kV; hydrodynamic injection, 1 s; detection at 214 nm.

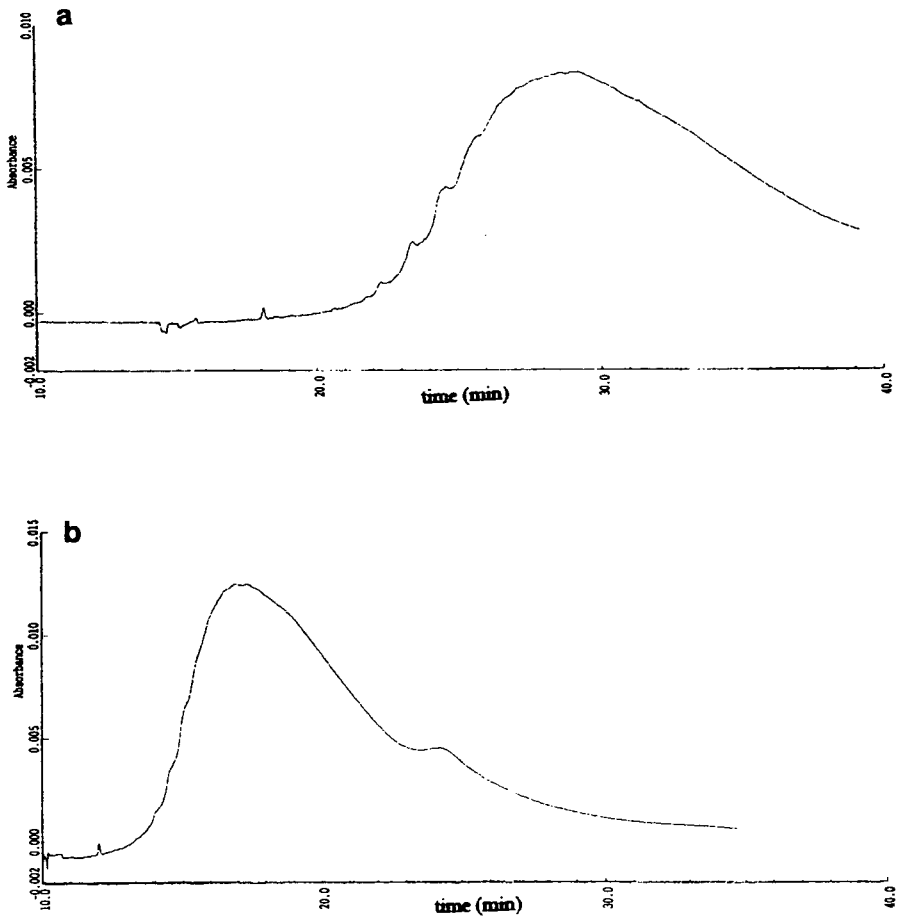

Fig. 6. Analysis by capillary electrophoresis of the bases of sulfonation used in the preparation of industrial anionic surfactants. Operating conditions as in Fig. 5. (a) Linear dodecylbenzene; (b) tetrapropylbenzene.

mixtures, and the electropherograms appear as broad and badly resolved peaks. However, it must be noted that the two mixtures of industrial alkylaromatics have very different electrophoretic behaviours under the operating conditions used. The components of tetrapropylbenzene, which are essentially ramified compounds, show migration times shorter than those of the linear dodecylbenzene components. These different behaviours result from a difference in interaction between these complex mixtures components and the SDS of the pseudo-stationary phase. The different interactions come from the lower hydrophobicity of ramified alkylbenzenes.

Considering this partial setback and the fact that increasing the amount of SDS in the mobile phase results in improved resolution, we performed the analysis of these two industrial bases of sulfonation with electrophoretic systems characterized by a higher concentration of SDS than previously (i.e., 50 m*M*), the other parameters remaining constant. Some resolution is also obtained both with linear dodecylbenzene and tetrapropylbenzene when the SDS concentration reaches 75 m*M*. This improvement in resolution is obtained to the detriment of analysis time, which increases with increasing volume of the pseudo-stationary phase.

In order to improve the resolution in time units, we tried increasing temperature of the electrophoretic medium from 30 to 40°C. As predicted by the theory, at this higher temperature the total analysis time is again acceptable, even with high SDS concentrations. This is due to the decrease in viscosity of the mobile phase, which causes an increase in the electroosmotic flow velocity.

However, a 100 m*M* concentration of SDS in the electrophoretic medium is required to obtain a satisfactory analysis of these two industrial bases of sulfonation. The corresponding electropherograms are reported in Fig. 7. In order to allow comparison of the electrophoretic behaviours, we also reported in Fig. 7 the elution range of the model alkylbenzenes under the same operating conditions.

These series of analyses indicated the following. (i) As would be expected, because of the synthesis processes used, the linear dodecylbenzene and tetrapropylbenzene are in fact complex mixtures. (ii) These two bases of sulfonation are characterized by relatively broad distributions. Effectively, the components of the linear dodecylbenzene elute at migration times extend-

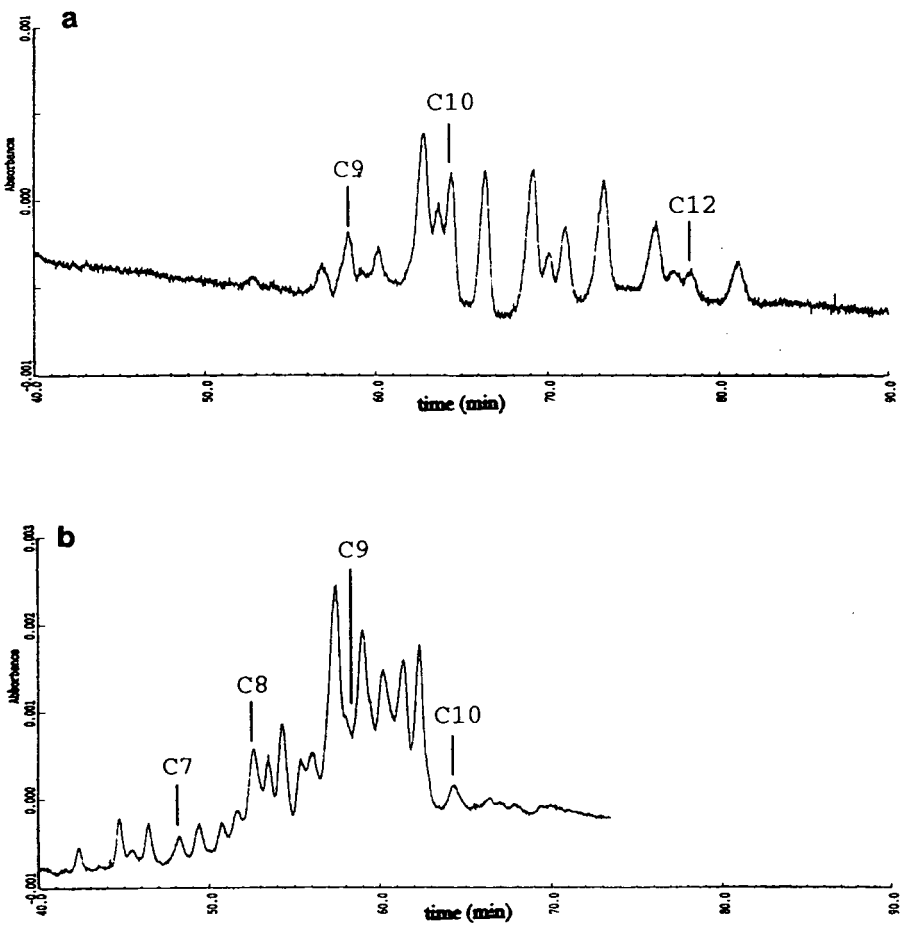

Fig. 7. Analysis by capillary electrophoresis of the bases of sulfonation used in the preparation of industrial anionic surfactants. Operating conditions: electrolyte, 5 m*M* NaH_2PO_4–2.5 m*M* $Na_2B_4O_7 \cdot 10H_2O$ buffer (pH 9); [SDS], 100 m*M*; [2-propanol] 40% (v/v); temperature, 40°C; applied voltage, 30 kV; hydrodynamic injection, 1 s; detection at 214 nm. (a) Linear dodecylbenzene; (b) tetrapropylbenzene.

ing respectively from those of *n*-octylbenzene and *n*-tridecylbenzene, whereas those of the tetrapropylbenzene elute between the migration times of *n*-hexylbenzene and *n*-undecylbenzene. This result justifies the designation "linear dodecylbenzene" attributed by the producer to the sulfonation base resulting from the condention of benzene on an industrial α-olefin centred on C_{12}. In contrast, we cannot provide such a direct justification for the "tetrapropylbenzene", as this is mainly constituted by a mixture of ramified alkylbenzenes, in contrast of the mixture of model alkylbenzenes which are all linear. (iii) The apparent electrophoretic mobilities of the components of the tetrapropylbenzene are lower than those observed with the linear dodecylbenzene. This result emphasizes again that the tetrapropylbenzene is essentially ramified. Effectively, for an identical number of carbons in the alkyl chain, hydrophobic interactions are weaker for a ramified chain than a linear chain and therefore the components of the industrial sulfonation base must have lower electrophoretic mobilities if they are more ramified. (iv) It must be emphasized that these structural hypotheses, established from the electrophoretic behaviour of the two sulfonation bases, were perfectly confirmed by their analysis using a combination of capillary gas chromatography and mass spectrometry. This method showed that the linear dodecylbenzene is composed of alkylbenzenes with side-chains from 10 to 13 carbons, each possessing positional isomers, and the tetrapropylbenzene is essentially a mixture of ramified alkylbenzenes.

As the complexity of the anionic surfactants that we intended to study seems to result mainly from the great diversity of the alkyl side-chains, we decided to analyse then directly under conditions similar to those selected during the study of their sulfonation bases, that is, in the presence of high concentrations of SDS and of organic co-solvent.

3.3. Analysis of industrial anionic surfactants

Three anionic surfactants commercialized by WITCO were examined: TRS 10-80, Sulframine AcB and Sulfo TPB.

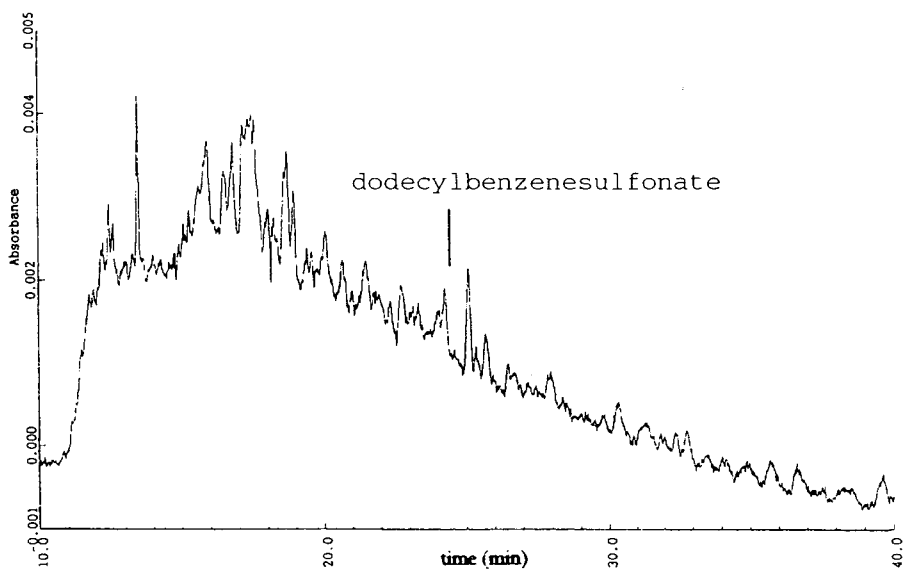

Fig. 8. Analysis of the anionic surfactant WITCO TRS 10-80 by capillary electrophoresis. Operating conditions: electrolyte, 6.25 m*M* borate–boric acid buffer, adjusted at pH 9; [SDS], 50 m*M*; [CH_3CN], 30% (v/v); temperature, 30°C; applied voltage, 30 kV; hydrodynamic injection, 1 s; detection at 214 nm.

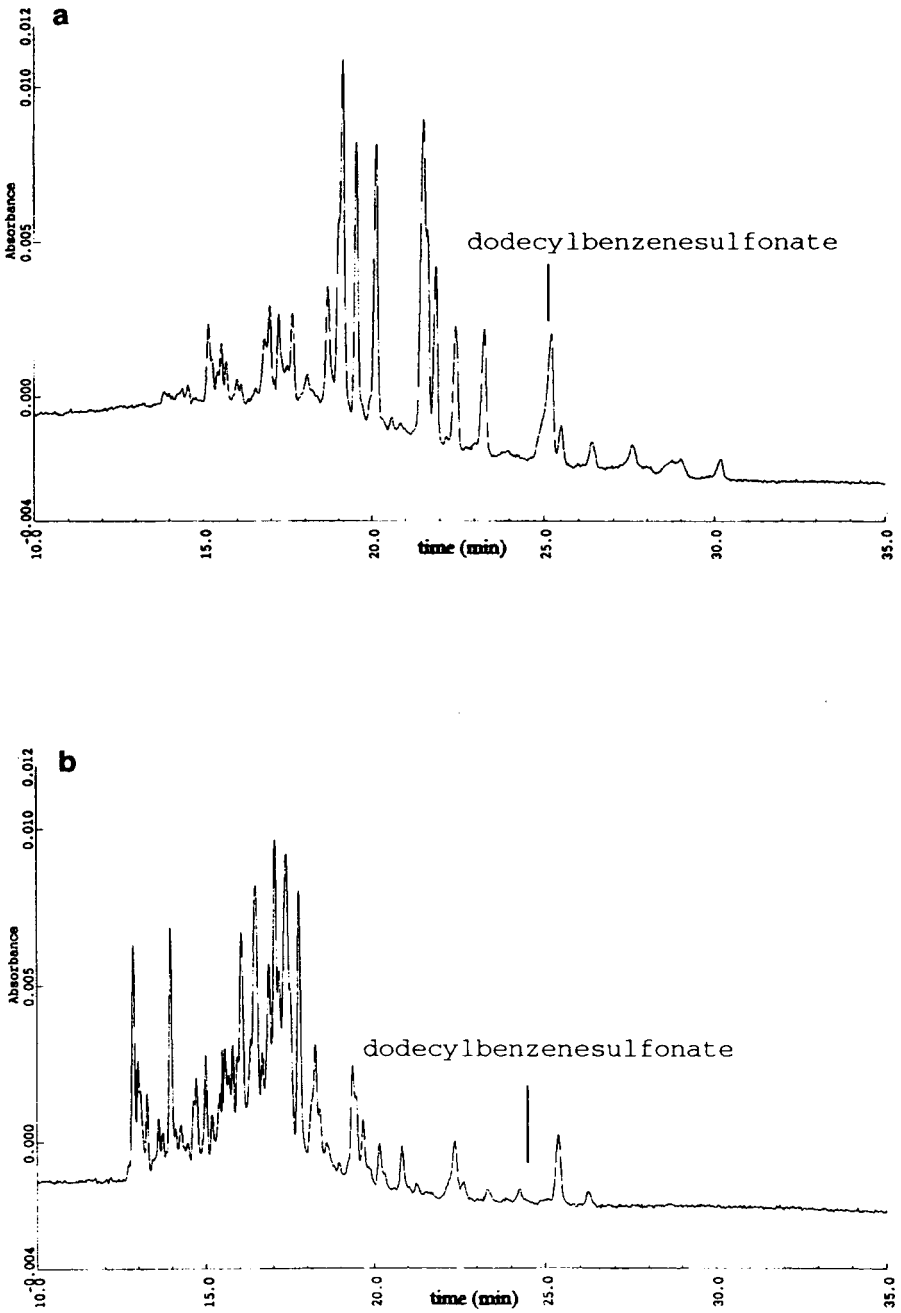

Fig. 9. Analysis of industrial anionic surfactants. Operating conditions as in Fig. 8. (a) WITCO Sulframine AcB; (b) WITCO Sulfo TPB.

Analysis of WITCO TRS 10-80

Considering the results obtained during the above study of the sulfonation bases, we decided to reconsider the analysis of TRS 10-80 WITCO with the following initial operating conditions: 6.25 m*M* borate–boric acid buffer (pH 9), 50 m*M* of SDS, temperature 30°C and a concentration of acetonitrile fixed in 5% steps.

As the amount of SDS was already large, we began this optimization by studying the influence on the resolution of substantial additions of acetonitrile because the amount of co-solvent in the mobile phase seemed to be, at a high SDS concentration, the other major parameter.

With the other operating parameters constant, we show in Fig. 8 the analysis of WITCO TRS 10-80 in the presence of a mobile phase containing 30% of acetonitrile. The results show that a large amount of acetonitrile, coupled with a moderate concentration of SDS, allows for the first time a relatively good separation of this complex matrix, better than the best results described previously [21], obtained using high-performance ion-exchange chromatography.

The selectivity of the electrophoretic system appears sufficient to obtain an acceptable resolution. However, this technique is still limited to the level of identification. Because of the large number of compounds separated, identification using spiking seems impossible. It appears essential, in order to complete the analysis of this complex mixture, to replace the classical UV detection with a more selective method allowing on-line identification.

After this positive result, we analysed under the same electrophoretic conditions the industrial anionic surfactants resulting from the sulfonation of alkylbenzenes obtained by condensation on benzene of either α-olefins centred around C_{12} ("linear dodecylbenzene") or tetramers of propylene ("tetrapropylbenzene"), as described above.

Analysis of WITCO Sulframine AcB

This anionic surfactant results from the sulfonation of linear dodecylbenzene. The electropherogram corresponding to the analysis of this mixture, under the conditions previously optimized with WITCO TRS 10-80, is shown in Fig. 9a.

As could be expected, because of the synthesis process used to prepare this product, it has a simpler matrix than WITCO TRS 10-80. However, in spite of this lesser complexity, identification by spiking is still difficult as few model molecules of this type are commercially available, a large number of syntheses would be required. The electrophoretic system developed appears to be efficient and relatively selective and allows one to separate many of the components of Sulframine AcB, particularly constitutional isomers of each homologous alkylbenzene with chain lengths of C_{10}–C_{13}.

Analysis of WITCO Sulfo TPB

This last surfactant results from the sulfonation of the tetrapropylbenzene base. The electropherogram corresponding to its analysis, under conditions previously optimized for WITCO TRS 10-80, is shown in Fig. 9b.

Comparison with the electropherogram obtained for Sulframine AcB (Fig. 9a) shows a greater complexity of Sulfo TPB, resulting in a poorer resolution. It appears also that apparent mobilities of the Sulfo TPB components are lower than those of the Sulframine AcB components, as evidenced by the comparison of the elution ranges of these two mixtures with the elution time of a standard compound (dodecylbenzenesulfonate, Fig. 9a and b). Therefore, sulfonated compounds possessing ramified alkyl side-chains have an electrophoretic behaviour clearly different from those of sulfonated compounds with linear chains. As in the case of alkylbenzenes, used as bases of sulfonation for the preparation of these two surfactants, this different electrophoretic behaviour results from the difference in hydrophobic interactions with SDS, which are weaker if the compound considered has a more ramified alkyl chain.

4. Conclusions

HPCE appears to be a particularly suitable technique for the resolution of complex mixtures

of surfactant molecules. Owing to the use of large amounts of an organic co-solvent, it was possible, for the first time, to resolve a matrix as complex as WITCO TRS 10-80.

Under operating conditions rather unusual in capillary electrophoresis, we analysed, with the same efficiency, surfactant formulations (WITCO Sulframine AcB and Sulfo TPB) and their bases of sulfonation (linear dodecylbenzene and tetrapropylbenzene). This broadens the application range of this technique from highly hydrophobic molecules to ionic molecules.

References

[1] J.D. Knight and R. House, *J. Am. Oil Chem. Soc.*, 36 (1959) 195.
[2] E.A. Sitzkorn and A.B. Carel, *J. Am. Oil Chem. Soc.*, 40 (1963) 57.
[3] S. Lee and N.A. Puttnam, *J. Am. Oil Chem. Soc.*, 44 (1967) 158.
[4] H.Y. Lew, *J. Am. Oil Chem. Soc.*, 14 (1972) 665.
[5] S. Nishi, *Buseki-Kuyaku*, 14 (1965) 917.
[6] S. Watanabe, M. Nukiyama,, F. Takagi, K. Tida and Y. Wada, *Shokuhin Eiseigaku Zasshi*, 16 (1975) 212.
[7] M. Imaida, T. Suminoto, M. Yada, M. Yoshida, K. Koyama and N. Kunita, *Shokmhin Eiseigaku Zasshi*, 16 (1975) 218.
[8] S. Matsutani, T. Shige and T. Nayai, *Yukagaku*, 28 (1979) 847.
[9] T.H. Lidicoet and L.H. Smithson, *J. Am. Oil Chem. Soc.*, 42 (1965) 1097.
[10] H.Y. Lew, *J. Am. Oil Chem. Soc.*, 44 (1967) 359.
[11] R. Dengi, *Tenside Deterg.* 10 (1973) 59.
[12] A. Nake, K. Tsuji and M. Yamanaka, *Anal. Chem.*, 52 (1980) 2275.
[13] A. Marcomini and W. Giger, *Anal. Chem.*, 59 (1987) 1709.
[14] M.A. Castles, B.L. Moore and S.R. Ward, *Anal. Chem.*, 61 (1989) 2534.
[15] A. Marcomini, S. Capri and W. Giger, *J. Chromatogr.*, 403 (1987) 243.
[16] A. Di Corcia, M. Marchetti, R. Samperi and A. Marcomini, *Anal. Chem.*, 63 (1991) 1179.
[17] A. Nakae and K. Kunihiro, *J. Chromatogr.*, 152 (1971) 137.
[18] D. Thomas and J.L. Rocca, *Analusis*, 7 (1979) 386.
[19] L.A. Verkruyse, R.V. Lewis, K.O. Meyers and S.J. Slater, *Proceedings of the 1983 SPE International Symposium on Oilfield and Geothermal Chemistry*, Society of Petroleum Engineers of AIME, Richardson, TX, 1983, paper SPE 11781, p. 105.
[20] S. Chen and D. Pietrzyk, presented at the *17th International Symposium on Column Liquid Chromatography*, Hamburg, 9–14 May 1994, poster.
[21] F.E. Suffridge and D.L. Taggart, *Proceedings of the 1977 SPE International Symposium on Oilfield and Geothermal Chemistry*, Society of Petroleum Engineers of AIME, Richardson, TX, 1977, paper SPE 6596, p. 75.
[22] P.L. Desbène, C. Rony, B. Desmazières and J.C. Jacquier, *J. Chromatogr.*, 608 (1992) 375.
[23] C. Tribet, R. Gaboriaud and P. Gareil, *J. Chromatogr.*, 609 (1992) 381.
[24] J. Romano, P. Jandik, W. Jones and P. Jackson, *J. Chromatogr.*, 546 (1991) 411.
[25] S. Terabe, *Micellar Electrokinetic Chromatography*, Beckman Instruments, Fullerton, CA, 1992.
[26] J. Vindevogel and P. Sandra, *Introduction to Micellar Electrokinetic Chromatography*, Hüthig, Heidelberg, 1992.
[27] C. Schwer and E. Kenndler, *Anal. Chem.*, 63 (1991) 1801.
[28] J. Bullock, *J. Chromatogr.*, 645 (1993) 169.
[29] P.L. Desbène and J.C. Jacquier, *J. Chromatogr.*, in preparation.
[30] Y. Walbroehl and J.W. Jorgenson, *Anal. Chem.*, 58 (1986) 479.
[31] H.T. Rasmussen and H.M. McNair, *J. Chromatogr.*, 516 (1990) 223.
[32] J. Vindevogel and P. Sandra, *Anal. Chem.*, 63 (1991) 1530.

ELSEVIER

Journal of Chromatography A, 689 (1995) 123–133

JOURNAL OF CHROMATOGRAPHY A

Preparative capillary isotachophoresis as a sample pretreatment technique for complex ionic matrices in high-performance liquid chromatography

M. Hutta*, D. Kaniansky, E. Kovalčíková, J. Marák, M. Chalányová, V. Madajová, E. Šimuničová

Department of Analytical Chemistry, Faculty of Natural Sciences, Comenius University, Mlynská Dolina CH-2, 84215 Bratislava, Slovak Republic

Received 22 July 1994

Abstract

Preparative capillary isotachophoresis (ITP) was studied for sample pretreatment in the high-performance liquid chromatography (HPLC) of ionogenic analytes present in complex ionic matrices (urine and humic substances). Sulphanilate, methyl (4-aminobenzenesulphonyl)carbamate (asulam), 2,4-dichlorophenoxyacetic acid (2,4-D) and 2-methyl-4-chlorophenoxyacetic acid (MCPA) served as model analytes. A high sample load of the ITP pretreatment was achieved by performing the preparative separations in tubes of 2.0 and 1.0 mm I.D. in the column-coupling configuration of the separation unit. The ITP separation according to ionic mobilities was combined with gradient elution HPLC in the ion-suppression mode to achieve highly dissimilar (orthogonal) separation systems in both techniques. The pretreatment provided the sample fraction for the HPLC analysis containing in addition to the analyte (sulphanilate) only ca. 2–3% of the urine matrix (spread along the complete elution profile) when a pair of discrete spacers defined the trapped constituents. Under these conditions the limit of detection for sulphanilate in urine could be reduced by more than two orders of magnitude. A high recovery of the pretreatment procedure [$99 \pm 1.5\%$ for a 1.7 ppm (w/w) concentration of sulphanilate] was typical. For asulam, 2,4-D and MCPA present in a humic matrix it was shown that the ITP pretreatment may also be effective for multi-residue procedures while favourable analytical characteristics of the pretreatment such as recovery and efficient sample clean-up are maintained.

1. Introduction

Sample pretreatment techniques (SPTs) play a key role in the trace analysis of ionogenic compounds by high-performance liquid chromatography (HPLC). There is a variety of SPTs based on different separation principles and applicable for this purpose [1,2]. The actual choice depends, mainly, on the physico-chemical properties of the analyte, the concentration range within which it is to be determined and the nature of the matrix. Many of the currently used SPTs provide a group isolation of the sample constituents. Although convenient in many instances, this can be a disadvantage when a trapped group contains a large number of sample constituents of close physico-chemical properties

* Corresponding author.

0021-9673/95/$09.50
SSDI 0021-9673(94)00854-X

as the risk of analyte peak overlap by matrix constituents may be high [3].

To solve these problems, high-efficiency SPTs are increasingly used and the analytical potential of such an approach is very convincing (see, e.g., Refs. [4–7]). SPTs based on electrophoretic principles and performed in instruments providing adequate separation efficiencies belong in this category. Convenient mainly for ionogenic analytes, they can be considered in many instances to be orthogonal to HPLC in terms of the separation principles. Zone electrophoresis (ZE) sample pretreatment as developed by Kok and co-workers [8–11] and various alternatives of preparative capillary isotachophoresis (ITP) [12–19] are especially promising. It can be deduced that from a general point of view ITP has some advantageous features as far as the sample pretreatment is concerned: (i) a high sample load capacity; (ii) the driving current is to a large extent employed for the transport of the separated constituents [20]; (iii) a well defined concentration of the separated constituents with a self-sharpening effect of the zone boundaries [21]; (iv) a predictable clean-up capability expressed in basic physico-chemical characteristics of the analytes (pK values, ionic mobilities) [22]; (v) the migration position of the analyte within the train of the ITP separands does not depend on the amount of sample once the electrolyte system for a given separation compartment guarantees its resolution [20].

Although the use of ITP for sample pretreatment in HPLC was proposed about 10 years ago [13,15], so far only limited attention has been paid to this subject [17,19]. This work was intended to study the potential of ITP pretreatment for anionic analytes present in matrices of high ionic complexity in combination with RP-HPLC with gradient elution. Such a combination was preferred as we would investigate the pretreatment of sample matrices containing constituents of highly varying hydrophobicity.

Usually, each sample type may require a specific approach as far as the sample pretreatment is concerned. Therefore, in a strict sense the use of any SPT should be evaluated in close relation with the matrix involved. However, as can be deduced from a statistical model of the peak overlap in multi-component chromatograms [3,23–26], classifications of matrices based on the saturation ratio (see below) make certain generalizations possible. In our experiments, urine, containing hundreds of acidic constituents at widely varying concentrations [27–29], was chosen as a matrix providing a discrete RP-HPLC profile under gradient elution in the ion-suppression mode with a very high sample component overlap. On the other hand, samples containing humic acids served as matrices of extremely high ionic complexity exhibiting under identical RP-HPLC conditions flat chromatographic profiles. Our study was focused on the clean-up capabilities of ITP, recoveries of the model analytes and the capabilities of the ITP pretreatment in multi-residue analysis.

2. Experimental

2.1. Instrumentation

A gradient chromatographic system consisting of two HPP 5001 pumps, a GP-2 gradient programming unit, an LCI-30 valve (20-μl sample loop) and an LCD 2040 UV–Vis detector (set at 254 or 240 nm) was obtained from Laboratorní přístroje (Prague, Czech Republic). The UV–Vis detector was connected to a CI 100 computing integrator and to a line recorder (Laboratorní přístroje). A 150 × 3 mm I.D. compact glass column packed with spherical Separon-RPS 5-μm silica-based polymeric sorbent was bought from Tessek (Prague, Czech Republic). The temperature of the column was maintained at 25 ± 1°C.

A CS isotachophoretic analyser (Villa-Labeco, Spišská Nová Ves, Slovak Republic) in a single-column mode was used for the analytical control of the fractionation. The column was provided with a 200 mm × 0.30 mm I.D. capillary tube made of fluorinated ethylene–propylene copolymer (FEP) and with a UVD-2 on-column photometric detector (Villa-Labeco). The detector was set at 254 nm. The driving current in the runs with this column was 50 μA.

Preparative experiments were carried-out using a discontinuous ITP fractionation unit [14,15] in the column-coupling configuration [30,31] constructed in this laboratory (Fig. 1). The pretreated samples were injected with the aid of an injection device [31] providing valve injection (50-μl sample loop), microsyringe injection (0–300 μl) or a combination of both. The preseparation column (II in Fig. 1) was provided with a 2.0 mm I.D. tube made of FEP. The final separation column was identical in design and was provided with a 1.0 mm I.D. tube made of FEP. The columns had on-column conductivity sensors [21] for monitoring of the separations to achieve proper timings in the switching of the columns and in the fractionation procedure (see below). The fractionation valve (V in Fig. 1) had a plunger with a 15-μl internal trapping loop. Electronic units of a CS isotachophoretic analyser (Villa-Labeco) were used in the preparative experiments without modification with the exception of the high-voltage power supply, which was reconstructed to deliver driving currents up to 1000 μA.

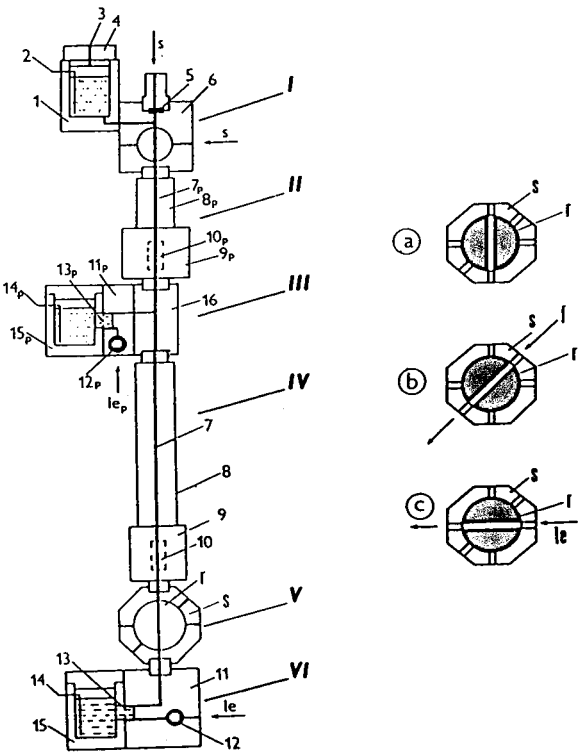

Fig. 1. ITP separation unit in the column-coupling configuration as used for the sample clean-up. I = Injection device; II = preseparation column; III = bifurcation block with the counter-electrode compartment for the preseparation column; IV = final separation column; V = fractionation (trapping) valve; VI = refilling block with electrode compartment for the final (trapping) separation column; 1 = terminating electrolyte compartment with a driving electrode (2) closed with a drilled (3) cap 4; 6 = injection valve with a septum (5) for microsyringe injection of the sample(s), s = sample introduction positions for the injection with a microsyringe (top) and with an internal sample loop in the rotor (right); 7, 7p = (capillary) tubes housed in columns (8, 8p) provided with conductivity detectors (10, 10p); 11, 11p = refilling blocks with needle valves (12, 12p); 15, 15p = leading electrolyte compartments with driving electrodes (14, 14p) separated from the channels in the refilling blocks (11, 11p) by membranes (13, 13p); 16 = bifurcation block; S, r = stator and rotor of the fractionation (trapping) valve, respectively; l_{ep}, l_e = positions for the refilling of the separation (p) and trapping columns, respectively. Operational algorithm for the fractionation valve: (a) position of the rotor of the fractionation (trapping) valve during the separation; (b) trapping of the desired fraction (f); (c) position for the refilling of the loop with the electrolyte solution (l_e).

2.2. Chemicals

Chemicals used for the preparation of the leading and terminating electrolyte solutions were bought from Serva (Heidelberg, Germany), Sigma (St. Louis, MO, USA) and Lachema (Brno, Czech Republic). Methylhydroxyethylcellulose 30 000 (Serva) purified on a mixed-bed ion exchanger (Amberlite MB-1; BDH, Poole, UK) was used as an anticonvective additive in the leading electrolyte solutions for the preparation column. Water from an Aqualabo two-stage demineralization unit (Aqualabo, Brno, Czech Republic) was further purified by circulation in a laboratory-made demineralization system made of polytetrafluorethylene and packed with Amberlite MB-1 mixed-bed ion exchanger. At the outlet water was filtered through a 0.45-μm filter (Gelman, Ann Arbor, MI, USA). The solutions used in the ITP experiments were prepared from freshly recirculated water.

Water doubly distilled from a glass apparatus

and methanol for HPLC (Merck, Darmstadt, Germany) were used for the preparation of the mobile phases. Mobile phase A was acidified with sulphuric acid diluted with water (1:1) to pH 2.0 and purified by percolation through a glass column packed with a coarse fraction (60–100 μm) of Separon-RPS (Tessek) immediately before the use.

2.3. Samples

Urine samples were obtained from healthy individuals (both male and female, mid-stream fraction). They were immediately diluted (seven-fold) with demineralized water to avoid gradual precipitation of the anionic constituents. When required, the samples or aliquots were spiked at appropriate concentrations with sulphanilic acid (Lachema). No preservatives were added to the samples and they were not subjected to any additional treatment.

Humic acid (Fluka, Buchs, Switzerland) of M_r. 600–1000 was dissolved in distilled water at a 500 mg/l concentration after gradual addition of NaOH to pH 6.0 under pH-meter control. After 24 h the sample was filtered (0.45 μm) and stored for further use. When required, the samples and/or aliquots were spiked at appropriate concentration levels with the selected pesticides. Asulam [methyl (4-aminobenzenesulphonyl)-carbamate], 2,4-D (2,4-dichlorophenoxyacetic acid) and MCPA (2-methyl-4-chlorophenoxy-acetic acid) (99% purity) were kindly provided by the Residue Laboratory of the Research Institute for Chemical Technology, (Bratislava, Slovak Republic).

2.4. ITP pretreatment procedure

The injected samples after the separation were trapped in the internal loop of the trapping valve (V in Fig. 1) by disconnecting the delivery of the driving current into the separation unit by the controller of the analyser. The timing for this disconnection was derived from the signal of the conductivity detector in the final separation column (10 in Fig. 1). The rotor of the trapping valve was then turned into the isolation positon (b in Fig. 1) and the fraction of interest was flushed out with water or mobile phase into a weighed eppendorf microvial. The trapping loop was refilled with the leading electrolyte (c in Fig. 1) and the rotor was turned into the working position (a in Fig. 1) to transport a further fraction into the loop by the driving current.

3. Results and discussion

3.1. Choice of sample matrices

Once the peak capacity of the column is given it is convenient to classify sample matrices according to the frequency with which the peak overlaps of the sample constituents can be expected [3]. In this context we can distinguish the following extreme types of the matrices:

(i) $n_c \gg m$ (n_c = peak capacity, m = number of sample components), i.e., the saturation factor (m/n_c) is very low and the chance of achieving complete resolution of the sample constituents is high. In such a situation sample clean-up is not necessary unless constituents having detrimental effects on the column performance are present or preconcentration of the analyte is needed.

(ii) $n_c \approx m$, i.e., the saturation factor is close to 1 and the number of detected peaks achieves a maximum number for a given column [3]. However, the number of single-component peaks which can be expected in such samples is very low [3]. Here, the use of SPTs is usually required to achieve a reasonable certainty of identification and/or a minimum bias in the quantification.

(iii) $n_c \ll m$, i.e. the saturation factor is high and the chance of detecting a single-component peak is negligible and also the number of peaks is considerably reduced (see, e.g., Fig. 1 in [3]). The use of SPTs for this type of sample matrices is essential.

With this classification in mind, sample matrices belonging into the last group were preferred for our evaluation of the sample pretreatment capabilities of ITP. Based on preliminary experiments with various samples of biological and environmental origins (urine, extract from

various plants, fermentation broths, soil extracts and humic acids), urine and humic acids were chosen as representatives of typical complex ionic matrices. Urine, having under our elution conditions (Table 1) chromatographic profiles with many peaks of widely varying heights (Fig. 2), contains hundreds of acidic constituents [27–29] and there is a very low probability of obtaining a pure sample constituent peak [3]. On the other hand, samples of humic acids, containing extremely large numbers of acidic constituents [32] and providing a minimum number of peaks with a flat chromatographic profile (see Fig. 9), represent a good example of a complex matrix with an equal spread of peaks over the retention time interval of current analytical interest (see Fig. 2 in Ref. [26]).

3.2. ITP pretreatment of urine

The ITP pretreatment was carried out in the separation unit shown schematically in Fig. 1 (for details see Experimental). The ITP separation conditions (Table 2) differentiated the separands mainly via the differences in their ionic mobilities [21]. This was a preferred ITP separation mode as the HPLC analyses of the ITP fractions were based on ion suppression. Such a combination of the separation systems has clear orthogonal features as hardly any relationship between the ionic mobilities and hydrophobicities of the compounds can be expected. In addition, these separation systems were fully compatible and the ITP fractions could be directly injected on to the HPLC column.

The chromatogram in Fig. 2 shows the elution

Table 1
Elution conditions used in HPLC runs

Column	Separon RPS (5 μm) CGC, 150 × 3 mm I.D.
Mobile phase A	water (pH 2, sulphuric acid) –1% (v/v) methanol
Mobile phase B	Methanol
Gradient	Linear: 2% B in A (0–4 min); from 2%–98% B (4–36 min); 98% B (36–46% min)
Flow-rate (ml/min)	0.5

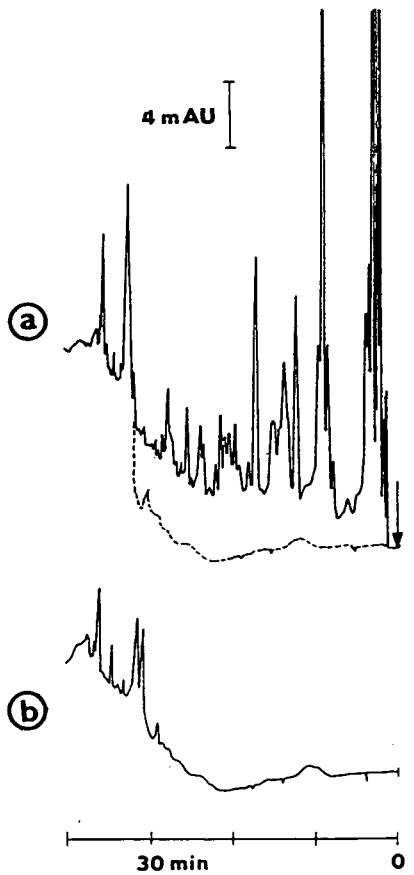

Fig. 2. Chromatographic profile of a urine sample. (a) Urine diluted (1:7 v/v) with doubly distilled water after collection (for the elution conditions see Table 1); (b) blank run under the same elution conditions as in (a). The dashed line in (a) marks the baseline as obtained in the blank run with the same detector setting.

profile of a diluted urine sample. By using the procedure described by Nagels and Creten [26] we found that this sample type is characterized by an exponential course of the frequency distribution of the relative peak heights (see Fig. 5). From the profile it can be seen that the baseline of the detection signal within the interval of retention times of analytical interest was considerably shifted relative to that obtained in the blank run. This shift represented 60.5% of the total area of the chromatogram [12% for a 0–2.9 mAU shift and 48.5% for a 0–4.5 mAU shift (AU = absorbance units)]. Only 39.5% of the

Table 2
Operational system and working conditions used in ITP runs

Parameter	Electrolyte	
	Leading[a]	Terminating[a]
Solvent	Water	Water
Anion	Cl^-	MES^-
Concentration (m*M*)	10	10
Counter ion	HIS	HIS
pH	6.0	6.0
Additive	HEC	–
Concentration (%, w/v)	0.2	–

Driving currents: preparative ITP, preseparation column (2.0 mm I.D.) = 1000 μA, trapping column (1.0 mm I.D.) = 500 μA; analytical ITP, monitoring, analytical column (0.3 mm I.D.) = 50μA.
[a] HEC = hydroxyethylcellulose; MES = morpholinethanesulphonate; HIS = histidine.

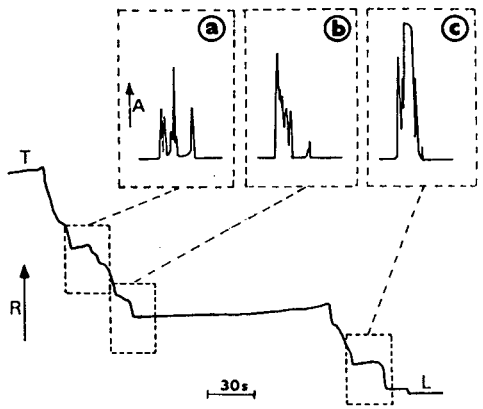

Fig. 3. ITP fractionation of urine. An isotachopherogram as obtained from the conductivity detector in the final (trapping) separation column for a 50-μl urine sample [diluted 1:7 (v/v) with doubly distilled water]. The trapped fractions (a–c) are marked by dashed boxes on the isotachopherogram. Panels at the top show isotachopherograms as obtained for the collected fractions in a single column ITP unit (see Experimental). For the electrolyte system and the driving currents, see Table 2. L, T = leading and terminating zones, respectively; A, R = increasing light absorption and resistance, respectively.

total area corresponded to the detected peaks. An estimate of the number of eluted sample constituents based on the statistical theory of component overlap is uncertain for such multicomponent chromatograms [23–25]. Nevertheless, if we assume that the detected constituents have molar absorptivities at the detection wavelength (254 nm) in the range 10^3–10^4 l mol^{-1} cm^{-1} we can state that the constituents responsible for a shifted baseline were present in the sample at 0.1–1.0 ppm concentrations whereas those forming the peaks corresponded to concentrations up to several tens of ppm. These simple estimates indicate that for the determination of the analyte present in urine at a 1 ppm concentration or less the use of a high-efficiency SPT can be very beneficial.

The isotachopherograms in Fig. 3 were obtained in the pretreatment of the same urine sample as used in the chromatography profiling (Fig. 2). The ITP fractions (marked by dashed boxes on the isotachopherogram as registered by the conductivity detector) were checked by analytical ITP (see the panels at the top) and finally separated by HPLC (Fig. 4). From the chromatograms of the fractions it can be seen that although the ITP pretreatment reduced the baseline shift relative to that of the untreated sample only fraction (a) was sufficiently clean to make the determinations at 0.01–0.1 ppm concentrations of the analytes possible. From the analyses of fractions (b) and (c) it is apparent that they contained separands of widely varying hydrophobicities. This suggests that the ITP pretreatment (providing the fractions within well defined effective mobility intervals) and HPLC were based on different separation principles. It is also clear that the relative peak heights of the constituents present in the fractions are exponentially distributed (Fig. 5).

Typical reproducibilities of the ITP fractionation are illustrated in Figs. 6 and 7. While the ITP control of the fractions indicates perfect reproducibility of the procedure from the HPLC runs, we can see slight differences in the peak heights for some of the separands. This can be due in part to the presence of mixed zones in the ITP pretreatment and also to some fluctuations in the migration velocities of the constituents leading to slight changes in the compositions of the trapped fractions. However, the main drawbacks of the pretreatment were in a relatively low clean-up efficiency. Whereas, for example, in

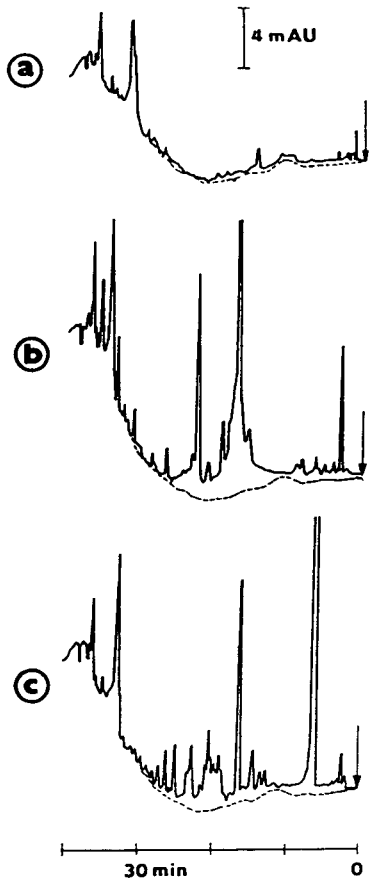

Fig. 4. Chromatograms to the separations of the ITP fractions of urine. (a)–(c) ITP fractions as obtained in the run shown in Fig. 3. The dashed lines mark actual baselines as obtained in the blank runs under identical elution conditions. For the elution conditions see Table 1.

fraction (a) the constituents present represented 3% of the original material, in fraction (b) it was 17% and in fraction (c) 20%. The rest of the urine components (60%) can be attributed to those migrating in the untrapped parts of the ITP train, to anionic constituents migrating with lower effective mobilities than that of the terminating anion and to cationic and uncharged sample constituents. To reduce the number of constituents present in the trapped fractions and strictly define potential interferents, experiments with appropriately chosen spacing constituents were carried out (for general information on the use of spacers in ITP see Ref. [33] and refer-

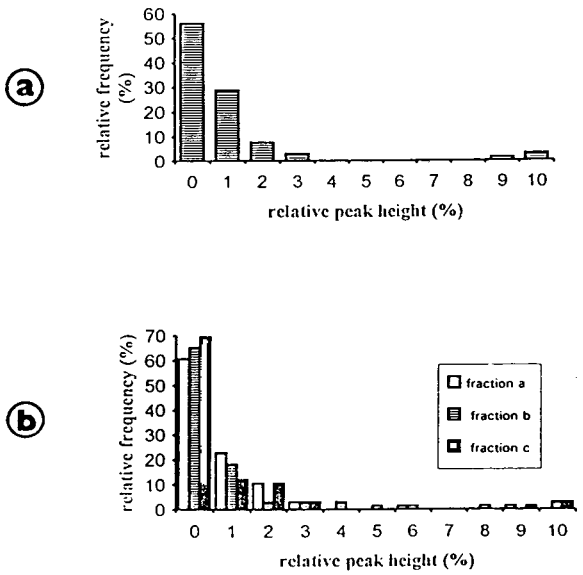

Fig. 5. Frequency distribution of relative peak heights on chromatograms as calculated for (a) urine and (b) its ITP fractions. The data were obtained for a 1% relative peak height resolution and 2σ peak density (0.0147). For further details, see the text.

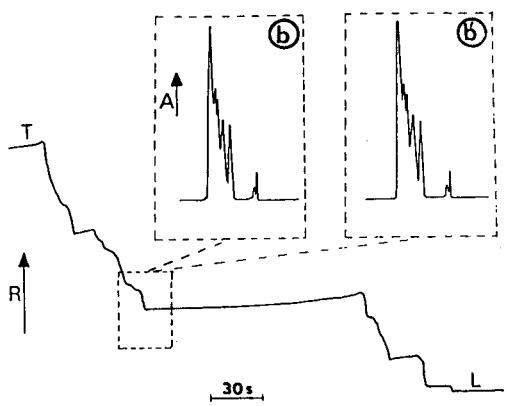

Fig. 6. Reproducibility of the ITP fractionation of urine as evaluated by the ITP monitoring. The trapped fraction is marked by a dashed box on the isotachopherogram as registered by the conductivity detector in the final (trapping) separation column. A 50-μl volume of a diluted urine sample (1:7, v/v) was taken for the fractionation. Isotachopherograms in the panels at the top (b and b′) show typical reproducibilities in the fractionation as evaluated by the ITP monitoring of the fractions. For further details concerning the ITP working conditions, see the legend to Fig. 3.

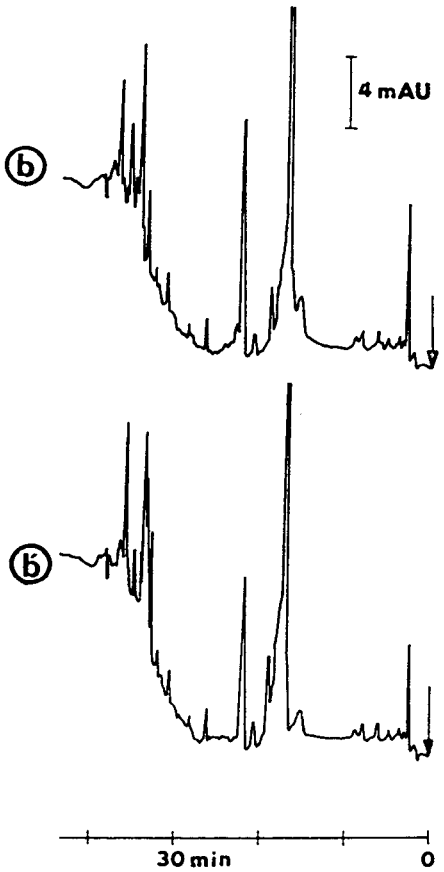

Fig. 7. Reproducibility of the ITP fractionation as evaluated by the HPLC monitoring. The same fractions as in Fig. 6 were monitored by HPLC under the elution conditions given in Table 1.

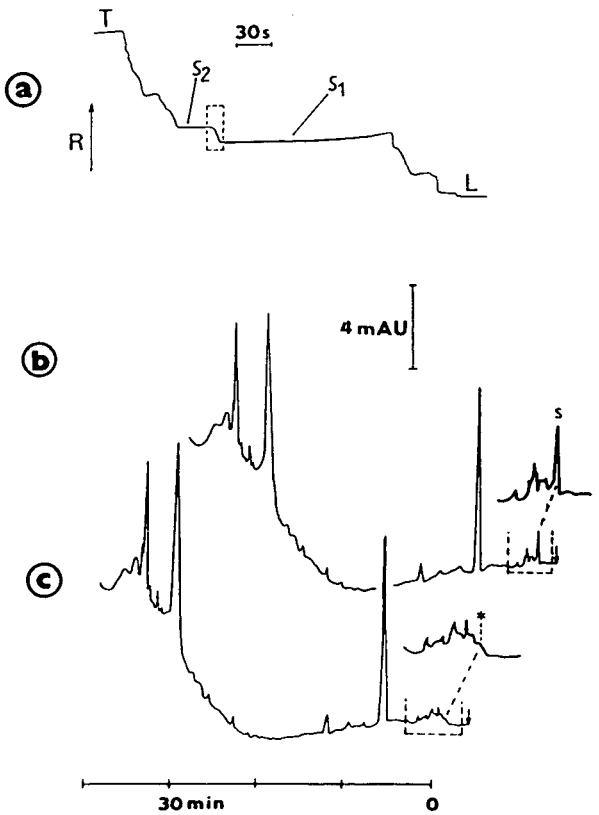

Fig. 8. HPLC analysis of sulphanilate in urine combined with the ITP sample pretreatment. (a) Isotachopherogram from the isolation of sulphanilate (present in urine at a 1.7 ppm concentration); the analyte was spaced by iminodiacetate (S_1) and β-bromopropionate (S_2) and the isolated fraction is marked by a dashed box on the isotachopherogram. (b) HPLC of the sulphanilate fraction isolated as in (a). (c) HPLC identical fraction from the unspiked urine sample. For the elution conditions, see Table 1. The ITP pretreatment was carried out under the same conditions as in Fig. 3.

ences cited therein). Sulphanilic acid, currently not present in urine [27–29], served as a model analyte in these experiments. The spacing constituents were chosen by a computer-based search [22] and iminodiacetate (S_1 in Fig. 8a) and β-bromopropionate (S_2 in Fig. 8a) were found to provide a narrow mobility gap, thus accommodating besides the analyte only a minimum number of matrix constituents. Chromatograms of the relevant ITP fractions (Fig. 8b and c) clearly illustrate a considerable improvement in the sample clean-up by using this ITP approach. For example, when the fraction from the unspiked urine (Fig. 8c) is compared with the untreated sample (Fig. 2a) and with the identical fraction without the use of spacers (Fig. 4b), the improvement achieved in the clean-up is considerable. We found that in this way the signal due to matrix constituents eluted in the position of sulphanilate was reduced ca. 150-fold. Such a background reduction enabled us to detect sulphanilate at a 0.1 ppm concentration. The use of spacing constituents in the pretreatment gave fractions with very reproducible profiles (see Fig. 8b and c) while recovery of sulphanilate as

determined at 1.7 ppm concentration was in the range 99 ± 1.5% (for three parallel runs with three different urine samples).

No disturbances due to the presence of spacers and counterionic constituents in the ITP fractions were observed in the HPLC analyses. To avoid potential problems associated with the injection of hydroxyethylcellulose on to the HPLC column, the leading electrolyte employed in the trapping column was used without this additive. Here, the electroosmotic flow was efficiently suppressed by coating the walls of the capillary tube by a high-molecular-mass derivative of methylhydroxyethylcellulose [34].

3.3. ITP pretreatment of humic matrices

Humic and fulvic acids are present in various environmental samples. As discussed above, they consist of very large numbers of components with different physico-chemical properties [32]. Under our gradient elution conditions the sample of humic acids caused a considerable shift of the baseline relative to that registered in the blank run (Fig. 9). The only peak was detected in the dead retention volume. This peak was probably due to inorganic constituents (the humic acid sample is claimed to contain 10–15% of ash) and in part also to unretained, highly hydrophilic fulvic acids.

In the HPLC analysis, humic substances of polymeric nature can precipitate at the top of the column. We found that after 5–10 runs with such samples the pressure resistance of the column increased considerably and a layer originating from humic substances was deposited on the column bed. This problem can be partially solved by washing the column with 0.1% ammonia solution after each run. This, however, negatively influences the column life owing to gradual decomposition of the bonded phase.

The distribution diagram for humic matrix shown in Fig. 10 differs significantly from that obtained for urine and its fractions (Fig. 5). Not considering the retention times between the first and sixth minutes, it resembles that expected for a sample matrix of an ideal complexity [26]. In ITP humic acids behave analogously and they

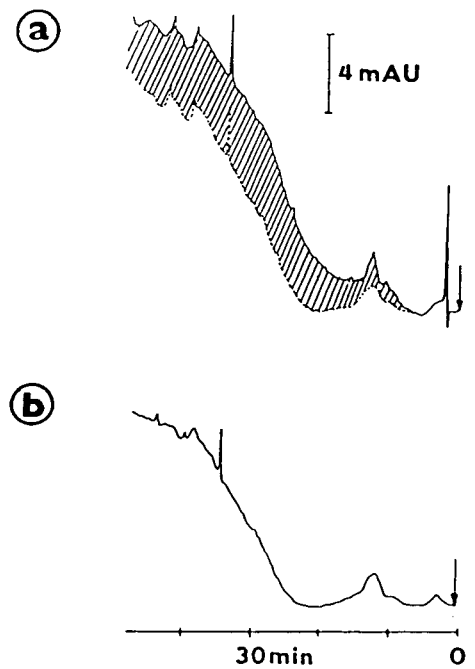

Fig. 9. HPLC profile of a humic acid sample at a detection wavelength of 240 nm. (a) 20-μl volume of the sample contained the acids at a 0.5 g/l concentration; (b) blank run under the same elution conditions (Table 1) as in (a). The shaded area in (a) indicates the shift of the detection signal on injection of the sample.

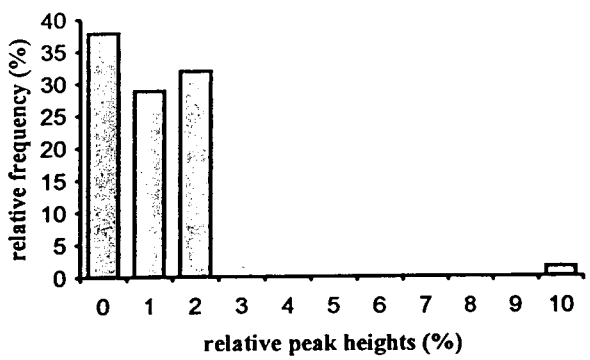

Fig. 10. Frequency distribution of relative peak heights on a chromatogram as calculated for a humic acid sample. The data were obtained for the sample as in Fig. 9 for a 1% relative peak height resolution and 2σ peak density (0.0147).

provide continuous mobility gradients [19,35]. A model sample containing acidic pesticides in a large excess of humic acids served for the evaluation of the ITP pretreatment for this type of matrix. As stated in the introduction, our intention was to carry out the pretreatment for a multi-residue analysis of anionogenic analytes of widely differing hydrophobicities. To meet these requirements, an ITP separation according to ionic mobilities was preferred. This is a favourable separation mode when analytes of close molecular masses (or, better, molecular mass/charge number ratios) are to be isolated as a group because the ionic mobilities are related to the molecular masses of ionogenic separands [36].

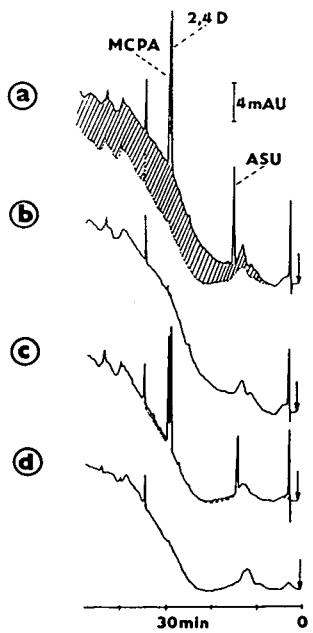

Fig. 11. ITP pretreatment for a multi-residue HPLC analysis of pesticides present in a humic matrix. (a) HPLC profile for asulam (14 ppm), 2,4-D (18 ppm) and MCPA (18 ppm) present in humic matrix (0.5 g/l of humic acids). (b) HPLC profile of the same humic acid sample as in (a). (c) HPLC profile of a humic acid sample (0.5 g/l) spiked with asulam (10 ppm), 2,4-D (14 ppm) and MCPA (14 ppm) after ITP pretreatment (the dashed line marks the baseline for a blank run). (d) HPLC profile of the corresponding ITP fraction from a blank preparative ITP run. For the ITP pretreatment conditions, see Table 2. The elution conditions are given in Table 1.

Therefore, in our particular case glutamate and pelargonate, covering a narrow mobility span under the separation conditions employed (Table 2), were suitable spacing constituents for the pesticides studied. Consequently, the trapped ITP fractions contained in addition to the pesticides only 2.5% of the original humic material (see also Fig. 11) detected within the elution window. The recoveries of the analytes under these conditions were in the range 95–100% for a 0.2–20 ppm concentration span. The chromatograms obtained in these experiments (Fig. 11) suggest that the ITP pretreatment did not significantly improve the detectability of the pesticides. This is, however, what could be expected for such a flat chromatographic profile of the matrix. Nevertheless, considering an empirical equation derived by Nagels and Creten [26], elimination of the baseline shift due to the pretreatment procedure has a positive impact on the determination limits of the pesticides. Obviously, considerable prolongation of the column life by using the ITP pretreatment should also be included in the overall analytical gain.

4. Conclusions

ITP sample pretreatment performed in tubes of 1–2 mm I.D. combined with discontinuous isolation of the analytes of interest provided a highly efficient sample preparation alternative for the HPLC of ionogenic analytes present in complex ionic matrices. Such I.D.s of the ITP separation compartment, favouring a high sample load [20], sufficiently eliminated dispersive effects of the increased heat production on the profiles of the ITP zone boundaries [21]. In addition, the ITP pretreatment could be performed in the separation mode having apparent orthogonal features relative to that used in HPLC (separations according to ionic mobilities vs. separation in the ion-suppression mode). The separation media in both ITP and HPLC were fully compatible so that no further operations with the sample fractions were needed before injection on to the HPLC column.

Optimum separation conditions for the ITP

pretreatment (the electrolyte system and spacing constituents) can be found very quickly by a computer-aided search when the migration characteristics of the analytes (pK values, ionic mobilities) are known [22]. From the practical point of view this is an obvious advantage as a number of experiments needed to find suitable sample pretreatment conditions can be reduced to a minimum.

ITP clean-up was effective in reducing the limits of detection in HPLC by 2–3 orders of magnitude while the recoveries of the analytes were in the range 98–100%. Our results show that multi-residue applicability of the ITP pretreatment for the ionogenic analytes is feasible. However, a perfect sample clean-up can be expected mainly for analytes with close ionic mobilities.

References

[1] H. Lingeman, R.D. McDowall and U.A.Th. Brinkman, *Trends Anal. Chem.*, 10 (1991) 48.

[2] K. Zech and R.W. Frei, *Selective Sample Handling and Detection in High-Performance Liquid Chromatography, Part B*, Elsevier, Amsterdam, 1989.

[3] J.M. Davis and J.C. Giddings, *Anal. Chem.*, 55 (1983) 418.

[4] F. Munari and K. Grob, *J. Chromatogr. Sci.*, 28 (1990) 61.

[5] E.A. Hogendoorn and U.A.Th. Brinkman, *J. Chromatogr.*, 644 (1993) 307.

[6] K.D. Bartle, I. Davies, M.W. Raynar, A.A. Clifford and J.P. Kithinji, *J. Microcol. Sep.*, 1 (1989) 63.

[7] H.J. Cortes, *J. Chromatogr.*, 626 (1992) 3.

[8] W.Th. Kok, *Chromatographia*, 24 (1987) 442.

[9] W.Th. Kok, K.-P. Hupe and R.W. Frei, *J. Chromatogr.*, 436 (1988) 421.

[10] A.J.J. Debets, R.W. Frei, K.-P. Hupe and W.Th. Kok, *J. Chromatogr.*, 465 (1989) 315.

[11] A.J.J. Debets, K.-P. Hupe, U.A. Th. Brinkman and W.Th. Kok, *Chromatographia*, 29 (1990) 217.

[12] E. Kenndler and D. Kaniansky, *J. Chromatogr.*, 209 (1981) 306.

[13] A.C. Schoots and F.M. Everaerts, *J. Chromatogr.*, 227 (1983) 328.

[14] D. Kaniansky, V. Zelenská and I. Zelenský, *J. Chromatogr.*, 256 (1983) 126.

[15] D. Kaniansky, V. Madajová, M. Hutta and I. Žilková, *J. Chromatogr.*, 286 (1984) 395.

[16] T. Hirokawa, J.-Y. Hu, K. Umeda, G. Kimura, H. Ikeda, F. Nishiyama and Y. Kiso, *J. Chromatogr.*, 513 (1990) 297.

[17] P.J.M. Hendriks, H.A. Claessens, T.H.M. Noij, F.M. Everaerts and C.A. Cramers, *Chromatographia*, 33 (1992) 539.

[18] T. Hirokawa and Y. Kiso, *J. Chromatogr. A*, 658 (1994) 343.

[19] P.J.M. Hendriks, *Thesis*, University of Technology, Eindhoven, 1994.

[20] F.E.P. Mikkers, F.M. Everaerts and J.A.F. Peek, *J. Chromatogr.*, 168 (1979) 293.

[21] F.M. Everaerts, J.L. Beckers and Th.P.E.M. Verheggen, *Isotachophoresis–Theory, Instrumentation and Applications*, Elsevier, Amsterdam, 1976.

[22] J. Marák, J. Laštinec, D. Kaniansky and V. Madajová, *J. Chromatogr.*, 509 (1990) 287.

[23] J.M. Davis and J.C. Giddings, *Anal. Chem.*, 57 (1985) 2168.

[24] D.P. Herman, M.-F. Gonnord and G. Guiochon, *Anal. Chem.*, 56 (1984) 995.

[25] M. Martin and G. Guiochon, *Anal. Chem.*, 57 (1985) 289.

[26] L.J. Nagels and W.L. Creten, *Anal. Chem.*, 57 (1985) 2706.

[27] I. Molnár, C. Horvath and P. Jatlow, *Chromatographia*, 11 (1978) 260.

[28] T. Hanai and J. Hubert, *J. Chromatogr.*, 239 (1982) 527.

[29] H.M. Liebich and C. Foerst, *J. Chromatogr.*, 525 (1990) 1.

[30] F.M. Everaerts, Th.P.E.M. Verheggen and F.E.P. Mikkers, *J. Chromatogr.*, 169 (1979) 21.

[31] D. Kaniansky, *Thesis*, Comenius University, Bratislava, 1981.

[32] E.M. Thurman and R.L. Malcolm, in R.F. Christman and E.T. Gjessing (Editors), *Aquatic and Terrestrial Humic Materials*, Ann Arbor Sci. Publ., Ann Arbor, MI, 1983, p. 1.

[33] D. Kaniansky, V. Madajová, J. Marák, E. Šimuničová, I. Zelenský and V. Zelenská, *J. Chromatogr.*, 390 (1987) 51.

[34] M. Koval', D. Kaniansky, M. Hutta and R. Lacko, *J. Chromatogr.*, 325 (1985) 151.

[35] P. Kopáček, D. Kaniansky and J. Hejzlar, *J. Chromatogr.*, 545 (1991) 461.

[36] O. Fujishita, M. Hirokawa, K. Nakashima, S. Higuchi, K. Otsubo, T. Aoyama and H. Karasawa, *Chem. Pharm. Bull.*, 36 (1988) 3985.

ELSEVIER

Journal of Chromatography A, 689 (1995) 135–148

JOURNAL OF CHROMATOGRAPHY A

Utilization of fluorescein sodium salt in laser-induced indirect fluorimetric detection of ions separated by capillary zone electrophoresis☆

P.L. Desbène[a,b,*], C.J. Morin[a,b], A.M. Desbène Monvernay[a,b], R.S. Groult[c]

[a]*Laboratoire d'Analyse des Systèmes Organiques Complexes, Université de Rouen, IUT, 43 Rue Saint Germain, 27000 Evreux, France*

[b]*IRFMP, Université de Rouen, 76134 Mont Saint Aignan Cédex, France*

[c]*Beckman France, 92 Chemin des Bourdons, 93220 Gagny, France*

First received 30 January 1994; revised manuscript received 1 August 1994

Abstract

Indirect detection, the principles of which were demonstrated some years ago, has attracted renewed interest in both UV–visible and fluorimetric detection. This paper reports the implementation of laser-induced indirect fluorimetric detection using a commercially available detector and its association with high-performance capillary electrophoresis for the determination of inorganic ions. In order to optimize the response sensitivity, the fluorescent agent being fluorescein sodium salt, the influence of the fluorescein sodium salt concentration, the ionic strength, the electrolyte pH and the gain on the signal-to-noise ratio were studied successively, the injection mode being either electrokinetic or hydrodynamic. In the case of a 75 μm I.D. fused-silica capillary, detection limits were in the ppb range or about 10 ppb for alkali metal cations using injection in the electrokinetic or in the hydrodynamic mode, respectively. As the detection system used had its maximum sensitivity at basic pH, the use of a complexing agent was required in order to perform the determination of alkaline earth metal cations, because they precipitate or are adsorbed at basic pH. Therefore, using ethylenediaminetetraacetic acid sodium salt (EDTA), it is possible to analyse at pH 7.5, in less than 5 min, a mixture containing three alkaline earth metal cations (Ba^{2+}, Ca^{2+} and Mg^{2+}) and three transition metal cations (Fe^{3+}, Zn^{2+} and Cu^{2+}) in addition to the previously mentioned alkali metal cations (Li^{+} and K^{+}).

1. Introduction

High-performance capillary electrophoresis is a recent analytical technique which appears to be one of the most powerful techniques for the separation of a broad range of complex matrices including both inorganic anions and cations and neutral or potentially ionizable molecules [1]. However, it presents some limitations. In particular, it still suffers from the lack of a sensitive and universal detector. A neat way of overcoming the lack of universality of detection systems was to use indirect detection, already widely used in high-performance liquid chromatography [2–25].

Ionic capillary electrophoresis has been used to determine both anions and cations. However,

* Corresponding author.

☆ Presented at the *6th International Symposium on High Performance Capillary Electrophoresis, San Diego, CA, 31 January–3 February 1994.*

0021-9673/95/$09.50
SSDI 0021-9673(94)00757-8

there is at present a greater diversity of the mixtures analysed in the case of anions than in the case of cations. Inorganic anion separations were performed in the presence of an electrophoretic buffer containing a chromophore, to obtain the background signal, and an electroosmotic flow reverser. Effectively, in the case of anions and in contrast to cations, the electroosmotic flow must be at least decreased, or even reversed, in order to shorten the analysis time. From literature data, it appears that potassium chromate is the most widely used absorbing agent [26–34]. Other compounds absorbing in the UV region were also used to obtain a background signal, for instancé pyromellitic acid [35], potassium phthalate [27,36] and potassium benzoate [27]. The most frequently used modifiers or reversers of electroosmotic flow are quaternary ammonium surfactants such as tetradecyltrimethylammonium bromide [31] or CIA Pak OFM Anion BT (Millipore–Waters) [26–29, 32–34,36]. However, this modifier or reverser of electroosmotic flow can also be diethylenetriamine [30] or hexamethonium hydroxide [35]. Such electrophoretic systems were also used to separate organic anions that do not possess chromophoric groups, e.g., alkylsulfonates and organic acids [27,31].

In the case of cation determination, the analytical approach is akin to that mentioned above for the determination of anions. Effectively, as a great number of cations are transparent in the UV range, it is often necessary to use indirect spectrometric detection (UV or fluorimetric) and less frequently conductimetric detection [37].

Initially, Aguilar et al. [38] separated by capillary zone electrophoresis (CZE) the cations of transition metals, Fe^{2+}, Cu^{2+} and Zn^{2+}, as cyano complexes, spectrophotometric detection being performed at 214 nm. More recently, the same group separated the Au^{+} and Ag^{+} cations, again complexed, and with UV detection (214 nm) [39]. However, the vizualisation of most separations of cations is performed by means of indirect photometric detection techniques. Foret et al. [40] separated a mixture of fourteen lanthanides using an electrophoretic buffer containing α-hydroxyisobutyric acid (HIBA), as complexing reagent, and creatine, as a chromophoric agent, to generate the background signal. Effectively, because of the similitude of the electrophoretic mobilities of some cations, it is necessary to introduce a supplementary mechanism of separation. According to the literature, complexation is frequently used with this aim. Chen and Cassidy [41] analyzed a mixture of lanthanides by CZE using as complexing agent HIBA, the electrophoretic buffer being composed of acetic acid and benzylamine. However, the factors influencing the selectivity of complexed cations were essentially studied by Weston and co-workers [42–44], the complexing agent being systematically HIBA. HIBA is the most commonly used complexing agent for the separation of cations, in association with indirect UV photometric detection [40–46]. However, Beck and Engelhardt [47] have recently developed an electrophoretic buffer containing imidazole, in association with indirect UV detection, for the separation of alkali and alkaline earth metal cations. Similarly, Riviello and Harrold [48] recently proposed a new electrophoretic system for the determination of alkali and alkaline earth metal and ammonium cations in association with indirect UV detection. This new electrophoretic system was based on the utilization of Cu(II) as the primary component of the electrolyte, the system selectivity being adapted by addition of a crown ether, 18-crown-6, as complexing agent.

Several workers have proposed the use of laser-induced fluorimetric detection in the presence of complexing agents to determine alkali and alkaline earth metal cations. Gross and Yeung [49] were the first to use indirect fluorimetric detection to determine alkali and alkaline earth metal cations by CZE. They used quinine sulfate to generate the background signal. More recently, Bächmann et al. [50] used in the same way indirect fluorimetric detection in the separation of alkali and alkaline earth metal cations. They developed a new electrophoretic system based on the association of Ce(II) and 18-crown-6, the latter being the complexing agent allowing the electrophoretic system selectivity to be adjusted. Swaile and Sepaniak [51]

used the fluorescence of complexes of 8-hydroxyquinoline with a large number of metallic cations, the chelating agent not presenting native fluorescence, and visualized by direct fluorescence a mixture of Ca^{2+}, Mg^{2+} and Zn^{2+} cations.

As laser-induced fluorimetric detection is now commercially available, we considered the development of a new electrophoretic system allowing the use of indirect fluorimetric detection and compatible with the detector without modification of this latter. As this detector has excitation and emission wavelengths in the visible range, all the electrophoretic systems previously described for the indirect fluorimetric detection of inorganic cations are ineffectual, the detectors used by different workers being equipped with lasers operating in the UV range. Considering the characteristics of the laser associated with the commercial fluorimetric detector we utilized, we decided to examine the potential offered by the sodium salt of fluorescein as a fluorescent reagent generating the background signal, with a view to detecting alkali, alkaline earth and transition metal cations separated by CZE.

Moreover, as the fluorescence intensity of fluorescein sodium salt is a function of pH, and that it is essential to operate in a basic medium, we therefore studied the possibilities offered by ethylenediaminetetraacetic acid (EDTA) as chelating agent, because alkaline earth metal cations become insoluble or are adsorbed on the capillary wall at such pH values.

2. Experimental

2.1. Reagents

All solutions, electrolytes and standards were prepared using 18-MΩ water generated by an Alpha-Q laboratory water purification system (Millipore, Bedford, MA, USA). The alkali, alkaline earth and transition metal cation standards were prepared from salts (nitrate or chloride, purity ≥ 99.99%) obtained from Aldrich France (La Verpillière, France). Citric acid and its sodium salt and sodium tetraborate utilized for the preparation of buffers and the disodium salt of EDTA used as a complexing agent (purity 99+%) were purchased from Aldrich France and used as received. Fluorescein sodium salt, providing the fluorescence background, was also purchased from Aldrich France and was used as received.

2.2. Preparation of electrolytes and standards

The electrolytes used were prepared from solutions made daily, containing the fluorescein sodium salt on the one hand and on the other hand the suitable buffer (citric acid and its sodium salt, sodium tetraborate or disodium salt of EDTA). In the case of EDTA, the pH was adjusted by addition of sodium hydroxide. After dilution, the electrolytes were systematically degassed for 20 min using sonication and their pH was measured before use, at the experimental temperature. It must also be mentioned that all the vessels used for the preparation of the analyte solutions and of the electrolytes were made of polypropylene (Polylabo-Block, Strasbourg, France). The disposable sample vials were made of siliconed polypropylene and were also purchased from Polylabo-Block. Dilutions were performed using Gilson (Villiers Le Bel, France) electronic automatic pipettes, equipped with disposable cones made of polypropylene.

2.3. Apparatus

All experiments were carried out on a P/ACE 2100 system (Beckman, Fullerton, CA, USA) fitted with an on-column argon laser-based fluorescence detector (λ_{exc} = 488 nm, λ_{em} = 520 nm) and monitored by a PS/2 computer (IBM, Greenock, UK) using P/ACE software or Gold software (Beckman). Data collection was performed using the same software. Samples were loaded by pressure injection [injection pressure 0.5 p.s.i. (1 p.s.i. = 6894.76 Pa)] or electromigration (applied voltage 10 kV) into a fused-silica capillary. The capillary columns used were untreated with respect to any covalently bonded stationary phase. Before use, several solutions were flushed through the capillary in the follow-

ing order: 0.1 *M* NaOH, water, 0.1 *M* HCl, water, buffer solution. These capillaries were 57 cm × 75 μm I.D. Injections were made at the high-voltage anode and cations were eluted to the grounded cathode. Indirect fluorimetric detection was performed at 520 nm through the capillary 50 cm from the inlet. The pH values of the electrolytes were measured using a Beckman Model ϕ pH meter at the analysis temperature.

3. Results and discussion

As mentioned above, because of the characteristics of the laser-induced fluorimetric detector utilized, at both the excitation and emission wavelengths, there was only a limited choice of fluorescence agents that could be used to provide the background signal. Among the commercially available fluorescence agents, fluorescein sodium salt appeared as the most suitable, as it offers maximum absorption at 492 nm and a maximum re-emission at 518 nm, very close to the optical characteristics of the detector. This fluorescence agent has the drawback, however, of a pH-dependent fluorescence intensity. We searched for a pH range allowing an acceptable fluorescence intensity to be maintained and still to have the possibility of modulating the electroosmotic flow using this parameter. As shown in Fig. 1, the fluorescence intensity of fluorescein is constant only in highly basic media, in a range where the electroosmotic flow velocity is independent of pH. However, in the pH range 7–9, this intensity is still hardly modified but the electroosmotic flow is noticeably changed.

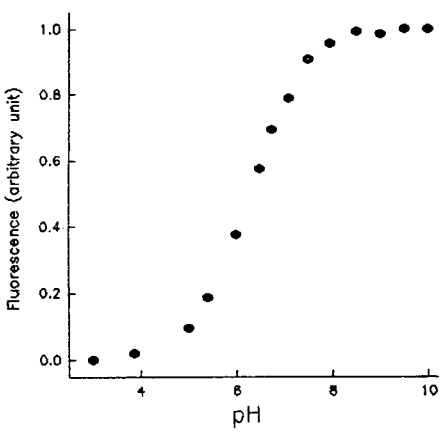

Fig. 1. Evolution of the fluorescence of fluorescein as a function of pH.

We then optimized the fluorescein concentration in the mobile phase, as Kuhr and Yeung [52] showed that the limit concentration detectable is a function of this parameter in indirect detection.

3.1. Influence of the fluorophore concentration on the detection system sensitivity

In order to optimize the detection system sensitivity, we studied the influence of fluorescein sodium salt concentration on the signal-to-noise ratio. The electrolyte pH was settled at pH 9.2, i.e., where the fluorophore intensity is maximum. We used potassium *n*-butylbenzene sulfonate as the test sample because it has an electrophoretic mobility similar to that of the fluorophore. Foret et al. [53] proved that in indirect detection, the sensitivity obtained for a sample ion is greater if its mobility is similar to the mobility of the ion used to provide the background signal. As reported in Table 1, a range of fluorophore concentrations of 10^{-8}–10^{-4} *M* was explored.

Table 1 shows that the maximum sensitivity is obtained with a 10^{-5} *M* fluorescein sodium salt concentration. Below this concentration, the background signal is not very stable and above it the difference between the initial background signal and the signal perturbed by the sample elution is no longer perceptible. Therefore, subsequent experiments were systematically performed using 10^{-5} *M* fluorescein sodium salt. Moreover, it is worth mentioning that increasing the photomultiplier gain resulted, as expected, in an enhancement of fluorescence but did not allow the signal-to-noise ratio to be improved.

We then still had to optimize the ionic strength of the electrophoretic medium and the injection parameters in order to attain the greatest sensitivity possible. As these two parameters are intimately related, because a concentration effect of the sample appears when low-conductivity samples are injected, consequently allowing

Table 1
Evolution of the signal-to-noise ratio as a function of the fluorescein sodium salt concentration

$[n-BuC_6H_4SO_3K]$ (mM)	Fluorescein sodium salt concentration (M)				
	10^{-8}	10^{-7}	10^{-6}	10^{-5}	10^{-4}
10	35	40	52	54	53
1	6	18	19	17	15
0.1	1.3	1.8	2	2.4	2.3

Electrolyte, 12.5 mM $Na_2B_4O_7$ (pH 9.2); temperature, 30°C; applied voltage, 30 kV; injection, hydrodynamic (injection time = 5 s).

larger injection volumes [54,55], we optimized these two parameters jointly. The two classical injection modes used in capillary electrophoresis, i.e., hydrodynamic and electrokinetic, were successively studied. The test sample was a mixture of lithium and potassium salts, both at 10^{-4} M concentration.

3.2. *Influence of the ionic strength of the electrolyte on the system sensitivity. Comparison of electrokinetic and hydrodynamic injection*

As demonstrated by Fig. 2, the signal-to-noise ratio is strongly dependent on the ionic strength of the electrolyte constituting the mobile phase in the case of hydrodynamic injection. Within the electrolyte concentration range explored (10–50 mM), the detection system sensitivity is maximum at a sodium borate concentration of 10 mM. Similar variations were observed in the electrokinetic injection mode but they were less important. Using this injection mode within the same concentration range, the sensitivity increased when the sodium tetraborate concentration decreased from 50 to 10 mM.

Therefore, we determined first the detection limit of lithium and potassium using an electrolyte with a sodium tetraborate concentration of 10 mM, using both the hydrodynamic and electrokinetic injection modes.

As the sample band injected has a very low conductivity, an important concentration effect is observed, allowing relatively large sample volumes to be injected, while keeping a constant system efficiency and consequently a constant separation quality [54,55].

At this concentration and with a 57 cm × 75 μm I.D. capillary, it was possible to use injection times up to 30 s, resulting in a pronounced improvement in the detection sensitivity. Beyond this limit, the signal-to-noise ratio remains nearly constant, while a drift of the baseline is observed before the system peak corresponding to the electroosmotic flow (water

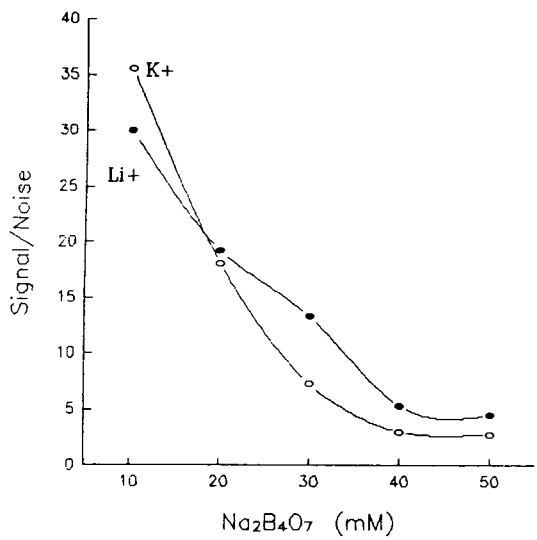

Fig. 2. Evolution of the signal-to-noise ratio, in the hydrodynamic injection mode, as a function of the ionic strength of the electrolyte in the mobile phase. Operating conditions: fused silica-capillary 57 cm × 75 μm I.D.; applied voltage, 10 kV; temperature, 30°C; sample, mixture of $LiNO_3$(10^{-4} M) and KNO_3 (10^{-4} M); electrolyte, $Na_2B_4O_7$ (pH 9.2); fluorescein concentration, 10^{-5} M; detection, fluorimetric ($\lambda_{exc.}$ = 488 nm, $\lambda_{detect.}$ = 520 nm).

peak), accompanied by peak broadening resulting in a noticeable loss of efficiency.

The detection thresholds obtained under these conditions for lithium and potassium are reported in Table 2. Further, as the sensitivity of the detection system seems to increase when the mobile phase electrolyte becomes more diluted, we also determined the detection thresholds of these two cations in the case of a mobile phase containing 2.5 m*M* sodium tetraborate at pH 9.2 (Table 2). The following comments can be made based on these results. (i) With a sodium salt being used to provide the background signal, laser-induced fluorimetric indirect detection appears far more sensitive in the case of lithium than with potassium. Whatever the electrolyte concentration in the mobile phase and the injection mode used, the detection threshold of potassium is 3–6 times greater than that of lithium. (ii) Whatever the cation (lithium or potassium) and the electrolyte concentration in the mobile phase, electrokinetic injection results in a greater sensitivity than hydrodynamic injection. This has already been reported by Weston et al. [46] using indirect UV detection. (iii) This detection system appears to be more sensitive if the electrolyte concentration in the mobile phase is lower. For instance, lithium and potassium cations at a 10^{-6} *M* concentration are not detected if a 10 m*M* sodium tetraborate electrolyte is used, but they are detected without difficulty at this concentration if an electrolyte containing 2.5 m*M* sodium tetraborate is used. As shown by Table 2, the sensitivity is improved tenfold if the sodium tetraborate concentration in the mobile phase is decreased from 10 to 2.5 m*M*. This last concentration is the lower limit of the electrolyte buffer effect.

The sensitivity thresholds obtained in indirect fluorimetric detection (39.5 and 3.6 ppb for potassium and 15 and 0.7 ppb for lithium in the hydrodynamic and electrokinetic injection modes, respectively) are comparable to the best detection limits reported in the literature for the same cations [50,51].

Considering these results, we then studied the potential offered by this new detection system for alkaline earth and transition metal cations.

3.3. Application to the analysis of mixtures of alkali, alkaline earth and transition metal cations

As the fluorophore used to provide the background signal, fluorescein, gives a noticeable fluorescence only in a basic medium, the determination of alkaline earth and transition metals appeared impossible in such a medium because these ions were adsorbed and/or precipitated on the negatively charged capillary wall at basic pH. Inhibition of adsorption could be achieved only by suppressing the cation charges or, better, by charging them negatively. Therefore, we considered the use of complexation. Such a strategy appeared necessary as Jandik et al. [43] has previously demonstrated that com-

Table 2
Detection thresholds obtained using laser-induced indirect fluorimetric detection, with fluorescein sodium salt as fluorophore

Cation	$[Na_2B_4O_7]$ (m*M*)	Detection limit (ppb)[a]	
		Hydrodynamic injection[b]	Electrokinetic injection[c]
K^+	10	390	44
	2.5	39.5	3.6
Li^+	10	119	8
	2.5	15	0.7

Fused-silica capillary, 57 cm × 75 μm I.D.; applied voltage, 10 kV; temperature, 30°C.
[a] Detection limit = 3 × signal-to-noise ratio.
[b] Injection pressure 0.5 p.s.i.; time 30 s.
[c] Injection voltage 10 kV; time 30 s.

plexation is required to separate some transition and alkaline earth metal cations, even in acidic medium, because their individual electrophoretic mobilities are insufficient to allow a satisfactory resolution. Different complexing agents have been used, HIBA in acetic medium and indirect UV detection [40,41,44,45] and 8-hydroxyquinolinesulfonic acid in basic medium and direct fluorimetric detection, the latter complexing agent giving fluorescent complexes with Ca(II), Mg(II) and Zn(II) [51]. As we are operating in a basic medium, and in the presence of a fluorophore providing a background signal, none of these approaches could be totally satisfactory. Consequently, we considered, developing a new complexing system compatible with the basic medium utilized and not leading to the formation of fluorescing complexes with metals. As the EDTA anion is known to give, in basic medium, octaedral complexes with a large number of cations, with the structure shown, and these complexes are more or less stable according to the nature of the cation (Table 3), we studied its potential for the determination by capillary electrophoresis of alkali, alkaline earth and transition metal cation mixtures.

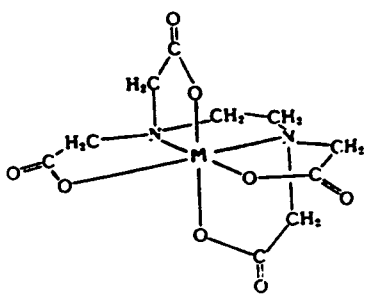

First we examined the influence of EDTA concentration on the electrophoretic behaviour of a test sample containing Ba^{2+}, Ca^{2+}, Mn^{2+} and Zn^{2+} cations at pH 9.2 and for a 10^{-5} *M* concentration of fluorescein sodium salt. As the pH changes as a function of EDTA concentration it was adjusted to 9.2 by addition of sodium hydroxide. The evolution of the effective electrophoretic mobilities of the different cations studied as a function of EDTA concentration is reported in Fig. 3.

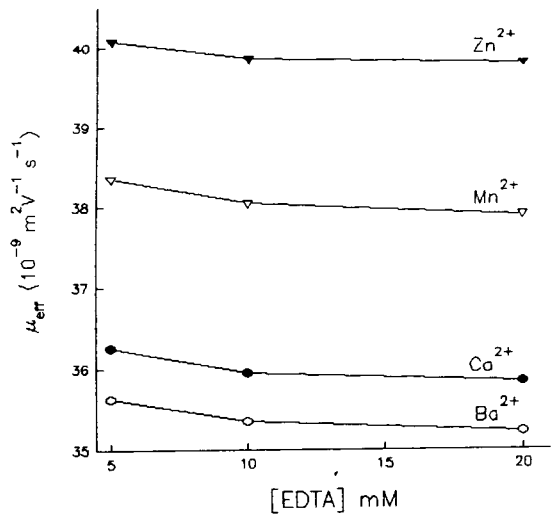

Fig. 3. Evolution of the electrophoretic behaviour of some alkaline earth and transition metal cations as a function of EDTA concentration. Operating conditions: fused-silica capillary, 57 cm × 75 μm I.D.; applied voltage, 30 kV; temperature, 30°C; electrolyte, EDTA of variable concentration, pH adjusted to 9.2 by addition of sodium hydroxide; fluorescein concentration, 10^{-5} *M*; injection, hydrodynamic (injection time = 2 s); detection, fluorimetric ($\lambda_{exc.}$ = 488 nm, $\lambda_{detect.}$ = 520 nm).

It is clear that the electrophoretic system selectivity does not change as a function of EDTA concentration for the cations studied, in spite of the fact that their electrophoretic mobilities increase as a function of the latter. Under these conditions, as the previous study of the signal-to-noise ratio as a function of the electrolyte ionic strength had shown that the sensitivity is enhanced at weak ionic strengths, we choose a 5 m*M* concentration of EDTA to complete this study.

Moreover, EDTA presents several acidities. The three weaker acidities are characterized, in pure water and at 0.1 *M* ionic strength, by pK_a values of 2.75, 6.25 and 10.38 [56]. Therefore, a study of the electrophoretic behaviour of transition and alkaline earth metal cations as a function of pH appeared necessary. We report this evolution in Fig. 4 for the above-mentioned cations.

As can be seen in Fig. 4a, there is no noticeable change in the selectivity as a function of pH.

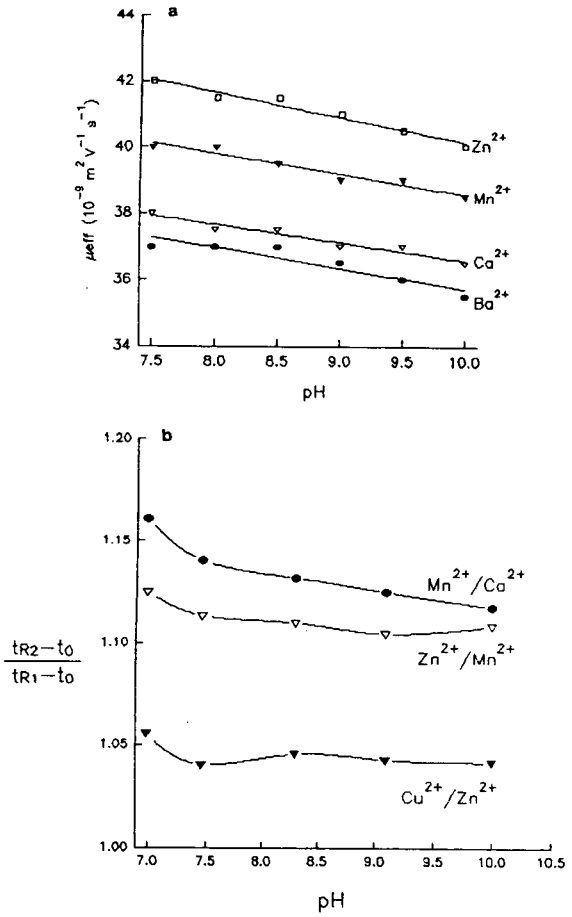

Fig. 4. Evolution of the electrophoretic behaviour of some alkaline earth and transition metal cations as a function of pH of the electrolyte: (a) electrophoretic mobilities; (b) ratio of corrected migration times $(t_{R2}-t_0)/(t_{R1}-t_0)$. Operating conditions: identical with those in Fig. 3, with the exception of the electrolyte, 5 m*M* EDTA, adjusted to a convenient pH by addition of sodium hydroxide.

As the electroosmotic flow velocity is strongly related to pH in the range 7–9, it also seemed worth, considering the above-mentioned results relative to selectivity, to study the evolution of the ratio of the corrected migration times of the different analyte species (Fig. 4b). Under these conditions, the differences in the electrophoretic behaviour should have been enhanced when the mobile phase pH decreased. This is effectively what we observed, although the phenomenon became noticeable only below pH 7.5 (Fig. 4b). Moreover, the electrophoretic system efficiency is hardly dependent of pH variations in the range 7–9. For instance, for Mn^{2+}, the efficiency varies from 223 000 theoretical plates at pH 9.0 to 206 000 theoretical plates at pH 7.0. Therefore, the resolving power of the electrophoretic system is obviously greater at pH 7.0 than at pH 9.2, this better resolution being obtained to the detriment of the analysis time.

As we also intended to obtain the greatest possible detection sensitivity, a compromise had to be found for the value of pH because the intensity of induced fluorescence is strongly dependent on pH below pH 9 in the case of fluorescein. Facing this dilemma, the choice of an electrolyte containing 5 m*M* EDTA adjusted to pH 7.5 by addition of sodium hydroxide appeared to be an acceptable compromise between the resolution and the sensitivity of the electrophoretic system. At such a pH value, the resolving power is already fairly good and the system sensitivity is not too lowered. We report in Fig. 5 the analysis of a mixture of alkali, alkaline earth and transition metals performed under these conditions.

This separation shows that two system peaks appear in the electropherogram. The first, corresponding to water, allows the determination of the electroosmotic flow velocity under the operating conditions, while the second is attributed to one of the various ionic forms of EDTA existing at this pH. These two electrophoretic peaks, due to the displacement of fluorophore molecules, appear logically as negative signals. Their attribution was confirmed, without any doubt, by injecting, under the same operating conditions, pure water on the one hand and EDTA on the other. Further, the migration time of the electroosmotic flow having been determined, it appears that the analyte cations are not all complexed by EDTA. Lithium and potassium cations, which elute before the electroosmotic flow, still possess a positive charge under these operating conditions. This is not surprising, as can be seen from the literature data concerning the complexation of cations by EDTA [56] reported in Table 3.

These two cations having charges opposite to

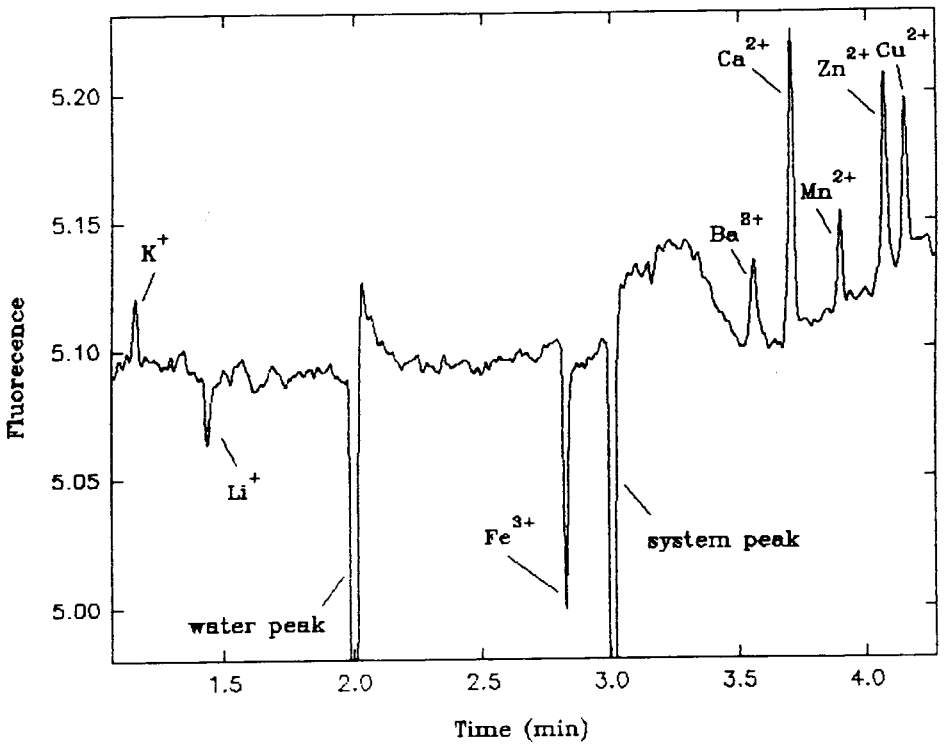

Fig. 5. Separation of alkali, alkaline earth and transition metal cations by CZE under the optimum conditions. Operating conditions: fused silica capillary, 57 cm × 75 μm I.D.; applied voltage, 30 kV; temperature, 30°C; electrolyte, 5 m*M* EDTA, adjusted to pH 7.5 by addition of sodium hydroxide; fluorescein concentration, 10^{-5} *M*; injection, hydrodynamic (injection time = 2 s); detection, fluorimetric ($\lambda_{exc.}$ = 488 nm, $\lambda_{detect.}$ = 520 nm).

Table 3
Complexation constants with EDTA in aqueous solution at 25°C [56] and equivalent ionic conductivity [57] of some alkali, alkaline earth and transition metal cations

Cation	Log *K*	Λ_0 (10^{-4} m^2 S mol^{-1})
Li^+	2.8	38.66
Ba^{2+}	7.8	63.6
Sn^{2+}	8.6	–
Mg^{2+}	8.7	53.0
Ca^{2+}	10.7	59.47
Mn^{2+}	14.0	53.5
Co^{2+}	16.3	55
Cd^{2+}	16.5	54
Zn^{2+}	16.5	–
Ni^{2+}	18.6	50
Cu^{2+}	18.8	53.6
Fe^{3+}	25.1	–
K^+	–	73.48
Na^+	1.7	50.08

the fluorophore charge, as fluorescein is negatively charged at pH 7.5, according to Kuhr and Yeung [52] an enhancement of fluorescence due to electrostatic attraction should be observed, resulting in positive peaks. This is in fact observed with the potassium cation. In contrast, lithium is visualized as a negative peak. This seemingly anomalous response results from the differences in the solvation of these cations, which are evidenced by their different equivalent ionic conductances Λ [57] and by their different electrophoretic mobilities, which are directly proportional to their equivalent ionic conductances [42].

The apparently opposite fluorescence behaviours of Li^+ and K^+ cations can be rationalized if the importance of the perturbation of the background fluorescence due to the electrolyte during the elution of a sample (here a cation) possessing

a charge opposite to the fluorophore charge, here the sodium salt of fluorescein, is evaluated. This perturbation of fluorescence can be calculated with the help of the treatment developed by Ackermans et al. [58] in the case of the indirect UV detection of a sample possessing the same charge as the chromophoric ion. In the present case, the intensity of fluorescence of a binary electrolyte AB, in the absence of any sample ion, is given by the equation

$$I_F^E = I_0(\phi_A\varepsilon_A + \phi_B\varepsilon_B)lc_A^E$$

where ε_A and ε_B are the molecular absorptivities of the electrolyte ions, ϕ_A and ϕ_B are the fluorescence efficiencies of the electrolyte ions, c_A^E and c_B^E are the electrolyte ion concentrations, with $c_A^E = c_B^E$, l is the optical path length and I_0 is the incident light intensity. In the presence of a sample ion, the fluorescence intensity becomes

$$I_F^S = I_0(\phi_X\varepsilon_X + \phi_B\varepsilon_B)lc_X^S + I_0(\phi_A\varepsilon_A + \phi_B\varepsilon_B)lc_A^S$$

where ε_X, ε_B and ϕ_X, ϕ_B are the molecular absorptivities and the fluorescence efficiencies of the sample ion and the counter ion, respectively, c_X^S is the sample ion concentration in the mobile phase and c_A^S and c_B^S are the concentrations of the ions constituting the electrolyte in the presence of the sample ion, with $c_A^S = c_B^S$.

The perturbation of the background fluorescence intensity in the presence of a sample is

$$\Delta I_F = I_F^S - I_F^E$$

or

$$\Delta I_F = I_0(\phi_X\varepsilon_X + \phi_B\varepsilon_B)lc_X^S + I_0(\phi_A\varepsilon_A + \phi_B\varepsilon_B)lc_A^S - I_0(\phi_A\varepsilon_A + \phi_B\varepsilon_B)lc_A^E$$

If the ion A is the fluorophore ($\phi_A \neq 0$) and if the other ions present in the mobile phase are not fluorescent (sample ion X and counter ions B), i.e., $\phi_X = \phi_B = 0$, the relationship giving the fluorescence intensity perturbation becomes:

$$\Delta I_F = I_0\phi_A\varepsilon_A lc_A^S - I_0\phi_A\varepsilon_A lc_A^E \quad (1)$$

Under these conditions, the Kohlrausch regulation equation [59] is, in agreement with Dismukes and Alberty [60],

$$\frac{c_A^E}{m_A^0} + \frac{c_B^E}{m_B^0} = \frac{c_A^S}{m_A^0} + \frac{c_B^S}{m_B^0} + \frac{c_X^S}{m_X^0} \quad (2)$$

where m_A^0, m_B^0, and m_X^0 are the absolute mobilities of the ions A and B in the electrolyte and of the sample ion X, respectively.

In the case of a fluorophoric ion A charged oppositely to the X sample ion, taking in account the electroneutrality equations, on the one hand in the electrolyte $c_A^E = c_B^E$ and on the other in the electrolyte containing the sample ion X $c_A^S = c_X^S + c_B^S$, the Kohlrausch regulation, Eq. 2, becomes

$$\frac{c_A^E}{m_A^0} + \frac{c_A^E}{m_B^0} = \frac{c_A^S}{m_A^0} + \frac{c_A^S - c_X^S}{m_B^0} + \frac{c_X^S}{m_X^0}$$

$$c_A^E = c_A^S + \frac{m_A^0(m_B^0 - m_X^0)}{m_X^0(m_B^0 + m_A^0)} \cdot c_X^S \quad (3)$$

or

$$c_A^E = c_A^S + \lambda_X c_X^S$$

with

$$\lambda_X = \frac{m_A^0(m_B^0 - m_X^0)}{m_X^0(m_B^0 + m_A^0)}$$

Taking in account Eq. 3, the perturbation of the fluorescence intensity in the presence of a sample ion becomes

$$\Delta I_F = -I_0\phi_A\varepsilon_A l\lambda_X c_X^S \quad (4)$$

Consequently, the presence of a sample X possessing a charge opposite to the charge of the fluorophore A used to generate the background signal results in a decrease in the fluorescence intensity, giving a negative peak, if $\lambda_X > 0$ ($m_B^0 > m_X^0$), i.e., if the absolute mobility of the analyte sample is smaller than the mobility of the ion associated with the fluorophore. This is the case with the Li^+ cation which has an absolute mobility smaller than that of Na^+ (see Table 3), which is the counter ion of the fluorophore (sodium salt of fluorescein). In addition, it results in the enhancement of the fluorescence, giving a positive peak, if $\lambda_X < 0$ ($m_B^0 < m_X^0$), i.e., if the absolute mobility of the analyte ion is greater

than that of the counter ion associated with the fluorophore. This is the case with the K^+ cation, which has an absolute mobility greater than that of Na^+ (see Table 3) associated with the fluorophore. Finally, it results in the total disappearance of the signal if the absolute mobility of the analyzed ion is exactly the same as the absolute mobility of the ion associated with the fluorophore.

The situation is far more complex in the case of the cations effectively complexed by EDTA. The metallic ions (M) complexing the EDTA base (B) increase the apparent strength of the EDTA conjugate (HB) of this base, owing to the displacement of the dissociation equilibrium [61,62]

$$i\mathrm{H_2O} + i\mathrm{HB} \rightleftharpoons i\mathrm{B} + i\mathrm{H_3O^+}$$
$$i\mathrm{B} + \mathrm{M} \rightleftharpoons \mathrm{MB}_i$$
$$i\mathrm{H_2O} + i\mathrm{HB} + \mathrm{M} \rightleftharpoons \mathrm{MB}_i + i\mathrm{H_3O^+}$$

Consequently, if lithium and potassium cations, which give poorly stable complexes with the EDTA anion, have little influence on the EDTA acidity and therefore on pK_a values, it is different in the case of metallic cations giving stable complexes with EDTA anion. Important displacements of the dissociation equilibrium of EDTA have been reported [61,62] in the case of these cations, resulting in a considerably decreased value of the final acidity constant pK_a. In such conditions, the apparent electrophoretic mobility of the analyte cations is the result of the electrophoretic mobilities of both the non-complexed cation (μ_{cat}) and its EDTA complex (μ_{compl}):

$$\mu_{app} = (1 - x)\mu_{cat} + x\mu_{compl}$$

where x is the molar fraction of the cations complexed by EDTA.

Obviously, the molar fraction is directly dependent on the complexation constant. The experimental electrophoretic mobilities must be directly related to the complexation constants of the different ions. This is effectively observed in the case of divalent cations, as evidenced by the comparison of the elution order and complexation constants reported in Table 3.

In the same way, the electrophoretic behaviour of the only trivalent cation analyzed, Fe^{3+}, can be explained by the formation of a very stable complex with EDTA (Table 3), conferring a total charge of about one electron to this cation and resulting in an experimental electrophoretic mobility smaller than the values obtained with divalent cations. Thus the analyte species, i.e., the complex Fe^{3+}–EDTA presenting a negative charge, is visualized, in agreement with Kuhr and Yeung [52], as a negative peak, due to the electrostatic repulsion with the negatively charged fluorophore at this pH.

As with the alkali metal cations K^+ and Li^+, the decrease of the fluorescence intensity during the elution of the Fe^{3+} cation, i.e., during the elution of the negatively charged Fe^{3+}–EDTA complex, can be rationalized by using a treatment directly transposed from that developed by Ackermans et al. [58]. The fluorescence perturbation is the given by the following relationship:

$$\Delta I_F = -I_0 \phi_A \varepsilon_A l \lambda'_X c^S_X \quad (5)$$

with

$$\lambda'_X = \frac{m^0_A(m^0_B + m^0_X)}{m^0_X(m^0_B + m^0_A)}$$

This equation shows that in the case of a sample ion X with the same charge as the fluorophore ion A, which is the case with the Fe^{3+}–EDTA complex in the presence of fluorescein sodium salt, its elution will result in a negative peak owing to a systematic decrease in fluorescence, whatever the value of its absolute mobility, because λ'_X is systematically positive.

In the case of divalent cations, which are partially complexed by EDTA anion, their visualization can be explained by a mixed mechanism, represented by the Eqs. 4 and 5. As their absolute mobility is systematically greater than the mobility of the sodium cation associated with the fluorophore, they give (in agreement with Eq. 4) an increase in the fluorescence in their non-complexed form. In contrast, their complexation by EDTA results in a decrease in the fluorescence intensity (Eq. 5). Consequently, the intensity of the peaks must decrease as a func-

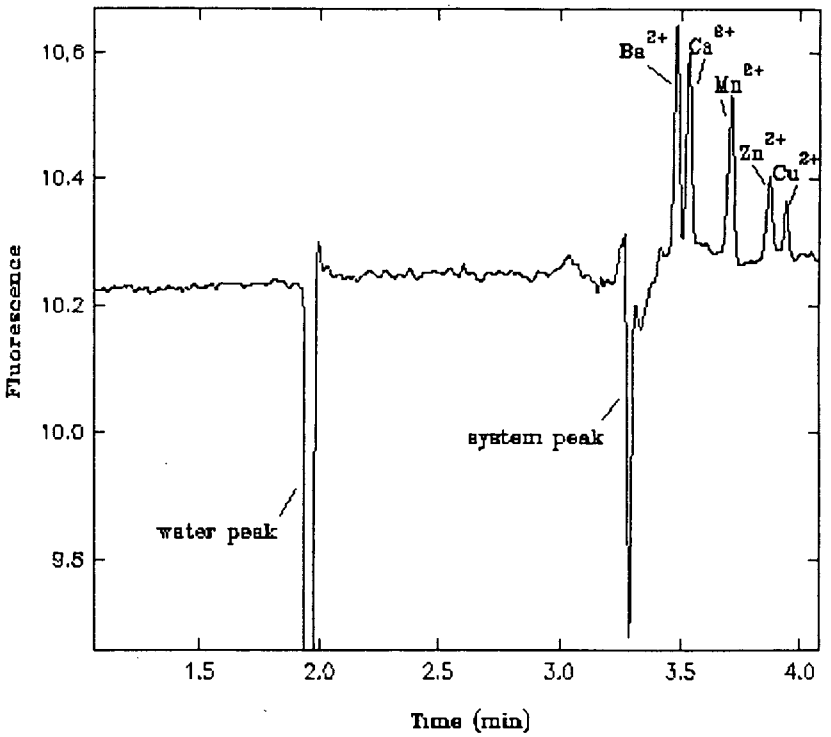

Fig. 6. Separation by CZE of five alkaline earth and transition metals cations injected in equal amounts using hydrodynamic injection (injection time = 2 s). Concentration of each cation, 10^{-4} *M*. Operating conditions as in Fig. 5.

tion of the importance of the complexation of divalent cations by EDTA. This is effectively observed in Fig. 6, and the results are those expected from divalent cation–EDTA–fluorescein mixed complexes [56,63].

Finally, other divalent alkaline earth and transition metal cations can be separated using this electrophoretic system (Table 4). Unfortunately, the selectivity and the efficiency of the electrophoretic system utilized are not sufficient to allow their separation in the presence of the five divalent cations previously determined. Because of their too similar effective electrophoretic mobilities (Table 4), Ni^{2+} co-elutes with Zn^{2+},

Table 4
Effective electrophoretic mobilities of alkali, alkaline earth and transition metal cations determined in the presence of 5 m*M* EDTA at pH 7.5

Cation	μ_{eff} (10^{-9} m^2 V^{-1} s^{-1})	Cation	μ_{eff} (10^{-9} m^2 V^{-1} s^{-1})
Ba^{2+}	37	Co^{2+}	41
Ca^{2+}	38	Zn^{2+}	42
Mg^{2+}	40	Ni^{2+}	42
Mn^{2+}	40	Cu^{2+}	42.5
Cd^{2+}	40		

and similarly Mg^{2+} and Cd^{2+} co-elute with Mn^{2+}.

We completed this study by the determination of detection thresholds in the presence of EDTA. The detection limits of the various alkaline earth and transition metals cations are reported in Table 5.

The comparison of the detection thresholds, in the hydrodynamic injection mode, in the present case (i.e., in the presence of EDTA and at pH 7.5), for the lithium and potassium cations, with those obtained previously with the same fluorophore, fluorescein sodium salt, for the same cations without EDTA and at pH 9.2 (Table 2) indicates a noticeable loss of sensitivity. The system developed in the presence of EDTA (required for the determination in a basic medium of alkaline earth metal cations) is overall ten times less sensitive. This sensitivity loss is probably due to the pH of the electrolyte used, which is near neutral. Such operating conditions necessarily result in a decrease in the fluorescence emitted by the fluorescein utilized to provide the background signal. Under these conditions, the sensitivity limits obtained with lithium and potassium cations are only similar to those reached in indirect UV detection with a comparable optical path.

The detection limits of the alkaline earth cations and of the transition metals appear to be very satisfactory. In fact, the proposed electrophoretic system, which combines the fluorescein sodium salt (as fluorophore) and EDTA (as complexing agent), leads to slightly improved sensitivities compared with those obtained previously for this type of cation, the detection limits obtained varying between tens and hundreds of ppb.

4. Conclusions

From this study, it appears that the use of the fluorescein sodium salt at pH 9 leads to a well adapted electrophoretic system for the detection and determination of lithium and potassium cations. In fact, very high sensitivities can be obtained for these two cations (in the ppb range) if the injection is performed in the electrokinetic mode. With hydrodynamic injection, which is better adapted in a quantification context, the detection limits, even if slightly higher, appear to be acceptable, in the tens of ppb range. Concerning the determination of alkaline earth and transition metal cations, as the separation could not be performed with the fluorescein sodium salt alone, a noticeable decrease in the detection sensitivity was observed for the Li^+ and K^+ cations because of the electrolytic system used (fluorescein sodium salt–EDTA, pH 7.5). Nevertheless, this electrolyte, which combines fluorescein and EDTA, appears to be of great interest for the determination of alkaline earth and transition metal cations as it leads to low detection limits for these ions. Taking into account the satisfactory results obtained in this study, we shall study in the near future the potential of this electrophoretic system for the determination of organic and inorganic anions and also organic cations.

Table 5
Detection limits obtained in laser-induced indirect fluorimetric detection using hydrodynamic injection and the fluorescein sodium salt as fluorophore in the presence of EDTA

Cation	Detection limit[a] (ppb)	Cation	Detection limit[a] (ppb)
Li^+	74	Mn^{2+}	28
K^+	300	Zn^{2+}	22
Ba^{2+}	80	Cu^{2+}	18
Ca^{2+}	20	Fe^{3+}	100

Fused-silica capillary, 57 cm × 75 μm I.D.; applied voltage, 30 kV; temperature, 30°C.
[a] Detection limit = 3 × signal-to-noise ratio.

References

[1] S.F.Y. Li, *Capillary Electrophoresis —Principles, Practice and Applications*, Elsevier, Amsterdam, 1992.
[2] J. Crommen, B. Fransson and G. Sibill, *J. Chromatogr.*, 142 (1977) 283.
[3] J. Crommen and P. Herné, *J. Pharm. Biomed. Anal.*, 2 (1984) 241.
[4] P. Herné, M. Renson and J. Crommen, *Chromatographia*, 19 (1984) 274.
[5] A. Laurent and R. Bourdon, *Ann. Pharm.*, 36 (1978) 453.
[6] N. Parris, *Ann. Biochem.*, 100 (1979) 260.
[7] G. Schill and E. Arvidsson, *J. Chromatogr.*, 492 (1989) 299.
[8] M. Denkert, L. Hackzell, G. Schill and E. Sjogren, *J. Chromatogr.*, 218 (1981) 31.
[9] L. Hackzell, T. Rydberg and G. Schill, *J. Chromatogr.*, 282 (1983) 179.
[10] W.E. Barber and P.W. Carr, *J. Chromatogr.*, 260 (1983) 89; 301 (1984) 25; 316 (1984) 211.
[11] B.A. Bidlingmeyer, *J. Chromatogr.*, 186 (1979) 419.
[12] B.A. Bidlingmeyer and F.V. Warren, *Anal. Chem.*, 54 (1982) 1282.
[13] T. Granasambandan and H. Freiser, *Anal. Chem.*, 54 (1982) 1282; 54 (1982) 2379.
[14] J.E. Parkin, *J. Chromatogr.*, 287 (1984) 457; 303 (1984) 436.
[15] J.E. Parkin and H.T. Lau, *J. Chromatogr.*, 314 (1984) 488.
[16] T. Takeuchi and D. Ishii, *J. Chromatogr.*, 403 (1987) 324.
[17] T. Takeuchi, K. Murase and D. Ishii, *J. Chromatogr.*, 445 (1988) 139.
[18] S. Banerjee, *Anal. Chem.*, 57 (1985) 2590.
[19] S. Banerjee and M.A. Castogivanni, *J. Chromatogr.*, 396 (1987) 169.
[20] S. Banerjee and J.R. Steimers, *Anal. Chem.*, 57 (1985) 1476.
[21] W.D. Pfeffer, T. Takeuchi and E.S. Yeung, *Chromatographia*, 24 (1987) 123.
[22] T. Takeuchi and E.S. Yeung, *J. Chromatogr.*, 366 (1986) 145; 370 (1986) 83.
[23] J. Ye, R.P. Baldwin and K. Ravichandran, *Anal. Chem.*, 58 (1986) 240.
[24] D.R. Bobbitt and E.S. Yeung, *Anal. Chem.*, 56 (1984) 1577; 57 (1985) 271.
[25] S. Maketon, E.S. Otterson and J.G. Tarter, *J. Chromatogr.*, 368 (1986) 395.
[26] S. Grocott, I. Jefferies, T. Bowser, J. Carnevale and P. Jackson, *J. Chromatogr.*, 602 (1992) 257.
[27] J. Romano, P. Jandik, W. Jones and P. Jackson, *J. Chromatogr.*, 546 (1991) 411.
[28] W. Jones and P. Jandik, *J. Chromatogr.*, 546 (1991) 445.
[29] B. Wildman, P. Jackson, W. Jones and P. Alden, *J. Chromatogr.*, 546 (1991) 459.
[30] K. Hargadon and B. McCord, *J. Chromatogr.*, 602 (1992) 241.
[31] W. Buchberger and P. Haddad, *J. Chromatogr.*, 608 (1992) 59.
[32] D. Salomon and J. Romano, *J. Chromatogr.*, 602 (1992) 219.
[33] G. Bondoux, P. Jandik and W. Jones, *J. Chromatogr.*, 602 (1992) 79.
[34] J. Nair and C. Izzo, *J. Chromatogr.*, 640 (1993) 445.
[35] M. Harrold, M. Wojtusik, J. Riviello and P. Henson, *J. Chromatogr.*, 640 (1993) 463.
[36] B. Kenney, *J. Chromatogr.*, 546 (1991) 423.
[37] X. Huang, T. Pang, M. Gordon and R. Zare, *Anal. Chem.*, 59 (1987) 2747.
[38] M. Aguilar, X. Huang and R. Zare, *J. Chromatogr.*, 480 (1989) 427.
[39] M. Aguilar, A. Farran and M. Martinez, *J. Chromatogr.*, 635 (1993) 127.
[40] F. Foret, S. Fanali, A. Nardi and P. Bocek, *Electrophoresis*, 11 (1990) 780.
[41] M. Chen and R. Cassidy, *J. Chromatogr.*, 602 (1992) 227.
[42] A. Weston, P. Brown, P. Jandik, W. Jones and A. Heckenberg, *J. Chromatogr.*, 593 (1992) 289.
[43] P. Jandik, W. Jones, A. Weston and P. Brown, *LC · GC*, 9 (1991) 634.
[44] A. Weston, P. Brown, A. Heckenberg, P. Jandik and W. Jones, *J. Chromatogr.*, 602 (1992) 249.
[45] M. Koberda, M. Konkowski, P. Younberg, W. Jones and A. Weston, *J. Chromatogr.*, 602 (1992) 235.
[46] A. Weston, P. Brown, P. Jandik, A.L. Heckenberg and W. Jones, *J. Chromatogr.*, 608 (1992) 395.
[47] W. Beck and H. Engelhardt, *Chromatographia*, 33 (1992) 313.
[48] J. Riviello and M. Harrold, *J. Chromatogr.*, 652 (1993) 385.
[49] L. Gross and E.S. Yeung, *Anal. Chem.*, 62 (1990) 427.
[50] K. Bächmann, J. Boden and I. Haumann, *J. Chromatogr.*, 626 (1992) 259.
[51] D. Swaile and M. Sepaniak, *Anal. Chem.*, 63 (1991) 179.
[52] W. Kuhr and E. Yeung, *Anal. Chem.*, 60 (1988) 2642.
[53] F. Foret, S. Fanali, L. Ossicini and P. Bocek, *J. Chromatogr.*, 470 (1989) 299.
[54] A. Vinther and H. Soeberg, *J. Chromatogr.*, 559 (1991) 3 and 27.
[55] D. Burgi and R. Chien, *Anal. Chem.*, 63 (1991) 2042.
[56] A. Ringbon, *Les Complexes en Chimie Analytique*, Dunod, Paris, 1967.
[57] J. Dean (Editor), *Lange's Handbook of Chemistry*, McGraw-Hill, New York, 13th ed., 1985, pp. 5–28.
[58] M.T. Ackermans, F.M. Everaerts and J.L. Beckers, *J. Chromatogr.*, 549 (1991) 345.
[59] F. Kohlrausch, *Ann. Phys. Chem.*, 62 (1897) 209.
[60] E.B. Dismukes and R.A. Alberty, *J. Am. Chem. Soc.*, 76 (1954) 191.
[61] R. Pribil, *Applied Complexometry*, Pergamon Press, Oxford, 1982.
[62] R. Pribil, *Analytical Applications of EDTA and Related Compounds*, Pergamon Press, Oxford, 1972.
[63] E.B. Sandell and H. Onishi, *Photometric Determination of Traces of Metals*, Wiley, New York, 1978.

ELSEVIER

Journal of Chromatography A, 689 (1995) 149–156

JOURNAL OF CHROMATOGRAPHY A

Isotachophoretic separation of rare earth ions I. Separation behaviour of yttrium and fourteen lanthanide ions forming complexes with tartaric acid and α-hydroxyisobutyric acid

Takeshi Hirokawa*, Wen Xia, Yoshiyuki Kiso[1]

Applied Physics and Chemistry, Faculty of Engineering, Hiroshima University, Kagamiyama 1, Higashi-hiroshima 724, Japan

First received 18 July 1994; revised manuscript received 2 September 1994

Abstract

A leading electrolyte for the isotachophoretic separation of yttrium ion from lanthanide ions was developed, consisting of 20 m*M* ammonia solution containing 0.5 m*M* tartaric acid and 8 m*M* α-hydroxyisobutyric acid (HIB) as complex-forming agents. The pH of the solution was adjusted to 4.8 by adding acetic acid. Using the electrolyte system developed, the separation behaviour of fifteen rare earth ions was studied in comparison with a simple HIB system. It was revealed that the addition of tartaric acid lowered the separability of adjacent pairs of medium and heavy lanthanide ions to two-thirds of that of HIB system, instead of the successful separation of Dy and Y. The electrolyte system developed was applied to the separation of a rare earth ore sample containing Y as one of the major components.

1. Introduction

The fourteen lanthanide cations can be separated by isotachophoresis (ITP) by using a leading electrolyte containing a complexing agent, α-hydroxyisobutyric acid (HIB) [1,2]. A typical leading electrolyte is 20 m*M* ammonia solution containing 10 m*M* HIB buffered to pH 4.8 by adding acetic acid, which is used in combination with a suitable terminating electrolyte, e.g., 10 m*M* carnitine hydrochloride solution. By using the above operational electrolyte system, referred to hereafter as the HIB system, the lanthanide cations can be separated in order of increasing atomic number. The separability between the adjacent pairs of lanthanide ions is not constant but varies periodically, forming four different subgroups (tetrad effect [3]) from 27 nmol/C (Eu–Gd pair) to 309 nmol C^{-1} (Gd–Tb pair) [4].

The HIB system can be successfully applied to the analysis of rare earth ores such as monazite, of which light lanthanides are the major component [5]. However, when the HIB system was applied to different rare earth ores containing significant amounts of Y^{3+}, a problem arose in that Y^{3+} and Dy^{3+} could not be separated to form a mixed zone and accurate analysis was

* Corresponding author.

[1] Present address: Hijiyama Women's College, Ushita-shin-machi, Hiroshima 732, Japan.

0021-9673/95/$09.50
SSDI 0021-9673(94)00872-8

impossible. As rare earth ores such as ion-adsorption-type ore and Xenotime ore contain Y^{3+} and Dy^{3+} with considerable abundances, another operational electrolyte system is necessary to permit the isotachophoretic separation of these two elements. The low separability of Y^{3+} and Dy^{3+} is due to the similarity of the absolute mobilities and stability constants of their HIB complexes [6]. Effective separation of these cations is therefore impossible when HIB alone is used as a complexing agent.

Recently, we have studied the isotachophoretic separation behaviour of twenty kinds of metal ions, including La^{3+}, Ce^{3+}, Gd^{3+}, Lu^{3+} and Y^{3+}, using leading electrolytes containing tartaric acid as the complex-forming agent [7]. The separation behaviour of the four lanthanide ions and Y^{3+} in the above electrolyte system was different from that of the HIB system. That is, the decreases in the effective mobilities of Gd^{3+} and Lu^{3+} with respect to tartaric acid concentration were very similar to each other, but the decrease was different from that of Y^{3+}. This suggested the possible separation of Y^{3+} from lanthanide ions by adding tartaric acid to the HIB system as another complex-forming agent.

The aim of this study was to develop an operational electrolyte system suitable for the separation of Y^{3+} from lanthanide ions and to demonstrate the utility of the electrolyte system in the analysis of a real rare earth ore containing both types of ions.

2. Experimental

2.1. Samples

An equimolar mixture containing Tb^{3+}, Dy^{3+} and Y^{3+} (1.67 m*M*) was used to optimize the tartaric acid concentration in the leading electrolyte. Another equimolar mixture of fifteen rare earth ions (Y^{3+} and the fourteen lanthanide ions: La^{3+}, Ce^{3+}, Pr^{3+}, Nd^{3+}, Sm^{3+}, Eu^{3+}, Gd^{3+}, Tb^{3+}, Dy^{3+}, Ho^{3+}, Er^{3+}, Tm^{3+}, Yb^{3+} and Lu^{3+}) was used to assess the separability of the electrolyte system developed. The concentration of each component was 0.33 m*M*. These test mixtures were prepared from stock solutions of the chlorides (5 m*M*), which were prepared by dissolving the compounds in purified water.

A 2 g l^{-1} solution of an ion-adsorption-type rare earth ore was prepared as follows: 0.5 g of the ore powder was dissolved in a PFTE vessel by adding 5 ml of concentrated hydrochloric acid, then evaporated to dryness by using a 500 W lamp to remove excess hydrochloric acid. Subsequently, 5 ml of water were added and the mixture was evaporated to dryness again. Finally, the chloride residue was dissolved in deionized water to 250 ml. The pH of the sample solution prepared was 2.6.

2.2. Operational electrolyte system

The operational electrolyte systems used are summarized in Table 1. The leading electrolytes containing different concentration of tartaric acid and HIB were prepared by mixing two leading electrolytes: 20 m*M* ammonia solution containing 10 m*M* HIB and 20 m*M* ammonia solution containing 2.5 m*M* tartaric acid. The pH of both solutions was adjusted to 4.80 by adding acetic acid. The terminating electrolyte was a 10 m*M* solution of carnitine hydrochloride. All the electrolytes contained 0.1 mass-% hydroxypropylcellulose (HPC) to suppress electroendosmosis. The electrolyte systems containing both HIB and tartaric acid as complexing agents are referred as the HIB–Tar system. A Horiba (Tokyo, Japan) Model F7-AD expanded pH meter was used for pH measurements.

2.3. Chemicals

The rare earth chlorides were of guaranteed grade (GR) from Katayama Chemical (Osaka, Japan). Powdered ion-adsorption-type rare earth ore (a mixture of rare earth oxides) was obtained from Nippon Kogyo (Tokyo, Japan). Hydrochloric acid was of ultrapure grade from Merck (Darmstadt, Germany). The complexing agents α-hydroxyisobutyric acid (GR) and tartaric acids (GR) and HPC (extra pure) were obtained from Tokyo Kasei (Tokyo, Japan). The viscosity of a

Table 1
Operational electrolyte system for isotachophoresis

Leading electrolyte	20 m*M* NH_3 solution
Complexing agent	(1) 10 m*M* α-hydroxyisobutyric acid (HIB)
	(2) 8.4 m*M* HIB, 0.4 m*M* tartaric acid
	(3) 8.0 m*M* HIB, 0.5 m*M* tartaric acid
	(4) 7.6 m*M* HIB, 0.6 m*M* tartaric acid
	(5) 7.2 m*M* HIB, 0.7 m*M* tartaric acid
	(6) 5.0 m*M* HIB, 1.25 m*M* tartaric acid
pH buffer	Acetic acid
pH	4.80
Additive	0.1 mass-% hydroxypropylcellulose
Terminating electrolyte	10 m*M* carnitine hydrochloride
Additive	0.1 mass-% hydroxypropylcellulose

2% (w/w) HPC aqueous solution was 1000–4000 cP at 20°C according to the specification.

2.4. Isotachophoretic apparatus and R_E measurement

The detector for ITP was a high-frequency contactless conductivity detector (HFCCD) [8], which was used in combination with the separation unit of a Labeco (Sp. Nova Ves, Slovakia) ZKI-001 isotachophoretic analyser. The separation column used consisted of a preseparation capillary (10 cm × 0.5 mm I.D. or 20 cm × 0.5 mm I.D.) and a main capillary (20 cm × 0.25 mm I.D.). The migration current in the preseparation stage was 125 μA and it was decreased to 50 μA while detecting zones. When the short preseparation tube was used, the amount of electric charge applied until the detection of the terminating zone was 0.27 C in the blank run, and 0.37 C for the long run. The high-voltage power supply was that for a Shimadzu (Kyoto, Japan) IP-2A system. Measurements were carried out at 25°C in a temperature-controlled room.

The qualitative index used was R_E, defined as the ratio of the potential gradient [$E(\mathrm{Vcm}^{-1})$] of the sample zones (E_S) to that of the leading zone (E_L) [9]. When a conductivity detector is used, it is equal to the ratio of specific resistance (ρ) of each zone. As the output signal of the HFCCD showed a non-linear response to the specific resistance of the zones [8], the signal obtained was converted into the specific resistance using a fourth-order polynomial expression of the output voltage. The expression was obtained using KCl solutions with known specific resistance. Na^+ and Li^+ were used as the internal standard to correct slight drift of the HFCCD signals. The simulated R_E values were 1.495 and 1.963, respectively.

3. Results and discussion

3.1. Separation of Y^{3+} from lanthanide ions

To optimize the tartaric acid concentration in the leading zone for the separation of Y^{3+} from lanthanide ions, the separability of an equimolar test mixture of Tb^{3+}, Y^{3+} and Dy^{3+} was examined using six leading electrolytes as shown in Table 1. It should be noted that the concentration of both tartaric acid and HIB in the electrolytes were different with each other.

Fig. 1 shows the isotachopherograms obtained for the test mixture (sample amount = 1.67 nmol × 3). It is obvious that the separability among the above ions depended sensitively on the tartaric acid concentration. When the tartaric acid concentration (C_{Tar}) was 0.5 m*M* (Fig. 1b) and 0.6 m*M* (Fig. 1c), Tb^{3+}, Y^{3+} and Dy^{3+} were separated in that order. However, the separation was impossible, when C_{Tar} was 0.4 and 0.7 m*M* (Fig. 1d). The HIB concentration (C_{HIB}) in the leading electrolyte was 8, 7.6, 8.4 and 7.2 m*M*, respectively.

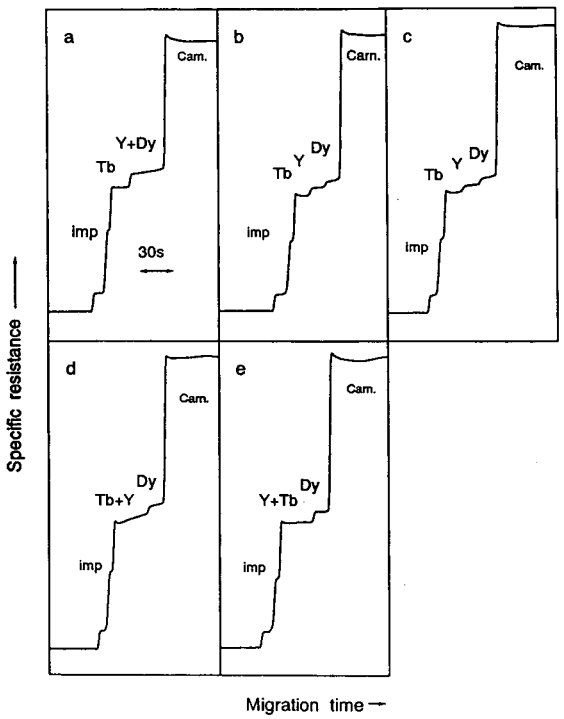

Fig. 1. Isotachopherograms of an equimolar mixture of Tb^{3+}, Y^{3+} and D^{3+} (1.67 mM 1 μl) obtained by using five leading electrolytes containing different concentrations of tartaric acid and HIB. Imp = electrolyte impurity. Migration current 50 μA. See Table 1 for details of the electrolyte systems used. C_{Tar} = (a) 0; (b) 0.5; (c) 0.6; (d) 0.7; (e) 1.25 mM.

Next the separation efficiency (nmol C^{-1}) of six rare earth ions (Eu^{3+}, Gd^{3+}, Tb^{3+}, Y^{3+}, Dy^{3+} and Ho^{3+} in order of migration) was measured for adjacent pairs by using the method reported previously [4]. The results are summarized in Table 2 together with the values observed for the HIB system [4]. Obviously from Table 2, the separation efficiency of the HIB–Tar system was ca. two-thirds of that of the HIB system. The separation efficiency of the Tb–Y and Y–Dy pairs was especially sensitive to the tartaric acid concentration because of the small effective mobility difference. In the analysis of real samples, therefore, the tartaric acid concentration should be optimized considering the abundance of Tb, Y and Dy. The separation of Tb, Y and Dy was thus achieved by using the HIB–Tar system, but the addition of tartaric acid decreased the separability of adjacent pairs of medium and heavy lanthanide ions.

Table 2
Separation efficiency observed for equimolar binary mixtures of adjacent lanthanide ions

Ions	Separation efficiency (nmol C^{-1})[a]		
	HIB[b]	HIB–Tar	
		C_{Tar} = 0.5 mM	C_{Tar} = 0.6 mM
Eu–Gd	27	0	0
Gd–Tb	309	220	166
Tb–Y		10	35
Tb–Dy	245	166	158
Y–Dy		100	75
Dy–Ho	197	137	112
Ce–Pr	180	166	176

The electrolyte systems were as in Table 1.
[a] Total amount of the separands/applied charge. Accuracy is ±5 nmol C^{-1}.
[b] Observed values for the HIB system [4].

3.2. Separation behaviour of rare earth ions

Fig. 2 shows the isotachopherograms of an equimolar mixture of the fifteen rare earth ions obtained by using three different leading electrolytes. When the HIB system was used, as shown in Fig. 2a, Y^{3+} and Dy^{3+} had the same step height. Although the same step height of separands at the isotachophoretic steady state does not always mean an imperfect separation [7], ITP–PIXE (particle-induced X-ray emission) analysis revealed that most of Y^{3+} and Dy^{3+} formed a mixed zone. The composition of the zone front suggested the effective mobility of Y^{3+} was slightly larger than that of Dy^{3+} [4].

When the HIB–Tar system (C_{Tar} = 0.5–0.6 mM) was used, Y^{3+} and Dy^{3+} were separated as expected (Fig. 2b). However, the Eu^{3+} and Gd^{3+} zones had the same step height, and the zone was also a true mixed zone according to ITP–PIXE analysis. The low separability of Eu^{3+} and Gd^{3+} is mainly caused by the fact that the stability constants of $Eu(AcO)_n^{3-n}$ complexes are larger than those of $Gd(AcO)_n^{3-n}$ complexes

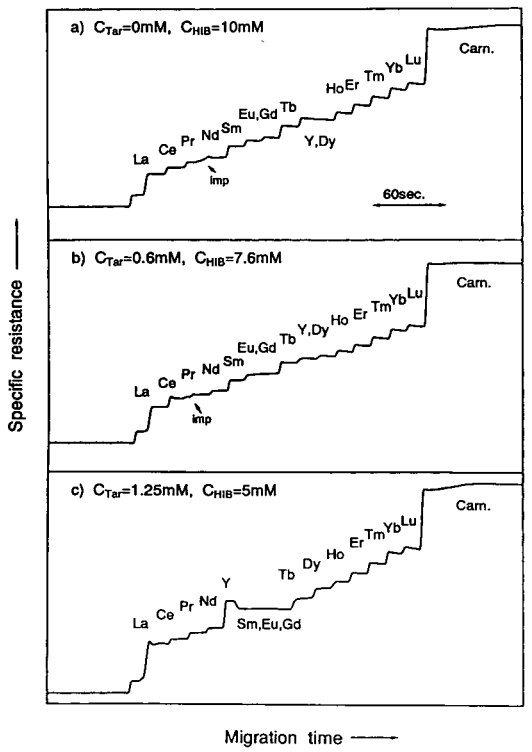

Fig. 2. Isotachopherograms of an equimolar mixture of fifteen rare earth ions (0.33 mM, 5 μl) obtained by using three different leading electrolytes. Electrolyte systems as in Table 1. Imp = electrolyte impurity. Migration current 50 μA.

[10], contrary to the HIB case. It seems that the stability constants of Eu–tartrate complexes are larger than those of Gd–tartrate complexes, similarly to the acetate complexes. When the tartaric concentration was increased and the HIB concentration was decreased, as shown in Fig. 2c, the Y^{3+} zone migrated before the Sm^{3+}, Eu^{3+} and Gd^{3+} mixed zone in an enforced manner [11]. The separability decrease on addition of tartaric acid was not observed for light lanthanide ions, as shown in Table 2 for Ce and Pr.

Table 3 shows the R_E values of the fifteen rare earth ions observed for the HIB system and the HIB–Tar system (C_{Tar} = 0, 0.4, 0.5, 0.6 and 0.7 mM). The effective mobilities of the rare earth ions were given as $\bar{m}_L/R_E$ from the definition of R_E, where $\bar{m}_L = 72.5 \cdot 10^{-5}$ cm^2 V^{-1} s^{-1} accord-

Table 3
R_E values of rare earth ions observed by using five leading electrolytes

Rare earth ion	Electrolyte system[a]				
	1	2	3	4	5
C_{Tar} (mM)[b]	0	0.4	0.5	0.6	0.7
C_{HIB} (mM)[c]	10	8.4	8.0	7.6	7.2
La	2.24	2.33	2.42	2.40	2.43
Ce	2.45	2.54	2.69	2.68	2.71
Pr	2.59	2.72	2.80	2.78	2.81
Nd	2.72	2.80	2.90	2.88	2.91
Sm	3.01	3.09	3.22	3.18	3.21
Eu	3.16	3.25	3.41	3.35	3.37
Gd	3.25	3.29	3.44	3.35	3.37
Tb	3.55	3.57	3.74	3.64	3.72
Y	3.79	3.73	3.90	3.75	3.72
Dy	3.79	3.80	3.98	3.88	3.89
Ho	3.97	3.96	4.15	4.04	4.05
Er	4.19	4.16	4.36	4.25	4.26
Tm	4.42	4.37	4.60	4.47	4.49
Yb	4.66	4.61	4.86	4.72	4.74
Lu	4.83	4.77	5.03	4.87	4.90
T[d]	5.65	5.85	5.94	6.17	5.98

[a] Electrolyte numbers as in Table 1.
[b] C_{Tar} = total concentration of tartaric acid.
[c] C_{HIB} = total concentration of α-hydroxyisobutyric acid.
[d] Terminating zone.

ing to our simulation. Clearly from Table 3, the R_E values of rare earth ions increased slightly on adding tartaric acid, in spite of the decrease in HIB concentration. When the concentration was 0.6 mM, for example, the effective mobility of Y^{3+} ($20.5 \cdot 10^{-5}$ cm^2 V^{-1} s^{-1}) was between those of Tb^{3+} ($21.1 \cdot 10^{-5}$ cm^2 V^{-1} s^{-1}) and Dy^{3+} ($20.1 \cdot 10^{-5}$ cm^2 V^{-1} s^{-1}) and consequently the separation was achieved. This suggested that the stability constants of Y–tartrate complexes are smaller than those of Dy–tartrate complexes.

As it was expected that better resolution might be obtained by increasing the HIB concentration, a leading electrolyte containing 10 mM HIB and 0.5 mM tartaric acid was applied to the rare earth elements. Although the separation of Eu and Gd was slightly improved, no clear steps were observed between the zones. When the HIB concentration was increased to 11 mM, the recovery of Lu began to decrease. It was less than 50% when the concentration was 12 mM.

This might be explained by the effective mobility of Lu at the transient state being smaller than that of the terminator (H^+) when the HIB concentration was higher than 10 m*M*.

3.3. Analysis of an ion-adsorption-type ore

An ion-adsorption-type ore containing a considerable amount of Y was analysed by using the HIB–Tar operational electrolyte system. Fig. 3 shows the isotachopherograms of the ore sample (2 g l^{-1}) obtained by using three different electrolyte systems [C_{Tar} = (a) 0, (b) 0.6 and (c) 1.25 m*M*. The volume injected was 3 μl. Obviously from Fig. 3a, Y^{3+} and Dy^{3+} merged into a zone when the HIB system was used, but they were separated with the HIB–Tar system (Fig. 3b). C_{Tar} was selected as 0.6 m*M* rather than 0.5 m*M* considering the separability shown in Table 2, because the abundance of Dy in the sample was greater than that of Tb. If Y and Dy are the targets of the analysis, a higher concentration of tartaric acid may be suitable, as shown in Fig. 3c.

The zone passing times of the major components in the rare earth ore sample were measured by varying the sample volume by using the HIB–Tar system and the HIB system to show the differences in separability. The results are shown in Figs. 4 and 5. In addition to the point that Y and Dy can be analysed separately by using HIB–Tar system, it is clear that better separability was obtained for Pr and Nd. Concerning Ce, the coincidence of the step with that of an electrolyte impurity (unidentified) made the zone passing time unstable. When the HIB system was used, a better result was obtained for Ce, as shown in Fig. 5. Figs. 4 and 5 show that the zone passing times per unit amount of sample were almost identical.

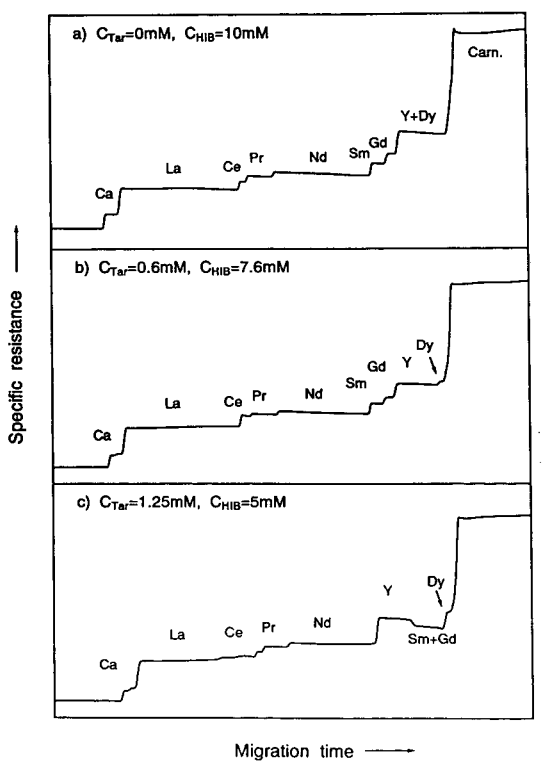

Fig. 3. Isotachopherograms of an ion-adsorption-type rare earth ore (2 g l^{-1}, 3 μl) obtained by using the HIB system and the HIB–Tar system (C_{Tar} = 0.6 and 1.25 m*M*).

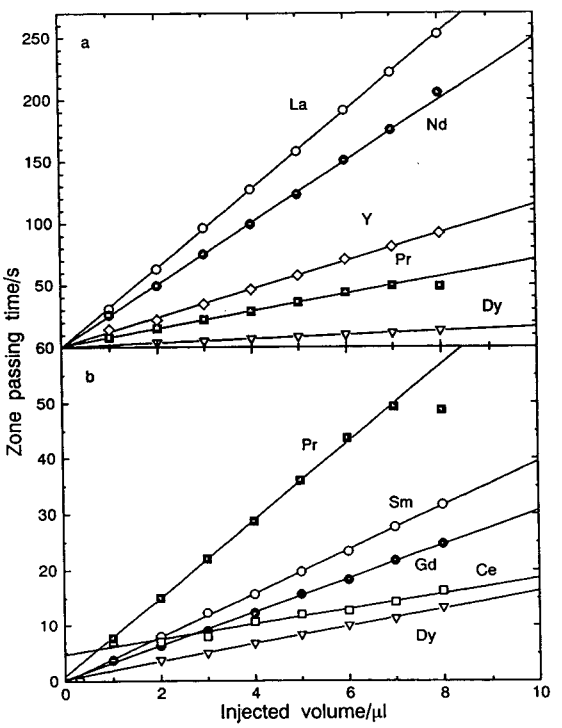

Fig. 4. Zone passing time vs. injection volume for an ion-adsorption-type rare earth ore (2 g l^{-1}) obtained by using the HIB–Tar system. Migration current 50 μA.

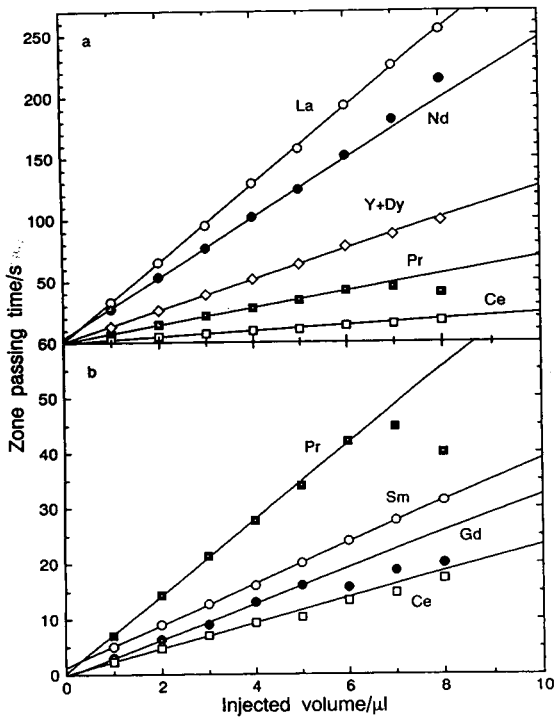

Fig. 5. Zone passing time vs. injection volume of an ion-adsorption-type rare earth ore (2 g l^{-1}) obtained by using the HIB system. Migration current 50 μA.

Table 4 summarizes the analytical results for the ore sample obtained by ITP, together with those given by PIXE and ITP–PIXE. Good agreement was obtained for the major components. Accurate results were obtained by ITP even for the minor components such as Ce and Dy, the abundances of which were 2 mass–%. ITP appears to be the most convenient method for determining rare earth elements at such a level of abundance. The elements with abundances of the order of 0.1% (w/w) can be determined by applying much more charge with the use of a longer capillary.

It is very convenient if the fifteen rare earth ions (lanthanide and yttrium ions) can be separated simultaneously using one electrolyte system. However, such a separation is impossible at present. The two electrolyte systems described in this paper are necessary for the analysis. In addition, Sc^{3+} was not treated in this study, as it has high stability constants even with acetate ions and it could not be detected as cations in ITP.

The capillary zone electrophoretic separation of lanthanides was reported by Foret et al. [12]. We modified the reported electrolyte system (30

Table 4
Analytical results for an ion-adsorption-type rare earth ore

Rare earth ion	ITP [10 μl (2 g l^{-1})]		ITP–PIXE [14 μl (2 g l^{-1})]		PIXE [5 μl (0.8 g l^{-1})]	
	μg	Mass-%[a]	μg	Mass-%[a]	μg	Mass-%[a]
La	5.539	36.68	7.425	35.96	1.020	35.22
Ce	0.300	1.98	0.431	2.09	0.083	2.87
Pr	1.211	8.02	1.747	8.46	0.260	8.98
Nd	4.725	31.29	6.465	31.31	0.860	29.7
Sm	0.710	4.70	1.001	4.85	0.135	4.66
Eu	–		0.145	0.70	0.039	1.35
Gd	0.649	4.30	0.674	3.26	0.115	3.97
Tb	–		0.104	0.50	0.035	1.21
Dy	0.302	2.00	0.405	1.96	0.054	1.86
Ho	0.052	0.34	0.073	0.35	0.007	0.2
Er	0.134	0.89	0.164	0.79	0.010	0.35
Tm	–		0.040	0.19	0.008	0.3
Yb	0.131	0.87	0.135	0.65	0.015	0.52
Lu	–		0.021	0.10	0.008	0.3
Y	1.347	8.92	1.820	8.81	0.247	8.53
Total	15.100		20.650		2.896	

[a] Mass-% = mass of a rare earth element/total mass of rare earth elements ×100.

m*M* creatinine–acetate buffer containing 4 m*M* HIB) by adding tartaric acid and applied the modified electrolyte system to the separation of rare-earth elements. However, satisfactory separation was not obtained for Tb, Y and Dy. This may be closely related to the fact that the pH and the ionic strength of the separated zones can be regarded as constant in CZE but they are not constant in ITP.

Acknowledgements

We thank Dr. Bohuslav Gaš, Dr. Jiri Zuska and Dr. Jiri Vacik for providing the high-frequency contactless conductivity detector used in this work. We also thank Iva Zuskova for her help in remeasuring the R_E values.

References

[1] I. Nukatsuka, M. Taga and H. Yoshida, *J. Chromatogr.*, 205 (1981) 95.
[2] T. Hirokawa, N. Aoki and Y. Kiso, *J. Chromatogr.*, 312 (1984) 11.
[3] L.J. Nugent, *J. Inorg. Nucl. Chem.*, 32 (1970) 3485.
[4] J. Hu, T. Hirokawa, F. Nishiyama and Y. Kiso, *J. Chromatogr.*, 589 (1992) 339.
[5] J. Hu, T. Hirokawa, F. Nishiyama, Y. Kiso, K. Ito and E. Shoto, *J. Chromatogr.*, 594 (1992) 371.
[6] J.E. Powell et al., in K.S. Vorres (Editor), *Rare Earth Research II*, Gordon and Breach, New York, 1964, p. 509.
[7] T. Hirokawa, W. Xia, K. Nakamura, I. Tanaka, F. Nishiyama, Y. Kiso, B. Gaš and J. Vacik, *J. Chromatogr. A*, 663 (1994) 245.
[8] B. Gaš, M. Demjanenko and J. Vacik, *J. Chromatogr.*, 192 (1980) 253.
[9] T. Hirokawa, M. Nishino, N. Aoki, Y. Kiso, Y. Sawamoto, T. Yagi and J. Akiyama, *J. Chromatogr.*, 271 (1983) D1.
[10] A. Sonesson, *Acta Chem. Scand.*, 12 (1958) 1937.
[11] F.M. Everaerts, J.L. Beckers and Th.P.E.M. Verheggen, *Isotachophoresis – Theory, Instrumentation and Applications*, Elsevier, Amsterdam, 1976.
[12] F. Foret, S. Fanali, A. Nardi and P. Boček, *Electrophoresis*, 11 (1990) 780.

ELSEVIER

Journal of Chromatography A, 689 (1995) 157–163

JOURNAL OF CHROMATOGRAPHY A

Short communication

Determination of C_{60} and C_{70} fullerenes in geologic materials by high-performance liquid chromatography

Dieter Heymann[a,*], L.P. Felipe Chibante[b], Richard E. Smalley[b]

[a]*Department of Geology and Geophysics, Rice University, P.O. Box 1892, Houston, TX 77251, USA*

[b]*Department of Chemistry and Quantum Institute, Rice University, P.O. Box 1892, Houston, TX 77251, USA*

First received 13 July 1994; revised manuscript received 30 September 1994

Abstract

It is demonstrated that high-performance liquid chromatography (HPLC) is an excellent and reliable analytical method for the determination of the C_{60} and C_{70} fullerenes extracted from geologic samples because the analysis is carried out at room temperature, is non-destructive (fullerenes can be recovered), and is easily calibrated with synthetic fullerenes. The determination of fullerenes in geologic materials is greatly empowered by the pre-separation of fullerenes from organics on a "big" HPLC column.

1. Introduction

When fullerenes were first discovered to be formed spontaneously in condensing carbon vapors [1], it was suggested that they might be widely distributed in the Universe. Subsequent searches for fullerenes in interstellar media and meteorites [2,3–5] have thus far been unsuccessful, but C_{60} and C_{70} have been reported to occur in the ejecta associated with an impact crater on the Long Duration Exposure Facility Spacecraft [6]. On the earth, C_{60} and C_{70} have been reported to occur in certain samples of shungite, a meta-anthracite coal from a deposit near Shunga, Russia [7], and in "fulgurite", a substance formed when lightning strikes certain soils or rocks [8]. Also in clay from the Cretaceous–Tertiary (K–T) boundary [9,10] and in carbonaceous matter from the Sudbury impact structure, Ontario, Canada [11].

Analyses of fullerenes have generally used mass spectrometry of either laser-vaporized or thermally heated samples. While this is often a good technique, we are concerned that, given the levels of a few parts-per-billion (ppb) [9,11], or parts-per-million (ppm) [11] at which fullerenes occur in geologic materials, the fullerenes may not volatilize efficiently from the surrounding matter, and that the high temperature and gas-phase conditions required in the analysis may inadvertently produce fullerenes that were not originally present in the sample. Instead we have used high-performance liquid chromatography (HPLC) of toluene extracts together with direct photo diode array (PDA) detection of the UV–visible absorption spectrum of the separated fullerenes.

HPLC is carried out at room temperature, hence the probability that fullerenes are formed

* Corresponding author.

0021-9673/95/$09.50
SSDI 0021-9673(94)00941-4

during the measurement is nil. Moreover, the retention times and peak areas, both salient properties of the substance to be determined, can be easily calibrated with standard solutions of synthetic C_{60} and C_{70}. The analysis is non-destructive and the fullerenes can be recovered after they emerge from the instrument. Whereas these positive aspects of HPLC have been evident to us for quite some time, we have encountered considerable skepticism, especially with regards to the sensitivity of the method. To engender a better understanding of the application of HPLC to the search for fullerenes in geologic samples we present here our cumulative experience of several years together with new results on the pre-separation of fullerenes from large amounts of organic substances.

2. Experimental

For our search for fullerenes in geologic materials we have assumed that significant fractions of C_{60} and C_{70}, if present, can be extracted from the materials by treatment with solvents such as toluene, and that the yields would probably increase upon the crushing, powdering, and ultimately, the demineralization of samples. Yet, even after the dissolution of inorganic minerals by repeated treatment with HCl and HF (i.e. demineralization), we can only recover those fullerene molecules which are not encased in chemical structures which prevent their dissolution in toluene. Hence, a failure to find fullerenes does not necessarily mean that these are not present in the sample.

Both non-demineralized and demineralized samples were placed in glassware, adequate amounts of HPLC-grade toluene were added, and the slurries were then sonicated for at least four hours. Next, the slurries were transferred to a Soxhlet thimble (the emerging fluids were, of course, collected) and the solids were washed by Soxhlet treatment using the collected fluids themselves for the washing. This procedure also brought about a good first separation of fluid and solids. Only centrifugation was used for additional separation when needed.

It has long been known that fullerenes are vulnerable to ultraviolet radiation [12], heating in air [13], and exposure to ozone [14]. We have therefore avoided strong irradiation and heating above 60°C of any solid sample, or any toluene extract, which means that reductions of fluid volumes by evaporation were done at reduced pressure. However, we have used the vulnerability to heating in air for cleaning all glassware at 500°C for at least 12 hours.

The end product of the treatment of a geologic sample was always a volume between 0.1 and 1.0 ml of filtered toluene, with, or without fullerenes, but nearly always with some organics dissolved in it. The HPLC instrument into which 25 μl of this solution was injected consisted of two Waters 510 pumps, an U6K injector, a 3.9 × 300 mm Nova-Pak silica-bonded C-18 column (called the "small" column) and a 996 photo diode array (PDA) taking UV–Vis absorption spectra of the fluid emerging from the column every 2 seconds. The PDA can take spectra in the range 210–640 nm, but our spectra were taken only in the range 310–430 nm (or sometimes 300 to 450 nm) because the toluene in the mobile phase absorbs too strongly below 310 nm and because the absorption by amounts of fullerene from geologic samples above 430 nm was negligibly small.

The mobile phase was commonly a 40:60 toluene–methanol mix flowing at 2.00 ml/min. For these conditions, the retention times of C_{60} and C_{70} were around 6.50 and 11.3 min respectively. Higher proportions of toluene were also used, depending on the sample. These separations with a stronger mobile phase gave the usual decrease in run time, narrower peaks and reduced resolution.

3. Results and discussion

3.1. Instrument performance

Fig. 1 shows chromatograms of the injection of: (A) 0.99 nanogram synthetic C_{60} and 1.06 ng synthetic C_{70}; (B) 4.95 and 5.32 ng of the fullerenes; and (C) of 49.5 and 53.2 ng of the

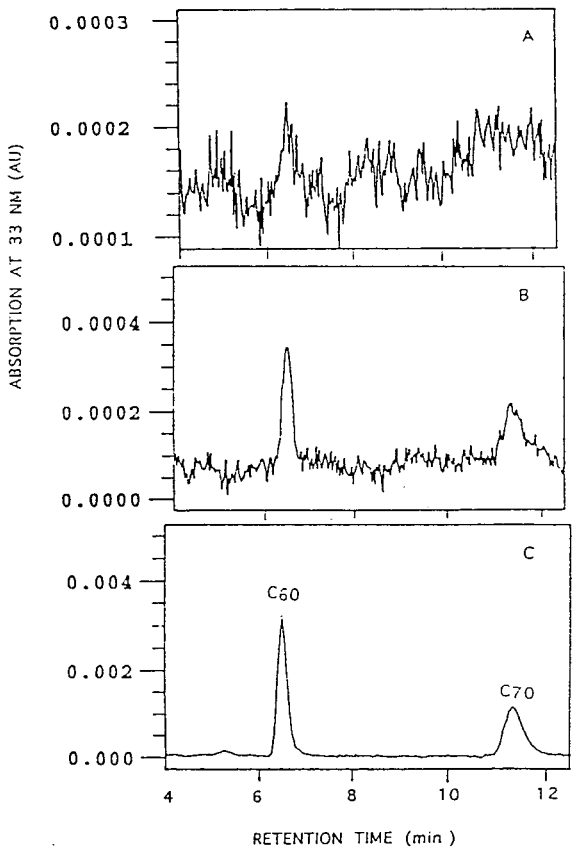

Fig. 1. Chromatograms of 25 μl-aliquots of increasingly concentrated solutions of synthetic fullerenes in toluene. The amounts are given in the text. All three chromatograms (A, B, and C) were generated under identical conditions. The small column was used. The mobile phase was 1.20 ml/min methanol and 0.80 ml/min toluene. An absorption spectrum was taken by the PDA detector every 2 s in the range 300 to 450 nm, but the chromatograms were constructed from absorption data at 330 nm, where the C_{60} spectrum has a local maximum. The chromatograms are shown from 4 to 12.5 min because only a meaningless peak corresponding to the dead time of the column is present between 0 and 4 min.

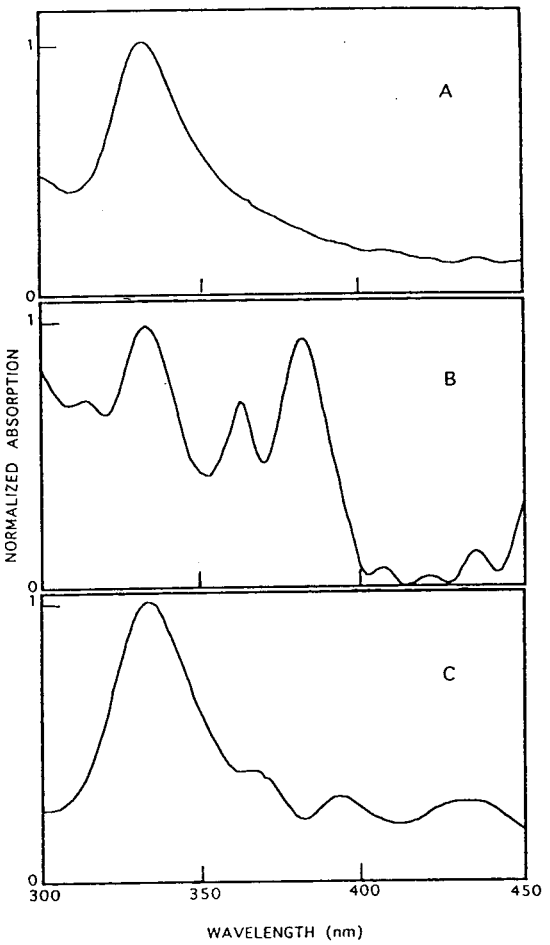

Fig. 2. The identification of fullerenes based on retention times and absorption spectra. A and B are absorption spectra in the wavelength range 300 to 450 nm at 6.47 and 11.35 min, the known retention times of C_{60} and C_{70}, for the injection of about 50 ng of each of the fullerenes. C is the absorption spectrum at the retention time of C_{60} for the injection of about 5 ng of that fullerene. The noise level of the PDA prevents the obtaining of a good C_{70} spectrum from the injection of 5 ng of that fullerene. The spectra are normalized such that absorption at maximum is 1.000. Actually the specific absorption of C_{70} at 330 nm is only about 0.6 times that of C_{60}. For identification of the fullerenes by both retention time and convincing absorption spectra, the minimum amounts required for injection are about 5 ng C_{60} and 20 ng C_{70}.

fullerenes. The first four minutes of the chromatograms are not shown as they only contain a peak at 1.2 min, which has no practical significance as it corresponds to the dead time of the column.

Fig. 2A and 2B show the absorption spectra of C_{60} and C_{70} in the range 300 to 450 nm, obtained at 6.47 min and 11.35 min from the injection of about 50 ng of fullerenes. Fig. 2C shows the C_{60} spectrum at 6.46 min from the injection of about 5 ng of fullerenes. The absorption spectrum for C_{70} for the injection of 5.32 ng of that fullerene

is greatly distorted by the noise of the PDA, hence is not shown. The C_{60} spectrum is greatly distorted by PDA noise for the injection of about 1 ng. Therefore, whereas the limit of detection from chromatograms alone is about 1 ng for C_{60} and 5 ng for C_{70}, when one requires that convincing absorption spectra must be paired with retention times, these limits must be raised to about 5 ng and 20 ng respectively. Fortunately we have been able to extract significantly larger amounts of fullerenes from our geologic samples.

Fig. 3 shows that the response of the PDA at 330 nm is linear in the range of concentrations of 20 to 20 000 ng per ml. A linear regression fit to the data yielded an integrated C_{60} peak area of 2237 ± 180 μVs (micro-volt-second) per ng injected. The fit for C_{70} (data not shown) yielded 1342 ± 121 μVs per ng injected. These areas are roughly 20, respectively 10 times larger than typical blank values obtained by the injection of pure toluene at the salient retention times. Ten replicate analyses of the 2000 ng/ml standard (50 ng injected) have yielded a standard deviation from the mean of $\pm 8\%$ of the peak area.

3.2. Pre-separation

Toluene extracts of geologic samples always contain from small to large amounts of organic substances, including pure hydrocarbons to compounds which contain O, N, S, and other elements. Polar compounds such as alcohols, ketones, aldehydes, acids, etc. tend to have shorter retention times than the C_{60} and C_{70} fullerenes on the C_{18}-bonded column used, and non-polar molecules tend to have increasingly longer retention times as their molecular weights increase. A major problem arises with all of these substances when their cumulative absorptions compete with those of the fullerenes.

Let us consider in some detail the example of a clay from the Cretaceous–Tertiary (K–T) boundary at Woodside Creek, New Zealand. It had long been known that the basal layer of the boundary seam at that K–T locality, which is about 2 cm thick, was rich in iridium and other platinum-group metals [15], as well as in various forms of elemental carbon, including soot [16,17], all putatively due to the after-effects of a

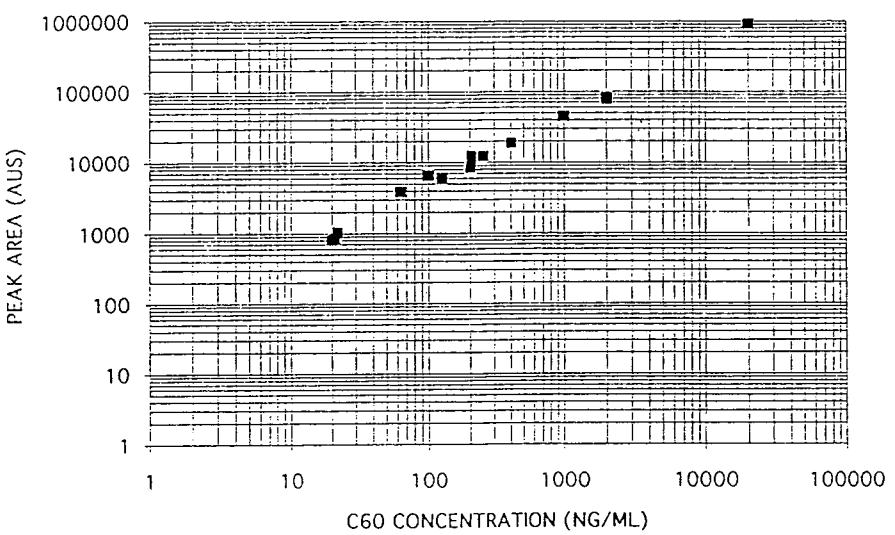

Fig. 3. Peak area as a function of C_{60} concentration in toluene solutions as determined with 25 μl-injections. Multiple injections were done for every value of concentration. A least-squares fit for this particular calibration yielded: 2237 ± 180 μVs per ng injected for C_{60} and 1342 ± 121 μVs per ng injected for C_{70} (analogous plot not shown).

gigantic crater-forming impact at Chicxulub, Yucatan, Mexico, some 65 Ma ago. Since the soot was thought to have formed by world-wide wildfires [16,17], we speculated that it might be attended by a complement of fullerenes.

Six samples of clay, ranging in weight from 68 to 201 gram, were treated with toluene. The extracts were pale yellow. Upon HPLC analysis the clays turned out to contain extractable C_{60} in the range 0.32 to 5.4 ppb. Fig. 4A shows a typical chromatogram of one of these extracts.

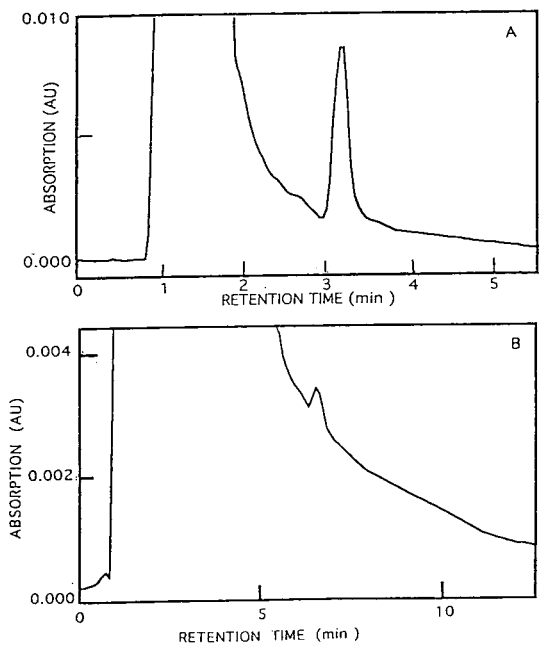

Fig. 4. A: Chromatogram from an extract of a clay sample from the Cretaceous–Tertiary boundary site of Woodside Creek, New Zealand. With a mobile phase of 1.00 ml/min methanol and 1.00 ml/min toluene, the retention times of C_{60} and C_{70} (little, if any present in the extract) were 3.18 min and 4.48 min respectively. The large and broad peak which crests at 1.5 min is due to organics also extracted from the clay. B: Chromatogram from an extract of a demineralized clay sample from the Cretaceous–Tertiary boundary site of Woodside Creek, New Zealand. The mobile phase used was 1.20 ml/min methanol and 0.80 ml/min toluene. The organics peak is huge, and baseline is not reached even after 12.5 min. The C_{60} peak at 6.48 min is riding on a substantial tail of the organics peak. The C_{70} peak was expected at 11.3 min. No peak was detected at that time.

The rather broad peak cresting at 1.5 min is due to organics extracted along with the C_{60}, whose peak occurs at 3.18 min. The C_{70} peak was expected at 4.48 min. Apparently this sample contained little, if any C_{70}. Although the C_{60} peak is riding on the tail of the organics, their interference with determining the peak area is only modest. However, when we succeeded recently in destroying most of the inorganic minerals of another clay sample of 250 gram by treatment with HCl and HF, and when we treated the carbon-rich residue with toluene, we obtained a strongly orange colored solution, obviously richer in organics than any we had previously obtained. We shall not be concerned here with the causes for the increased yield of organics, but with their effect on the detection of the fullerenes. Fig. 4B shows the chromatogram of the extract. It is overwhelmingly dominated by the organics peak and its huge tail. It is seen that the extract contained just enough C_{60} for its peak (6.48 min) to stick out above the organics background, but small amounts of C_{70} (expected at 11.3 min), if present, could be totally masked by the tail of the organics peak.

3.3. Preparative study

In order to deal with problems such as this, we obtained a column with the same stationary C-18 phase, but with internal dimensions of 19 × 300 mm (the "big" column). As mobile phase we used 10 ml/min each of methanol and toluene. Up to 2.0 ml of extract could be injected into the system. To test the efficacy of separation and recovery, we spiked fullerene-free organics obtained by the extraction of soot produced by the burning of a crude fossil oil from the Brent field in the North Sea with 396 ng C_{60} and 426 ng C_{70}. A sample of this mixture was analyzed on the small column (Fig. 5A). The remainder was then injected into the big (prep) column and the emerging fluids were collected from one minute before to one minute after the retention times of C_{60} and C_{70}, sufficient to catch more than 90% of the emerging fullerenes (Fig. 5B). The volume of the combined fullerene fluids was then

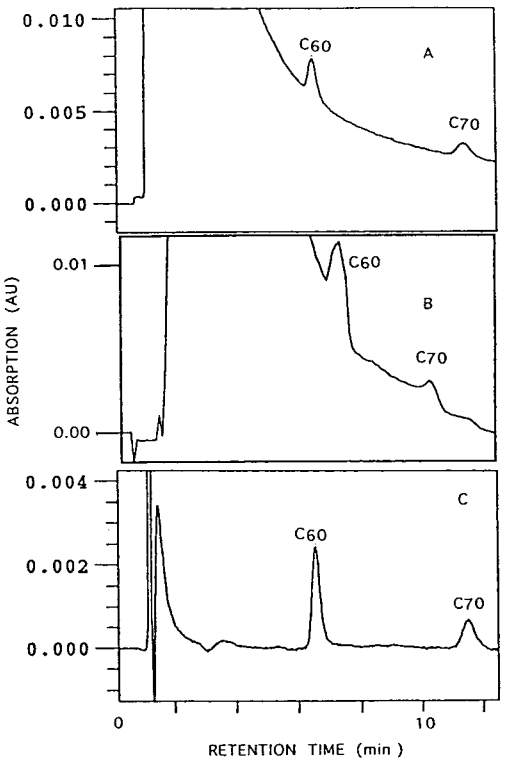

Fig. 5. Three chromatograms which illustrate the testing of the big column. A mixture was made of fullerene-free organics with 396 ng C_{60} and 426 ng C_{70} in toluene. Chromatogram A was obtained from an injection of this mixture. The amounts of the fullerenes were sufficiently large so that their peaks are seen to ride on the tail of the organics peak. Chromatogram B was taken while the organics and fullerenes progresses through the big column. Chromatogram C was taken after separation. Note the injection peak and the very modest organics peak (the negative excursion between the two peaks is quite common). By 4 min into the analysis, the PDA is back to zero level. The fullerene peaks are unencumbered by organics. Their absorption spectra (not shown) are identical to those of C_{60} and C_{70}.

reduced to less than 0.5 ml by evaporation at reduced pressure. A sample of this fluid was injected for analysis into the small column (Fig. 5C). Fig. 5 shows from A to C the succession of salient chromatograms. At the top is the chromatogram of the non-separated mix, showing the fullerene peaks riding on a the tail of a large organics peak similar to the one in Fig. 4B. The sample was so rich in organics that the PDA became saturated. The next chromatogram was recorded as the substances migrated down the big column. One can see the peaks of C_{60} and C_{70} at about 7 and 10 min riding on the tail of the organics peak. The PDA was saturated for this injection as well. The chromatogram at the bottom shows the extract after separation. There is still a small organics peak at the beginning of the chromatogram, but zero baseline is reached after about 4 min and the peaks of the fullerenes are unencumbered by organics. The recoveries were 365 ng C_{60} and 390 ng C_{70}, which correspond to very good yields of 92% and 91%, respectively.

With the test successful, we proceeded to treat the Woodside Creek sample in analogous fashion. Fig. 6A shows the progression of organics and fullerenes through the big column and the bottom chromatogram (4 to 12.5 min only, because the organics peak is very small) is from the injection of the combined recovered C_{60} and C_{70} fractions evaporated to a volume of 0.12 ml.

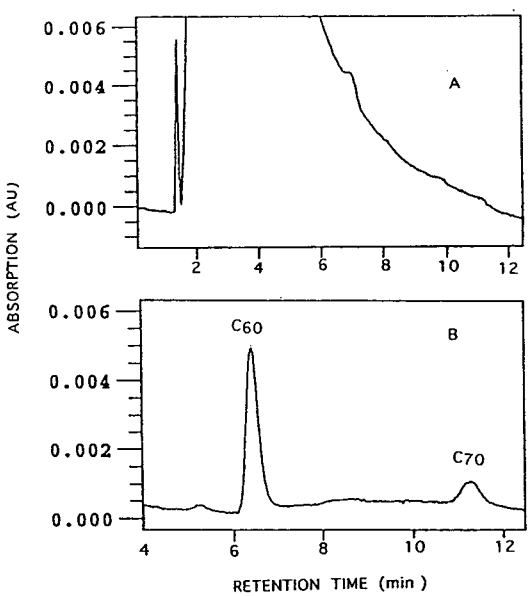

Fig. 6. These chromatograms are analogues of chromatograms B and C of Fig. 5, but for the extract from the demineralized Woodside Creek sample. The chromatogram of the separated extract is shown only from 4 to 12.5 min. The organics peak in it is very small. The peak at 6.44 min was identified by its spectrum as C_{60}. The peak at 11.3 min gave only a distorted C_{70} spectrum. The substance of the peak is, however, most likely C_{70}.

With an assumed recovery of 90%, the amounts of extracted fullerenes were 496 ng C_{60} and 171 ng C_{70}, which correspond to contents of 2.0 ppm and 0.68 ppb in the clay, and a C_{70}/C_{60} ratio of 0.34. Perhaps the most remarkable aspect of this result is that we had not been able to reveal C_{70} in the chromatograms of the earlier extracts of clay samples from Woodside Creek. One possible reason is that the separation as carried out here has removed organics to the extent that they no longer mask the C_{70} presence in the chromatogram.

A word of caution is in order. We found that the sensitivity of the PDA detector decreased substantially, by almost a factor of two, after large amounts of organics (the peak at 1.5 min!) had passed through it. We think that some organic compounds were partially decomposed photochemically when they passed through the PDA detector, hence that a thin absorbing film of products was deposited on the walls of the analytical cell. We were able to restore the sensitivity to about 0.8 times its original value by washing the detector with methanol and acetone. We conclude that the safest procedure is to determine the retention times of the fullerenes on the large column with synthetic, pure C_{60} and C_{70}, and to run organics-rich samples with the PDA turned off. The times when sample collection should begin or end depend, of course, on the widths of the fullerene peaks.

Acknowledgements

This research was funded in part by the National Science Foundation and the Robert A. Welch Foundation. We thank the Department of Geology and Geophysics of Rice University for the purchase of the big column.

References

[1] H.W. Kroto, J.R. Heath, S.C. O'Brien, R.F. Curl and R.E. Smalley, *Nature*, 318 (1985) 162.
[2] D.K. Bohme, *Chem. Rev.*, 92 (1992) 1487.
[3] R.D. Ash, S.S. Russell, I.P. Wright, C.T. Pillinger and J.W. Arden, *Lunar Planet. Sci.*, Vol. XXII, The Lunar and Planetary Institute, Houston, Texas, 1991, pp. 35–37.
[4] I. Gilmour, S.S. Russell, J. Newton, C.T. Pillinger, J.W. Arden, T.J. Dennis, J.P. Hare, H.W. Kroto, R. Taylor and D.R.M. Walton, *Lunar Planet. Sci.*, Vol. XXII, The Lunar and Planetary Institute, Houston, Texas, 1991, pp. 445–446.
[5] M.S. DeVries, K. Reihs, H.R. Wendt, W.G. Golden, H.E. Hunziker, R. Fleming, E. Peterson and S. Chang, *Geochim. Cosmochim. Acta*, 57 (1993) 933.
[6] F. Radicati Di Brozolo, T.E. Bunch, R.H. Fleming and J. Macklin, *Nature*, 369 (1994) 37.
[7] P.R. Buseck, S.J. Tsipurski and R. Hettich, *Science*, 257 (1992) 215.
[8] T.K. Daly, P.R. Buseck, P. Williams and C.F. Lewis, *Science*, 259 (1993) 1599.
[9] D. Heymann, W.S. Wolbach, L.P.F. Chibante, R.R. Brooks and R.E. Smalley, *Geochim. Cosmochim. Acta*, 58 (1994) 3531.
[10] D. Heymann, L.P.F. Chibante, R.R. Brooks, W.S. Wolbach and R.E. Smalley, *Science*, 256(1994) 645.
[11] L. Becker, J.L. Bada, R.E. Winans, J.E. Hunt, T.E. Bunch and B.M. French, *Science*, 256 (1994) 642.
[12] R. Taylor, J.P. Parsons, A.G. Avent, S.P. Rannard, T.J. Dennis, J.P. Hare, H.W. Kroto and D.R.M. Walton, *Nature*, 351 (1991) 277.
[13] L.P.F. Chibante, C. Pan, M.L. Pierson, R.E. Haufler and D. Heymann, *Carbon*, 31 (1993) 185.
[14] L.P.F. Chibante and D. Heymann, *Geochim. Cosmochim. Acta*, 57 (1993) 1879.
[15] L. Alvarez, W. Alvarez, F. Asaro and H.V. Michel, *Science*, 208 (1980) 1095.
[16] W.S. Wolbach, R.S. Lewis and E. Anders, *Science*, 230 (1985) 167.
[17] E. Anders, W.S. Wolbach and I. Gilmour, in J.S. Levine (Editor), *Global Biomass Burning*, The MIT Press, Cambridge, MA, 1991, pp. 485–492.

ELSEVIER

Journal of Chromatography A, 689 (1995) 164–169

JOURNAL OF CHROMATOGRAPHY A

Short communication

Determination of urea and its thermal decomposition products by high-performance liquid chromatography

Manfred Koebel*, Martin Elsener

Paul Scherrer Institute, CH-5232 Villigen, Switzerland

First received 18 July 1994; revised manuscript received 26 September 1994

Abstract

The thermal decomposition of urea can yield a wide variety of products; apart from ammonia and isocyanic acid, addition compounds of higher molecular mass may appear. In order to detect their presence in exhaust gases from a selective catalytic reduction (SCR) process using urea as a reducing agent, a chromatographic method was developed. The chromatographic separation is performed on an anion-exchange column using a phosphate buffer (pH 7) as eluent and UV detection at 190 nm. The method allows the simultaneous determination of neutral compounds (urea, biuret, melamine, ammeline) and of anions (cyanurate, isocyanate, acetate, formate, nitrite, nitrate, etc.). The value of the method for optimizing urea-SCR process design is illustrated.

1. Introduction

In recent years, urea has found increasing application as a selective reducing agent for nitrogen oxides (NO_x) from combustion processes. At the Paul Scherrer Institute we have been investigating the selective catalytic reduction of NO_x from diesel exhaust gases since 1988 [1,2].

Urea is usually atomized as a 40% aqueous solution into the hot exhaust gas (250–450°C) in front of the selective catalytic reduction (SCR) catalyst and decomposes primarily into ammonia and isocyanic acid according to

$$NH_2CONH_2 \rightarrow NH_3 + HNCO \quad (1)$$

In addition of this decomposition, larger molecules may also be formed as a result of secondary reactions deriving from the highly reactive isocyanic acid. Trimerizations leads to cyanuric acid, a very stable ring compound. Addition of isocyanic acid to urea forms biuret. Other possible compounds include ammeline, ammelide, melamine, melam and melem. It has therefore been argued that the urea-SCR process could potentially emit new by-products of questionable toxicity. It is also possible that the formation of these compounds could increase the problem of particulate emissions.

High-performance liquid chromatography was deemed the method of choice for determining this variety of possible compounds, but the search for the appropriate combination of column and eluent was complicated.

Preliminary experiments were made using various reversed-phase columns, water or 5 m*M* phosphate buffer (pH 7) as eluent and UV

* Corresponding author.

0021-9673/95/$09.50
SSDI 0021-9673(94)00922-8

detection at 196 nm. They were based on work concerning the determination of cyanuric acid as described by Tucker and Blade [3] and by Briggle et al. [4]. The columns tried included Waters Novapak C_{18} and Puresil C_{18}, LiChrospher RP-18, cyano (Brownlee) and phenyl (Brownlee).

It was observed that urea and cyanuric acid could be separated on these columns, but that urea eluted too early. When real samples (exhaust gas absorbed in water) were injected it was apparent that urea was hardly retained, appearing together with the solvent peak. This was realized because ammonium ions in the sample, also absorbing at 196 nm, simulated huge amounts of urea. Considering the very polar nature of urea and its low molecular mass, this result may be expected. This problem was also pointed out by Palfi-Ledniczky et al. [5], who resorted to a polar silica column and 2-propanol–butanol–water mixtures as the eluent.

A further literature search with the emphasis on the determination of urea revealed that columns with ion-exchange properties might be a better approach to solving this type of problem. Wills et al. [6] used an anion-exchange column and sodium hydroxide as the eluent to separate various amines and urea in marine food samples. Wolff et al. [7] describe the determination of urea, glycerophosphorylcholine, betaine and various sugars on a cation-exchange column in the calcium form with water as the eluent. Müller [8] determined urea, creatinine and uric acid in human serum and urine by ion-pair reversed-phase HPLC using a μBondapak C_{18} column and 1.25 mmol/l tetrabutylammonium phosphate as the eluent.

Subsequent tests with an anion-exchange column of low exchange capacity and phosphate buffer showed that urea is sufficiently retarded to separate it from the solvent/ammonium peak and that cyanuric acid may also be determined at this pH. This is due to the fact that the first pK_a of cyanuric acid is at about 6.5 and it is therefore partially ionized at pH 7.0. In our case an added advantage is that isocyanic acid may be determined in the same chromatogram.

2. Experimental

2.1. Chromatographic apparatus

An ion chromatograph (Waters ILC-1) was used, with minor modification, employing a UV–Vis detector (Waters Model 486) instead of the normal conductivity detector. For maximum sensitivity of the urea peak, the wavelength was set to 190 nm. The pump was a Waters Model 590 and the eluent was delivered at flow-rates between 0.5 and 1.0 ml/min (see below). The anion-exchange column was a Waters IC-Pak A HC, No. 26770, a polymethacrylate-based resin with quaternary ammonium groups and an exchange capacity of about 30 μequiv./ml. Its dimensions are 150 mm × 4.6 mm I.D. The injector (Waters ILC I) was fitted with a 20-μl sample loop and the data acquisition software was Baseline 810 (Waters).

2.2. Reagents and eluents

Screening for the optimum eluent composition led to a solution of 5 m*M* NaH_2PO_4 in ultra-pure water (obtained with a Waters Milli-Q system), with the pH adjusted to 7.00 with LiOH. The influence of other additions is discussed below.

Standard solutions of the compounds expected were prepared in ultra-pure water with chemicals of at least technical purity (>98%). They included urea, biuret, cyanuric acid, sodium cyanate, ammeline, melamine, formic acid, sodium acetate, sodium chloride, bromide, sodium nitrite, sodium nitrate, sodium carbonate, amidosulfonic acid and ammonium carbamate. In the case of free acids these were roughly neutralized using LiOH.

2.3. Sampling method

Sampling of flue gas was made with the gas-sampling apparatus shown in Fig. 1. An important feature is the two glass frits that provide intimate mixing of the gas phase and the absorbing liquid; only by this measure can the higher molecular mass compounds such as urea and

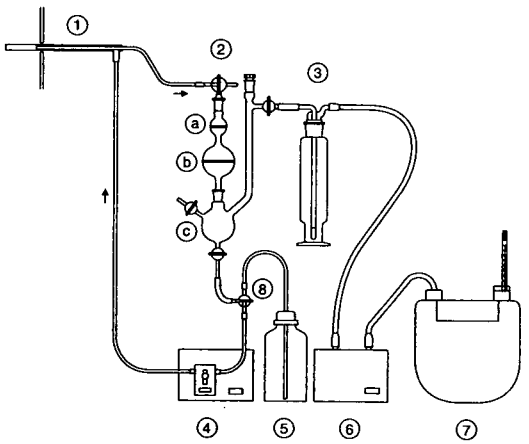

Fig. 1. Gas sampling apparatus. 1 = Heated gas probe; 2 = absorption unit with fritted glass filters: (a) glass frit, 30 mm diameter, P100, (b) glass frit, 60 mm diameter, P40, and (c) collecting vessel, 100 ml; 3 = safety wash bottle, 200 ml; 4 = dosing pump; 5 = bottle with absorption liquid (deionized water); 6 = vacuum pump; 7 = gas meter; 8 = three-way valve.

biuret be trapped efficiently, as they tend to form aerosols.

The vacuum pump 6 draws a constant sample gas stream from the heated gas probe through the absorption unit and the safety gas bottle. The total gas volume is measured by the gas meter 7. The absorption liquid stored in the bottle 5 is added to the gas sample at the T-shaped heated gas probe by means of the dosing pump 4, with the three-way valve 8 switched to the appropriate position. In order to obtain the best limit of detection, the volume of absorption liquid is limited to 15 ml, and this may be obtained by turning valve 8 to the position "recycle the absorption liquid". Water was used for absorption and the washed gas volume was 20–40 l. Before injection into the chromatograph, the sample solution was brought to the same phosphate concentration and pH as for the eluent in a final volume of 20 ml.

2.4. Chromatographic method

The flow-rate was set to 0.5 ml/min during the first 10 min, then it was increased to 1.0 ml/min. Calibration graphs for the main components of interest (urea, biuret, melamine, cyanuric acid and isocyanic acid) using peak areas were linear over a wide range (0.5–100 mg/l). Therefore, for the analysis of exhaust gas sample solutions, a single-point calibration without internal standard was made daily using a standard mixture containing 5 mg/l each of urea, biuret, melamine, cyanuric acid and sodium isocyanate.

3. Results and discussion

3.1. Method optimization

Various compositions of phosphate buffer and potassium sulfate varying also in pH were explored. The addition of potassium sulfate had almost no effect on the retention times of the early-eluting neutral species (urea, biuret, melamine), but speeds up the elution of the later-eluting ionized species (isocyanic acid, chloride, nitrate, etc.). Two eluent compositions proved particularly successful:

(a) 1 m*M* NaH_2PO_4 + 5 m*M* K_2SO_4 in high-purity water, pH adjusted to 7.00 with LiOH. Potassium sulfate was added in order to speed up the elution of the late-eluting ions (cyanate, nitrate). The disadvantage of this eluent is that the peak of an unknown substance in some real exhaust gas samples coincides exactly with that of cyanate. As we believe that late-eluting species are generally of ionic nature, this should also be the case for the unknown substance.

(b) 5 m*M* NaH_2PO_4 in high-purity water, pH adjusted to 7.00 with LiOH. The retention times of the early-eluting, non-ionic species urea and biuret are identical with those using eluent (a), but the later-eluting species are further delayed. Cyanate does not suffer interference from the unknown species in real exhaust gas samples. This eluent was therefore adopted in the final analytical procedure.

The pH value of 7 is a working compromise in so far as some expected compounds are pH-sensitive. Ammonia is essentially present in protonated form, i.e., as ammonium ion; it will

therefore be excluded from the ion exchanger, which itself possesses positive fixed charges of quaternary ammonium ions. This effect of Donnan exclusion from the pores leads to rapid elution of ammonium ion together with the solvent peak. For cyanuric acid ($pK_a \approx 6.5$), about half will be present as the anion and therefore will be retained by an ionic mechanism. Isocyanic acid ($pK_a \approx 3.7$) is determined as the anion working at a pH at which hydrolysis is also negligible.

In order to obtain a good separation of the urea peak from the injection peak, a low flow-rate of 0.5 ml/min was chosen. However, this flow-rate led to very long retention times with eluent (b) for the late-eluting anions such as nitrate (which is usually present in the samples). In order to shorten the analysis time, the flow-rate was increased after the first 10 min to 1.0 ml/min with eluent (b). In this way nitrate eluted after about 31 min. Sulfate eluted very late (ca. 50 min), but with a very broad peak, so that a subsequent injection made at 35 min gave no perturbation in the next analysis.

3.2. Typical results

Fig. 2 shows a typical chromatogram of the five main compounds of interest (standard mixture with 5 ppm each of urea, biuret, melamine, cyanuric acid and sodium cyanate). Table 1 shows typical retention times and limits of detection in solution. The latter is defined as the concentration corresponding to a peak height of 400 μV or 0.0004 absorbance units.

Table 1
Typical retention times and limits of detection for major compounds

Compound	Retention time (min)	Detection limit (mg/l)
Urea	3.9	0.2
Biuret	5.0	0.025
Ammeline	5.2	0.015
Melamine	7.2	0.012
Acetate	8.5	0.4
Formate	~10	n.a.[a]
Carbonate	~10	n.a.
Cyanuric acid	12.5	0.1
Chloride	13.6	1
Nitrite	19.0	0.15
Isocyanate	21	1
Nitrate	31	0.15

[a] n.a. = Not available.

Fig. 3 shows a chromatogram of a typical exhaust gas sample at a relatively low engine load (25 kW) corresponding to a low catalyst temperature of 230°C. Fig. 4 shows an analogous chromatogram corresponding to a high load (75 kW) and a high catalyst temperature of 400°C. In

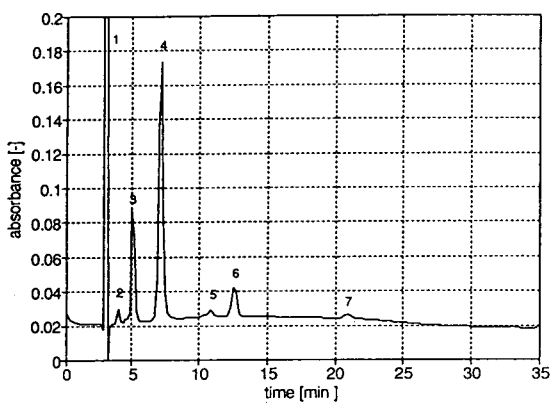

Fig. 2. Test chromatogram for 5 ppm each of (2) urea, (3) biuret, (4) melamine, (6) cyanuric acid and (7) sodium isocyanate. 1 = Injection peak; 5 = flow-rate switching "spike".

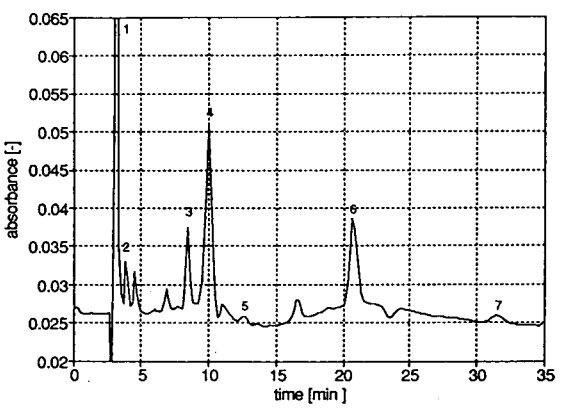

Fig. 3. Representative chromatogram of exhaust gas sample solution at low engine load. 1 = Injection peak; 2 = urea; 3 = acetate; 4 = carbonate; 5 = cyanuric acid; 6 = isocyanate; 7 = nitrate. The other peaks were not identified.

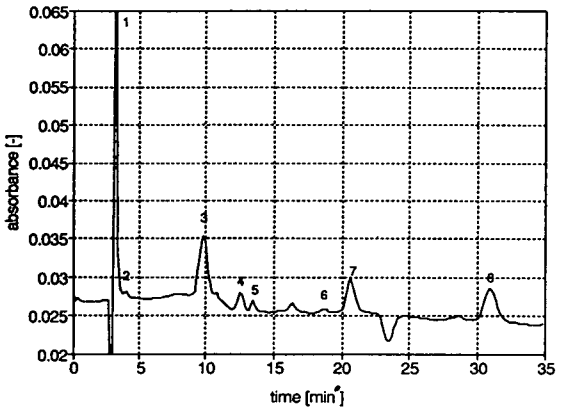

Fig. 4. Representative chromatogram of exhaust gas sample solution at high engine load. 1 = Injection peak; 2 = urea; 3 = carbonate; 4 = cyanuric acid; 5 = chloride; 6 = nitrite; 7 = isocyanate; 8 = nitrate.

both instances the amount of urea injected in front of the catalyst was relatively high, so that an ammonia emission of about 100 ppm in the exhaust gas after catalyst was obtained.

The method allows the simultaneous determination of ionic and neutral compounds. The small, non-ionic compounds, e.g., urea and biuret, appear early in the chromatogram; the ionic species, being more strongly retained, appear much later. A comparison of the elution volumes with the estimated column void volume suggests that the mechanism leading to the short retention times of neutral compounds can hardly involve ion exclusion [9]. For these compounds an additional interaction with the resin must be postulated, probably having the character of adsorption or partitioning, or both. The very polar character of the column may play a role here. The anions are presumed to be retained by the well known mechanism of ion exchange.

3.3. Application of the method to the urea-SCR process

The proposed method was used to study the formation of by-products of the urea-SCR process. The main compounds that could be detected were urea, isocyanic acid and cyanuric acid. Their level increases together with the emission of ammonia when the addition of urea is increased. The level of urea addition is usually defined as the stoichiometric parameter $\alpha = 2 \cdot$ urea/NO (mol/mol). As can be seen from the main reaction of urea-SCR, $\alpha = 1.0$ corresponds to stoichiometric addition of urea:

$$2NH_2CONH_2 + 4NO + O_2 \rightarrow 4N_2 + 4H_2O + 2CO_2 \quad (2)$$

Other compounds attributable to the use of urea, i.e., biuret, ammeline and melamine, could not be found in significant amounts. We may mention here also the presence of acetic acid at low engine loads (or low catalyst temperatures) and two unknown substances eluting after 16.5 and 28.5 min. The substance eluting at 16.5 min was only detectable when urea was injected.

Urea could only be detected at the lowest catalyst temperature (230°C; next higher temperature 330°C). The gas concentration was 0.8 mg/m_N^3 at $\alpha = 1.0$ and reached 2.3 mg/m_N^3 at $\alpha = 1.1$ (corresponding to an ammonia emission of ca. 100 ppm). However, an ammonia emission of ca. 100 ppm would already be prohibitive by itself.

Isocyanic acid could only be found in significant amounts at $\alpha = 1.0$ and higher. Here also the highest emission was found at the lowest catalyst temperature of 230°C (11 mg/m_N^3 at $\alpha = 1.1$). This may be due to the fact that at lower temperature greater amounts of gaseous urea enter the catalyst, and are only decomposed there into isocyanic acid and ammonia. Isocyanic acid itself has a finite rate of hydrolysis, leading to ammonia and carbon dioxide.

The emissions of cyanuric acid are very low, i.e. below 0.5 mg/m_N^3, under all conditions. The highest levels again occur at the highest α-values, but the temperature dependence is reversed relative to that of urea and isocyanic acid.

Summarizing these results, we can see that the emission of the higher molecular mass compounds urea and cyanuric acid is low under all the conditions examined. An appreciable increase in the emission of particulates is therefore not to be expected, even at moderate super-stoichiometric levels of urea addition. In any

event, such high values of α are not relevant in practice, as they produce an unacceptably high ammonia emission.

We believe that these low emission values also reflect the good design of the present SCR equipment [2]: perfect mixing of gas stream and urea solution (air atomizing nozzle), comparatively low space velocity in the catalyst (ca. 12 000 h^{-1}, 100 cells/in.^{2}), etc. Under less ideal conditions the emission of urea, cyanuric acid and isocyanic acid is likely to be higher. The method developed and reported here is therefore a useful tool for optimizing SCR-process design.

Acknowledgements

The financial support of the Swiss Federal Office of Energy (BEW) is gratefully acknowledged. Our thanks are also due to Mr. F. Mayer, Swiss Federal Institute of Technology, Zurich, for valuable suggestions concerning the choice of the chromatographic column, and to Dr. J. Highfield for careful reading of the manuscript.

References

[1] M. Koebel, M. Elsener and H.P. Eicher, *Tech. Rundsch.*, 82, No. 49 (1990) 74–79; see also *BWK*, No. 3, Special Luftreinhaltung, E24-E32, 1991.
[2] M. Koebel, *VDI-Ber.*, 1019 (1993) 195–211.
[3] S.P. Tucker and L.M. Blade, *Anal. Lett.*, 25 (1992) 2265–2277.
[4] Th.V. Briggle, L.M. Allen, R.C. Duncan and C.D. Pfaffenberger, *J. Assoc. Off. Anal. Chem.*, 64 (1981) 1222–1226.
[5] M. Palfi-Ledniczky, G. Dénes and K. Ujszaszy, *Chromatographia*, 24 (1987) 847–848.
[6] R.B.H. Wills, J. Silahahi and M. Wootton, *J. Liq. Chromatogr.*, 10 (1987) 3183–3191.
[7] S.D. Wolff, P.H. Yancey, T.S. Stanton and R.S. Balaban, *Am. J. Physiol.*, 256 (1989) F954–956.
[8] H. Müller, *Fresenius' Z. Anal. Chem.*, 332 (1988) 464–467.
[9] D.T. Gjerde and J.S. Fritz, *Ion Chromatography*, Hüthig, Heidelberg, 1987, Ch. 10.

ELSEVIER

Journal of Chromatography A, 689 (1995) 170–174

JOURNAL OF CHROMATOGRAPHY A

Short communication

Detection of benzthiazide by high-performance liquid chromatography–thermospray mass spectrometry

Yunje Kim[a], Songja Park[a], Jongsei Park[a], Won Lee[b,*]

[a]*Doping Control Centre, Korea Institute of Science and Technology, P.O. Box 131, Seoul 130-650, South Korea*

[b]*Research Institute for Basic Sciences and Department of Chemistry, Kyung Hee University, Seoul 130-701, South Korea*

First received 6 April 1994; revised manuscript received 15 August 1994

Abstract

Benzthiazide, a banned drug in the Olympic Games, is difficult to confirm by GC–MS after methylation of urine extracts. Organic acids are added to the LC effluent to detect this drug by LC–thermospray (TSP) MS. An organic acid with a small pK_a value is useful for detecting benzthiazide in the positive-ion mode. In the negative-ion mode, the highest sensitivity for benzthiazide was obtained by using $HOCH_2COOH$. When LC–TSP-MS is used to detect benzthiazide, FCH_2COOH and $ClCH_2COOH$ are useful organic acids in the positive-ion mode and $HOCH_2COOH$, CH_3CH_2COOH and FCH_2COOH in the negative-ion mode. FCH_2COOH is useful in both the positive- and negative-ion modes. $ClCH_2COOH$ is a useful organic acid for detecting the molecular ion of benzthiazide.

1. Introduction

Benzthiazide (Fig. 1), a diuretic, has been included in the list of banned drugs since the 1988 Winter and Summer Olympic Games. This drug is misused to reduce the body mass and to increase the urine flow, leading to a decrease in the concentration of other doping agents [1]. This drug is currently subjected to a screening method using high-performance liquid chromatography with UV detection [2]. However, confirmation of positive cases could not be achieved by gas chromatography–mass spectrometry (GC–MS) after methylation of the urine extracts, as used to detect diuretics [3]. In this work, we tried to detect benzthiazide by liquid chromatography–mass spectrometry (LC–MS) using a commercial thermospray (TSP) interface.

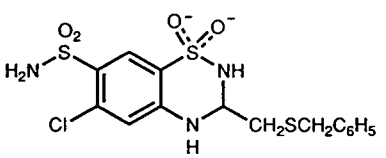

Fig. 1. Structure of benzthiazide.

When CH_3COONH_4 in the LC effluent (volatile buffer as an ionizing additive) was used to detect benzthiazide in the positive-ion mode of LC–TSP-MS, the drug could not be detected. We therefore tried to detect benzthiazide by using an LC effluent containing a different organic acid (FCH_2COOH, $ClCH_2COOH$, CH_3CH_2COOH, $HOCH_2COOH$ and SCH_2COOH), and the sensitivities of the drug to each of these acids in the LC effluent were compared.

* Corresponding author.

0021-9673/95/$09.50
SSDI 0021-9673(94)00904-X

2. Experimental

2.1. Chemicals

Water obtained with a Milli-Q water purification system (Millipore) was used throughout. Acids used in the mobile phase (Table 1) and methanol were of analytical-reagent grade from Merck (Darmstadt, Germany). Benzthiazide was obtained from Sigma (St. Louis, MO, USA).

2.2. Instrumentation

The HPLC system was Model HP 1090A (Hewlett-Packard, Palo Alto, CA, USA) equipped with an autoinjector for use in LC–MS. A Hewlett-Packard HP 5988A LC–TSP-MS system with an HP 9000-300 quadrupole mass spectrometer was used and a Model 7946 instrument was employed for data acquisition and processing.

2.3. Liquid chromatographic conditions

Solvent A consisted of 0.2 *M* of each carboxylic acid (HCOOH, CH_3CH_2COOH, $HOCH_2COOH$, $HSCH_2COOH$, $ClCH_2COOH$ or FCH_2COOH) and 0.2 *M* aqueous ammonia (1:1, v/v) and solvent B was methanol. The solvents were degassed and thoroughly purged with helium. The mobile phase composition was A–B (75:25), the flow-rate was 0.8 ml/min and the amount of benzthiazide injected was 2 μg.

2.4. Thermospray and mass spectrometric conditions

The TSP interface foreline pump maintained a pressure of 13.3–26.6 Pa in the cold trap, and two spectrometer diffusion pumps maintained a pressure of $2.66 \cdot 10^{-5}$–$5.32 \cdot 10^{-5}$ Pa in the manifold. The TSP temperatures were as follows: stem, 108–115°C (the stem temperature was determined by probe survey and was a temperature of 95% vaporization of mobile phase); tip, 180–205°C; and ion source, 276°C. In all the experiments the filament-on mode (ionization by an electron beam) was used. In this mode of operation, conventional negative-ion chemical ionization (NICI) can be carried out using the vaporized mobile phase as the CI reagent gas [4].

3. Results and discussion

In the negative-ion mode of the TSP buffer ionization process, it is assumed that the molecule studied by LC–MS contains hydrogen and is represented by HM; the anion of the additive, R^-, is the conjugate base of the organic acid in the LC effluent. When HM and R^- collide, there are two competing processes that can lead to products:

$$HM + R^- \rightleftharpoons HMR^- \quad (1)$$

$$HM + R^- \rightleftharpoons M^- + HR \quad (2)$$

Because Eq. 1 involves the formation of a hydrogen bond for almost all polar molecules,

Table 1
Physico-chemical properties of organic acids used in the mobile phase

Ionization solution	Molecular mass	Ion detection range (*m/z*)		pK_a	Boiling point (°C)
		Positive	Negative		
CH_3CH_2COOH	74.08	170–570	200–600	4.87	141
$HOCH_2COOH$	76.05	175–575	230–630	3.83	Decomposes
$HSCH_2COOH$	92.12	205–605	330–730	3.68	120
FCH_2COOH	78.04	170–570	240–640	2.95	168
$ClCH_2COOH$	94.05	235–635	270–670	2.92	189

this reaction is always favourable thermochemically [5]. The gas-phase acidity of HM may be compared with that of another acid, HR, whose conjugate base, R^-, competes with M^- for the proton in Eq. 2. The smaller the gas-phase acidity, the stronger is HM as an acid and the weaker is M^- as a base. Therefore, if the ionization process in TSP is in the gas phase, then the additive R^- will form HR from HM by proton abstraction when HR has a higher gas-phase acidity. In Fig. 2, all the spectra have an M^- ion, m/z 430, but do not have an HMR^- adduct ion. It is suggested that the gas-phase acidity of benzthiazide is lower than that of the organic acid. As a result, the proton affinity of benzthiazide must be weaker than that of the organic acid because this compound acts as a proton donor [6]. Therefore, if an organic acid with a higher pK_a value is used to detect benzthiazide, this drug is hardly detected by LC–TSP-MS. Fig. 3 shows that benzthiazide can be detected in the positive-ion mode by using

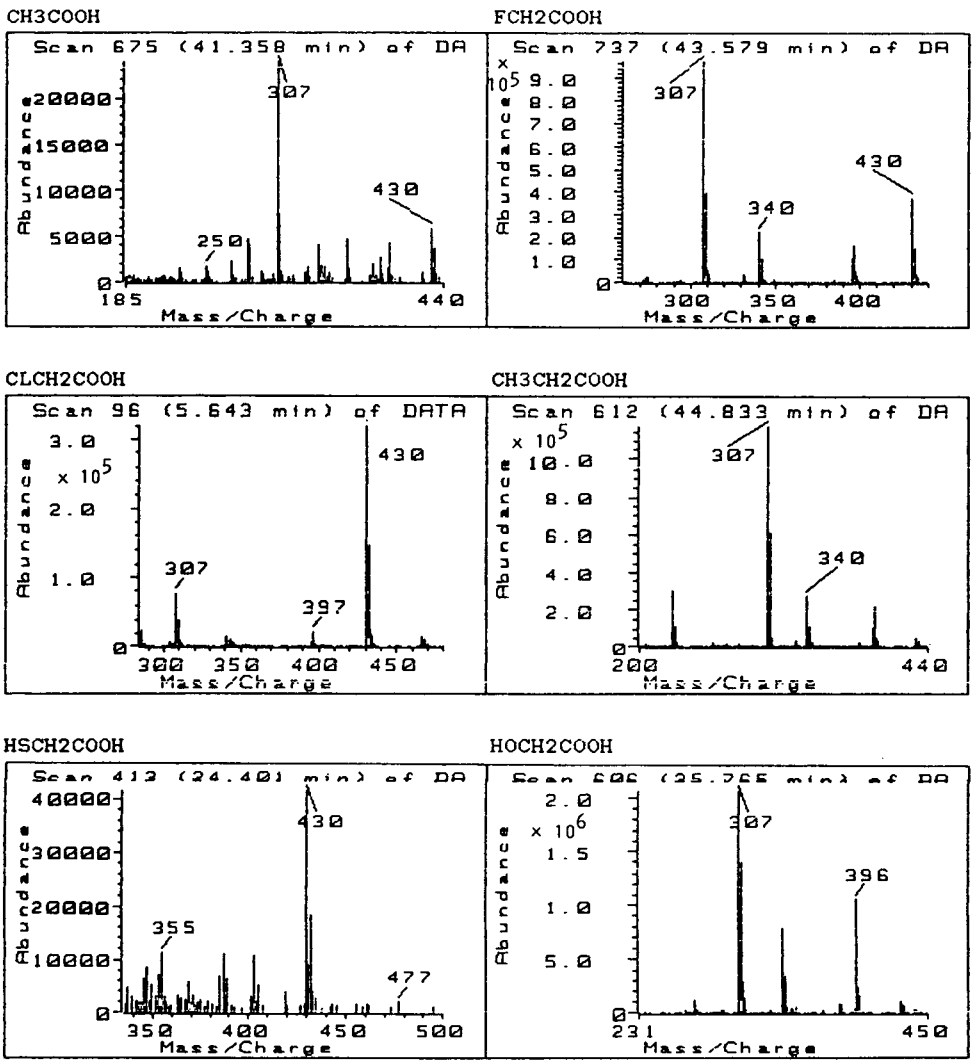

Fig. 2. Spectra of benzthiazide obtained with the use of different organic acids in LC–TSP-MS in the negative-ion mode.

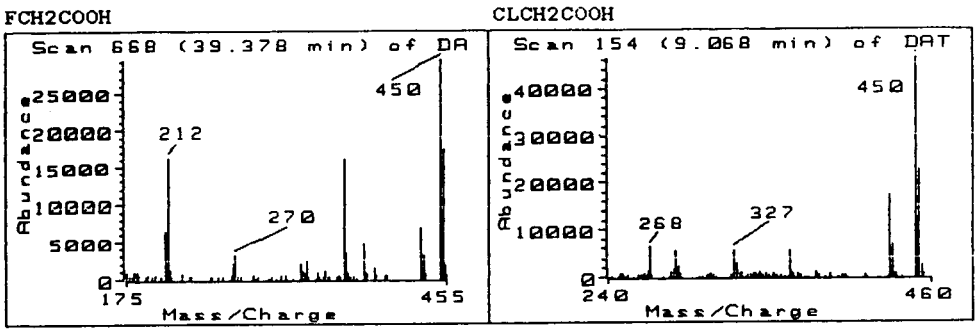

Fig. 3. Spectra of benzthiazide obtained with two organic acids in LC–TSP-MS in the positive-ion mode.

FCH_2COOH and $ClCH_2COOH$, which have smaller pK_a values than the other organic acids (see Table 1). We can predict that this drug will generate more $[MNH_4]^+$ adduct ion than $[MH]^+$ ion owing to smaller pK_a value and the proton affinities of FCH_2COOH and $ClCH_2COOH$, and the results show that the $[MNH_4]^+$ ion is the base peak.

When GC–MS was used to detect benzthiazide, it could not be detected by applying methylation to decrease the polarity. LC–MS in the positive-ion mode also could not detect this drug using CH_3COONH_4, which is generally used in LC–TSP-MS for the buffer ionization process. However, Table 2 shows that, in spite of using the positive-ion mode, the peak area of benzthiazide is $6.0 \cdot 10^4$ (FCH_2COOH) and $8.6 \cdot 10^4$ ($ClCH_2COOH$). In addition, in spite of using the positive-ion mode, the sensitivity of benzthiazide using these organic acids is higher than that in the negative-ion mode using CH_3COOH or $HSCH_2COOH$. Benzthiazide in the negative-ion mode shows the highest sensitivity when $HOCH_2COOH$ is used ($418.9 \cdot 10^4$). CH_3CH_2COOH ($201.7 \cdot 10^4$) and FCH_2COOH ($173.1 \cdot 10^4$) also give relatively high sensitivities. These three organic acids in the negative-ion mode give larger peak areas of benzthiazide than do the other acids. Therefore, if it is required to detect benzthiazide by LC–TSP-MS, FCH_2COOH or $ClCH_2COOH$ with a low pK_a value is useful in the positive-ion mode and $HOCH_2COOH$, CH_3CH_2COOH or FCH_2COOH is useful in the negative-ion mode. FCH_2COOH is a useful organic acid in both the positive- and negative-ion modes. The peak intensity of benzthiazide when using $ClCH_2COOH$ is lower than that with the other organic acids ($HOCH_2COOH$, CH_3CH_2COOH or FCH_2COOH), and the $[M]^-$ ion of benzthiazide is the base peak. This result is different from that with the fragment ion at m/z 307 as the base peak when the other organic acids are used. We assume that this is due to the boiling point of $ClCH_2COOH$ (189°C) being higher than those of the other acids (see Table 1); an organic acid with a high boiling point may remove fragment ions by pyrolysis because it is able to accommodate the input heat [7]. Hence $ClCH_2COOH$ is a useful acid for detecting the molecular ion of benzthiazide. When using FCH_2COOH and $ClCH_2COOH$, the sensitivity for benzthiazide was predicted to be higher than that with the other organic acids as in negative-ion chemical ionization (NICI) in GC–MS

Table 2
Comparison of sensitivity for benzthiazide with different organic acids in the positive- and negative-ion modes

Organic acid	Peak area ($\times 10^4$)	
	Positive-ion mode	Negative-ion mode
CH_3COOH	N.D.[a]	4.3
FCH_2COOH	6.0	173.1
$ClCH_2COOH$	8.6	43.9
$HOCH_2COOH$	N.D.	418.9
CH_3CH_2COOH	N.D.	201.7
$HSCH_2COOH$	N.D.	7.5

[a] N.D. = not detected.

because an element (F and Cl, respectively) with high electronegativity is substituted. However, benzthiazide showed lower sensitivity when these organic acids were used than with the use of CH_3CH_2COOH and $HOCH_2COOH$ because it did not generate an $[HMR]^-$ adduct ion.

4. Conclusions

Because the gas-phase acidity of benzthiazide is high, an organic acid with a small pK_a value is useful for detecting this drug by LC–TSP-MS in the positive-ion mode. The base peak of benzthiazide is the $[MNH_4]^+$ adduct ion. When LC–TSP-MS in the negative-ion mode is used to detect benzthiazide, the highest sensitivity is obtained using $HOCH_2COOH$. In the positive-ion mode FCH_2COOH and $ClCH_2COOH$ are useful organic acids, and in the negative-ion mode $HOCH_2COOH$, CH_3CH_2COOH and FCH_2COOH are useful. FCH_2COOH is useful in both the positive- and negative-ion modes. If $ClCH_2COOH$, with a high boiling point, is used to detect benzthiazide in LC–TSP-MS, this acid is useful to detect the molecular ion of benzthiazide because the base peak of this drug is the $[M]^-$ ion.

Acknowledgement

This work was supported in part by the program of Basic Sciences Research (BRSI-94-3439), Ministry of Education, 1994.

References

[1] F.T. Delbeke and M. Debackere, *J. Pharm. Biomed. Anal.*, 3 (1985) 141.
[2] S.F. Cooper, R. Massse and R. Dugal, *J. Chromatogr.* 489 (1989) 65.
[3] C. Fagerlund, P. Hartvig and B. Lindstrom, *J. Chromatogr.*, 168 (1979) 107.
[4] D. Barcello, *Org. Mass Spectrom.*, 24 (1989) 219.
[5] C.E. Parker, R.W. Smith, S.J. Gaskell and M.M. Bursey, *Anal. Chem.*, 58 (1986) 1661.
[6] M.M. Bursey, C.E. Parker, R.W. Smith and S.J. Gaskell, *Anal. Chem.*, 57 (1985) 2597.
[7] M.L. Vestal and G.J. Fergusson, *Anal. Chem.*, 57 (1985) 2373.

ELSEVIER

Journal of Chromatography A, 689 (1995) 175–176

JOURNAL OF CHROMATOGRAPHY A

Book Review

Perfumery—Practice and Principles, by R.R. Calkin and J.S. Jellinek, Wiley, New York, Chichester, 1994, XIV + 287 pp., price £58.00, US$ 80.50, ISBN 0-471-58934-9.

The book is divided into five parts with 20 chapters covering 250 pages with additional pages for an appendix on chemical structural information and on perfumes, raw materials and bases. It ends with a bibliography, an index of perfumery raw materials and a general subject index.

The first part addresses basic skills and techniques in perfumery. It describes in 7 chapters (72 pages) what it takes to be a perfumer, the technique of smelling, classification of perfumery raw materials, and the technique of matching or imitation of existing perfumes. The last one is the only chapter which has included a description of an instrumental, analytical tool, namely gas chromatography. Part I gives an overview of the training of perfumers, without going too much into details. Simplification of some aspects and many good examples help readers outside the field of perfumery to understand the complexity of the subject, but are unsatisfying to the scientist in the field.

The second part on aesthetics and fundamentals of composition (22 pages) includes a chapter on the biological basis of aesthetics (the function of smell in nature and its implications on the work of the perfumer), the structure of a perfume, its balance between simplicity and complexity, as well as a chapter on the use of bases, the building blocks of perfumery. This part describes traditional approaches in perfumery and does not reflect the tools and methods used in modern fragrance research. The authors describe in a practical way the relation between top, middle, and base note of a perfume; information derived from their long experience in this field.

Part III (39 pages) is devoted to studies in fine fragrance. It mainly contains a description of selected great perfumes like l'Air du Temps, Chanel No. 5, Opium, Cabochard, and many others. The perfumes are grouped into families according their underlying accords, showing nicely the descent or evolution of a new perfume.

Aspects of creative perfumery are discussed in Part IV (61 pages). Aesthetic and technical considerations for perfumes in functional products (products other than alcoholic fragrances) bring up the parameters which influence the performance of a fragrance: volatility (vapour pressure), water solubility, inherent odour strength, odour value and odour volume. Problems of stability and compatibility are discussed as well. This part shows best the scientific side of creative perfumery, which in the future will become more and more important, and partly replace the mystery of perfumery art.

The final part is devoted to scientific fundamentals (43 pages). It begins with the explanation of chemical structures of perfumery materials, followed by a chapter on chemical reactions in perfumery (e.g. Schiff bases, hydrolysis, oxidation etc.). It is not clear for whom these

SSDI 0021-9673(94)01077-3

chapters are beneficial. The chemistry is very basic, starting with the explanation, that the carbon atom is tetravalent and ending with examples of the relation between odour and functional groups. The physical basis and psychophysics of perfumery are described in the last two chapters. Influence of molecular size and structure on volatility is shown, but no reference or description is given, how volatility can be measured. Persistence, fixation and substantivity are among other terms, which are explained in their practical implications, but no attempt is made to provide information, how such important parameters are determined. The same applies for threshold value, slope (dose/response curve) and odour value.

This text book is of high value to those interested in the art and craft of perfumery. It can be recommended not only to junior perfumers, but as well to persons from sale and marketing interested in practical aspects of perfumery. Unfortunately its value as a reference book is limited, due to an incomplete bibliography, which contains only 53 references of which 44 are from 1990 and older. For the chromatographer it may be disappointing, after reading in the preface about the importance of GC and GC–MS, to find only a very basic description of the technique without any reference to state of the art in headspace analysis or micropreparative isolations.

Dübendorf, Switzerland R. Schwarzenbach

Chromatography in the Petroleum Industry

Edited by **E.R. Adlard**

Journal of Chromatography Library, Volume 56

Petroleum mixtures consist primarily of relatively unreactive complex hydrocarbons covering a wide boiling range. Such mixtures are difficult to separate by most analytical techniques. Therefore, the petroleum industry has for many years played a leading role in the development of chromatographic methods of analysis. Since the last book specifically concerned with chromatographic analysis of petroleum appeared 15 years ago, numerous advances have been made including developments in liquid and supercritical fluid chromatography, the advent of silica capillary columns with bonded stationary phases and the commercial availability of new selective detectors.

The current book contains chapters written by experts concerning the analysis of mixtures ranging from low boiling gases to waxes and crude oils.

Although the volume is specifically aimed at the petroleum analyst, there is much information of general interest which should be of benefit to a very wide readership.

Contents:

©1995 452 pages Hardbound
Price: Dfl. 435.00 (US$ 255.75)
ISBN 0-444-89776-3

ELSEVIER
An imprint of Elsevier Science

ORDER INFORMATION

ELSEVIER SCIENCE B.V.
P.O. Box 330
1000 AH Amsterdam
The Netherlands
Fax: +31 (20) 485 2845

For USA and Canada:
P.O. Box 945, New York
NY 10159-0945
Fax: +1 (212) 633 3680

US$ prices are valid only for the USA & Canada and are subject to exchange rate fluctuations; in all other countries the Dutch guilder price (Dfl.) is definitive. Customers in the European Union should add the appropriate VAT rate applicable in their country to the price(s). Books are sent postfree if prepaid.

PRINCIPAL COMPONENTS

By **D.L. Massart** and **P.J. Lewi**

This attractively packaged set, comprising 4 videos, a manual and a software package, is an introduction to the use of principal components analysis (PCA) and related methods in chemometrics. Emphasis has been placed on the use of PCA to display graphically the structure of data sets or to extract graphically information from such a set (display methods). However, links are provided to several other important methods, such as evolving factor analysis, principal component regression and partial least squares.

In order to induce students to learn PCA, and convince them of the usefulness of the methods, several real-life examples have been included. These examples have been chosen to illustrate the generality of the data analysis approach. The data pertain to food, industrial and environmental analysis, animal experimentation, medicinal chemistry, virology and epidemiology. In the software section an additional example concerned with food analysis has been added. Section 3 of the manual contains a complete list of figures. This allows the user to look at some of the figures in a more leisurely fashion or to re-read text which has been heard when viewing the videos. Some of the visuals and some of the texts (occasionally shortened) have been included in this section.

Two types of software augment this series. The first is a tutorial version of a commercial software package called SPECTRAMAP, which has been modified for didactical use. SPECTRAMAP is a performant software for methods derived from PCA that gives excellent display quality.

The other type of software is a listing of a MATLAB® program. In order to understand completely a mathematical algorithm or method, the authors recommend the user to program it himself, using MATLAB®. In this way the user can also obtain all the intermediate results, thereby understanding what happens with a data set when analyzed by PCA. This section also contains an additional data set with which the user can experiment with the software. Some hints are given in to teachers and self-learners on how to use the material to optimize results.

Contents: VIDEOS:

Part A: Principal components as display method.
Part B: Display variables and relationships between variables and objects.
Part C: Singular value decomposition; Eigenvalues; Evolving factor analysis; Software and exercises.
Part D: The display of latent variables in tabulated data.

A 25-minute demonstration video, containing a representative selection from all four video tapes is available at cost price.

ELSEVIER

An imprint of Elsevier Science

MANUAL:

1. Introduction.
2. Proposed didactical concepts.
3. List of Visuals.
4. Software Section.

4A. SPECTRAMAP (P.J. Lewi, J. Van Hoof, M. Nijs).
4B. A MATLAB program for principal components analysis (M. Massart).

©1994 Complete set VHS PAL
Price: Dfl. 1750.00 (US$1000.00)
ISBN 0-444-81622-4
Complete set VHS NTSC
Price: Dfl. 1750.00 (US$1000.00)
ISBN 0-444-81655-0
Manual
Price: Dfl. 65.00 (US$37.00)
ISBN 0-444-81653-4
Demonstration copy
VHS PAL Video
Price: Dfl. 50.00 (US$28.50)
ISBN 0-444-81980-0
Demonstration copy
VHS NTSC Video
Price: Dfl. 50.00 (US$28.50)
ISBN 0-444-81979-7

Additional copies of the manual may be ordered separately.

ORDER INFORMATION

ELSEVIER SCIENCE B.V.
P.O. Box 330
1000 AH Amsterdam
The Netherlands
Fax: +31 (20) 5862 845

For USA and Canada
P.O. Box 945
Madison Square Station
New York, NY 10159-0945
Fax: +1 (212) 633 3680

US$ prices are valid only for the USA & Canada and are subject to exchange rate fluctuations; in all other countries the Dutch guilder price (Dfl.) is definitive. Customers in the European Union should add the appropriate VAT rate applicable in their country to the price(s). Books are sent postfree if prepaid.

PUBLICATION SCHEDULE FOR THE 1995 SUBSCRIPTION

Journal of Chromatography A and *Journal of Chromatography B: Biomedical Applications*

MONTH	O 1994	N 1994	D 1994	J 1995	
Journal of Chromatography A	683/1 683/2 684/1	684/2 685/1 685/2 686/1	686/2 687/1 687/2 688/1 + 2	689/1 689/2 690/1 690/2	The publication schedule for further issues will be published later.
Bibliography Section					
Journal of Chromatography B: Biomedical Applications				663/1 663/2	

INFORMATION FOR AUTHORS

(Detailed *Instructions to Authors* were published in *J. Chromatogr. A*, Vol. 657, pp. 463–469. A free reprint can be obtained by application to the publisher, Elsevier Science B.V., P.O. Box 330, 1000 AH Amsterdam, Netherlands.)

Types of Contributions. The following types of papers are published: Regular research papers (full-length papers), Review articles, Short Communications and Discussions. Short Communications are usually descriptions of short investigations, or they can report minor technical improvements of previously published procedures; they reflect the same quality of research as full-length papers, but should preferably not exceed five printed pages. Discussions (one or two pages) should explain, amplify, correct or otherwise comment substantively upon an article recently published in the journal. For Review articles, see inside front cover under Submission of Papers.

Submission. Every paper must be accompanied by a letter from the senior author, stating that he/she is submitting the paper for publication in the *Journal of Chromatography A* or *B*.

Manuscripts. Manuscripts should be typed in **double spacing** on consecutively numbered pages of uniform size. The manuscript should be preceded by a sheet of manuscript paper carrying the title of the paper and the name and full postal address of the person to whom the proofs are to be sent. As a rule, papers should be divided into sections, headed by a caption (*e.g.*, Abstract, Introduction, Experimental, Results, Discussion, etc.). All illustrations, photographs, tables, etc., should be on separate sheets.

Abstract. All articles should have an abstract of 50–100 words which clearly and briefly indicates what is new, different and significant. No references should be given.

Introduction. Every paper must have a concise introduction mentioning what has been done before on the topic described, and stating clearly what is new in the paper now submitted.

Experimental conditions should preferably be given on a *separate* sheet, headed "Conditions". These conditions will, if appropriate, be printed in a block, directly following the heading "Experimental".

Illustrations. The figures should be submitted in a form suitable for reproduction, drawn in Indian ink on drawing or tracing paper. Each illustration should have a caption, all the *captions* being typed (with double spacing) together on a *separate sheet*. If structures are given in the text, the original drawings should be provided. Coloured illustrations are reproduced at the author's expense, the cost being determined by the number of pages and by the number of colours needed. The written permission of the author and publisher must be obtained for the use of any figure already published. Its source must be indicated in the legend.

References. References should be numbered in the order in which they are cited in the text, and listed in numerical sequence on a separate sheet at the end of the article. Please check a recent issue for the layout of the reference list. Abbreviations for the titles of journals should follow the system used by *Chemical Abstracts*. Articles not yet published should be given as "in press" (journal should be specified), "submitted for publication" (journal should be specified), "in preparation" or "personal communication".

Vols. 1–651 of the *Journal of Chromatography*; *Journal of Chromatography, Biomedical Applications* and *Journal of Chromatography, Symposium Volumes* should be cited as *J. Chromatogr.* From Vol. 652 on, *Journal of Chromatography A* (incl. Symposium Volumes) should be cited as *J. Chromatogr. A* and *Journal of Chromatography B: Biomedical Applications* as *J. Chromatogr. B.*

Dispatch. Before sending the manuscript to the Editor please check that the envelope contains four copies of the paper complete with references, captions and figures. One of the sets of figures must be the originals suitable for direct reproduction. Please also ensure that permission to publish has been obtained from your institute.

Proofs. One set of proofs will be sent to the author to be carefully checked for printer's errors. Corrections must be restricted to instances in which the proof is at variance with the manuscript.

Reprints. Fifty reprints will be supplied free of charge. Additional reprints can be ordered by the authors. An order form containing price quotations will be sent to the authors together with the proofs of their article.

Advertisements. The Editors of the journal accept no responsibility for the contents of the advertisements. Advertisement rates are available on request. Advertising orders and enquiries can be sent to the Advertising Manager, Elsevier Science B.V., Advertising Department, P.O. Box 211, 1000 AE Amsterdam, Netherlands; Tel: 31 (20) 485 3796; Fax: 31 (20) 485 3810. Courier shipments to street address: Molenwerf 1, 1014 AG Amsterdam, Netherlands. *UK*: T.G. Scott & Son Ltd., Tim Blake, Portland House, 21 Narborough Road, Cosby, Leics. LE9 5TA, UK; Tel: (0116) 2750 521/2753 333; Fax: (0116) 2750 522. *USA and Canada*: Weston Media Associates, Daniel S. Lipner, P.O. Box 1110, Greens Farms, CT 06436-1110, USA; Tel: (203) 261 2500; Fax: (203) 261 0101.

Capillary Electrophoresis

Principles, Practice and Applications

By **S.F.Y. Li**

Journal of Chromatography Library Volume 52

"Everything seems to be there, any detection system you have ever dreamed of, any capillary coating, enough electrolyte systems to saturate your wits, and more, and more.
...by far the most thorough book in the field yet to appear."

Journal of Chromatography

" It is almost encyclopaedic in its coverage and all chapters are extremely well referenced. This will facilitate any search for original information on any aspect of CE."

Talanta

"This is a useful book that serves several audiences. The author is to be commended for putting together a thoughtful, complete, and thoroughly useful reference."

Analytical Chemistry

This book covers all aspects of CE, from the principles and technical aspects to the most important applications. It is intended to meet the growing need for a thorough and balanced treatment of CE. The book will serve as a comprehensive reference work. Both the experienced analyst and the newcomer will find the text useful.

Contents: 1. Introduction. Historical Background. Overview of High Performance CE. Principles of Separations. Comparison with Other Separation Techniques. **2. Sample Injection Methods.** Introduction. Electrokinetic Injection. Hydrodynamic Injection. Electric Sample Splitter. Split Flow Syringe Injection System. Rotary Type Injector. Freeze Plug Injection. Sampling Device with Feeder. Microinjectors. Optical Gating. **3. Detection Techniques.** Introduction. UV-Visible Absorbance Detectors. Photo-diode Array Detectors. Fluorescence Detectors. Laser-based Thermooptical and Refractive Index Detectors. Indirect Detection. Conductivity Detection. Electrochemical Detection. Mass Spectrometric Detection. **4. Column Technology.** Uncoated Capillary Columns. Coated Columns. Gel-filled Columns. Packed Columns. Combining Packed and Open-Tubular Column. **5. Electrophoretic Media.** Electrophoretic Buffer Systems. Micellar Electrokinetic Capillary Chromatography. Inclusion Pseudophases. Metal-complexing Pseudophases. Other Types of Electrophoretic Media. **6. Special Systems and Methods.** Buffer Programming. Fraction Collection. Hyphenated Techniques. Field Effect Electroosmosis. Systematic Optimization of Separation. **7. Applications of Capillary Electrophoresis.** Biomolecules. Pharmaceutical and Clinical Analysis. Inorganic Ions. Hydrocarbons. Foods and Drinks. Environmental Pollutants. Carbohydrates. Toxins. Polymers and Particles. Natural Products. Fuel. Metal Chelates. Industrial Waste Water. Explosives. Miscellaneous Applications. **8. Recent Advances and Prospect for Growth.** Recent Reviews on CE. Advances in Injection Techniques. Novel Detection Techniques. Advances in Column Technology. Progress in Electrolyte Systems. New Systems and Methods. Additional Applications Based on CE. Future Trends. Subject index.

©1992 1st reprint 1993 608 pages
Hardbound
Price: Dfl. 395.00 (US$225.75)
ISBN 0-444-89433-0
1st repr. as a Paperback 1993
Price: Dfl. 200.00 (US$114.25)
ISBN 0-444-81590-2

ELSEVIER
An imprint of Elsevier Science

ORDER INFORMATION
ELSEVIER SCIENCE B.V.
P.O. Box 330
1000 AH Amsterdam
The Netherlands
Fax: +31 (20) 5862 845
For USA and Canada
P.O. Box 945
Madison Square Station
New York, NY 10159-0945
Fax: +1 (212) 633 3680

US$ prices are valid only for the USA & Canada and are subject to exchange rate fluctuations; in all other countries the Dutch guilder price (Dfl.) is definitive. Customers in the European Union should add the appropriate VAT rate applicable in their country to the price(s). Books are sent postfree if prepaid.

0021-9673(19950106)689:1;1-M